SACRIFICIAL POLYMERS FOR RAPID MANUFACTURING OF BIOINSPIRED VASCULAR MATERIALS

BY

MAYANK GARG

DISSERTATION

Submitted in partial fulfillment of the requirements
for the degree of Doctor of Philosophy in Materials Science and Engineering
in the Graduate College of the
University of Illinois at Urbana-Champaign, 2020

Urbana, Illinois

Doctoral Committee:

Professor Nancy Sottos, Chair
Professor Jeffrey Moore
Assistant Professor Christopher Evans
Assistant Professor Qian Chen

ABSTRACT

Synthetic vascular systems, inspired by hierarchical vascular networks for mediating heat and mass transport in biological structures, have gained tremendous interest in the fields of microfluidics, soft robotics, microelectronics, battery packaging, and civil infrastructure. Strategies for fabrication of vascular networks include pullout, dissolution, melting, or evaporation of sacrificial templates (metal wires, fugitive inks, photoresists) embedded in a host matrix to leave hollow conduits ranging from microns to meters in length. Most sacrificial materials cannot be easily templated into complex interconnected architectures or are unable to withstand thermomechanical stresses during integration into structural thermosets and fiber-reinforced polymer composites (FRPCs).

Catalyst-assisted thermal depolymerization of poly(lactic acid) (PLA) templates containing an organometallic compound enables manufacturing of complex vasculature in thermosets and FRPCs for self-healing, thermal regulation, and electromagnetic reconfigurability applications. However, this vascularization method is a two-step energy-intensive process that requires sustained external heating to first polymerize the thermoset matrix, and then to depolymerize the embedded sacrificial PLA templates into volatile products (ca. 200 °C for 12 hours). Moreover, vaporization of sacrificial components (VaSC) with PLA is only suitable for host matrices that withstand these extreme conditions. Residual organometallic catalyst also remains on the channel walls, which may hamper subsequent functionalization of the microchannels. In this dissertation, we explore new sacrificial polymers that depolymerize at lower temperatures than PLA to reduce the energy consumption for making vascular structures and expand the scope of VaSC to a broader range of host matrices. Next, we investigate a more energy-efficient strategy for rapid

manufacturing of vascular materials in a single-step by harnessing the energy from exothermic curing of the host matrix.

New organometallic catalysts are pursued for lowering the VaSC temperature and time for PLA in epoxy-based matrices with a glass transition temperature (T_g) ca. 155 °C. Depolymerization of PLA films blended with various surface areas and concentrations of tin (II) oxalate and tin (II) acetate catalysts are compared via mass loss in a thermogravimetric analyzer (TGA). A 10x improvement in mass loss kinetics of PLA is observed with tin acetate. PLA films blended with tin acetate are then embedded in a host matrix and successfully evacuated in a heated oven at temperatures as low as 170 °C after 12 hours to create microchannels with less catalytic residue on the walls. A lower temperature limit for VaSC within a practical time (12 h) is reported near the melting temperature of PLA ca. 160 °C.

Vascularization at lower temperatures with a five-fold reduction in thermal energy consumption than PLA is demonstrated with a metastable polymer known as cyclic poly(phthalaldehyde) (cPPA). cPPA is synthesized and solvent-processed into laser-cut films, fibers, and printed templates. Mass loss before (TGA) and after embedding into a host matrix (VaSC) is compared to determine successful vascularization protocols. A mass loss kinetics model derived from the TGA experiments reveals a ca. 32 kJ/mol reduction in activation energy for depolymerization of cPPA compared to PLA, allowing vascularization within 1 hour at 110 °C. Residue-free channel walls are obtained in epoxy-based matrices with T_g between 42-65 °C.

A further 50 °C reduction in VaSC temperature is achieved with acid-catalyzed depolymerization of poly(propylene carbonate) (PPC) templates. PPC containing a latent photoacid generator (PAG) is melt-processed into fibers and filaments near 150 °C, which is easily depolymerized below the extrusion temperature after activating the PAG. This orthogonal trigger approach allows melt-extrusion into mechanically robust templates that sustain bending loads without brittle fracture and are readily incorporated in host matrices with low T_g after photoactivation. Residue-free vasculature is achieved after exposure to temperatures between 50-100 °C after 1-12 hours. A 100x increase in the pre-exponential factor for the Arrhenius-based mass loss kinetics of PPC compared to cPPA facilitates the faster depolymerization of PPC at such low temperatures.

In the final part of the thesis, we investigate concurrent depolymerization of embedded sacrificial templates during frontal polymerization (FP) of a dicyclopentadiene (DCPD) matrix to create vascular thermosets and FRPCs within minutes under ambient conditions. The heat generated during FP of DCPD is sufficient for complete depolymerization of cPPA and PPC fibers and printed templates without an additional external heat source. A thermochemical computational model based on experimental parameters provides insights into the processing window for coupled polymerization and depolymerization reactions. Bioinspired thermosets with redundant vascular networks are fabricated with this single-step approach. In addition, vascular FRPCs are manufactured within seconds at room temperature, reducing fabrication time by three orders of magnitude and processing energy by four orders of magnitude compared to the current PLA VaSC method. This one-step, energy-efficient processing route can propel industrial-scale manufacturing of bioinspired vascular structures for biomedical, transportation, and energy applications.

To Mom, Dad, and Hamanshu for their unending love.

To my friends and family, for all your encouragement.

Thank you all for existing.

ACKNOWLEDGEMENTS

I will begin by expressing my gratitude to the two people who invested their energy, confidence, and research expertise consistently in my graduate journey- Professor Nancy Sottos and the late Professor Scott White. You have provided me numerous opportunities to explore my scientific curiosity and encouraged me to lead in more ways than I ever imagined. Bossman, you will be dearly missed. It has been a privilege to witness Professor Jeffrey Moore drive the vision of the Autonomous Materials Systems (AMS) research group with his deep-rooted motivation from nature. Thank You for staying by my side in more than one Marathon and showing me what it means to work as a team.

I extend my thanks to Professor Philippe Geubelle for his persistent efforts in revealing the beauty that is captured in simple equations. I admire your zeal for discussing science from dawn to dusk. I also want to thank Professor Christopher Evans and Professor Qian Chen for serving on my thesis committee and their feedback in this project. I extend my gratitude to Beckman Institute’s Imaging Technology Group (ITG) microscopy suite and the Aerospace Engineering (AE) machine shop for providing their expertise and equipment to make progress towards my research goals. This work has been financially supported by the Air Force Office of Scientific Research (AFOSR grant # FA 9550-16-1-0017, Center of Excellence in Self-healing, Regeneration, and Structural Remodeling) and the PPG-MRL Graduate Research Fellowship.

I am indebted to Ashley Trimmell and Erica Malloch for ensuring a smooth research experience at the University of Illinois Urbana Champaign (UIUC) through their consistent and quick assistance with various administrative tasks. I am grateful to numerous Sottos-White and

AMS group members (present and former) who have provided their assistance and feedback on countless experiments, instruments, documents, and presentations. My mentors Jason Patrick, Mostafa Yourdkhani, Ozgur Capraz, Anthony Coppola, Stephen Pety, and Thu Doan have guided me personally and professionally throughout this journey. My mentees Adam Ladd, Jacob Komenda, Yiqiao (Sophie) Liu, David Nejdl, and Sashank Peravali have been instrumental in bringing my collaborative projects to fruition. I cherish these professional relationships turn into friendships.

I consider myself extremely lucky to have the essential support system at UIUC and back home to persevere on this path with its ups and downs while enjoying the priceless moments that have entangled our lives. To all the people who have endured this process with me- my parents (Jaspal and Amita), brother (Hamanshu), cousins, grandmother (Savitri), aunts and uncles, undergrad friends (Dhruv, Vatsal, Rachit, Arpit, Akshay, Nikhil, Aaditya, Nikita), UIUC friends (Faraz, Dylan, Leah, Tony and Kali, Pranjali, Shachi and Saurabh, Kelly, Jia, Julie)- Thank You for helping me write a chapter in the thesis of my life! I hope to meet you all in person after the COVID-19 situation improves.

(Chapter 2) I extend my gratitude to the following people: Members (present and former) of the AMS group at UIUC: Prof. Jason Patrick, Dr. Stephen Pety, Dr. Anthony Griffin, Prof. Xiang Zhang, Prof. Philippe Geubelle, and Prof. Paul Braun; Department of Chemistry collaborators: Dr. Yurun Miao and Prof. Kenneth Suslick; Catherine Wallace and Dianwen Zhang of ITG; Dr. Chris Mangun of CU Aerospace.

(Chapter 3) I extend my gratitude to the following people: Members (present and former) of the AMS group at UIUC: Adam Ladd, Jia En Aw, Evan Lloyd, Prof. Xiang Zhang, Dr. Hector

Lopez Hernandez, and Prof. Mostafa Yourdkhani; Dr. Leilei Yin of ITG; Greg Milner and Lee Booher of the AE machine shop.

(Chapter 4) I extend my gratitude to the following people: Members (present and former) of the AMS group at UIUC: Jacob Komenda, David Nejdl, Sashank Peravali, Sophie Liu, Adam Ladd, Prof. Paul Braun, and Prof. Xiang Zhang; Greg Milner and Lee Booher of the AE machine shop.

(Chapter 5) This project would not have been possible without the guidance and collaboration of so many people: Members (present and former) of the AMS group at UIUC: Dr. Ian Robertson, Jia En Aw, Prof. Xiang Zhang, Polette Centellas, Leon Dean, Evan Lloyd, Sophie Liu, Nil Parikh, Prof. Mostafa Yourdkhani, Prof. Jeffrey Moore, Prof. Philippe Geubelle, Dr. Anthony Griffin, and Dr. Christopher Montgomery; Dr. Leilei Yin, Travis Ross, and Jose Vazquez of ITG; Kyle Cheek and Jeff Smith of the Mechanical Engineering machine shop.

TABLE OF CONTENTS

CHAPTER 1

INTRODUCTION

Biological materials such as leaves, lungs, and bones possess hierarchical vascular networks that mediate heat and mass transport in response to external and internal stimuli to sustain complex living systems [1]. Interconnected vessels mediate nutrient and liquid transport inside multifunctional load-bearing structural biomaterials such as bone and wood for sustenance, growth, and repair [2]. Synthetic fiber-reinforced polymer composites (FRPCs) possess outstanding mechanical properties, promoting use in aviation, automotive, marine, and energy industries [3]–[6]. However, FRPCs remain quiescent to external stimuli with limited functionality.

Fabrication of FRPCs with embedded hollow microchannels using "sacrificial" precursors has garnered significant research interest in the past two decades, resulting in environmentally adaptive structures with self-repair [7]–[10], active cooling [11]–[14], and electromagnetic reconfigurability [15] functionalities. The state-of-the-art manufacturing method [15], [16] for making vascular FRPCs involves embedding a solid polymer as a placeholder in a liquid resin (**Figure 1.1a**), followed by curing of the host matrix (**Figure 1.1b**) and evacuation of the sacrificial template by an additional heating cycle (**Figure 1.1c**) to create a hollow replica (**Figure 1.1d**). This process is both energy- and time-intensive, and limited to high-temperature resistant host matrices. New sacrificial polymers are needed to reduce the energy footprint of the fabrication process and expand vascularization to a broader range of host matrices.

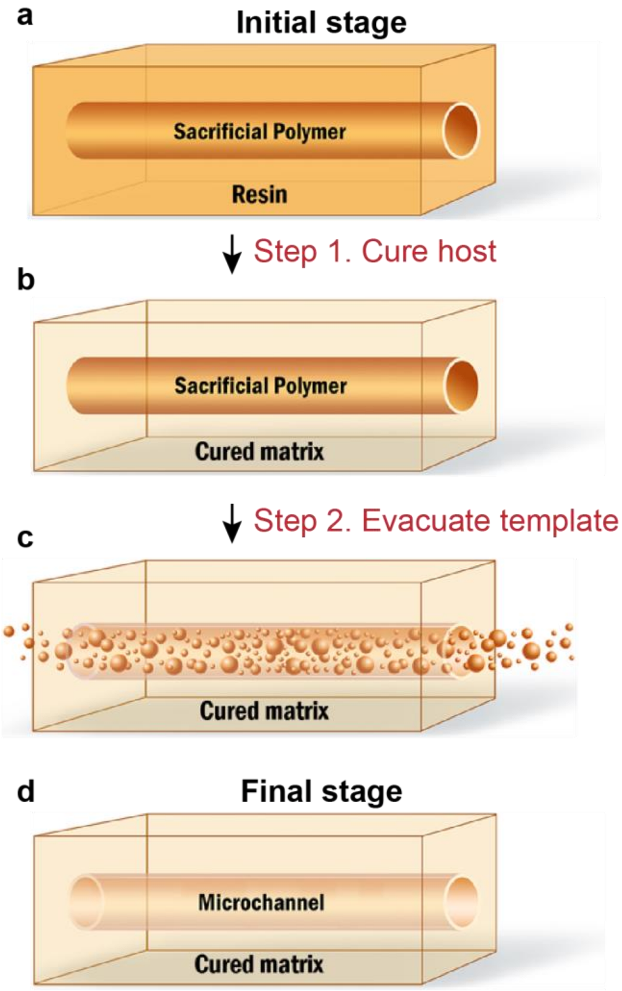

Figure 1.1. Fabrication of microvascular structures using a two-step process. (a) A sacrificial polymer template is embedded in a host resin and (b) post-cured in an oven. (c) The thermoset matrix is then exposed to a higher temperature to evacuate the gaseous monomers during depolymerization of the template and (d) leave a hollow replica of the initial architecture.

This chapter describes the function and formation of biological vascular materials. Existing strategies for fabricating bioinspired structures with embedded microfluidic networks are summarized across multiple fields, focusing on the limitations of existing sacrificial precursors for making structural vascular materials. Finally, the design criteria for new sacrificial polymers and host matrices to streamline the manufacturing of microvascular thermosets and FRPCs are introduced.

1.1 Vascular networks in biological systems: formation and function

1.1.1 Redundant vascular networks for multifunctionality

Biological systems contain vascular pathways to deliver biochemical fluids for maintaining metabolic and homeostatic functions including respiration, circulation, waste removal, sensing, thermal regulation, and self-repair [1]. For example, the interconnected vessels in a *Citrus limon* leaf (**Figure 1.2**) facilitate the distribution of hormones, sugars, and other metabolites in the plant through transpiration [17]. Besides sustenance through capillary action, these vessels also transport water to the small pores in the leaves to reduce the leaf temperature by 10 °C through diffusion and evaporation of water [18]. Even after arterial puncture (shown in red), the branched architecture maintains homeostasis by redirecting fluid flow through redundancy in the network. This interconnectivity is essential for survival after damage.

Figure 1.2 Redundant microvascular networks in a *Citrus limon* leaf. Figure adapted from [17]. The red circle highlights an arterial puncture, and the green-colored fluorescent dye reveals the interconnectivity of the network.

1.1.2 Self-repair and remodeling in structural vascular composites

Bone is an example of a load-bearing vascular biocomposite that remodels itself by resorbing old material and forming new material throughout its lifecycle [19]–[22]. The highly interconnected vascular structure of cortical bone tissue houses blood vessels and sensory nerves in its Haversian and Volkmann's canals (**Figure 1.3a**) for providing essential nutrients to the surrounding cells and maintaining its overall health. Mechanical and biological stimuli such as fracture or a change in loading [19]–[21], and high calcium demands during pregnancy and lactation [22] trigger bone remodeling through the formation of new vessels at anatomically distinct sites termed basic multicellular units (BMUs). As illustrated in **Figure 1.3**, vascularization along the longitudinal axis of the bone occurs through Haversian cutting cones inside concentrically wrapped lamellae known as osteons (ca. 200 μm diameter). In the case of a fracture in the bone tissue, cells known as osteoclasts resorb old bone to create tunnels in the damaged region (**Figure 1.3b**), which are then filled with capillaries, nerves, and connective tissue. Bone forming cells known as osteoblasts line the cutting cones behind the osteoclasts and deposit new bone to house blood vessels inside the newly created Haversian canals. Blood vessels supply essential nutrients to the surrounding tissue in this damaged region and restore the structural integrity of the bone. Vascularization through coordinated deposition and removal of material is a crucial feature in biological structural materials but remains an unmet challenge in structural thermosets and FRPCs.

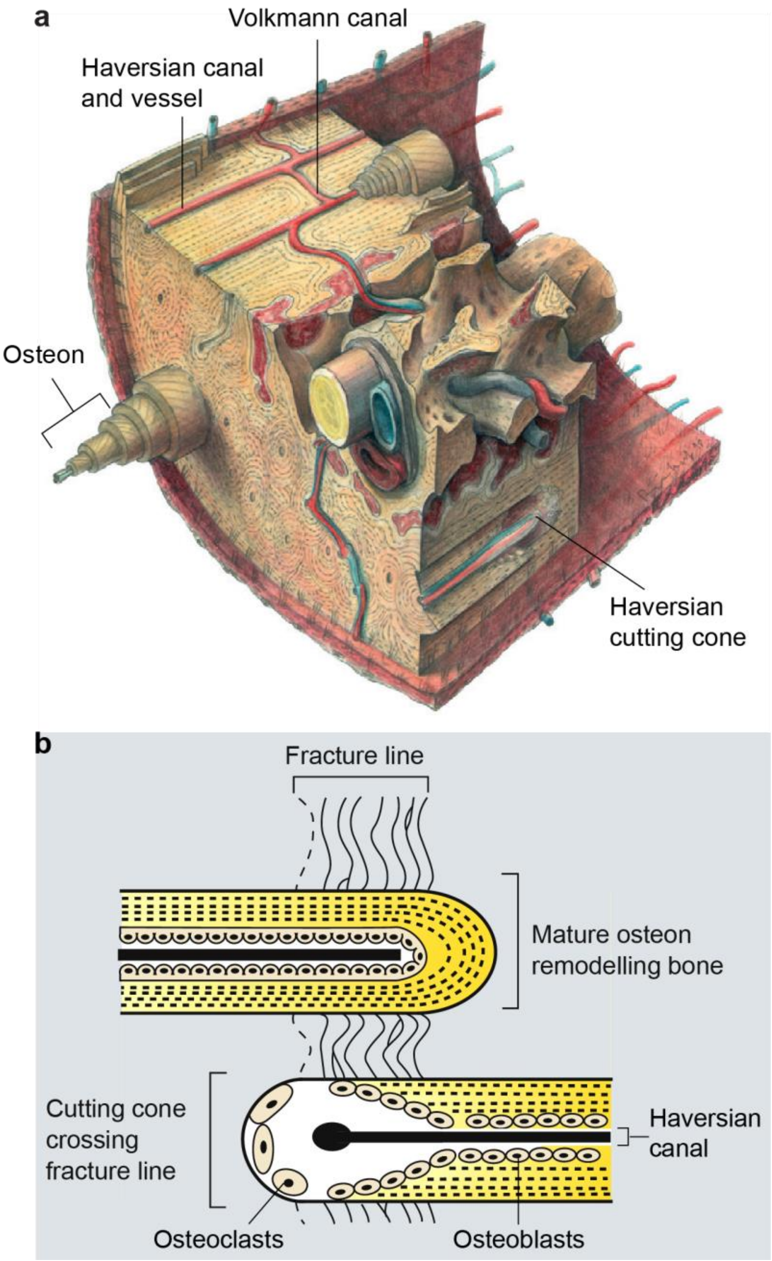

Figure 1.3. Structural remodeling in a bone. (a) A normal bone with interconnected canals housing blood vessels and sensor nerves. Figure adapted from [20]. (b) Formation of Haversian canals in a bone after damage. Figure adapted from [19].

1.2 Bioinspired synthetic vascular structures

1.2.1 Fabrication methods for vascularized materials

The creation of hollow conduits in polymeric host matrices provides liquid cooling and electrical insulation in microelectronics[23]–[27], cellular proliferation and gas capture in synthetic mimics [28]–[30], thermal management in heat exchangers and fiber-reinforced composites [13], [31], chemical reactions in redox flow batteries and solar microreactors [32]–[34], and material regeneration in self-healing structures [10], [35]. Several strategies have been reported to create microvascular structures including laser ablation [36], lithography [37], electrostatic discharge [38], and removal of a "placeholder" templates [15], [39]. In templating methods, the sacrificial metal [7], [40], wax-based fugitive ink [41], [42], or biopolymer [28], [43] templates are submerged/embedded in a host resin followed by matrix polymerization. The template is then removed through pullout [8], melting [41], [44], [45], or dissolution [28], [43], leaving a hollow replica inside the host matrix. This template removal strategy prevents the infiltration or collapse of cavities during fabrication and preserves the features (dimensions, morphology, and interconnectivity) of the resulting channels. Channel architecture varies in complexity from 1-D straight channels to 3-D interconnected networks (**Figure 1.4**). The choice of the host matrix material governs the selection of a sacrificial precursor and the method of template removal.

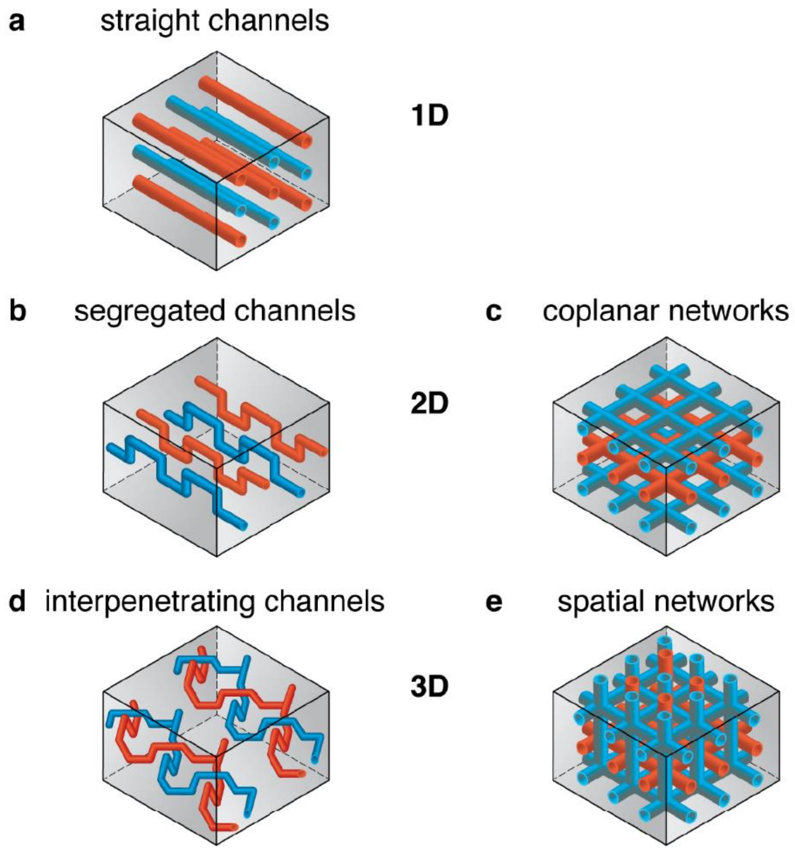

Figure 1.4 Vascular architectures of increasing complexity: (a) One-dimensional (1D) straight channels; (b) Two-dimensional (2D) segregated channels; (c) 2D coplanar interconnected networks; (d) Three- dimensional (3D) interpenetrating channels; (e) 3D spatial interconnected networks. Figure adapted from [9].

Vascularized materials have been used in biomedical as well as structural applications. Miller et al. [28] embedded 3D printed carbohydrate glass lattices in engineered tissues, which were dissolved by cellular media to create vascular channels that promoted cellular metabolic function in otherwise necrotic systems (**Figure 1.5a**). Grigoryan et al. [46] used projection stereolithography to selectively photopolymerize monolithic transparent hydrogels with entangled vascular networks for studying oxygenation and flow of human red blood cells in a proximate airway (**Figure 1.5b**). Cambié et al. [33], [34] fabricated photomicroreactors with planar microchannels by bonding two polydimethylsiloxane sheets with channels created through positive relief molds [33] or drilling holes into acrylic sheets [34]. Pharmaceutically relevant molecules were synthesized through the concentration of solar irradiation into the fluids flown through the channels (**Figure 1.5c**). Toohey et al. printed sacrificial fugitive ink scaffolds that were removed by melting to form microchannels networks inside thermoset epoxy-based matrices [41], [42], [47], [48]. Liquid healing agents were sequestered in the networks and used to heal damage repeatedly (**Figure 1.5d**).

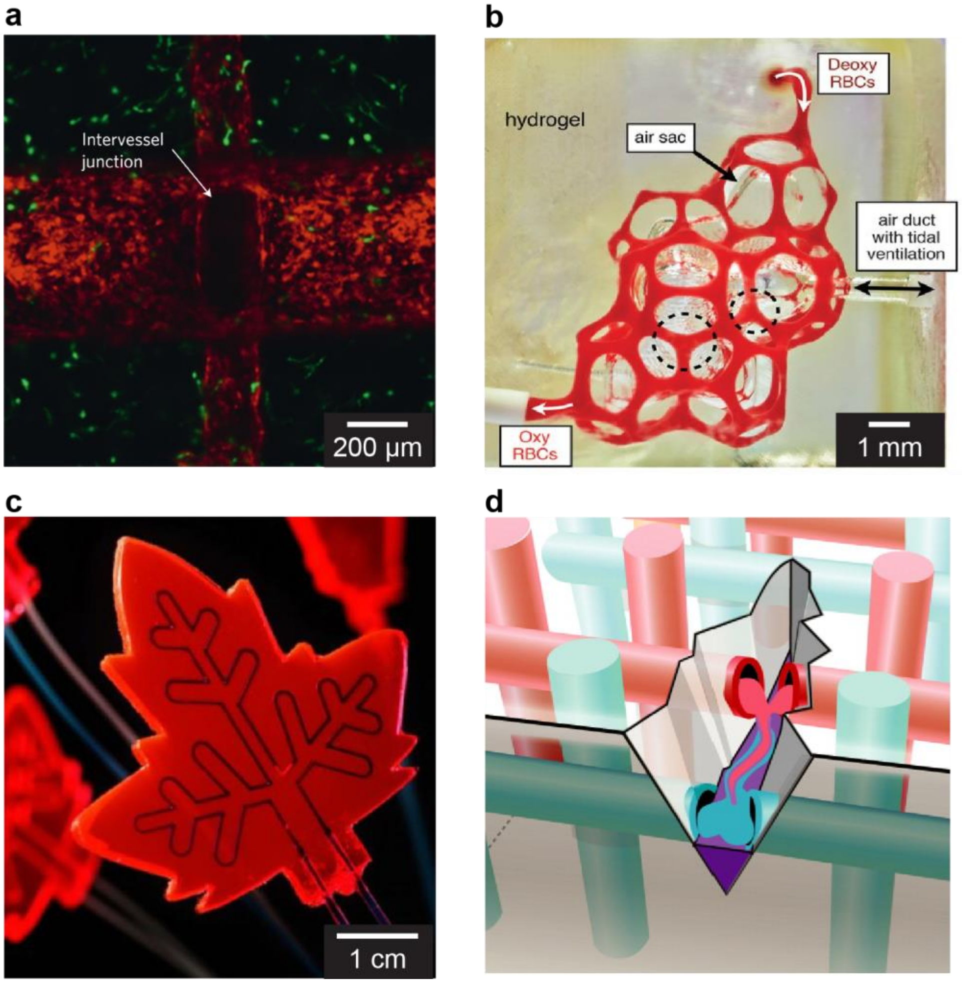

Figure 1.5. Applications of synthetic vascular materials. (a) Cell proliferation in engineered tissue [28]. (b) Respiration inspired photopolymerized microfluidics [46]. (c) Leaf-inspired photomicroreactors through lithography [33]. (d) self-healing polymers through melting f fugitive inks [47].

Most sacrificial precursors that require dissolution for removal are not suitable for structural polymeric materials. For example, neat thermosets and FRPCs made with epoxy-based resins are highly resistant to solvent penetration compared to hydrogels and other “soft” materials. The dissolution of the embedded interconnected templates is limited to the surface of the host structure, making it impractical to remove the templates within a reasonable amount of time.

Therriault et al. [44] successfully fabricated thermosets with 3D microvascular networks via the direct-write assembly of a wax scaffold that was infiltrated with a liquid resin, cured, and exposed to elevated temperature in a vacuum oven to melt and remove the template (**Figure 1.6**). This technique was used to introduce vascularization in an epoxy substrate with a coating [41]. Channel architecture was optimized to deliver liquid healing agents to the cracks in the coating [41], [42], [47], [48]. Complete removal of a sacrificial template by melting is not feasible when dominant capillary forces in channels with diameters below a hundred microns inhibit the escape of the molten material from the matrix [16]. Wax scaffolds are also too delicate to survive the temperatures and compaction pressures encountered in the processing of FRPCs.

Huang et al. [8] fabricated carbon-FRPCs by pull out of metal wires after curing the composite laminate to form 1D channels. Later, Trask et al. [40] embedded low melting temperature solder wires as sacrificial templates in the composite laminate and removed them using a combination of heat and vacuum to create hollow channels. These strategies are limited to planar geometries, limiting the mixing of two reactive fluids in self-healing applications [7], [40], [45], [49]–[51].

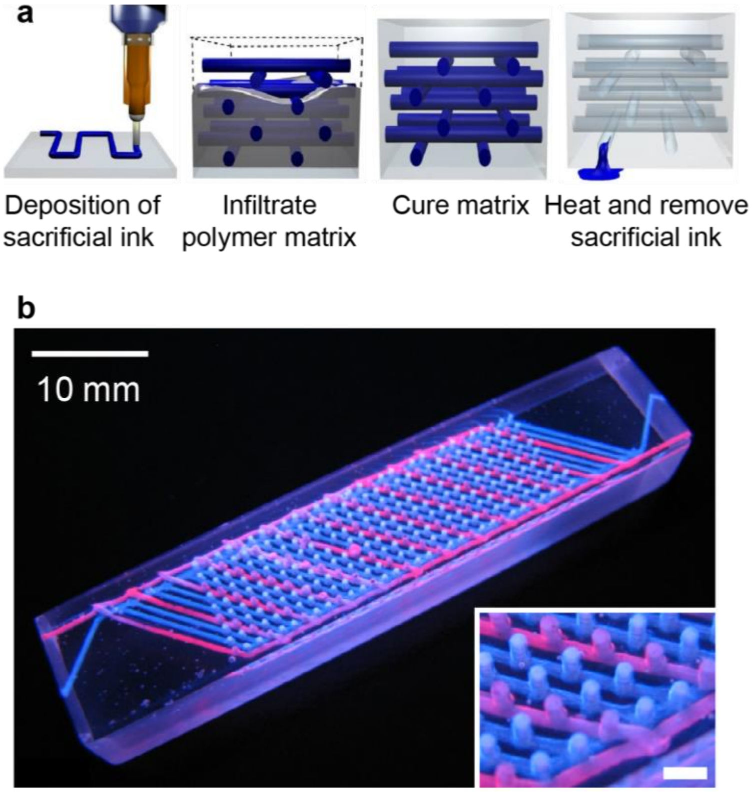

Figure 1.6. Three-dimensional interpenetrating vasculature in an epoxy matrix for self-healing coatings. (a) Direct ink writing of a fugitive wax scaffold, followed by resin infusion and subsequent removal through melting in a vacuum oven. Figure adapted from [44]. (b) Two chemically reactive liquid healing agents (red/blue) were delivered to the fractured surface through the vascular networks (scale bar for inset is 2 mm). Figure adapted from [42].

1.2.2 Vaporization of sacrificial components (VaSC) for microvascular FRPCs

Thermal vaporization of sacrificial polymer templates is widely used in the microelectronics packaging to create partially and fully enclosed cavities for electrical insulation and thermal management [39], [52], [53]. Since this concept relies on the escape of gaseous products, fully encapsulated templates can be removed to create cavities with transverse dimensions in the nanometers to millimeters range. Inspired by this template vaporization method, Esser-Kahn et al. developed a robust method to create thermosets and FRPCs with interconnected vascular networks [15]. This technique, termed vaporization of sacrificial components (VaSC), involved solidification of a host matrix with embedded sacrificial templates followed by their removal using a combination of heat and vacuum to leave behind a hollow inverse replica of the original template (**Figure 1.7**).

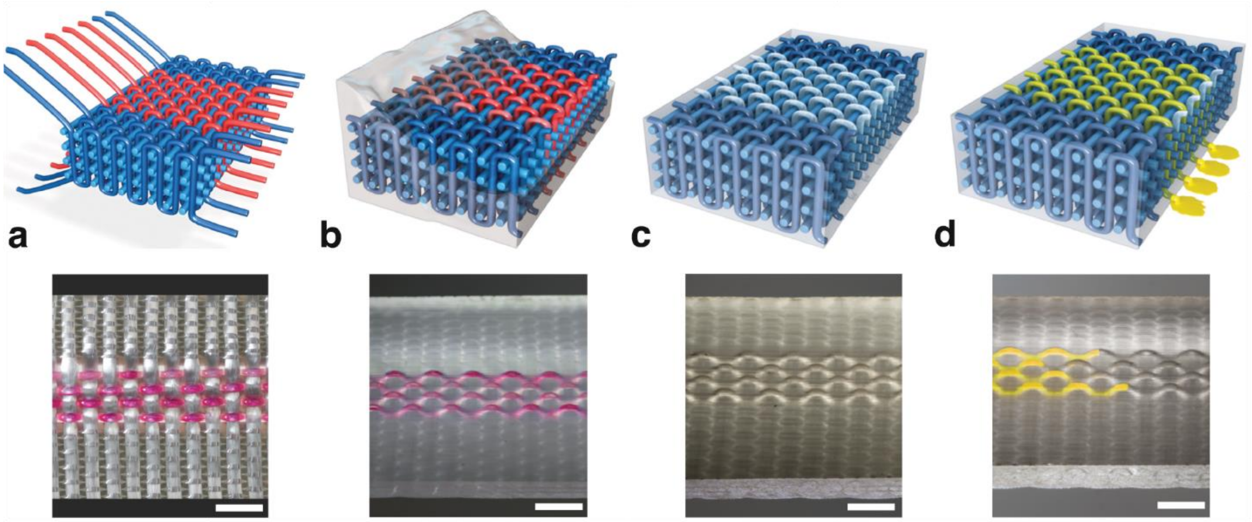

Figure 1.7. Manufacture of multifunctional microvascular fiber-reinforced composites through VaSC. (a) 3D glass reinforcement textile preform co-woven with 500 μm diameter sacrificial z-fibers (pink). (b) liquid thermosetting epoxy resin infiltration followed by matrix solidification and composite post-curing. (c) sacrificial fiber evacuation via thermal depolymerization at 200 °C under vacuum. (d) fluid circulation (yellow) through newly created 3D microvasculature (scale bars = 5 mm). Figure adapted from [15].

The sacrificial polymer was poly(lactic acid) (PLA) blended with an organometallic catalyst, which promotes depolymerization at elevated temperatures (ca. 200 °C) [54]. PLA has been melt-processed into fibers (1D), sheets (2D), and additively printed (3D) templates with high fidelity [16]. These templates maintained thermomechanical integrity during integration into the glass- or carbon-FRPC [9]–[12], [55]. VaSC with sacrificial PLA has produced high-performance multifunctional structures with bioinspired functions such as self-healing and active cooling (**Figure 1.8**).

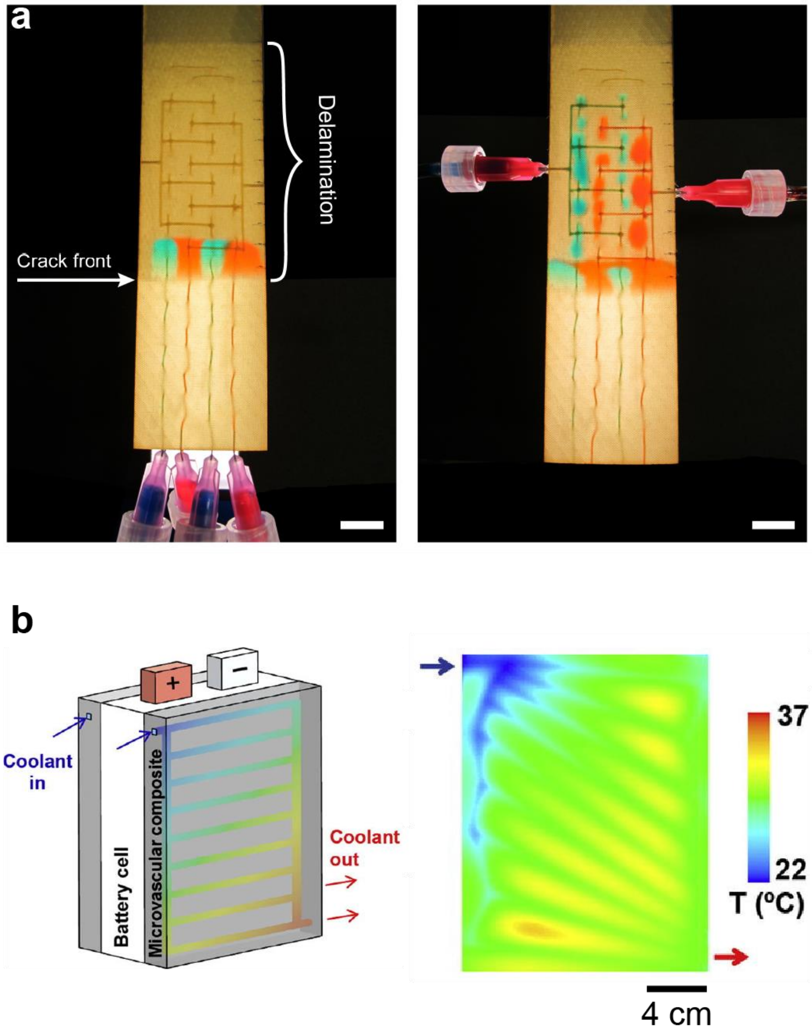

Figure 1.8. Multifunctional microvascular structural materials. (a) Self-healing with two-part healing agents (red/blue) being delivered in the midplane of a delaminated FRPC through isolated (left) and interconnected (right) microvascular networks (scale bars are 10 mm) [9]. (b) The surface temperature profile of a carbon-FRPC panel for battery packaging in electric vehicles with a 2D microvascular network. The composite panel is exposed to a constant heat flux on one side but flowing liquid coolant through the microchannels helps maintain its temperature within the nominal range. Figure adapted from [12].

1.2.3 Limitations of VaSC

The VaSC method is a lengthy two-step process that requires significant energy to cure the neat matrix or composite and to depolymerize the PLA into volatile products (ca. 200 °C for 12 hours). The combined thermal cycle for curing and vascularizing a Bisphenol A based epoxy matrix (BPA-epoxy) in a 0.8 m^3 vacuum oven consumes more than 10^8 joules of energy (see **Appendix A**). The thermal energy consumption scales with part size. For example, curing the fuselage of a Boeing 777x airplane in an autoclave for one day consumes greater than 10^{11} joules, which is equivalent to the energy consumption of nine US households over a full year [56]. Adding a VaSC cycle to the fabrication sequence at this scale further increases the energy input. VaSC of PLA templates is also limited to matrices that can sustain ca. 200 °C without significant thermomechanical deformation/degradation. Additionally, the organometallic catalyst used to promote thermal depolymerization of PLA remains as residue on the channel walls [57], [58]. New sacrificial polymers that depolymerize at lower temperatures than PLA will help reduce the energy consumption for making vascular FRPCs and expand the scope of VaSC to a broader range of host matrices.

1.3 Requirements of sacrificial and host materials

The most important requirement for a sacrificial polymer is the ability to depolymerize into volatile products at the temperatures and time scales of interest. Additional attributes related to synthesis, processing, and compatibility with host matrix include:

- Bulk availability or synthesis scalability of the sacrificial polymer with high molecular weights (hundreds of kDa) to facilitate processing.

- Melt- or solvent-processability into complex architectures that resist deformation and breakage during integration into the host structure (tensile strength > 23 MPa for automated weaving with fiber-reinforcement [15]).
- Compatibility with the host matrix. Ideally, the sacrificial polymer and the host matrix should not have any physical or chemical interactions which could either inhibit the depolymerization of the sacrificial template or prevent the escape of its depolymerization products.

Stimuli-responsive polymers that depolymerize partially or entirely into small molecules after exposure to thermal, optical, and chemical stimuli [59] have been developed for drug delivery [60]–[62], micro- and nano-lithography [63], [64], polymer recycling [65]–[68], and payload release [69], [70] (**Figure 1.9**). Most of these polymers fail to meet the above requirements of a sacrificial polymer for vascularization despite their ability to undergo rapid depolymerization at low temperatures. Sagi et al. synthesized self-immolative polyurethanes for drug delivery that were triggered to depolymerize at one end of the polymer chain using specific protein molecules [60]. Dilauro et al. reported ion-sensitive poly(phthalaldehyde) microcapsules that depolymerized and released desirable chemical payloads after contact with fluoride ions [71]. In these examples, the trigger-sensitive molecule grafted at the polymer chain end is cleaved using a stimulus followed by an unzipping reaction from the active site. Zhang et al. designed UV sensitive chain-shattering polymers for rapid depolymerization through a burst-release mechanism by simultaneously cleaving the trigger moieties present on every single monomer in the polymer backbone [69]. Baker et al. thermoformed poly(benzyl ether)s into different shapes that were depolymerized completely into small molecules for recycling purposes [65]. Most of these stimuli-responsive polymers require long and multistep polymer synthesis procedures, do not yield desirable mechanical properties for sacrificial templates, and need contact or dissolution in liquid media to facilitate the depolymerization reaction, making them unsuitable for VaSC applications due to various reasons discussed in the previous section.

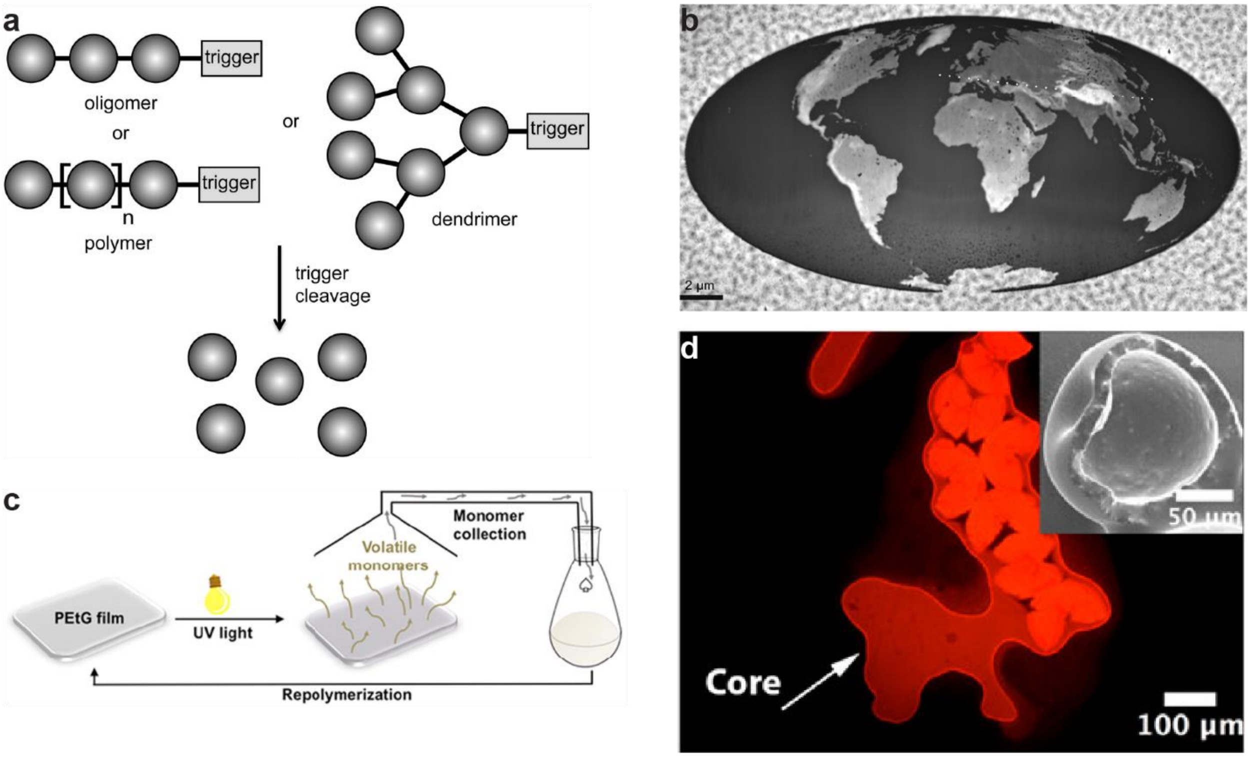

Figure 1.9. Sacrificial polymers developed for a range of applications. (a) Drug delivery through a cascade of reactions in self-immolative polycarbamates [72]. (b) Nanolithography via thermal depolymerization of linear poly(phthalaldehyde) [73]. (c) Recycling with photocontrolled depolymerization of poly(ethyl glyoxylate) [67]. (d) Payload release by acid triggered depolymerization of cPPA [74].

1.3.1 Promising sacrificial polymers

Solid-state depolymerization into volatile monomers under mild temperature conditions (ca. 100 °C) has been reported for only a few sacrificial polymer systems. Cyclic poly(phthalaldehyde) (cPPA) is a unique metastable ring polymer that is kinetically trapped to exist above its ceiling temperature of ca. -36 °C [75]. Rapid depolymerization of cPPA from a solid state into its monomeric building blocks is observed after the polymer ring is cleaved by thermal and acidic triggers[76]–[79]. Complete depolymerization of solvent processed cPPA has been reported for transient film substrates [78]–[80] and microcapsule payload release [74], but templating into fibers and printed structures for VaSC applications has not yet been achieved.

Poly(propylene carbonate) (PPC) is another sacrificial polymer that is heavily used for creating air gaps in microelectronic devices [25], [39], [52], [81], [82]. Thermal depolymerization of neat PPC occurs at relatively high temperatures (ca. 200 °C), but lower temperature depolymerization of solvent-cast PPC films (ca. 100-180 °C) has been demonstrated using acidic and basic triggers[83], [84].

1.3.2 Promising host matrices

Thermoset FRPCs require sustained external heating (several hours) to drive the matrix curing reaction. New strategies for faster curing at lower temperatures are desirable to reduce the thermal energy and time consumption for fabricating vascular composite structures. Alternative approaches for rapid crosslinking (within minutes) of the matrix such as snap-cure resins [85], heated molds [86], and frontal polymerization [87] have emerged as viable manufacturing routes for FRPCs compared to bulk curing. The first two strategies rely on external heating throughout the curing cycle, which scales with the part size. In contrast, frontal polymerization (FP) has emerged as an alternative strategy for transforming liquid monomers into functionally graded polymers and FRPCs [88]. Recently, Robertson et al. reported an energy-efficient FP of dicyclopentadiene (DCPD) and high-performance FRPCs [89]. During FP a localized heat trigger initiates a self-sustaining exothermic reaction wave that cures DCPD monomer into a solid poly(DCPD) matrix without any further energy input. Pot-life (minutes to hours) and the speed of curing of the resin during FP are highly influenced by the concentration of the catalyst and the choice and the concentration of inhibitor.

All of the released enthalpy during FP of DCPD is not required to sustain the reaction. Similar to the process of bone vascularization through coordinated material deposition and removal (discussed in **Section 1.1)**, synchronizing the resin curing process with triggered depolymerization of an embedded sacrificial template through the internal heat generated by the surrounding matrix presents itself as an interesting opportunity for reducing the overall energy footprint for fabricating vascular materials.

1.4 Goals

There are three main material and processing goals for manufacturing vascular structures (**Figure 1.10**) through less energy-intensive protocols with the promising sacrificial and host materials proposed in the previous section:

- Process sacrificial polymers into templates (fibers and printed architectures) that remain thermomechanically stable during integration into the host and compare the features of the resulting microchannels after depolymerization of the initial templates.
- Characterize the depolymerization of the templates before and after embedding into host matrices at significantly lower temperatures than VaSC with sacrificial PLA (< 150 °C). The trigger could be a combination of catalysts, light, and heat.
- Eliminate a sustained external heat source (e.g., an oven) for making vascular structures by utilizing the chemical enthalpy of the matrix to facilitate the curing and depolymerization reactions.

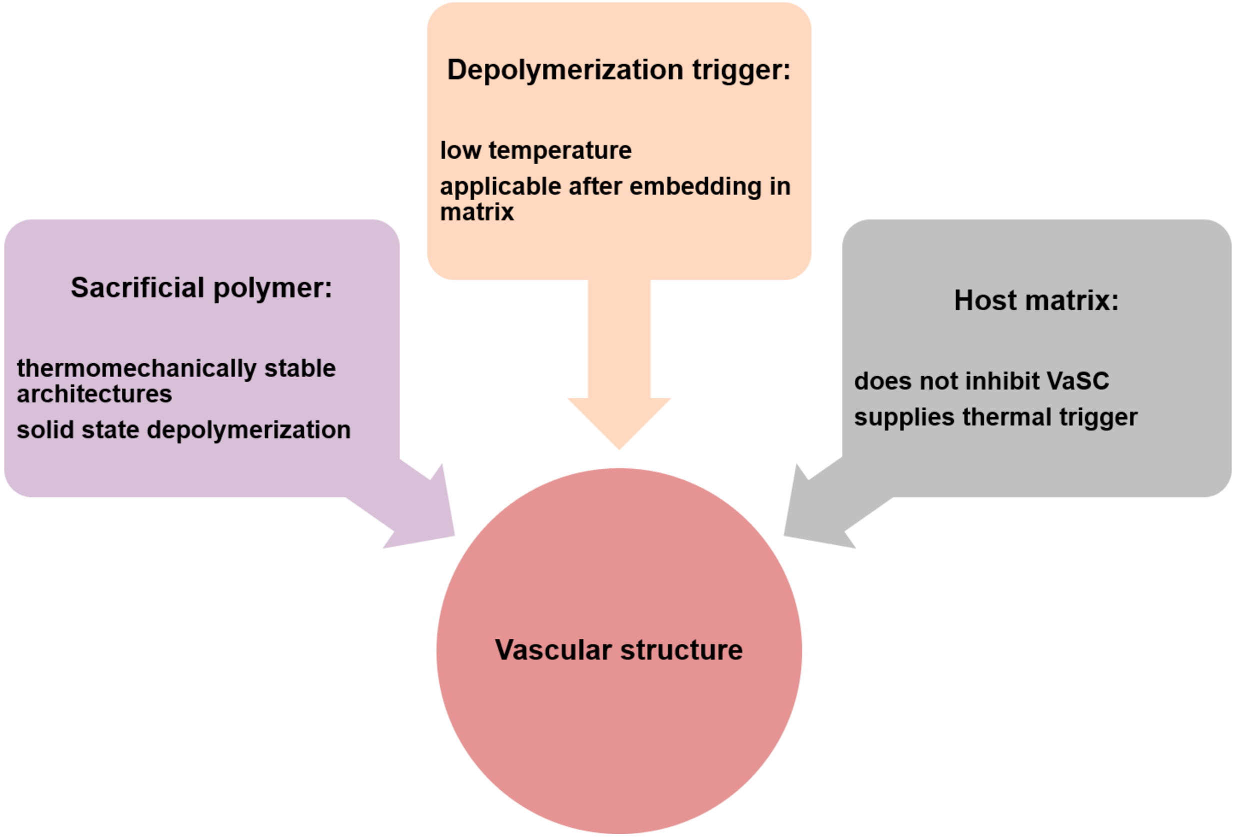

Figure 1.10. Material and process aspects for making a vascular structure: integration of the sacrificial polymer, evacuation of the templates using a depolymerization trigger to create high fidelity vascular networks, and compatibility of a host matrix that does not inhibit (or rather promotes) depolymerization of the sacrificial precursor.

1.5 Overview of dissertation

The primary objective of this dissertation is to develop a library of sacrificial polymers that thermally depolymerize rapidly at lower temperatures to enable more efficient manufacturing of vascular thermosets and FRPCs. Three different sacrificial polymers are investigated - PLA, cPPA, and PPC. The fidelity of the microchannels is evaluated using advanced microscopic techniques in different matrices, and a range of vascularization protocols are determined for each polymer system. The advantages and limitations along with the energy and time savings associated with each sacrificial system are discussed.

In Chapter 2, more efficient organometallic catalysts are investigated with the goal of lowering the VaSC temperature [58]. The effects of catalyst surface area, catalyst type, and catalyst loading on the depolymerization kinetics of sacrificial PLA films are analyzed. Successful vascularization protocols with reduced loadings of the more efficient catalyst at various temperatures are evaluated.

Chapter 3 describes the successful vascularization of several room-temperature-cured matrices through depolymerization of cPPA templates at much lower temperatures (ca 100 °C) than PLA. In Chapter 4, sacrificial PPC templates are investigated for vascularization in various host matrices at temperatures as low as 50 °C without compromising the energy savings compared to cPPA. A depolymerization kinetics model compares the activation energy for depolymerizing all the three sacrificial polymers and reveals key differences in the thermodynamic parameters that govern the rate of depolymerization at various temperatures.

Chapter 5 presents a one-step method for vascularization where polymerization of the matrix and the depolymerization of the sacrificial polymer are concurrently driven by the internal heat generation from the curing reaction of the host. Rapid vascularization (within minutes) of a frontally polymerizable resin under ambient conditions is achieved through the evacuation of both cPPA and PPC templates. Vascular FRPCs are manufactured within seconds at room temperature with this rapid process, saving fabrication energy by nearly four orders of magnitude and fabrication time by three orders of magnitude.

The conclusions of this dissertation and suggestions for future directions are summarized in Chapter 6.

1.6 References

[1] N. A. Campbell, J. B. Reece, M. R. Taylor, E. J. Simon, and J. L. Dickey, *Biology*. Benjamin Cummings, 2010.

[2] J.-Y. Rho, L. Kuhn-Spearing, and P. Zioupos, “Mechanical properties and the hierarchical structure of bone,” *Medical Engineering & Physics*, vol. 20, no. 2, pp. 92–102, Mar. 1998, doi: 10.1016/s1350-4533(98)00007-1.

[3] I. M. Daniel and O. Ishai, *Engineering Mechanics of Composite Materials*. New York: Oxford: Oxford University Press, 2006.

[4] P. Brøndsted, H. Lilholt, and A. Lystrup, “COMPOSITE MATERIALS FOR WIND POWER TURBINE BLADES,” *Annu Rev Mater Res*, vol. 35, no. 1, pp. 505–538, 2005, doi: 10.1146/annurev.matsci.35.100303.110641.

[5] K. Friedrich and A. A. Almajid, “Manufacturing Aspects of Advanced Polymer Composites for Automotive Applications,” *Appl Compos Mater*, vol. 20, no. 2, pp. 107–128, 2012, doi: 10.1007/s10443-012-9258-7.

[6] V. M. Karbhari and F. Seible, “Fiber Reinforced Composites – Advanced Materials for the Renewal of Civil Infrastructure,” *Appl Compos Mater*, vol. 7, no. 2/3, pp. 95–124, 2000, doi: 10.1023/a:1008915706226.

[7] C. J. Norris, I. P. Bond, and R. S. Trask, “The role of embedded bioinspired vasculature on damage formation in self-healing carbon fibre reinforced composites,” *Composites Part A*, vol. 42, no. 6, pp. 639–648, Jun. 2011, doi: 10.1016/j.compositesa.2011.02.003.

[8] C. Y. Huang, R. S. Trask, and I. P. Bond, “Characterization and analysis of carbon fibre-reinforced polymer composite laminates with embedded circular vasculature,” *Journal of The Royal Society Interface*, vol. 7, no. 49, pp. 1229–1241, Jun. 2010, doi: 10.1098/rsif.2009.0534.

[9] J. F. Patrick *et al.*, “Robust sacrificial polymer templates for 3D interconnected microvasculature in fiber-reinforced composites,” *Composites Part A: Applied Science and Manufacturing*, vol. 100, pp. 361–370, Sep. 2017, doi: 10.1016/j.compositesa.2017.05.022.

[10] J. F. Patrick *et al.*, “Continuous Self-Healing Life Cycle in Vascularized Structural Composites,” *Advanced Materials*, vol. 26, no. 25, pp. 4302–4308, Apr. 2014, doi: 10.1002/adma.201400248.

[11] S. J. Pety, P. X. L. Chia, S. M. Carrington, and S. R. White, “Active cooling of microvascular composites for battery packaging,” *Smart Mater Struct*, vol. 26, no. 10, p. 105004, 2017, doi: 10.1088/1361-665x/aa84e7.

[12] S. J. Pety, M. H. Y. Tan, A. R. Najafi, P. R. Barnett, P. H. Geubelle, and S. R. White, “Carbon fiber composites with 2D microvascular networks for battery cooling,” *International*

Journal of Heat and Mass Transfer, vol. 115, pp. 513–522, Dec. 2017, doi: 10.1016/j.ijheatmasstransfer.2017.07.047.

[13] A. M. Coppola, A. S. Griffin, N. R. Sottos, and S. R. White, “Retention of mechanical performance of polymer matrix composites above the glass transition temperature by vascular cooling,” *Composites Part A: Applied Science and Manufacturing*, vol. 78, pp. 412–423, Nov. 2015, doi: 10.1016/j.compositesa.2015.07.012.

[14] A. M. Coppola, L. G. Warpinski, S. P. Murray, N. R. Sottos, and S. R. White, “Survival of actively cooled microvascular polymer matrix composites under sustained thermomechanical loading,” *Compos Part Appl Sci Manuf*, vol. 82, pp. 170–179, 2016, doi: 10.1016/j.compositesa.2015.12.010.

[15] A. P. Esser-Kahn *et al.*, “Three-Dimensional Microvascular Fiber-Reinforced Composites,” *Advanced Materials*, vol. 23, no. 32, pp. 3654–3658, Jul. 2011, doi: 10.1002/adma.201100933.

[16] R. C. R. Gergely *et al.*, “Multidimensional Vascularized Polymers using Degradable Sacrificial Templates,” *Advanced Functional Materials*, vol. 25, no. 7, pp. 1043–1052, Dec. 2014, doi: 10.1002/adfm.201403670.

[17] E. Katifori, G. J. Szöllősi, and M. O. Magnasco, “Damage and Fluctuations Induce Loops in Optimal Transport Networks,” *Phys Rev Lett*, vol. 104, no. 4, p. 048704, 2010, doi: 10.1103/physrevlett.104.048704.

[18] D. M. Gates, “Transpiration and Leaf Temperature,” *Ann Rev Plant Physio*, vol. 19, no. 1, pp. 211–238, 1968, doi: 10.1146/annurev.pp.19.060168.001235.

[19] N. Little, B. Rogers, and M. Flannery, “Bone formation, remodelling and healing,” *Surg Oxf*, vol. 29, no. 4, pp. 141–145, 2011, doi: 10.1016/j.mpsur.2011.01.002.

[20] F. Härle and R. J. Boudrieau, “Oral and Maxillofacial Surgery in Dogs and Cats,” *Sect 1 Surg Biology*, pp. 7–13, 2012, doi: 10.1016/b978-0-7020-4618-6.00002-6.

[21] N. A. Sims and T. J. Martin, “Coupling the activities of bone formation and resorption: a multitude of signals within the basic multicellular unit.,” *Bonekey Reports*, vol. 3, p. 481, 2014, doi: 10.1038/bonekey.2013.215.

[22] A. Chamberlain and S. Forbes, “A preliminary study of microscopic evidence for lactation in cattle,” 2005, pp. 44–49.

[23] P. A. Kohl, “Air-Gaps for Electrical Interconnections,” *Electrochem Solid-state Lett*, vol. 1, no. 1, p. 49, 1999, doi: 10.1149/1.1390631.

[24] T. J. Spencer, P. J. Joseph, T. H. Kim, M. Swaminathan, and P. A. Kohl, “Air-Gap Transmission Lines on Organic Substrates for Low-Loss Interconnects,” *IEEE Transactions on*

Microwave Theory and Techniques, vol. 55, no. 9, pp. 1919–1925, 2007, doi: 10.1109/tmtt.2007.904326.

[25] R. Saha, N. Fritz, S. A. B. Allen, and P. A. Kohl, “Packaging-compatible wafer level capping of MEMS devices,” *Microelectronic Engineering*, vol. 104, pp. 75–84, Apr. 2013, doi: 10.1016/j.mee.2012.11.010.

[26] M. S. Bakir *et al.*, “Chip-to-Module Interconnections Using ‘Sea of Leads’ Technology,” *MRS Bulletin*, vol. 28, no. 1, pp. 61–67, Jan. 2003, doi: 10.1557/mrs2003.19.

[27] G. T. Ostrowicki, N. T. Fritz, R. I. Okereke, P. A. Kohl, and S. K. Sitaraman, “Domed and Released Thin-Film Construct—An Approach for Material Characterization and Compliant Interconnects,” *IEEE Transactions on Device and Materials Reliability*, vol. 12, no. 1, pp. 15–23, 2012, doi: 10.1109/tdmr.2011.2175927.

[28] J. S. Miller *et al.*, “Rapid casting of patterned vascular networks for perfusable engineered three-dimensional tissues,” *Nat Mater*, vol. 11, no. 9, pp. 768–774, 2012, doi: 10.1038/nmat3357.

[29] D. T. Nguyen, Y. T. Leho, and A. P. Esser-Kahn, “A three-dimensional microvascular gas exchange unit for carbon dioxide capture,” *Lab Chip*, vol. 12, no. 7, pp. 1246–1250, 2012, doi: 10.1039/c2lc00033d.

[30] J. A. Potkay, M. Magnetta, A. Vinson, and B. Cmolik, “Bio-inspired, efficient, artificial lung employing air as the ventilating gas,” *Lab Chip*, vol. 11, no. 17, p. 2901, 2011, doi: 10.1039/c1lc20020h.

[31] K. J. Maloney, K. D. Fink, T. A. Schaedler, J. A. Kolodziejska, A. J. Jacobsen, and C. S. Roper, “Multifunctional heat exchangers derived from three-dimensional micro-lattice structures,” *Int J Heat Mass Tran*, vol. 55, no. 9–10, pp. 2486–2493, 2012, doi: 10.1016/j.ijheatmasstransfer.2012.01.011.

[32] A. Z. Weber, M. M. Mench, J. P. Meyers, P. N. Ross, J. T. Gostick, and Q. Liu, “Redox flow batteries: a review,” *J Appl Electrochem*, vol. 41, no. 10, pp. 1137–1164, 2011, doi: 10.1007/s10800-011-0348-2.

[33] D. Cambié, F. Zhao, V. Hessel, M. G. Debije, and T. Noël, “A Leaf-Inspired Luminescent Solar Concentrator for Energy-Efficient Continuous-Flow Photochemistry,” *Angewandte Chemie Int Ed*, vol. 56, no. 4, pp. 1050–1054, 2016, doi: 10.1002/anie.201611101.

[34] D. Cambié *et al.*, “Energy-Efficient Solar Photochemistry with Luminescent Solar Concentrator Based Photomicroreactors,” *Angewandte Chemie Int Ed*, vol. 58, no. 40, pp. 14374–14378, 2019, doi: 10.1002/anie.201908553.

[35] S. R. White, J. S. Moore, N. R. Sottos, B. P. Krull, W. A. S. Cruz, and R. C. R. Gergely, "Restoration of Large Damage Volumes in Polymers," *Science*, vol. 344, no. 6184, pp. 620–623, 2014, doi: 10.1126/science.1251135.

[36] D. Lim, Y. Kamotani, B. Cho, J. Mazumder, and S. Takayama, "Fabrication of microfluidic mixers and artificial vasculatures using a high-brightness diode-pumped Nd:YAG laser direct write method.," *Lab on a chip*, vol. 3, no. 4, pp. 318–323, Nov. 2003, doi: 10.1039/b308452c.

[37] M. A. Unger, H.-P. Chou, T. Thorsen, A. Scherer, and S. R. Quake, "Monolithic Microfabricated Valves and Pumps by Multilayer Soft Lithography," *Science*, vol. 288, no. 5463, pp. 113–116, 2000, doi: 10.1126/science.288.5463.113.

[38] J.-H. Huang *et al.*, "Rapid Fabrication of Bio-inspired 3D Microfluidic Vascular Networks," *Advanced Materials*, vol. 21, no. 35, pp. 3567–3571, Sep. 2009, doi: 10.1002/adma.200900584.

[39] J. P. Jayachandran *et al.*, "Air-channel fabrication for microelectromechanical systems via sacrificial photosensitive polycarbonates," *Journal of Microelectromechanical Systems*, vol. 12, no. 2, pp. 147–159, Apr. 2003, doi: 10.1109/jmems.2003.809963.

[40] R. S. Trask and I. P. Bond, "Bioinspired engineering study of Plantae vascules for self-healing composite structures," *Journal of The Royal Society Interface*, vol. 7, no. 47, pp. 921–931, Apr. 2010, doi: 10.1098/rsif.2009.0420.

[41] K. S. Toohey, N. R. Sottos, J. A. Lewis, J. S. Moore, and S. R. White, "Self-healing materials with microvascular networks," *Nat Mater*, vol. 6, no. 8, pp. 581–585, Aug. 2007, doi: 10.1038/nmat1934.

[42] C. J. Hansen, W. Wu, K. S. Toohey, N. R. Sottos, S. R. White, and J. A. Lewis, "Self-Healing Materials with Interpenetrating Microvascular Networks," *Advanced Materials*, vol. 21, no. 41, pp. 4143–4147, Nov. 2009, doi: 10.1002/adma.200900588.

[43] L. M. Bellan, S. P. Singh, P. W. Henderson, T. J. Porri, H. G. Craighead, and J. A. Spector, "Fabrication of an artificial 3-dimensional vascular network using sacrificial sugar structures," *Soft Matter*, vol. 5, no. 7, pp. 1354–1357, 2009, doi: 10.1039/b819905a.

[44] D. Therriault, S. R. White, and J. A. Lewis, "Chaotic mixing in three-dimensional microvascular networks fabricated by direct-write assembly," *Nat Mater*, vol. 2, no. 4, pp. 265–271, 2003, doi: 10.1038/nmat863.

[45] C. J. Norris, I. P. Bond, and R. S. Trask, "Interactions between propagating cracks and bioinspired self-healing vascules embedded in glass fibre reinforced composites," *Composites Science and Technology*, vol. 71, no. 6, pp. 847–853, Apr. 2011, doi: 10.1016/j.compscitech.2011.01.027.

[46] B. Grigoryan *et al.*, “Multivascular networks and functional intravascular topologies within biocompatible hydrogels,” *Science*, vol. 364, no. 6439, pp. 458–464, 2019, doi: 10.1126/science.aav9750.

[47] B. J. Blaiszik, S. L. B. Kramer, S. C. Olugebefola, J. S. Moore, N. R. Sottos, and S. R. White, “Self-Healing Polymers and Composites,” *Annual Review of Materials Research*, vol. 40, no. 1, pp. 179–211, Jun. 2010, doi: 10.1146/annurev-matsci-070909-104532.

[48] A. R. Hamilton, N. R. Sottos, and S. R. White, “Self-Healing of Internal Damage in Synthetic Vascular Materials,” *Adv Mater*, vol. 22, no. 45, pp. 5159–5163, 2010, doi: 10.1002/adma.201002561.

[49] C. J. Norris, J. A. P. White, G. McCombe, P. Chatterjee, I. P. Bond, and R. S. Trask, “Autonomous stimulus triggered self-healing in smart structural composites,” *Smart Materials and Structures*, vol. 21, no. 9, p. 094027, Sep. 2012, doi: 10.1088/0964-1726/21/9/094027.

[50] C. J. Norris, I. P. Bond, and R. S. Trask, “Healing of low-velocity impact damage in vascularised composites,” *Composites Part A: Applied Science and Manufacturing*, vol. 44, pp. 78–85, Jan. 2013, doi: 10.1016/j.compositesa.2012.08.022.

[51] I. P. S. Qamar, N. R. Sottos, and R. S. Trask, “Grand challenges in the design and manufacture of vascular self-healing,” *Multifunct Mater*, vol. 3, no. 1, p. 013001, 2020, doi: 10.1088/2399-7532/ab69e2.

[52] E. Uzunlar and P. A. Kohl, “Size-Compatible, Polymer-Based Air-Gap Formation Processes, and Polymer Residue Analysis for Wafer-Level MEMS Packaging Applications,” *Journal of Electronic Packaging*, vol. 137, no. 4, pp. 041001–13, Dec. 2015, doi: 10.1115/1.4030952.

[53] E. Uzunlar, J. Schwartz, O. Phillips, and P. A. Kohl, “Decomposable and Template Polymers: Fundamentals and Applications,” *Journal of Electronic Packaging*, vol. 138, no. 2, pp. 020802–15, Jun. 2016, doi: 10.1115/1.4033000.

[54] H. Dong *et al.*, “Chemical Treatment of Poly(lactic acid) Fibers to Enhance the Rate of Thermal Depolymerization,” *ACS Applied Materials & Interfaces*, vol. 4, no. 2, pp. 503–509, Feb. 2012, doi: 10.1021/am2010042.

[55] K. R. Hart *et al.*, “Repeated healing of delamination damage in vascular composites by pressurized delivery of reactive agents,” *Composites Science and Technology*, vol. 151, pp. 1–9, Oct. 2017, doi: 10.1016/j.compscitech.2017.07.027.

[56] A. J. Timmis *et al.*, “Environmental impact assessment of aviation emission reduction through the implementation of composite materials,” *Int J Life Cycle Assess*, vol. 20, no. 2, pp. 233–243, 2014, doi: 10.1007/s11367-014-0824-0.

[57] H. Dong, “Synthetic Vascular Materials via a Vaporization of Sacrificial Component Approach,” 2013.

[58] M. Garg, S. R. White, and N. R. Sottos, “Rapid Degradation of Poly(lactic acid) with Organometallic Catalysts,” *Acs Appl Mater Inter*, vol. 11, no. 49, pp. 46226–46232, 2019, doi: 10.1021/acsami.9b17599.

[59] G. I. Peterson, M. B. Larsen, and A. J. Boydston, “Controlled Depolymerization: Stimuli-Responsive Self-Immolative Polymers,” vol. 45, no. 18, pp. 7317–7328, Sep. 2012, doi: 10.1021/ma300817v.

[60] A. Sagi, R. Weinstain, N. Karton, and D. Shabat, “Self-Immolative Polymers,” *Journal of the American Chemical Society*, vol. 130, no. 16, pp. 5434–5435, Apr. 2008, doi: 10.1021/ja801065d.

[61] M. E. Roth, O. Green, S. Gnaim, and D. Shabat, “Dendritic, Oligomeric, and Polymeric Self-Immolative Molecular Amplification,” *Chemical Reviews*, vol. 116, no. 3, pp. 1309–1352, Jan. 2016, doi: 10.1021/acs.chemrev.5b00372.

[62] A. D. Wong, M. A. DeWit, and E. R. Gillies, “Amplified release through the stimulus triggered degradation of self-immolative oligomers, dendrimers, and linear polymers,” *Advanced Drug Delivery Reviews*, vol. 64, no. 11, pp. 1031–1045, Aug. 2012, doi: 10.1016/j.addr.2011.09.012.

[63] H. Wu, T. W. Odom, D. T. Chiu, and G. M. Whitesides, “Fabrication of complex three-dimensional microchannel systems in PDMS.,” *Journal of the American Chemical Society*, vol. 125, no. 2, pp. 554–559, Jan. 2003, doi: 10.1021/ja021045y.

[64] C. K. Harnett, G. W. Coates, and H. G. Craighead, “Heat-depolymerizable polycarbonates as electron beam patternable sacrificial layers for nanofluidics,” *... Science & Technology B: ...*, vol. 19, no. 6, p. 2842, 2001, doi: 10.1116/1.1409383.

[65] M. S. Baker, H. Kim, M. G. Olah, G. G. Lewis, and S. T. Phillips, “Depolymerizable poly(benzyl ether)-based materials for selective room temperature recycling,” *Green Chemistry*, vol. 17, no. 9, pp. 4541–4545, 2015, doi: 10.1039/c5gc01090j.

[66] J.-B. Zhu, E. M. Watson, J. Tang, and E. Y. X. Chen, “A synthetic polymer system with repeatable chemical recyclability,” *Science*, vol. 360, no. 6387, pp. 398–403, Apr. 2018, doi: 10.1126/science.aar5498.

[67] B. Fan, J. F. Trant, R. E. Yardley, A. J. Pickering, F. Lagugné-Labarthet, and E. R. Gillies, “Photocontrolled Degradation of Stimuli-Responsive Poly(ethyl glyoxylate): Differentiating Features and Traceless Ambient Depolymerization,” *Macromolecules*, vol. 49, no. 19, pp. 7196–7203, Sep. 2016, doi: 10.1021/acs.macromol.6b01620.

[68] Y. Liu, H. Zhou, J.-Z. Guo, W.-M. Ren, and X.-B. Lu, “Completely Recyclable Monomers and Polycarbonate: Approach to Sustainable Polymers.,” *Angewandte Chemie (International ed. in English)*, vol. 56, no. 17, pp. 4862–4866, Apr. 2017, doi: 10.1002/anie.201701438.

[69] Y. Zhang, L. Ma, X. Deng, and J. Cheng, “Trigger-responsive chain-shattering polymers,” *Polymer Chemistry*, vol. 4, no. 2, pp. 224–228, 2013, doi: 10.1039/c2py20838e.

[70] A. P. Esser-Kahn, S. A. Odom, N. R. Sottos, S. R. White, and J. S. Moore, “Triggered Release from Polymer Capsules,” *Macromolecules*, vol. 44, no. 14, pp. 5539–5553, 2011, doi: 10.1021/ma201014n.

[71] A. M. Dilauro, A. Abbaspourrad, D. A. Weitz, and S. T. Phillips, “Stimuli-Responsive Core–Shell Microcapsules with Tunable Rates of Release by Using a Depolymerizable Poly(phthalaldehyde) Membrane,” *Macromolecules*, vol. 46, no. 9, pp. 3309–3313, May 2013, doi: 10.1021/ma400456p.

[72] R. J. Amir, N. Pessah, M. Shamis, and D. Shabat, “Self-Immolative Dendrimers,” *Angewandte Chemie Int Ed*, vol. 42, no. 37, pp. 4494–4499, 2003, doi: 10.1002/anie.200351962.

[73] A. W. Knoll *et al.*, “Probe-based 3-D nanolithography using self-amplified depolymerization polymers.,” *Advanced Materials*, vol. 22, no. 31, pp. 3361–3365, Aug. 2010, doi: 10.1002/adma.200904386.

[74] S. Tang, M. Yourdkhani, C. M. P. Casey, N. R. Sottos, S. R. White, and J. S. Moore, “Low-Ceiling-Temperature Polymer Microcapsules with Hydrophobic Payloads via Rapid Emulsion-Solvent Evaporation.,” *ACS Applied Materials & Interfaces*, vol. 9, no. 23, pp. 20115–20123, Jun. 2017, doi: 10.1021/acsami.7b05266.

[75] J. P. Lutz, O. Davydovich, M. D. Hannigan, J. S. Moore, P. M. Zimmerman, and A. J. McNeil, “Functionalized and Degradable Polyphthalaldehyde Derivatives,” *J Am Chem Soc*, vol. 141, no. 37, pp. 14544–14548, 2019, doi: 10.1021/jacs.9b07508.

[76] H. L. Hernandez *et al.*, “Accelerated Thermal Depolymerization of Cyclic Polyphthalaldehyde with a Polymeric Thermoacid Generator,” *Macromol Rapid Comm*, vol. 39, no. 11, p. 1800046, 2018, doi: 10.1002/marc.201800046.

[77] J. A. Kaitz, C. E. Diesendruck, and J. S. Moore, “End group characterization of poly(phthalaldehyde): surprising discovery of a reversible, cationic macrocyclization mechanism.,” *Journal of the American Chemical Society*, vol. 135, no. 34, pp. 12755–12761, Aug. 2013, doi: 10.1021/ja405628g.

[78] C. W. Park *et al.*, “Thermally triggered degradation of transient electronic devices.,” *Advanced Materials*, vol. 27, no. 25, pp. 3783–3788, Jul. 2015, doi: 10.1002/adma.201501180.

[79] H. L. Hernandez *et al.*, “Triggered Transience of Metastable Poly(phthalaldehyde) for Transient Electronics,” *Advanced Materials*, vol. 26, no. 45, pp. 7637–7642, Oct. 2014, doi: 10.1002/adma.201403045.

[80] O. P. Lee, H. L. Hernandez, and J. S. Moore, “Tunable Thermal Degradation of Poly(vinyl butyl carbonate sulfone)s via Side-Chain Branching,” *Acs Macro Lett*, vol. 4, no. 7, pp. 665–668, 2015, doi: 10.1021/acsmacrolett.5b00234.

[81] P. J. Joseph, P. Monajemi, F. Ayazi, and P. A. Kohl, “Wafer-Level Packaging of Micromechanical Resonators,” *IEEE Transactions on Advanced Packaging*, vol. 30, no. 1, pp. 19–26, 2007, doi: 10.1109/tadvp.2006.890220.

[82] H. A. Reed, C. E. White, V. Rao, S. A. B. Allen, C. L. Henderson, and P. A. Kohl, “Fabrication of microchannels using polycarbonates as sacrificial materials,” *Journal of …*, vol. 11, no. 6, pp. 733–737, Oct. 2001, doi: 10.1088/0960-1317/11/6/317.

[83] M. G. Cupta, P. J. Joseph, and P. A. Kohl, “Photoacid generators for catalytic decomposition of polycarbonate,” *Journal of Applied Polymer Science*, vol. 105, no. 5, pp. 2655–2662, 2007, doi: 10.1002/app.26343.

[84] O. Phillips, J. M. Schwartz, and P. A. Kohl, “Thermal decomposition of poly(propylene carbonate): End-capping, additives, and solvent effects,” *Polymer Degradation and Stability*, vol. 125, pp. 129–139, Mar. 2016, doi: 10.1016/j.polymdegradstab.2016.01.004.

[85] A. Cherniaev, Y. Zeng, D. Cronin, and J. Montesano, “Quasi-static and dynamic characterization of unidirectional non-crimp carbon fiber fabric composites processed by HP-RTM,” *Polym Test*, vol. 76, pp. 365–375, 2019, doi: 10.1016/j.polymertesting.2019.03.036.

[86] M. D. Silcock, C. Garschke, W. Hall, and B. L. Fox, “Rapid Composite Tube Manufacture Utilizing the QuickstepTM Process,” *J Compos Mater*, vol. 41, no. 8, pp. 965–978, 2007, doi: 10.1177/0021998306067261.

[87] J. A. Pojman, “Frontal Polymerization,” vol. 89, Wiley-VCH Verlag GmbH & Co. KGaA, 2010, pp. 45–67.

[88] J. A. Pojman, “Polymer Science: A Comprehensive Reference,” vol. 4, K. Matyjaszewski and M. Möller, Eds. Elsevier B.V., 2012, pp. 957–980.

[89] I. D. Robertson *et al.*, “Rapid energy-efficient manufacturing of polymers and composites via frontal polymerization,” *Nature*, vol. 557, no. 7704, pp. 223–227, May 2018, doi: 10.1038/s41586-018-0054-x.

CHAPTER 2

RAPID DEPOLYMERIZATION OF POLY(LACTIC ACID) WITH ORGANOMETALLIC CATALYSTS*

2.1 Introduction

Biological systems contain hierarchical vascular networks to mediate nutrient and fluid transport for repair, thermal regulation, and waste removal [1]. Incorporation of microchannels in synthetic matrices enables heat and mass transport in microfluidics [2]–[8], microelectronics [9]–[12], CO_2 sequestration [13], [14], flow batteries [15], heat exchangers [16], and environmentally adaptive structures [17]–[29]. Several subtractive (material removal) strategies have been adopted to create such microvascular structures including laser ablation [4], dissolution [2], [3], lithography [7], [8], [13], electrostatic discharge [30], melting [23], [31], [32], and template vaporization [9], [17], [20], [24], [25], [33]. Thermal vaporization of sacrificial polymer templates is a reliable strategy for fabricating vascular networks to promote electrical insulation and liquid cooling in microelectronics [34]–[38], and to enable self-healing [24]–[27], [39] and self-cooling [18], [33], [40] in thermoset polymers and composites. Poly(lactic acid) (PLA) is one such sacrificial polymer, with a huge market share in biomedical, food packaging, and other environmental applications due to biodegradability and ease of processing [41]. Esser-Kahn et al. [24] embedded PLA templates in fiber-reinforced composites to form vascular networks through the vaporization of sacrificial components (VaSC) technique. Sacrificial PLA templates treated with tin (II) oxalate (Sn(Oxa)) catalyst were embedded into a host thermoset matrix, and subsequent thermal treatment

---

*Sections of this chapter were published in [53] at elevated temperatures led to sublimation of the templates and formation of vascular networks [42]. This protocol for removal of catalyst-infused sacrificial PLA involved exposure to elevated temperatures (≈ 200 °C) in a vacuum oven for a long time (≈ 12 h). These conditions made this process energy-intensive and limited to high-temperature resistant host matrices while also resulting in significant discoloration due to oxidation of the matrix. A more efficient catalyst is needed to depolymerize the PLA more quickly and at lower temperatures to reduce the energy footprint of VaSC and prevent the degradation/deformation of host matrices that cannot sustain this high-temperature processing step.

Thermal depolymerization of PLA assisted by various catalysts has been pursued extensively for recycling purposes because the depolymerization onset temperature of neat PLA is relatively high (around 280 °C) [43]. Several metal-based catalysts including Al, Ti, Zn, Fe, Zr, Ca, and Mg, depolymerize PLA at lower temperatures [44]–[46]. Most reports on the influence of residual impurities on the thermal stability of PLA involve tin (II) 2-ethylhexanoate/tin octoate ($Sn(Oct)_2$) catalyst since it is highly efficient in transesterification reactions involving PLA polymerization [44], [45], [47]. Dong et al. [42] screened several Sn-based catalysts and reported that Sn(Oxa) and $Sn(Ac)_2$ were equally efficient catalysts for facilitating the depolymerization of sacrificial PLA (**Scheme 2.1**).

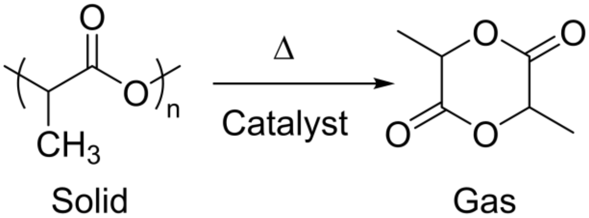

Scheme 2.1 Thermal depolymerization reaction of PLA facilitated by a metal catalyst.

The particle size/surface area of the catalysts in these screening procedures was either not reported [42] or inconsistent [44], despite the well-established understanding that changing the specific surface area (SSA) of a catalyst influences its activity. Nishida et al. [47] had concluded that several random depolymerization pathways involving transesterification reactions initiated the depolymerization of PLA containing Sn. This initiation was followed by zeroth-order kinetics suggesting that the heterogeneous surface of the Sn catalyst facilitates the PLA depolymerization and finally results in gaseous lactide monomers.

In this chapter, we investigate the relationship between catalyst SSA and PLA depolymerization performance. The catalytic activity of two organotin compounds for lowering PLA depolymerization temperature is compared in TGA experiments and modeling of the depolymerization kinetics. We report rapid depolymerization of PLA at lower temperatures and reduced catalyst loading compared to currently used protocols for Sn(Oxa)-enabled VaSC.

2.2 Materials and methods

2.2.1 Materials

PLA pellets (4043D, $M_\mathrm{w} \approx 150$ kDa) were obtained from Natureworks LLC. Tin oxalate (Sn(Oxa)) and tin acetate ($Sn(Ac)_2$) catalysts were procured from Sigma-Aldrich. All solvents including concentrated hydrochloric acid (HCl) (37%), dichloromethane (DCM), deionized water, and acetone were used as received from Sigma-Aldrich unless otherwise noted. Epoxy resin (Araldite LY 8605) and amine hardener (Aradur 8605) components were obtained from Huntsman Advanced Materials LLC and mixed using a mass ratio of 35 parts per hundred (pph) hardener to resin for making solid epoxy samples (hereon deemed epoxy 8605).

2.2.2 Catalyst processing and characterization

We dissolved 2 g Sn(Oxa) (as received) in 10 ml concentrated HCl for 20 min to create recrystallized Sn(Oxa) particles. The solution was diluted to 1 M HCl using DI water, and the mixture was centrifuged in 45 ml centrifuge tubes at 500 rpm for 5 min immediately after crystal formation was observed. The sediment was diluted with DI water and centrifuged again. The process was repeated three times to remove any residual HCl. The crystals formed were dried under vacuum at RT for 24 h. We mechanically sieved (U.S. Std. No. 500) Sn(Oxa) particles (< 25 μm), which were subsequently rotary ground using a high-speed rotary mixer (Col-Int Tech, FW-100) for 1 min to obtain particles of smaller size. A 5 g amount of rotary ground catalyst was dispersed in DCM in a 1000 ml glass beaker and sonicated for 10 min. The beaker was left undisturbed for larger particles to sediment. The supernatant was collected from the top 4 cm of the beaker after 4 h based on an approximation of Stokes's law [48] with the assumption that particles greater than one micron would have sunk below during that time. Subsequently, the supernatant was centrifuged at 5000 rpm for five minutes in 45 ml centrifuge tubes to collect the small particles. Sn(Oxa) (centrifuged) particles were dried at RT under vacuum for 24 h to remove any residual solvent before further use. $Sn(Ac)_2$ particles were used as received from the manufacturer and specific surface area (SSA) of all three samples were measured.

Scanning electron micrographs (SEM) were acquired on a Philips XL30 ESEM-FEG 450. Catalyst particles and epoxy 8605 samples containing microchannels were imaged at 15 kV and 20 kV respectively after sputter-coating the samples with gold/palladium for 70 s using a Denton Desk II TSC-turbo pumped unit. Energy-dispersive X-ray spectroscopy (EDS) was performed on the microchannels inside epoxy 8605 samples using an AMETEK® EDAX Octane Plus detector with a 20 kV electron source. The energy spectra were analyzed using the TEAM™ software (version 4.5.1). National Institute of Health's (NIH) Image J software was used for digital measurements on SEM micrographs of catalyst particles.

Raman spectra of the catalyst particles were acquired on a Horiba LabRAM HR 3D Raman Confocal Imaging Microscope with a 785 nm laser. Centrifugation of catalyst particle suspensions was performed on a Thermo Electron Corp IEC Multi Centrifuge.

The specific surface area (SSA) of catalyst particle samples (ca. 1 g) was calculated based on the multipoint Brunauer-Emmet-Teller (BET) method after measuring nitrogen adsorption isotherms at -196 °C in a Nova 2200e surface area and pore analyzer. (Quantachrome Instruments, Boynton Beach, FL). The SSA of Sn(Oxa) (recrystallized) particles was below the lower detectable limit of the instrument, so SEM images were analyzed to estimate the SSA using the following equation:

$$SSA = \frac{2(lb + bh + hl)}{\rho * lbh} \tag{2.1}$$

where, l is the length of the catalyst particle, b is the breadth of the catalyst particle, h is the height of the catalyst particle, and ρ is the density of catalyst particle (ρ (Sn(Oxa)) = 3.56 g/cm^3). The height of the particles was assumed to be equal to the breadth while calculating the surface area per particle.

Differential scanning calorimetry (DSC) was performed on a TA instruments Discovery DSC 250. For each experiment, a 3 mg catalyst sample measured using an analytical balance (XPE205, Mettler-Toledo) was transferred into aluminum hermetic DSC pans at room temperature and sealed. The heat flow for each catalyst sample was obtained under a constant ramp rate of 5 °C/min up to 240 °C.

2.2.3 Solvent casting and characterization of sacrificial films

A 1 g amount of PLA was dissolved in 4 ml DCM in a scintillation vial for 1 h at room temperature. Catalyst particles (3 wt. % of PLA) were sonicated in 1 ml DCM in another vial for 2 min. The catalyst-DCM mixture was added to the PLA-DCM mixture slowly and vortexed for 1 h to ensure good dispersion of catalyst. The mixture was poured into a 50 mm diameter Teflon lined Petri dish and dried in a fume hood for 24 h at RT to obtain films with thickness ≈ 300 µm. The films were subsequently dried under vacuum at 60 °C overnight to remove residual DCM. Subsequently, films with reduced wt. % of $Sn(Ac)_2$ catalyst were also made with the same procedure. All wt. % are w.r.t. PLA unless specified. Films were cut into small pieces for TGA and GPC experiments.

Analytical Gel Permeation Chromatography (GPC) analyses were performed on a system composed of a Waters (1515) Isocratic high-pressure liquid chromatography pump, a Waters (2414) Refractive Index Detector, a Waters (2707) 96-well autosampler, and a series of 4 Waters HR Styragel columns (7.8 x 300 mm, HR1, HR3, HR4 and HR5) in tetrahydrofuran (THF) at 30 °C. The GPC was calibrated using monodisperse polystyrene standards.

Thermogravimetric analysis (TGA) was performed on a TA instruments TGA Q500 in a nitrogen atmosphere, calibrated with nickel standards. For each experiment, the sample (ca. 10 mg) was weighed (± 0.001 mg) in a platinum crucible. For dynamic measurements, the mass loss was recorded during a heating cycle over the temperature range of 40 to 350 °C at a heating rate of 5 °C min^{-1}. For isothermal experiments, the temperature was ramped from 40 °C to the desired temperature at a rate of 10 °C min^{-1} and subsequently held at that temperature for 12 hours.

2.2.4 Cell casting and vascularization in epoxy matrix

Sacrificial films were cut into 18 mm long and 2 mm wide templates and embedded in an epoxy 8605 matrix using a cell-casting procedure (**Scheme 2.2**). First, the resin-hardener mixture was degassed at room temperature under 12 Torr vacuum for 45 min (Yamato ADP31 drying oven, Welch 1402 pump). The sacrificial films were then clamped between 2 silicone rubber gaskets (each 2 mm thick) attached to two rectangular glass plates coated with a PTFE release agent (MS-122AD, Miller-Stephenson). The epoxy mixture was carefully poured into the glass mold to cover the sacrificial films completely and cured for 24 h at RT followed by 8 h at 121 °C. Solid samples were then removed from the mold and cut using a Buehler Isomet saw into 16 mm x 8 mm x 4 mm samples, each containing a sacrificial film template embedded along the specimen length with transverse ends exposed to the surroundings.

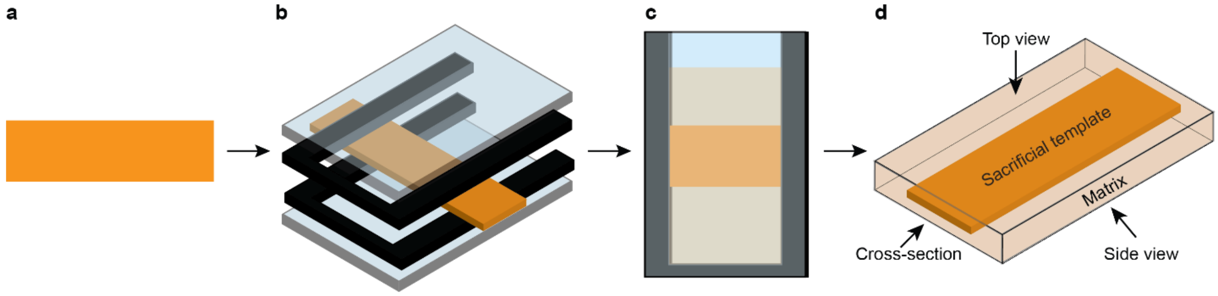

Scheme 2.2. Cell casting sacrificial templates in the thermoset matrix for vascularization experiments. (a) PLA film (orange). (b) Exploded isometric view of a film clamped by two rubber spacers (black) sandwiched between two glass plates (translucent blue). (c) Liquid resin (translucent brown) is poured in the cell casting mold to encapsulate the film. (d) The cured specimen is cut into shape with the transverse ends of the template exposed to the surrounding environment for VaSC experiments.

The mass of each sample was measured using a Mettler Toledo XPE 205 balance (±0.03 mg) before placing them in an evacuation oven (Jeio Tech Co. Ltd., OV-11). The temperature of the oven was increased from RT to the desired temperature under vacuum (≈ 0.5 Torr) and the isothermal temperature was held for a certain number of hours for vaporization of sacrificial components (VaSC) experiments before removing the specimens from the oven. The mass of the evacuated epoxy samples was measured again to calculate the mass loss of the specimens after VaSC. The evacuated microchannels were flushed with water to confirm if the channels were clear. These specimens were freeze-fractured before taking SEM micrographs and EDS spectra of the microchannels. These samples were then polished using a glycol-based polycrystalline diamond suspension on an Allied MetPrep 3™ with PH-4™ Power Head Grinder/Polisher (Allied High Tech Products Inclusive). Optical images of the cross-sections of the epoxy 8605 samples were obtained on a Keyence VHX-5000 digital microscope at 100x magnification.

2.3 Results and discussion

2.3.1 Effect of catalyst surface area on PLA depolymerization

Sn(Oxa) (as received) consisted of irregularly shaped particles, 1-100 µm in length (**Figure 2.1a**). Different mechanical grinding and recrystallization procedures were followed to obtain particles with significantly different surface areas. Sieving (**Figure 2.1b**) and subsequent rotary grinding (**Figure 2.1c**) resulted in particles smaller than Sn(Oxa) (as received), but larger particles were still present due to inhomogeneity in the grinding process. The rotary ground catalyst was then dispersed in DCM followed by centrifugation to isolate particles 1-3 µm in size (**Figure 2.1d**). The recrystallization procedure involving dissolution in concentrated HCl yielded relatively large particles in the 25-50 µm range (**Figure 2.1e**). No change in chemical composition was measured after the recrystallization process (**Figure 2.2**). Measured specific surface area (SSA) values of Sn(Oxa) (recrystallized) and Sn(Oxa) (centrifuged) particles are shown in **Table 2.1**. The SSA of Sn(Oxa) (centrifuged) particles was approximately 20 times higher than that of Sn(Oxa) (recrystallized) particles. The SSA of Sn(Oxa) (recrystallized) particles was below the lower detectable limit of the instrument, so SEM images were analyzed to estimate the SSA (**Table 2.2**).

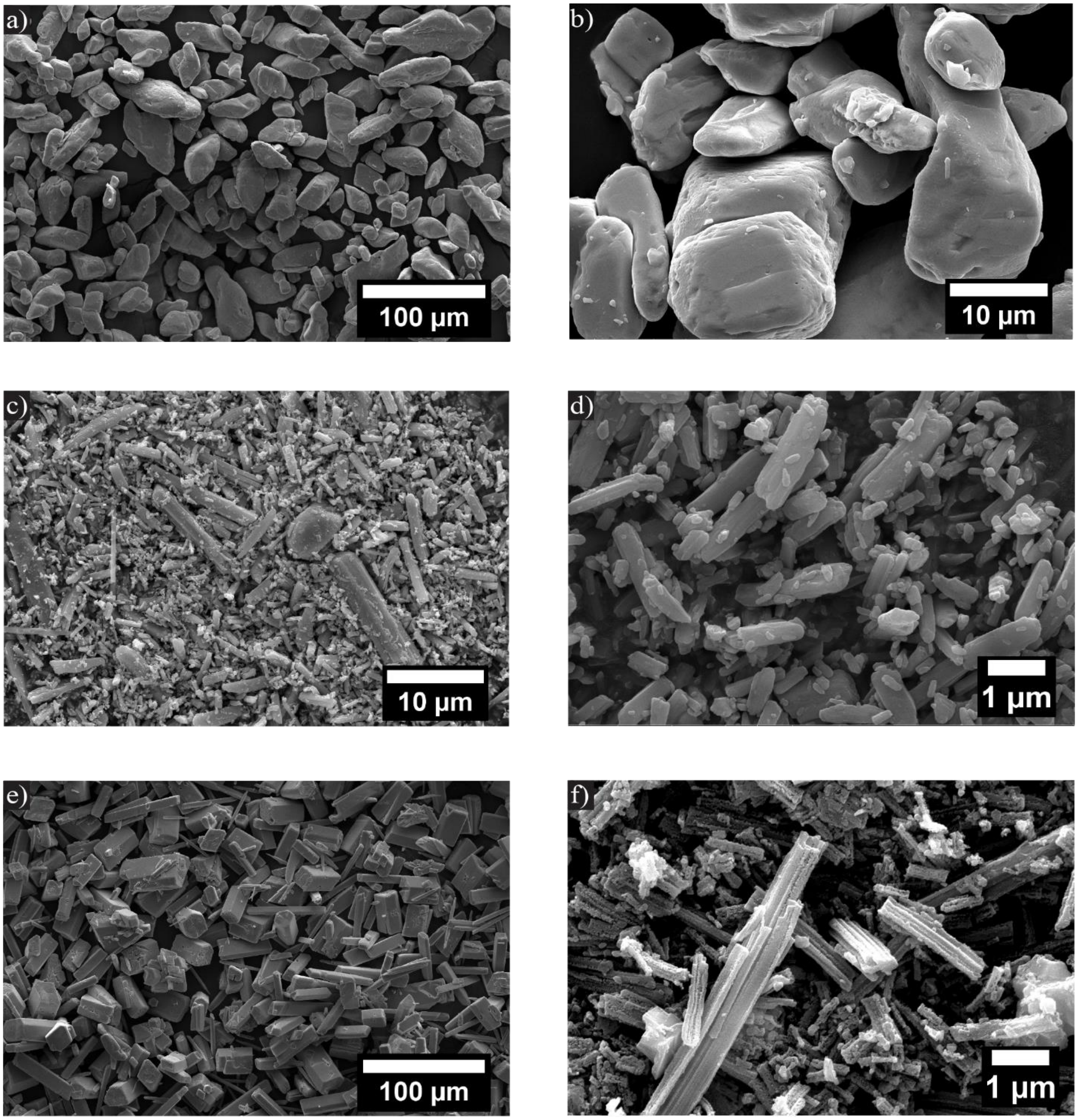

Figure 2.1. SEM micrographs of Sn(Oxa) and Sn(Ac)$_2$ catalysts at different stages of processing: (a) Sn(Oxa) (as received). (b) Sn(Oxa) (Sieved < 25 μm). (c) Sn(Oxa) (rotary ground). (d) Sn(Oxa) (centrifuged). (e) Sn(Oxa) (recrystallized). (f) Sn(Ac)$_2$ (as received).

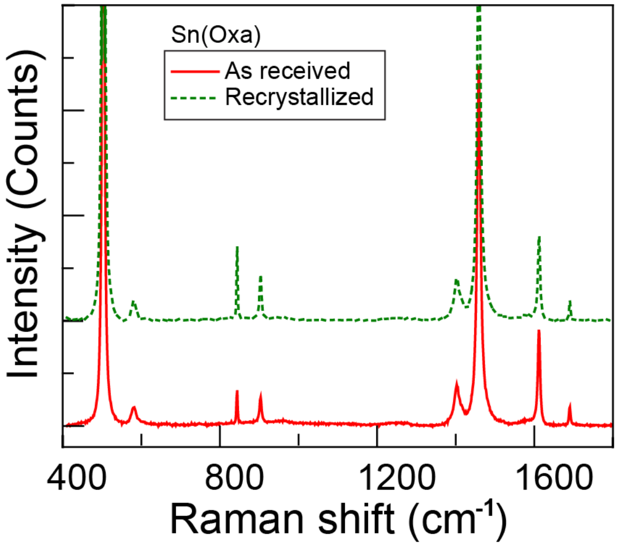

Figure 2.2. Raman spectra of as received (Fig 1.1a) and recrystallized (Fig 1.1e) Sn(Oxa) catalyst samples. Strong peaks at 1463 and 508 cm^{-1} represent carbon-oxygen and tin-oxygen bond interactions, respectively. Weak peaks at 908 and 847 cm^{-1} represent carbon-carbon interactions [49]. The spectra confirmed that no change in chemical composition occurred after the recrystallization process.

Table 2.1. Specific Surface Area (SSA) for different catalyst samples (from **Figure 2.1d-f**).

Catalyst	**Mean SSA (m^2/g)**
Sn(Oxa) (recrystallized)[1]	0.098 ± 0.04
Sn(Oxa) (centrifuged)[2]	2.1 ± 0.2
$Sn(Ac)_2$ (as received)[2]	5.0 ± 0.5

[1] Particle dimensions were measured using ImageJ software to obtain the estimated SSA (**Table 2.2**). The error represents 1 standard deviation from 100 measurements.

[2] SSA was measured using a BET instrument. The error represents 1 standard deviation from 3 samples.

Table 2.2. Mean particle dimensions (100 measurements each) and estimated SSA for Sn(Oxa) (recrystallized) particle samples using ImageJ software.

Catalyst	**Length (μm)**	**Breadth (μm)**	**Mean SSA (m^2/g)**
Sn(Oxa) (recrystallized)	34.6	13.7	0.09

Both types of Sn(Oxa) catalyst particles were blended with PLA at 3 wt. % concentration (w.r.t. PLA) and formed into films for subsequent depolymerization experiments. Reduction in the molecular weight of the starting polymer was not observed after film casting (**Table 2.3**). The depolymerization onset temperature (T_d) of films was measured at 5 % weight loss in dynamic TGA experiments and summarized in **Figure 2.3a**. The T_d for films with Sn(Oxa) (centrifuged) was 245 °C, which is 37 °C lower than films with Sn(Oxa) (recrystallized). The residual weight % after depolymerization for both samples was roughly equivalent to the initial catalyst concentration, implying no residual polymer byproducts remained. In isothermal TGA experiments at 200 °C, films with Sn(Oxa) (centrifuged) depolymerized completely into volatile products in less than 8 h (**Figure 2.3b**). In contrast, films with Sn(Oxa) (recrystallized) showed only 23 % weight loss after 12 h. This significant change in the PLA depolymerization kinetics is attributed to the total surface area of the catalyst in the vicinity of the polymer chains. The depolymerization time of PLA films with Sn(Oxa) (centrifuged) drastically increased as the dwell temperature in the isothermal TGA experiments was decreased below 200 °C (**Figure 2.4a**).

Table 2.3. Gel permeation chromatography (GPC) of PLA samples before and after solvent casting using DCM. Triple detection (using the refractive index, light scattering, and viscometer detectors) was used to obtain the weight average molecular weights. No significant reduction in average molecular weight was observed.

PLA Sample	**M_w (kDa)**	**PDI**
Neat 4043D pellet	149 ± 8 %	1.4
Neat 4043D film	157 ± 8 %	1.4
PLA/Sn(Oxa) (Centrifuged) film	162 ± 8 %	1.3

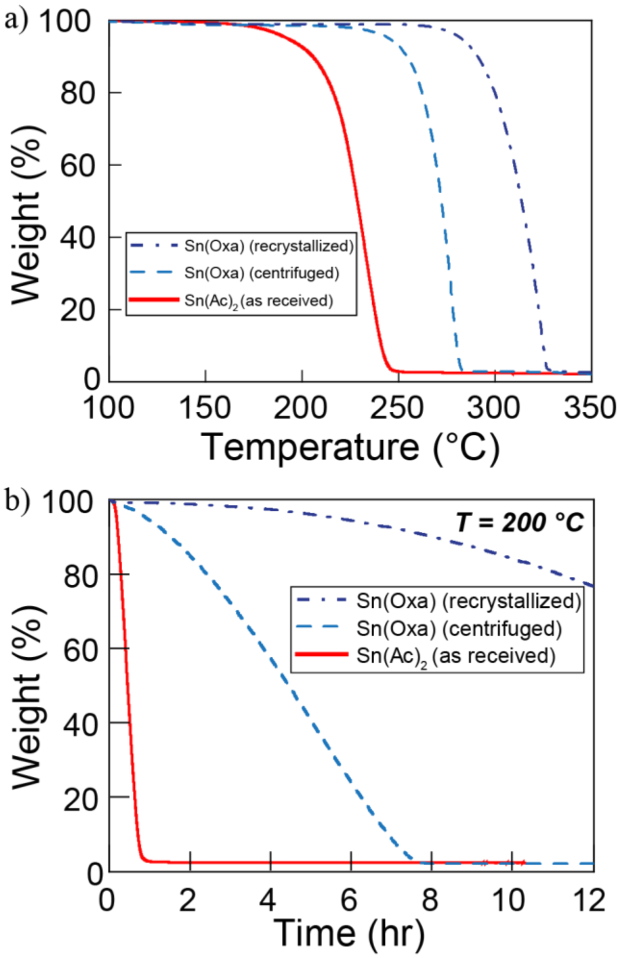

Figure 2.3. Thermal depolymerization of PLA films with 3 wt. % Sn(Oxa) (recrystallized and centrifuged) and Sn(Ac)$_2$ (as received) catalysts: (a) Dynamic TGA and (b) isothermal TGA at 200 °C. The depolymerization temperature decreased with the addition of Sn(Oxa) (centrifuged) catalyst with higher SSA and even more significantly with Sn(Ac)$_2$.

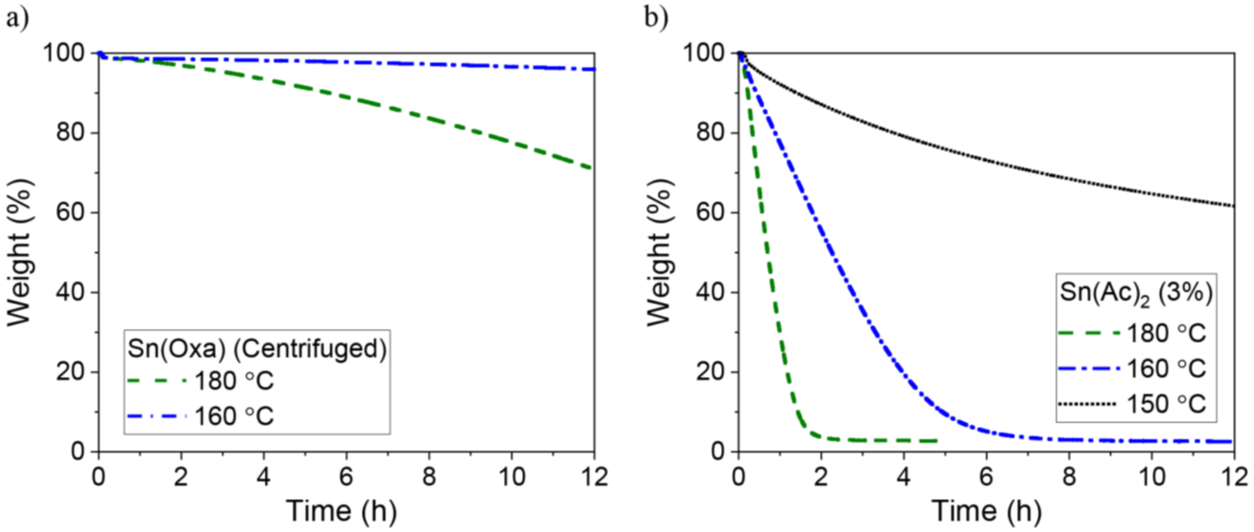

Figure 2.4. (a) Thermal depolymerization of PLA films with 3 wt. % Sn(Oxa) (centrifuged) catalyst at different isothermal temperatures in TGA. The depolymerization rate was significantly reduced below 200 °C and was negligible at 160 °C. (b) Thermal depolymerization of PLA films with 3 wt. % $Sn(Ac)_2$ (as received) catalyst at different isothermal temperatures in TGA. The depolymerization rate was significantly reduced at 150 °C, which is below the melting point of PLA (ca. 160 °C).

2.3.2 Improved catalyst for rapid depolymerization

Tin acetate ($Sn(Ac)_2$), another organometallic catalyst, was also investigated to accelerate the depolymerization kinetics of PLA. $Sn(Ac)_2$ (as received) consisted of rod-like structures in the 1-3 µm range (**Figure 2.1f**). The SSA of these particles was twice that of Sn(Oxa) (centrifuged) as summarized in **Table 2.1**. The T_d of films with 3 % $Sn(Ac)_2$ particles were 53 °C lower than that of Sn(Oxa) (centrifuged) and 90 °C lower than that of Sn(Oxa) (recrystallized) in dynamic TGA experiments (**Figure 2.3a**). In isothermal TGA at 200 °C, the time for complete depolymerization was substantially reduced to less than one hour using $Sn(Ac)_2$ catalyst (**Figure 2.3b**). Previously, Dong et al. compared the catalytic activity of Sn(Oxa) and $Sn(Ac)_2$ in depolymerizing PLA films and reported a similar T_d for both catalysts, but the SSA was not discussed [42]. In great contrast, here we observe a significant decrease in T_d during dynamic TGA experiments and a ten-fold decrease in PLA depolymerization time at 200 °C during isothermal TGA experiments with

$Sn(Ac)_2$ compared to Sn(Oxa). This substantial decrease in depolymerization time is unlikely due to the small change in the SSA from the Sn(Oxa) (centrifuged) catalyst. We hypothesize that the decrease in depolymerization temperature and time is related to the improved catalytic ability of $Sn(Ac)_2$ to carry out transesterification reactions in polymers.

A depolymerization kinetics model [50] that depends on the degree of PLA depolymerization at different temperatures was applied to obtain parameters that provide the best fit between the model and the TGA experiments (Equation 2.2).

$$\frac{\partial \alpha}{\partial t} = Aexp\left(-\frac{E}{RT}\right)(1-\alpha)^n \alpha^m \qquad 2.2$$

$$\alpha\,(t) = \frac{Intitial\ weight\ -\ Weight\ at\ time\ (t)}{Initial\ weight\ -\ Residual\ weight}$$

where, α (non-dimensional) denotes the degree of depolymerization/conversion of PLA; t (s) and T (K) denote time and temperature respectively; E (kJ/mol), A (s^{-1}), and R (8.314 $Jmol^{-1}K^{-1}$) denote activation energy, pre-exponential factor, and universal gas constant respectively; n and m denote two constants associated with the conversion that accounts for autocatalytic effects. We leveraged on an optimization scheme to seek parameters that provide the best fit between the model and three different temperatures for each catalyst. The activation energy (E) and pre-exponential factor (A) were kept within the expected range for PLA depolymerization with catalysts. The obtained parameters (**Table 2.4**) are then used to predict the TGA response at 180 °C for Sn(Oxa) (centrifuged) and 170 °C for $Sn(Ac)_2$, which match reasonably well with experiments. (**Figure 2.5**).

Table 2.4. Kinetic parameters obtained using isothermal TGA data for different catalysts.

Catalyst	Loading (wt. %)	*E* (kJ/mol)	*A* (s^{-1})	*m*	*n*
Sn(Oxa)	3	133	3.2×10^{10}	0.03	0.73
$Sn(Ac)_2$	3	122	4.2×10^{10}	0.33	0.12

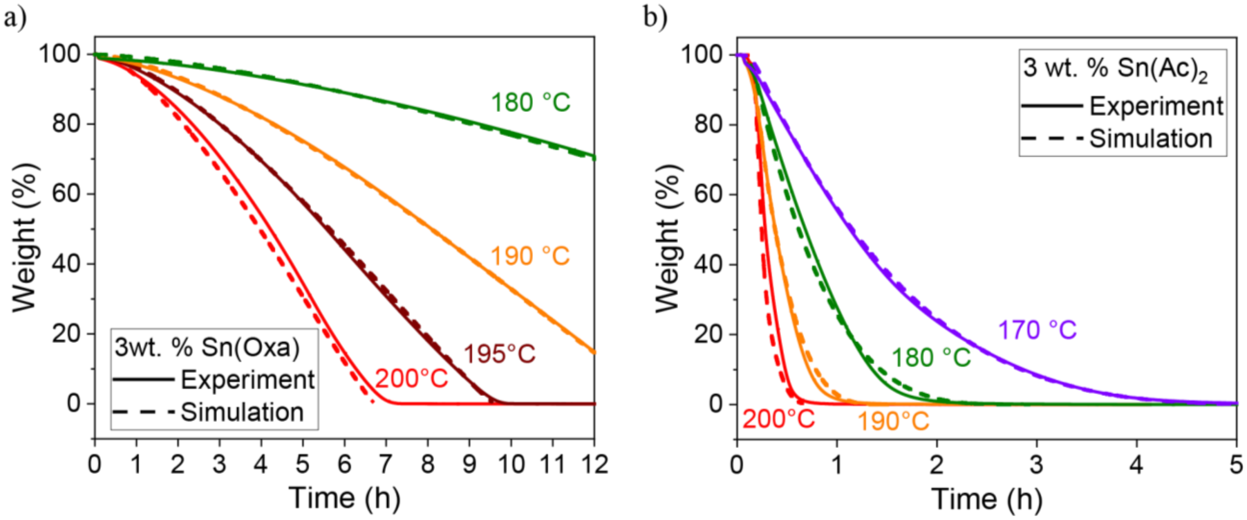

Figure 2.5. Comparison between isothermal TGA experiments (solid lines) and simulation (dashed lines) at different temperatures for PLA films containing 3 wt. % catalyst: (a) Sn(Oxa) (centrifuged) and (b) $Sn(Ac)_2$. The initial catalyst mass was subtracted from the experimental TGA data to compare mass loss solely due to PLA with simulations. Model optimization was performed using MATLAB. Simulation results were obtained in collaboration with Dr. Xiang Zhang.

The activation energy for films with 3% $Sn(Ac)_2$ catalyst is 122 kJ/mol, which is 11 kJ/mol lower than that for films with 3% Sn(Oxa) (centrifuged) (**Table 2.4**). This difference in activation energy results in reduced reaction time at lower temperatures for $Sn(Ac)_2$ catalyst (**Figure 2.5**). Additionally, the melting point of $Sn(Ac)_2$ has been reported as ~182 °C [51]. Our DSC experiments reveal the onset of melting as early as 160 °C (**Figure 2.6**). In contrast, no melting is observed for Sn(Oxa) since it is more thermally stable [52]. The melting of $Sn(Ac)_2$ likely contributes to the accelerated reaction kinetics since the liquid $Sn(Ac)_2$ will have a much higher surface area available for reaction compared to solid Sn(Oxa). This trend is also evident in the isothermal TGA experiment with $Sn(Ac)_2$ at 150 °C, in which the PLA depolymerization proceeds extremely slowly below the melting temperature onset of $Sn(Ac)_2$ (**Figure 2.4b**). The decomposition temperatures of Sn(Oxa) and $Sn(Ac)_2$ are 302 °C[52] and 238 °C [51], respectively. No signs of degradation for either catalyst were observed in the DSC experiments up to 200 °C. Moreover, the lower density of $Sn(Ac)_2$ (2.31 g/cm^3) compared to Sn(Oxa) (3.56 g/cm^3) results in increased volume (~ 35 %) of $Sn(Ac)_2$ for the same wt.% of both catalysts in PLA films. As a result, a higher volume (hence total surface area) of $Sn(Ac)_2$ for the same loading might be another contributing factor to the faster depolymerization of PLA.

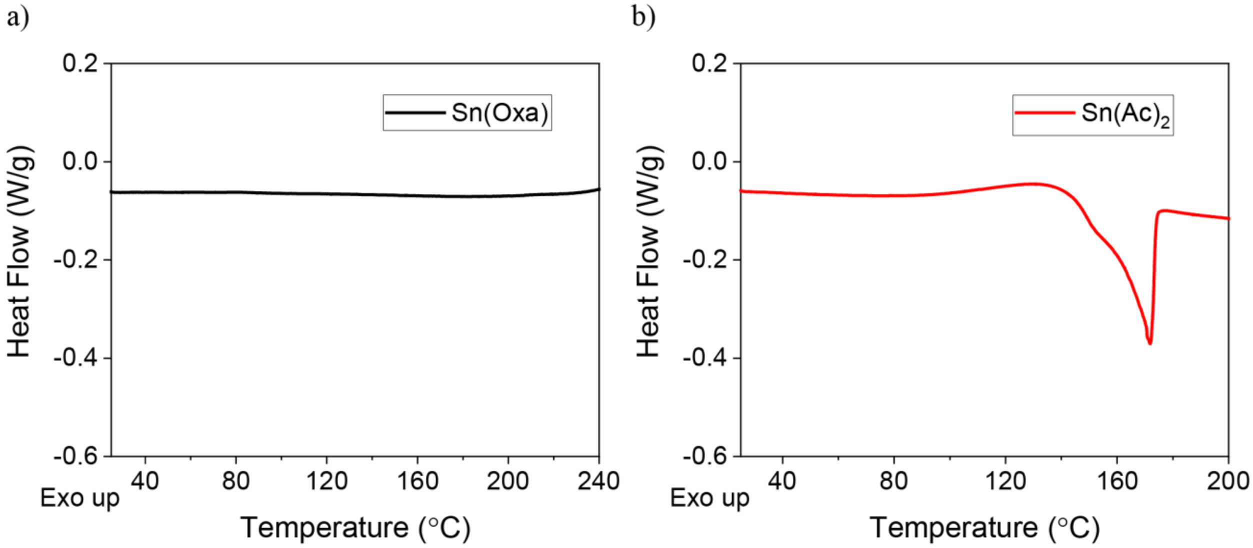

Figure 2.6. Differential scanning calorimetry (DSC) experiments on Sn(Oxa) and $Sn(Ac)_2$ catalysts at 5 °C/min.

2.3.3 *Reduced catalyst concentration*

Both Sn(Oxa) and $Sn(Ac)_2$ catalysts are stable up to 200 °C, and the residual catalyst unnecessarily remains after the vaporization of the PLA [42]. Because $Sn(Ac)_2$ catalyzed PLA films depolymerized extremely rapidly at 200 °C, films with a lower concentration (0.1 -2 %) of $Sn(Ac)_2$ were investigated to reduce the catalyst concentration required for complete depolymerization of PLA. Remarkably, the T_d of all films, including 0.1 % $Sn(Ac)_2$, were less than that for 3 % Sn(Oxa) (centrifuged) (**Figure 2.7a**). In isothermal TGA at 200 °C, all of the films with $Sn(Ac)_2$ depolymerized faster than films with 3 % Sn(Oxa) (centrifuged) (**Figure 2.7b**). Films with 0.1 % $Sn(Ac)_2$ depolymerized completely in less than half the time compared to 3 % Sn(Oxa) (Centrifuged) under the same conditions.

The half-life (time for 50 wt. % loss) of films with reduced loadings of $Sn(Ac)_2$ were also determined from isothermal TGA experiments at different temperatures (**Figure 2.7c**). Films with 0.5 % $Sn(Ac)_2$ had a half-life of 36 min at 200 °C, which was nearly seven times lower compared to the 265 min half-life of 3 % Sn(Oxa) (centrifuged) containing films. A drastic difference in the half-life of films with different loadings of $Sn(Ac)_2$ was observed at lower dwell temperatures. The half-life of PLA films with 3 % $Sn(Ac)_2$ at 160 °C was ca. 150 min compared to 394 min for 0.5 % $Sn(Ac)_2$ films. The half-life for films with 0.1 and 0.2 % $Sn(Ac)_2$ exceeded the maximum isothermal TGA experiment time of 720 min at 160 °C and are not reported here. In contrast, PLA films with 3 % Sn(Oxa) (centrifuged) incurred only 30 % weight loss at 180 °C and 3 % loss at 160 °C in 720 min (TGA in **Figure 2.4a**). Below 160 °C the catalytic depolymerization rate was drastically reduced, as the PLA as well as $Sn(Ac)_2$ are solid below this temperature. The diffusion of the catalyst in the solid PLA matrix is slower, leading to a significantly extended depolymerization time (**Figure 2.4b**). These findings suggest that $Sn(Ac)_2$ has improved catalytic activity for the PLA depolymerization reaction compared to Sn(Oxa) and leads to faster depolymerization at lower concentrations and temperatures. This rapid depolymerization kinetics can potentially reduce the energy and time required for converting PLA into volatile products for sacrificial and feedstock recycling applications. Hence, films blended with $Sn(Ac)_2$ were investigated as sacrificial templates for manufacturing vascular thermosets below temperatures previously reported for PLA with Sn(Oxa).

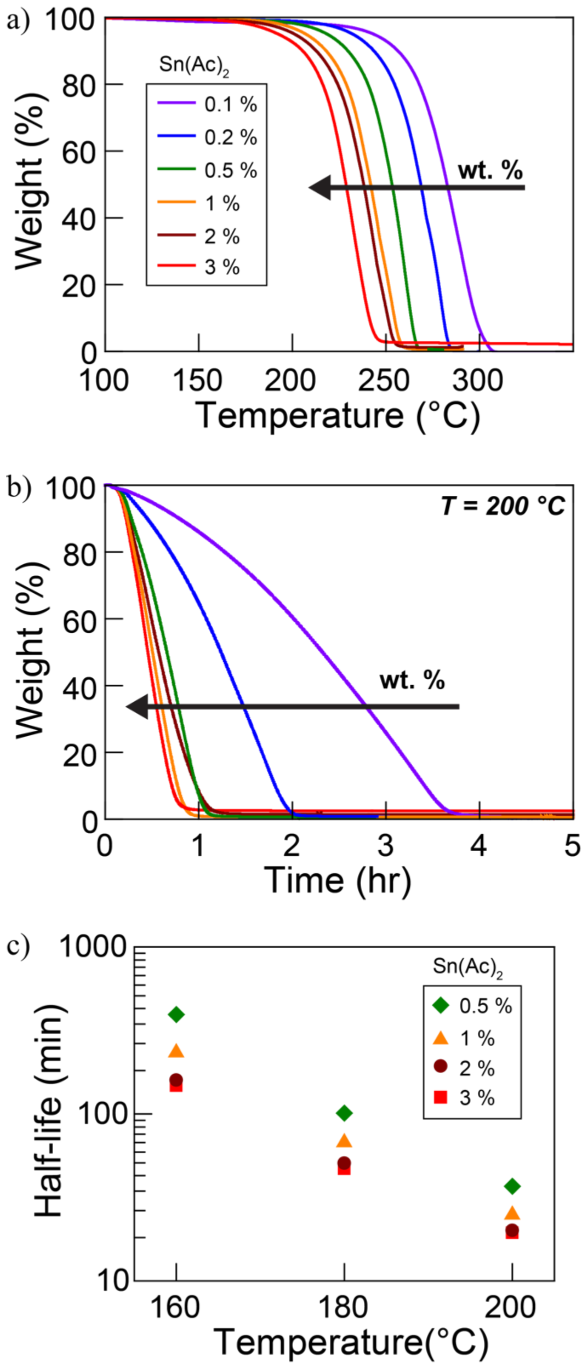

Figure 2.7. Effect of $Sn(Ac)_2$ catalyst concentration on PLA depolymerization: (a) Dynamic TGA and (b) isothermal TGA at 200 °C. (c) The half-life of PLA films at different temperatures in isothermal TGA (3 samples were used for each test, and the error bars of 1 SD are smaller than the size of the symbols).

2.3.4 Characterization of depolymerization in epoxy matrix

PLA films blended with different loadings of $Sn(Ac)_2$ were embedded in epoxy 8605 matrices and depolymerized at temperatures below 200 °C to demonstrate successful vascularization at lower temperatures. Complete evacuation of the depolymerization products from the matrix was verified through mass loss measurements of the templates and passing a flushing solvent through the resulting microchannel. Previously, an energy-intensive sacrificial PLA depolymerization step (200 °C for 12 hours in a vacuum oven) was required to create vascular networks in thermoset polymers and composites [24]. For reference, films with 3 % Sn(Oxa) (centrifuged) showed a mass loss of 97 % after vascularization of the epoxy matrix at 200 °C for 12 h, and the remaining mass corresponds to the initial loading of the catalyst since it is non-volatile under these conditions (**Table 2.5**). Significant discoloration due to oxidation of the epoxy matrix was also observed under these extreme VaSC conditions. Oxidation is undesirable and can alter the mechanical properties of the final thermoset polymers and composites (top specimen in **Figure 2.8**). In comparison, films with 3 % $Sn(Ac)_2$ were successfully vaporized to create microchannels in a much shorter time (3 hours) at the same temperature. Furthermore, films with 3 % $Sn(Ac)_2$ also evacuated completely from the epoxy matrix at 170 °C in 12 h, which was not possible with Sn(Oxa) based on TGA experiments (**Figure 2.4**). Films with lower $Sn(Ac)_2$ loading (1 %) were also depolymerized at 170 °C within 12 h to yield clear microchannels in the epoxy matrix. Minimal discoloration of the matrix was observed under these reduced VaSC temperatures (bottom specimen in **Figure 2.8**).

Table 2.5. Mass loss of PLA films in epoxy 8605 matrices after VaSC at different temperatures.

Catalyst	**Loading (wt. %)**	**Temperature (°C)**	**Time (h)**	**Mass loss$^{\Psi}$ (%)**
Sn(Oxa) (centrifuged)	3	200	12	97
$Sn(Ac)_2$	3	200	3	97
$Sn(Ac)_2$	3	170	12	97
$Sn(Ac)_2$	1	170	12	99

$^{\Psi}$Error in mass loss is ±1 % from 3 samples for each test

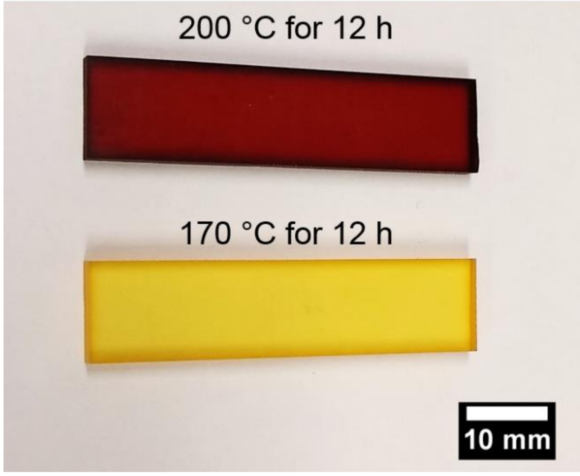

Figure 2.8. Epoxy 8605 samples after VaSC cycle at 200 °C for 12 hours (top) and 170 °C for 12 hours (bottom) showing a significant discoloration of the matrix (top) due to oxidation at 200 °C for a long time.

Optical cross-sections of the epoxy matrix before and after the vascularization step reveal that the microchannels were clear of any significant residue after the depolymerization of PLA (**Figure 2.9**). SEM of the sectioned epoxy samples revealed the presence of particles on the walls of these microchannels (**Figure 2.10**). Samples with 1 wt. % $Sn(Ac)_2$ catalyst had a smaller amount of residual catalyst present inside the channels and EDAX measurements inside the microchannel walls confirmed the presence of tin in these residual particles (**Figure 2.11**). Hence, sacrificial PLA templates embedded in a host matrix are depolymerized efficiently at substantially lower temperatures than 200 °C within reasonable times using $Sn(Ac)_2$ catalyst. Although the VaSC conditions were not optimized in this work, the isothermal TGA data indicate that the temperature can be reduced to 160° C, which is 40 °C lower than the current protocol with Sn(Oxa). $Sn(Ac)_2$ would allow faster vascularization of multifunctional thermoset polymers and composites at lower temperatures and reduced catalyst loadings without undesirable oxidation of the host matrix. Also, $Sn(Ac)_2$ enables reduced catalyst loadings without significantly compromising the PLA depolymerization rate at temperatures above 180 °C. This reduction is important for applications requiring microchannel functionalization, as large amounts of catalyst on the channel walls would interfere during their surface modification with different chemicals.

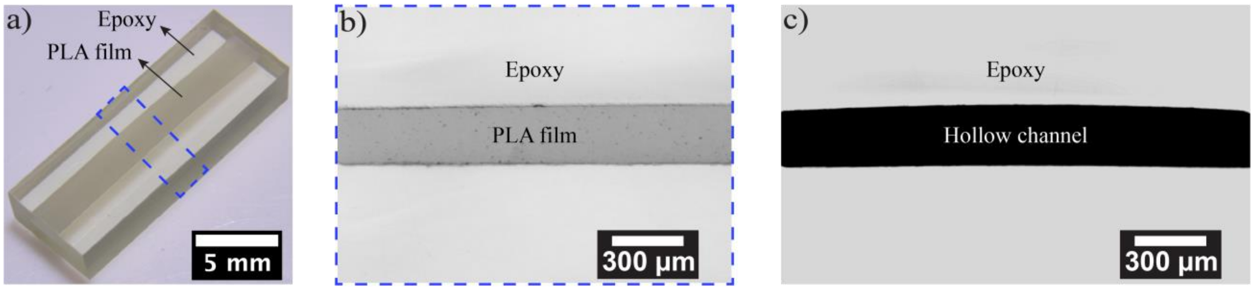

Figure 2.9. Optical micrographs before and after VaSC of PLA films containing 3 wt. % $Sn(Ac)_2$ in epoxy matrix: (a) Isometric view and (b) cross-sectional view before VaSC. (c) Cross-sectional view after VaSC showing complete removal of PLA film from the evacuated microchannel.

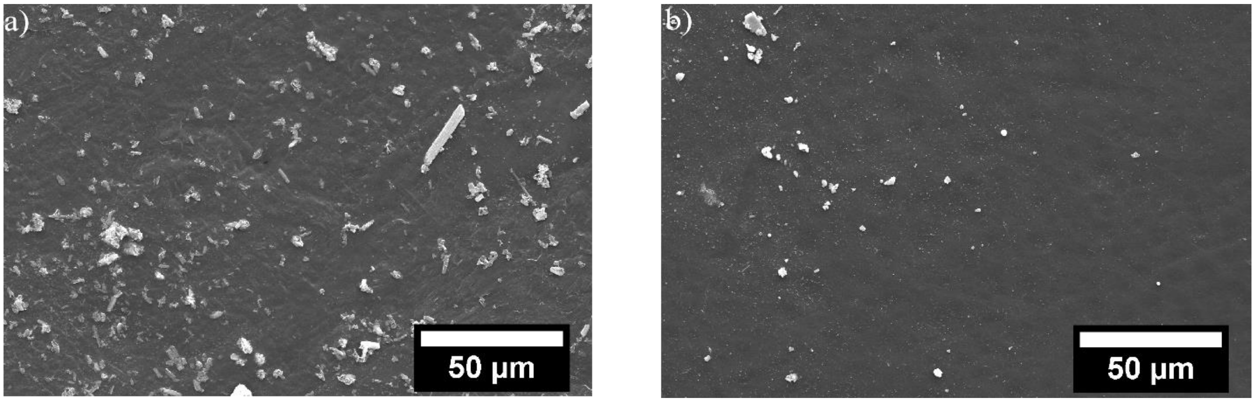

Figure 2.10. SEM micrographs of sectioned microchannels after VaSC of PLA films at 200 °C, containing 3 % catalyst in 8605 matrix: (a) Sn(Oxa) and (b) $Sn(Ac)_2$.

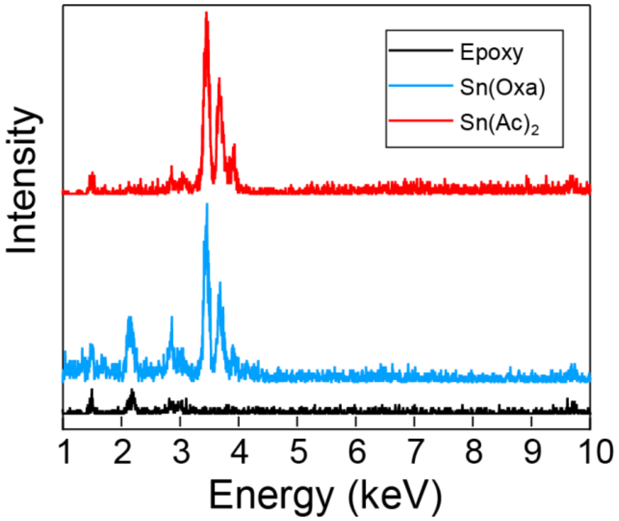

Figure 2.11. EDAX spectra of channel surfaces after VaSC (SEM in Figure 5). The neat epoxy surface showed mostly gold and palladium peaks near 2.1 keV and 2.8 keV, respectively. Peaks at 3.4, 3.7, and 3.9 keV confirmed the presence of tin in residue particles present in the microchannels containing Sn(Oxa) and Sn(Ac)$_2$ catalysts.

2.4 Summary

In this chapter, the effect of catalyst SSA and different catalyst types on the depolymerization of PLA films was investigated. A 20-fold increase in the surface area of Sn(Oxa) catalyst lowered the depolymerization onset of sacrificial PLA by 37 °C and reduced the total depolymerization time. The same concentration of Sn(Ac)$_2$ with slightly higher surface area further lowered the depolymerization onset temperature of PLA by 53 °C and drastically reduced its depolymerization time by more than an order of magnitude at 200 °C. Furthermore, PLA films with approximately one-tenth the concentration of Sn(Ac)$_2$ compared to Sn(Oxa) exhibited a lower depolymerization onset temperature, smaller half-life, and faster depolymerization at temperatures as low as 160 °C. Modeling of the depolymerization kinetics revealed lower activation energy for Sn(Ac)$_2$ catalyzed depolymerization compared to Sn(Oxa). Melting of the Sn(Ac)$_2$ catalyst during PLA depolymerization was confirmed by DSC experiments and likely contributed to the faster depolymerization kinetics. $Sn(Ac)_2$ facilitated the fabrication of microchannels in an epoxy matrix with less residue compared to Sn(Oxa), while further lowering the VaSC temperature by 30 °C (**Figure 2.12**). The use of $Sn(Ac)_2$ potentially enables faster removal of sacrificial PLA templates from host matrices at lower temperatures with minimal oxidation and discoloration of the host epoxy matrix compared to Sn(Oxa). However, unsuccessful vascularization was observed when epoxy samples with films containing 3% $Sn(Ac)_2$ were exposed to 150 °C for 12 hours due to much slower catalyst diffusion below the melting point (T_m) of PLA.

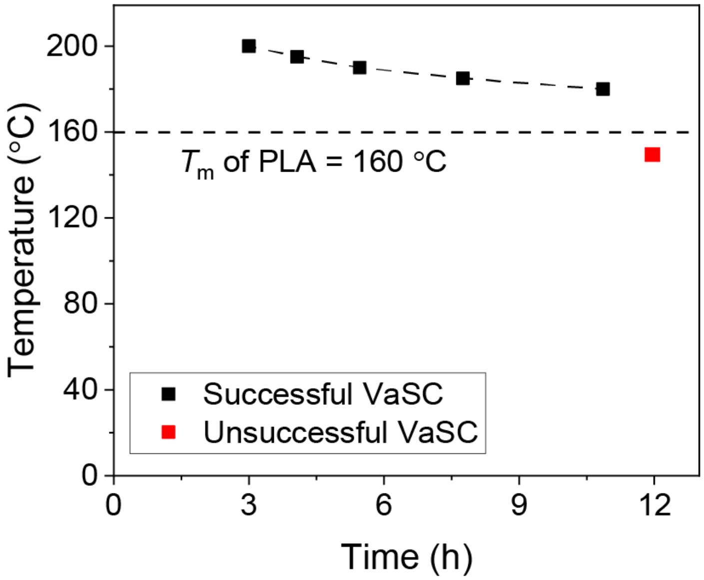

Figure 2.12. Successful VaSC protocols for PLA films containing 3 wt. % tin acetate catalyst. Vascularization is not observed below the melting point of PLA.

2.5 References

[1] N. A. Campbell, J. B. Reece, M. R. Taylor, E. J. Simon, and J. L. Dickey, *Biology*. Benjamin Cummings, 2010.

[2] L. M. Bellan, S. P. Singh, P. W. Henderson, T. J. Porri, H. G. Craighead, and J. A. Spector, “Fabrication of an artificial 3-dimensional vascular network using sacrificial sugar structures,” *Soft Matter*, vol. 5, no. 7, pp. 1354–1357, 2009, doi: 10.1039/b819905a.

[3] C. Gualandi, A. Zucchelli, M. F. Osorio, J. Belcari, and M. L. Focarete, “Nanovascularization of Polymer Matrix: Generation of Nanochannels and Nanotubes by Sacrificial Electrospun fibers,” *Nano Lett*, vol. 13, no. 11, pp. 5385–5390, 2013, doi: 10.1021/nl402930x.

[4] D. Lim, Y. Kamotani, B. Cho, J. Mazumder, and S. Takayama, “Fabrication of microfluidic mixers and artificial vasculatures using a high-brightness diode-pumped Nd:YAG laser direct write method.,” *Lab on a chip*, vol. 3, no. 4, pp. 318–323, Nov. 2003, doi: 10.1039/b308452c.

[5] Y. Zhou, “The recent development and applications of fluidic channels by 3D printing,” *J Biomed Sci*, vol. 24, no. 1, p. 80, 2017, doi: 10.1186/s12929-017-0384-2.

[6] W. Wu, A. DeConinck, and J. A. Lewis, “Omnidirectional Printing of 3D Microvascular Networks,” *Adv Mater*, vol. 23, no. 24, pp. H178–H183, 2011, doi: 10.1002/adma.201004625.

[7] C. Colosi *et al.*, “Microfluidic Bioprinting of Heterogeneous 3D Tissue Constructs Using Low-Viscosity Bioink,” *Adv Mater*, vol. 28, no. 4, pp. 677–684, 2015, doi: 10.1002/adma.201503310.

[8] M. A. Unger, H.-P. Chou, T. Thorsen, A. Scherer, and S. R. Quake, “Monolithic Microfabricated Valves and Pumps by Multilayer Soft Lithography,” *Science*, vol. 288, no. 5463, pp. 113–116, 2000, doi: 10.1126/science.288.5463.113.

[9] J. P. Jayachandran *et al.*, “Air-channel fabrication for microelectromechanical systems via sacrificial photosensitive polycarbonates,” *Journal of Microelectromechanical Systems*, vol. 12, no. 2, pp. 147–159, Apr. 2003, doi: 10.1109/jmems.2003.809963.

[10] P. J. Joseph, P. Monajemi, F. Ayazi, and P. A. Kohl, “Wafer-Level Packaging of Micromechanical Resonators,” *IEEE Transactions on Advanced Packaging*, vol. 30, no. 1, pp. 19–26, 2007, doi: 10.1109/tadvp.2006.890220.

[11] T. J. Spencer, Y.-C. Chen, R. Saha, and P. A. Kohl, “Stabilization of the Thermal Decomposition of Poly(Propylene Carbonate) Through Copper Ion Incorporation and Use in Self-Patterning,” *Journal of Electronic Materials*, vol. 40, no. 6, pp. 1350–1363, Mar. 2011, doi: 10.1007/s11664-011-1518-z.

[12] E. Uzunlar and P. A. Kohl, “Size-Compatible, Polymer-Based Air-Gap Formation Processes, and Polymer Residue Analysis for Wafer-Level MEMS Packaging Applications,” *Journal of Electronic Packaging*, vol. 137, no. 4, pp. 041001–13, Dec. 2015, doi: 10.1115/1.4030952.

[13] J. A. Potkay, M. Magnetta, A. Vinson, and B. Cmolik, “Bio-inspired, efficient, artificial lung employing air as the ventilating gas,” *Lab Chip*, vol. 11, no. 17, p. 2901, 2011, doi: 10.1039/c1lc20020h.

[14] D. T. Nguyen, Y. T. Leho, and A. P. Esser-Kahn, “A three-dimensional microvascular gas exchange unit for carbon dioxide capture,” *Lab Chip*, vol. 12, no. 7, pp. 1246–1250, 2012, doi: 10.1039/c2lc00033d.

[15] A. Z. Weber, M. M. Mench, J. P. Meyers, P. N. Ross, J. T. Gostick, and Q. Liu, “Redox flow batteries: a review,” *J Appl Electrochem*, vol. 41, no. 10, pp. 1137–1164, 2011, doi: 10.1007/s10800-011-0348-2.

[16] K. J. Maloney, K. D. Fink, T. A. Schaedler, J. A. Kolodziejska, A. J. Jacobsen, and C. S. Roper, “Multifunctional heat exchangers derived from three-dimensional micro-lattice structures,” *Int J Heat Mass Tran*, vol. 55, no. 9–10, pp. 2486–2493, 2012, doi: 10.1016/j.ijheatmasstransfer.2012.01.011.

[17] S. J. Pety, P. X. L. Chia, S. M. Carrington, and S. R. White, “Active cooling of microvascular composites for battery packaging,” *Smart Mater Struct*, vol. 26, no. 10, p. 105004, 2017, doi: 10.1088/1361-665x/aa84e7.

[18] S. J. Pety, M. H. Y. Tan, A. R. Najafi, P. R. Barnett, P. H. Geubelle, and S. R. White, “Carbon fiber composites with 2D microvascular networks for battery cooling,” *International Journal of Heat and Mass Transfer*, vol. 115, pp. 513–522, Dec. 2017, doi: 10.1016/j.ijheatmasstransfer.2017.07.047.

[19] S. J. Pety *et al.*, “Design of redundant microvascular cooling networks for blockage tolerance,” *Appl Therm Eng*, vol. 131, no. Int. J. Heat Mass Transf. 103 2016, pp. 965–976, 2018, doi: 10.1016/j.applthermaleng.2017.10.094.

[20] A. M. Coppola *et al.*, “Active Cooling of a Microvascular Shape Memory Alloy-Polymer Matrix Composite Hybrid Material ,” *Adv Eng Mater*, vol. 18, no. 7, pp. 1145–1153, 2016, doi: 10.1002/adem.201600020.

[21] A. M. Coppola, L. G. Warpinski, S. P. Murray, N. R. Sottos, and S. R. White, “Survival of actively cooled microvascular polymer matrix composites under sustained thermomechanical loading,” *Compos Part Appl Sci Manuf*, vol. 82, pp. 170–179, 2016, doi: 10.1016/j.compositesa.2015.12.010.

[22] R. Pejman *et al.*, “Gradient-based hybrid topology/shape optimization of bioinspired microvascular composites,” *Int J Heat Mass Tran*, vol. 144, p. 118606, 2019, doi: 10.1016/j.ijheatmasstransfer.2019.118606.

[23] K. S. Toohey, N. R. Sottos, J. A. Lewis, J. S. Moore, and S. R. White, “Self-healing materials with microvascular networks,” *Nat Mater*, vol. 6, no. 8, pp. 581–585, Aug. 2007, doi: 10.1038/nmat1934.

[24] A. P. Esser-Kahn *et al.*, “Three-Dimensional Microvascular Fiber-Reinforced Composites,” *Advanced Materials*, vol. 23, no. 32, pp. 3654–3658, Jul. 2011, doi: 10.1002/adma.201100933.

[25] J. F. Patrick *et al.*, “Continuous Self-Healing Life Cycle in Vascularized Structural Composites,” *Advanced Materials*, vol. 26, no. 25, pp. 4302–4308, Apr. 2014, doi: 10.1002/adma.201400248.

[26] J. F. Patrick *et al.*, “Robust sacrificial polymer templates for 3D interconnected microvasculature in fiber-reinforced composites,” *Composites Part A: Applied Science and Manufacturing*, vol. 100, pp. 361–370, Sep. 2017, doi: 10.1016/j.compositesa.2017.05.022.

[27] K. R. Hart *et al.*, “Repeated healing of delamination damage in vascular composites by pressurized delivery of reactive agents,” *Composites Science and Technology*, vol. 151, pp. 1–9, Oct. 2017, doi: 10.1016/j.compscitech.2017.07.027.

[28] C. J. Norris, J. A. P. White, G. McCombe, P. Chatterjee, I. P. Bond, and R. S. Trask, “Autonomous stimulus triggered self-healing in smart structural composites,” *Smart Materials and Structures*, vol. 21, no. 9, p. 094027, Sep. 2012, doi: 10.1088/0964-1726/21/9/094027.

[29] L. M. Dean, B. P. Krull, K. R. Li, Y. I. Fedonina, S. R. White, and N. R. Sottos, “Enhanced Mixing of Microvascular Self-Healing Reagents Using Segmented Gas–Liquid Flow,” *Acs Appl Mater Inter*, vol. 10, no. 38, pp. 32659–32667, 2018, doi: 10.1021/acsami.8b09966.

[30] J.-H. Huang *et al.*, “Rapid Fabrication of Bio-inspired 3D Microfluidic Vascular Networks,” *Advanced Materials*, vol. 21, no. 35, pp. 3567–3571, Sep. 2009, doi: 10.1002/adma.200900584.

[31] D. Therriault, S. R. White, and J. A. Lewis, “Chaotic mixing in three-dimensional microvascular networks fabricated by direct-write assembly,” *Nat Mater*, vol. 2, no. 4, pp. 265–271, 2003, doi: 10.1038/nmat863.

[32] C. J. Norris, I. P. Bond, and R. S. Trask, “Interactions between propagating cracks and bioinspired self-healing vascules embedded in glass fibre reinforced composites,” *Composites Science and Technology*, vol. 71, no. 6, pp. 847–853, Apr. 2011, doi: 10.1016/j.compscitech.2011.01.027.

[33] R. C. R. Gergely *et al.*, “Multidimensional Vascularized Polymers using Degradable Sacrificial Templates,” *Advanced Functional Materials*, vol. 25, no. 7, pp. 1043–1052, Dec. 2014, doi: 10.1002/adfm.201403670.

[34] P. A. Kohl *et al.*, “Air-gaps in 0.3 μm electrical interconnections,” *IEEE Electron Device Letters*, vol. 21, no. 12, pp. 557–559, 2000, doi: 10.1109/55.887464.

[35] T. J. Spencer, P. J. Joseph, T. H. Kim, M. Swaminathan, and P. A. Kohl, “Air-Gap Transmission Lines on Organic Substrates for Low-Loss Interconnects,” *IEEE Transactions on Microwave Theory and Techniques*, vol. 55, no. 9, pp. 1919–1925, 2007, doi: 10.1109/tmtt.2007.904326.

[36] M. S. Bakir *et al.*, “Chip-to-Module Interconnections Using ‘Sea of Leads’ Technology,” *MRS Bulletin*, vol. 28, no. 1, pp. 61–67, Jan. 2003, doi: 10.1557/mrs2003.19.

[37] G. T. Ostrowicki, N. T. Fritz, R. I. Okereke, P. A. Kohl, and S. K. Sitaraman, “Domed and Released Thin-Film Construct—An Approach for Material Characterization and Compliant Interconnects,” *IEEE Transactions on Device and Materials Reliability*, vol. 12, no. 1, pp. 15–23, 2012, doi: 10.1109/tdmr.2011.2175927.

[38] R. Saha, N. Fritz, S. A. B. Allen, and P. A. Kohl, “Packaging-compatible wafer level capping of MEMS devices,” *Microelectronic Engineering*, vol. 104, pp. 75–84, Apr. 2013, doi: 10.1016/j.mee.2012.11.010.

[39] C. J. Hansen, W. Wu, K. S. Toohey, N. R. Sottos, S. R. White, and J. A. Lewis, “Self-Healing Materials with Interpenetrating Microvascular Networks,” *Advanced Materials*, vol. 21, no. 41, pp. 4143–4147, Nov. 2009, doi: 10.1002/adma.200900588.

[40] A. M. Coppola, A. S. Griffin, N. R. Sottos, and S. R. White, “Retention of mechanical performance of polymer matrix composites above the glass transition temperature by vascular cooling,” *Composites Part A: Applied Science and Manufacturing*, vol. 78, pp. 412–423, Nov. 2015, doi: 10.1016/j.compositesa.2015.07.012.

[41] M. Niaounakis, *Biopolymers: Processing and Products*. Elsevier, 2014.

[42] H. Dong *et al.*, “Chemical Treatment of Poly(lactic acid) Fibers to Enhance the Rate of Thermal Depolymerization,” *ACS Applied Materials & Interfaces*, vol. 4, no. 2, pp. 503–509, Feb. 2012, doi: 10.1021/am2010042.

[43] Y. Aoyagi, K. Yamashita, and Y. Doi, “Thermal degradation of poly[(R)-3-hydroxybutyrate], poly[ε-caprolactone], and poly[(S)-lactide],” *Polymer Degradation and Stability*, vol. 76, no. 1, pp. 53–59, Jan. 2002, doi: 10.1016/s0141-3910(01)00265-8.

[44] Y. Fan, H. Nishida, T. Mori, Y. Shirai, and T. Endo, “Thermal degradation of poly(l-lactide): effect of alkali earth metal oxides for selective l,l-lactide formation,” *Polymer*, vol. 45, no. 4, pp. 1197–1205, Feb. 2004, doi: 10.1016/j.polymer.2003.12.058.

[45] D. Cam and M. Marucci, “Influence of residual monomers and metals on poly (L-lactide) thermal stability,” *Polymer*, vol. 38, no. 8, pp. 1–6, Apr. 2003, doi: 10.1016/s0032-3861(96)00711-2.

[46] M. NODA and H. OKUYAMA, “Thermal Catalytic Depolymerization of Poly(L-Lactic Acid) Oligomer into LL-Lactide: Effects of Al, Ti, Zn and Zr Compounds as Catalysts.,” *CHEMICAL & PHARMACEUTICAL BULLETIN*, vol. 47, no. 4, pp. 467–471, 1999, doi: 10.1248/cpb.47.467.

[47] H. Nishida, T. Mori, S. Hoshihara, Y. Fan, Y. Shirai, and T. Endo, “Effect of tin on poly(l-lactic acid) pyrolysis,” *Polymer Degradation and Stability*, vol. 81, no. 3, pp. 515–523, Jan. 2003, doi: 10.1016/s0141-3910(03)00152-6.

[48] S. Middleman, *An Introduction to Fluid Dynamics*. John Wiley & Sons Incorporated, 1998.

[49] D. Palacios, M. C. D'Antonio, A. C. González-Baró, and E. J. Baran, "Spectrochimica Acta Part A: Molecular and Biomolecular Spectroscopy," *Spectrochimica Acta Part A: Molecular and Biomolecular Spectroscopy*, vol. 77, no. 1, pp. 334–335, Sep. 2010, doi: 10.1016/j.saa.2010.04.037.

[50] P. Das and P. Tiwari, "Thermal degradation kinetics of plastics and model selection," *Thermochimica Acta*, vol. 654, pp. 191–202, Aug. 2017, doi: 10.1016/j.tca.2017.06.001.

[51] J. D. DONALDSON, W. Moser, and W. B. Simpson, "1147. Tin(II) acetates," *Journal of the Chemical Society (Resumed)*, no. 0, pp. 5942–5947, 1964, doi: 10.1039/jr9640005942.

[52] S. Kitabayashi and N. Koga, "Physico-geometrical mechanism and overall kinetics of thermally induced oxidative decomposition of tin(II) oxalate in air: Formation process of microstructural tin(IV) oxide," *Journal of Physical Chemistry C*, vol. 118, no. 31, pp. 17847–17861, Aug. 2014, doi: 10.1021/jp505937k.

[53] M. Garg, S. R. White, and N. R. Sottos, "Rapid Degradation of Poly(lactic acid) with Organometallic Catalysts," *Acs Appl Mater Inter*, vol. 11, no. 49, pp. 46226–46232, 2019, doi: 10.1021/acsami.9b17599.

CHAPTER 3

SACRIFICIAL CYCLIC POLY(PHTHALALDEHYDE) TEMPLATES FOR LOW-TEMPERATURE VASCULARIZATION OF POLYMER MATRICES

3.1 Introduction

Catalyst-assisted thermal depolymerization of poly(lactic acid) (PLA) templates embedded in thermoset polymers and composites enables the fabrication of complex multifunctional vascular structures [1]–[4]. However, PLA evacuation through the Vaporization of Sacrificial Components (VaSC) technique is energy-intensive (typically 200 °C for 12 hours), consuming 85 MJ of thermal energy for a one-meter long host structure [5], [6]. Furthermore, VaSC of PLA templates is limited to host matrices that can sustain this thermal treatment without deformation or degradation. The depolymerization temperature decreases to 170 °C with more efficient catalysts and a reduction in the molecular weight of the templates, but the evacuation time increases considerably at lower temperatures [3], [7]. Moreover, the catalyst particles remain on the microchannel surface after PLA depolymerization [6], [7], which may hinder subsequent functionalization of the vasculature. New sacrificial polymers that depolymerize at lower temperatures without catalysts are desirable for expanding vascularization to a broader range of host materials [2].

In addition to rapid depolymerization at low temperatures, sacrificial polymers must be melt- or solution-processable, possess sufficient molecular weight and good mechanical properties, and survive thermomechanical loads during integration into the host matrix. Depolymerization into gaseous products is preferred to enable complete evacuation of the high aspect ratio templates [2]. Compatibility between the matrix and the sacrificial polymer is also crucial since any physical or chemical interactions could inhibit the depolymerization and subsequent evaporation of the sacrificial templates [8].

Polymers that degrade in response to thermal, photo, and chemical stimuli are employed in recycling [9]–[11], triggered release [12]–[14], lithographic resists [15], and signal amplification [16]–[19]. Unfortunately, most stimuli-responsive polymers do not have good mechanical properties [9], [10], [19], and require contact with liquid media for facilitating the degradation reaction [11], [13], [19], [20]. Solvent access is limited to the exposed surfaces of the embedded templates in VaSC, making most stimuli-responsive polymers unsuitable for vascularization due to extremely slow diffusion-dominated degradation [2]. Linear poly(phthalaldehyde) (PPA) is a low ceiling temperature polymer that undergoes rapid depolymerization after exposure to different stimuli at moderate temperatures [21]. However, complex synthesis (10-15 days), low molecular weight (ca. 20 kDa), and poor benchtop stability at RT (days to weeks) limit PPA availability and processing options. Cyclic poly(phthalaldehyde) (cPPA) is a promising low ceiling temperature (-36 °C) [22] polymer that can be synthesized within a few hours with high molecular weight (hundreds of kDa) using a cationic polymerization reaction [23]. cPPA is stable at RT for months due to the absence of reactive chain ends, yet undergoes rapid unzipping from the solid state into an *ortho*-phthalaldehyde (*o*PA) monomer (**Scheme 3.1**) in response to mechanical, acidic, and thermal stimuli [23]–[30]. Solution-processed cPPA capsules and films have been used for functional payload release [14] and transient substrates [27], [28], [31]. Thermal processing of sacrificial polymers provides superior control over the mechanical properties and morphology of the resulting templates, which is desirable for VaSC applications [2], [3]. However, cPPA depolymerizes before observable glass or melt transition temperatures [23], [30] limiting its processability.

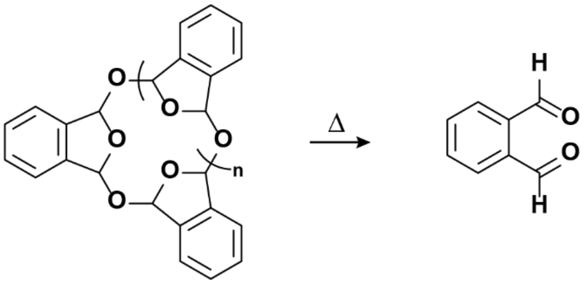

Scheme 3.1. Thermal depolymerization of cyclic poly(phthalaldehyde) (cPPA) to *o*PA monomer.

In this chapter, we investigate the processing and thermal depolymerization of sacrificial cPPA templates for creating microfluidic networks in a variety of host matrices. cPPA is formed into films, fibers, and printed templates through solution-based methods. Evacuation of these templates from several thermoset matrices is characterized at various temperatures and a low-temperature vascularization protocol is established for this new sacrificial polymer.

3.2 Materials and methods

3.2.1 Materials

High-performance liquid chromatography grade methanol, tetrahydrofuran (THF), and dichloromethane (DCM) were purchased from VWR. *ortho*-Phthalaldehyde (*o*PA) (99%) was procured from TCI America and purified by recrystallization as previously reported [23]. Dicyclopentadiene (DCPD), 2nd Generation Grubbs Catalyst (GC2), 5-ethylidene-2-norbornene (ENB), pentaerythritol tetrakis(3-mercaptopropionate) (tetrathiol), N,N-diglycidyl-4-glycidyoxyaniline (DGOA), (dimethylaminomethyl) phenol (catalyst 1), 5-(N-2,3-Dihydroxypropylacetamido)-2,4,6-triiodo-N,N′-bis(2,3-dihydroxypropyl)isophthalamide (Histodenz^{TM}) were purchased from Sigma Aldrich and used as received. EPON 828 and EPIKURE 3233 were obtained from Hexion. Clear PDMS (Sylgard 184) was purchased from

DOW Corning. Polytetrafluoroethylene (PTFE) Petri dish liners were purchased from Welch Fluorocarbon Inc. Glass plates and polyurethane gaskets were purchased from McMaster Carr. Glass syringes were purchased from Air-Tite Products Co. Inc.

3.2.2 cPPA Synthesis

The purified *o*PA (12 g) was dissolved in anhydrous DCM (96 ml). The solution was transferred to a nitrogen-environment Schlenk Line and cooled to -78 °C using an acetone/dry ice bath. Boron trifluoride diethyl etherate (2 mol %, 240 µl, 1.8 mmol) was added dropwise, and the stirred reaction was allowed to equilibrate for two hours at -78 °C. Pyridine (400 µl, 7.5 mmol) was added, and the stirred reaction was allowed to equilibrate for an additional two hours at -78°C. The polymer was precipitated dropwise into methanol, vacuum filtered, washed with diethyl ether, and dried for twenty-four hours under vacuum in a freeze drier (Labconco FreeZone 2.5 Liter Benchtop Freeze Dry System).

3.2.3 Solvent-cast cPPA films

Films were prepared using a modified procedure from the literature [23]–[25], [32]. Synthesized cPPA (800 mg) was dissolved in DCM (5 mL) and vortexed for 30 min to ensure full dissolution. The solution was drop-cast into a Teflon-lined Petri dish with a diameter of 50 mm. The evaporation rate of DCM was slowed by placing another Petri dish filled with DCM (10 mL) inside the film casting enclosure [32]. Slower evaporation was necessary to minimize surface defects and ensure uniform film thickness. The film was dried for 24 hours at room temperature (RT) in the saturated enclosure, followed by overnight drying under vacuum (0.3 Torr). Film thickness (ca. 250 µm) was controlled by adjusting the initial amount of cPPA in the casting solution. The cPPA films were annealed at 90 °C for 15 min to reduce any residual stresses resulting from the casting process and stored at -20 °C until further use. The annealed films were cut into 20 mm x 5 mm rectangular strips using a 90 W CO_2 laser-cutter (Full Spectrum Laser, Pro Series). The strips were cleaned with isopropyl alcohol to remove any residual monomer on the edges due to laser ablation and weighed on an analytical balance (XPE205, Mettler-Toledo, ±0.03 mg) before embedding into various host matrices.

3.2.4 Wet-spinning of cPPA fibers

Synthesized cPPA was dissolved at 30% (w/w) in different solvents and extruded inside a coagulation bath. Specifically, cPPA (1 g) was dissolved in THF (2.3 g) and vortexed overnight to create ca. 30% clear solution without any bubbles. A small amount of Nile Red dye was added to some solutions for visualization. The solution was transferred to a 5 mL glass syringe and mounted on a syringe pump (Legato 100, kd Scientific) followed by extrusion through a stainless-steel nozzle (Nordson EFD General Purpose Tips) submerged inside a measuring cylinder filled with methanol (1000 mL). Fibers with diameters ranging from 0.2 to 1.6 mm were made by varying nozzle gauges from 27 to 14. For example, a flow rate of 30 μL/min through a 22-gauge nozzle (internal diameter of 0.41 mm) yielded fibers with diameter ca. 0.4 mm. Fibers were kept submerged in methanol for ten minutes to complete the coagulation process and were subsequently dried overnight in a fume hood.

3.2.5 Solution-printing of cPPA templates

The printing ink (35% cPPA in THF) was prepared in a 3 mL syringe barrel (Optimum, Nordson EFD) and inserted into an HP3cc pneumatic dispensing tool (Nordson EFD). The barrel was fitted with a 20-gauge stainless-steel nozzle (Optimum, Nordson EFD). A custom regulator controlled the air pressure to drive the ink extrusion process.

The dispensing head was mounted on a robotic gantry (ABL9000, Aerotech Inc.) operated by a high-precision motion controller (A3200, Aerotech Inc.). A custom-designed software (RoboCAD 2.0) simultaneously controlled both the extrusion process and motion of the dispensing head. cPPA was extruded directly onto a glass plate submerged inside a methanol coagulation bath. The printed structures remained in the solvent bath for ten minutes and were subsequently removed and dried overnight in a fume hood.

3.2.6 Specimen fabrication for mass loss experiments

Sacrificial film strips (20 mm x 5 mm x 250 μm) were embedded inside a poly(dicyclopentadiene) (pDCPD) matrix using a half-casting procedure. GC2 (0.52 mg) was dispersed in toluene (200 μL) and sonicated for five minutes. The catalyst solution was transferred to a scintillation vial containing 4 g of endo-DCPD mixed with 5 wt.% ENB. 0.13 mg of GC2 per 1 g of DCPD-ENB mixture was maintained for all resin formulations. The DCPD resin (2 g) was first poured into a 50 mm diameter aluminum dish and allowed to partially gel at RT for 120 minutes. Each laser-cut cPPA strip (20.0 ± 1.0 mg) was placed on the gelled DCPD surface with a cotton swab, then allowed to adhere for 30 minutes. Another 2 g of resin was added on top of the film and the matrix was subsequently cured at RT for 24 hours, followed by another 24 hours in a 35 °C oven. Each cured specimen containing an embedded sacrificial cPPA film was cut (16 mm x 8 mm x 2 mm) using a low-speed wet saw to expose the transverse ends of the film to the surroundings.

The mass of all samples was measured before placing them in a heated vacuum oven (Jeio Tech Co. Ltd., OV-11) for VaSC experiments. Each specimen was sandwiched between two aluminum plates to ensure uniform heating. The temperature of the oven was increased from RT to the desired temperature under vacuum (0.5-1.0 Torr) and the isothermal temperature was held for 1-3 hours before cooling down to RT. The specimens were removed from the oven and their mass was measured to calculate the total mass loss after cPPA evacuation. The mass loss of neat pDCPD samples with similar dimensions as the VaSC specimens was also measured for each set of conditions.

The mass loss percentage of cPPA was determined using the following equations:

$$Mass\ loss\ (\%) = \frac{\Delta M_{cPPA}}{M_{cPPA}} * 100 \qquad 3.1$$

where ΔM_{cPPA} represents the mass loss solely due to cPPA evacuation and M_{cPPA} is the estimated mass of the cPPA strip embedded in the pDCPD sample calculated from the mass per unit length of each laser-cut rectangular film,

$$M_{cPPA} = \frac{M_i}{l_i} * l_f \qquad 3.2$$

where M_i is the initial mass, l_i is the initial length of the laser-cut cPPA strip before it was embedded inside the matrix (l_i = 20 mm), and l_f is the final length of the embedded strip after cutting the pDCPD sample.

The mass loss solely due to cPPA (ΔM_{cPPA}) is calculated:

$$\Delta M_{cPPA} = M_{before} - M_{after} - M_{DCPD} \qquad 3.3$$

where M_{before} and M_{after} are the mass of the entire pDCPD sample containing the cPPA film before and after VaSC, respectively. M_{DCPD} is the mass loss of the similarly sized neat pDCPD matrix at the specific temperature and time being evaluated.

3.2.7 Vascularization of cPPA fibers and printed templates in crosslinked matrices

Sacrificial fibers and printed structures were embedded in a pDCPD matrix using a cell casting procedure (**Scheme 2.2 in** Chapter 2). The templates were clamped between two U-shaped rubber gaskets (each 1 mm thick) attached to two rectangular glass plates. The DCPD resin mixture was carefully poured into the glass mold to cover the sacrificial templates completely and cured according to the prior procedure. Solid samples were then removed from the mold and cut using a low-speed wet saw (50 mm x 8 mm x 2 mm) to expose the transverse ends of the sacrificial components before VaSC.

Sacrificial templates were embedded in a thiol-based epoxy matrix using the same cell-casting procedure as for the pDCPD samples. However, for these samples the glass plates were coated with a PTFE release agent (MS-122AD, Miller-Stephenson) before the templates were clamped. DGOA, (7.5 g) was mixed with tetrathiol (9.9 g) at stoichiometry and stirred. Then catalyst 1 (174 mg) was added and the mixture was degassed at RT under 12 Torr vacuum for ten minutes (Yamato ADP31 drying oven, Welch 1402 pump). The resin-hardener mixture was poured into the glass mold containing the sacrificial elements and cured for 24 hours at RT. The specimens were cut with a low-speed wet saw to expose the transverse ends of the sacrificial templates for subsequent experiments.

Sacrificial templates were embedded in an amine-based epoxy matrix using the same cell-casting procedure as for the pDCPD samples. However, for these samples the glass plates were coated with a PTFE release agent (MS-122AD, Miller-Stephenson) before the templates were clamped. The resin EPON 828 (10 g) and the hardener EPIKURE 3233 (4.3 g) were mixed in a paper cup and degassed for 45 min at RT under 12 Torr vacuum (Yamato ADP31 drying oven, Welch 1402 pump). The resin-hardener mixture was poured into the glass mold and cured at RT for 24 hours, followed by 35 °C for 24 hours before cutting with a low-speed wet saw to expose the transverse ends of the sacrificial templates. These samples were then subjected to VaSC in a heated vacuum oven.

Sacrificial templates were embedded in a polydimethylsiloxane (PDMS) matrix using a cell-casting procedure similar to the epoxy matrix. The glass slides were not coated with the PTFE release agent. The PDMS prepolymer and curing agent were mixed in 10:1 ratio by weight and degassed for 10 minutes before pouring into the mold containing cPPA fibers. The samples were cured at RT for 24 hours, followed by 35 °C for 24 hours.

3.2.8 Depolymerization characterization

Molecular weights of synthesized cPPA solid, films, and fibers were obtained by analytical gel permeation chromatography (GPC) on the same system as described in Chapter 2. Each sample (10 mg) was fully dissolved in THF (1 mL), and this solution was injected via a 1 mL syringe into a 300 μL GPC vial through a 0.45 μm polytetrafluoroethylene (PTFE) filter to remove any undissolved particulates. Vials were inserted into the GPC autosampler tray and each sample was run with one injection (60 min) according to standard instrument protocol. Number and weight averaged molecular weights (M_n and M_w) were calculated using Wyatt's Astra 6 software through the integration of the signal peaks obtained from the RI detector using the latest PS calibration. All GPC analyses were performed in triplicates.

Differential scanning calorimetry (DSC) was performed with a TA instruments Discovery DSC 250. For each experiment, a 3 mg sample was measured using an analytical balance (XPE205, Mettler-Toledo) and transferred into an aluminum hermetic DSC pan at room temperature. The heat flow for each sample was obtained under a constant ramp rate of 10 °C/min up to 95 °C.

Mass loss of synthesized powder, films, and fibers (3 mg samples) in a nitrogen environment was measured on the TA instruments TGA Q500 system as described in Chapter 2. For dynamic tests, the mass loss was recorded during a heating cycle over the temperature range from 40 °C to 250 °C at a linear ramp rate of 5 °C/min. For isothermal tests, the temperature was ramped from 40 °C to 10 °C below the desired temperature at a linear ramp rate of 10 °C/min, then subsequently ramped to the desired temperature at a linear ramp rate of 5 °C/min to minimize temperature overshoot. The isothermal temperature was maintained for three to six hours for each test.

VaSC samples were polished using a glycol-based polycrystalline diamond suspension on an Allied MetPrep 3™ with PH-4™ Power Head Grinder/Polisher (Allied High Tech Products Inclusive) before optical and electron microscopy. Optical images of the pDCPD, epoxy, and PDMS samples before and after VaSC were obtained on a Keyence VHX-5000 digital microscope at 200x magnification. Scanning electron micrographs (SEM) were acquired on an FEI Quanta FEG 450 ESEM. Samples were imaged at 5 kV after sputter coating with gold/palladium for 70 s using a Denton Desk II TSC-turbo-pumped sputter coater.

Microchannels were visualized by X-ray computed microtomographic (µCT) imaging (Xradia MicroXCT-400 with TXM Controller software). µCT scans were conducted after infiltrating empty microchannels with a contrast dye (350 mg of Histodenz$^{\text{TM}}$ in 1 g DI water). Full 360° scans were obtained in rotation intervals of 0.4° with a 4x objective (5 µm per pixel) at 5 s exposure times with 40 kV (200 µA, 8W) source settings. Scan reconstructions were performed by a proprietary software and images were produced via Amira$^{\text{TM}}$ (v. 6.4.0).

3.3 Results and discussion

3.3.1 Vascularization characterization with sacrificial films

Drop-cast cPPA films were annealed and laser-cut into rectangular strips (**Figure 3.1a,b**). The mass loss of the cPPA films was monitored *ex situ* under dynamic and isothermal conditions using a thermogravimetric analyzer (TGA) (**Figure 3.2**). The depolymerization onset (T_d) of cPPA films (defined by 5% mass loss) was observed at 115 °C with complete mass loss at 140 °C in the dynamic TGA experiments at 5 °C/min (**Figure 3.2a**). In contrast, only 1% mass loss occurred for PLA films containing 3 wt. % tin (II) acetate [7] in this temperature range. Under isothermal conditions, significant mass loss of cPPA films occurred only at temperatures greater than 85 °C (**Figure 3.2b**). As the exposure temperature increased from 90 °C to 110 °C, the time required for complete mass loss decreased from 3.5 hours to less than 1 hour. The PLA films containing 3% tin (II) acetate catalyst again showed negligible mass loss after 4 hours at 110 °C (**Figure 3.2b**).

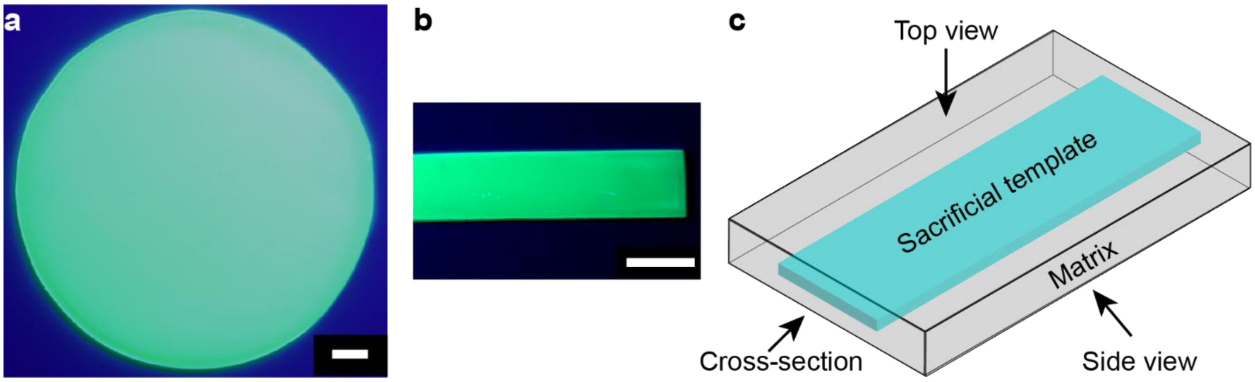

Figure 3.1. Specimen preparation for vascularization. Optical images of ca. 250 µm thick cPPA film (a) after solvent casting and (b) after laser-cutting (scale bars are 5 mm). (c) Schematic of a VaSC specimen showing a cPPA film embedded in a pDCPD matrix.

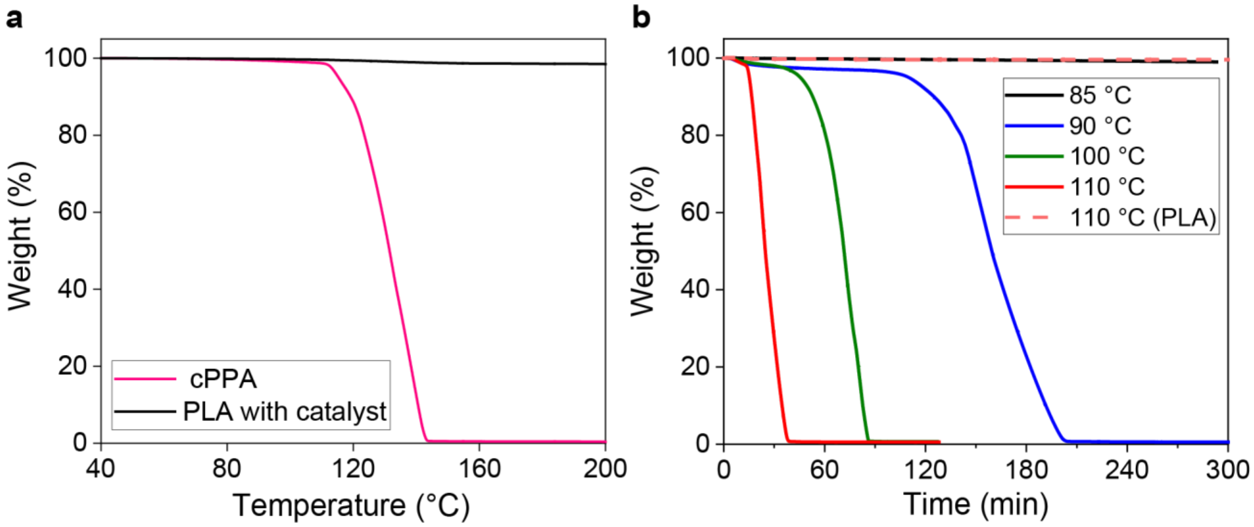

Figure 3.2. Mass loss of sacrificial polymer films under dynamic and isothermal conditions. (a) Dynamic TGA data for cPPA and PLA films at 5 °C/min showing complete mass loss of cPPA between 100 and 140 °C. PLA films containing 3 wt. % tin acetate ($Sn(Ac)_2$) catalyst did not show any mass loss in this temperature range. (b) Mass loss of cPPA films in isothermal TGA experiments. Mass loss of PLA film containing 3% $Sn(Ac)_2$ catalyst (Chapter 2) at 110 °C is indicated by the dashed red line.

Next, the cPPA films were embedded in a pDCPD matrix (**Figure 3.1c**), which will oxidize under the conditions required for vascularization with PLA templates (> 170 °C for 12 hours) [7]. The transverse ends of templates (cross-sectional view in **Figure 3.1c**) were exposed to the surrounding environment to facilitate the evacuation of gaseous monomer during the thermal cycle. Successful vascularization occurred with approximately 95% mass loss of the sacrificial template. Any small amount of residual monomer on the channel walls was easily flushed away with ethanol. Three hours of exposure at 90 °C resulted in blocked microchannels due to incomplete removal of cPPA with an average mass loss of 81% (**Figure 3.3**), which is in qualitative agreement with the mass loss data for the films alone.

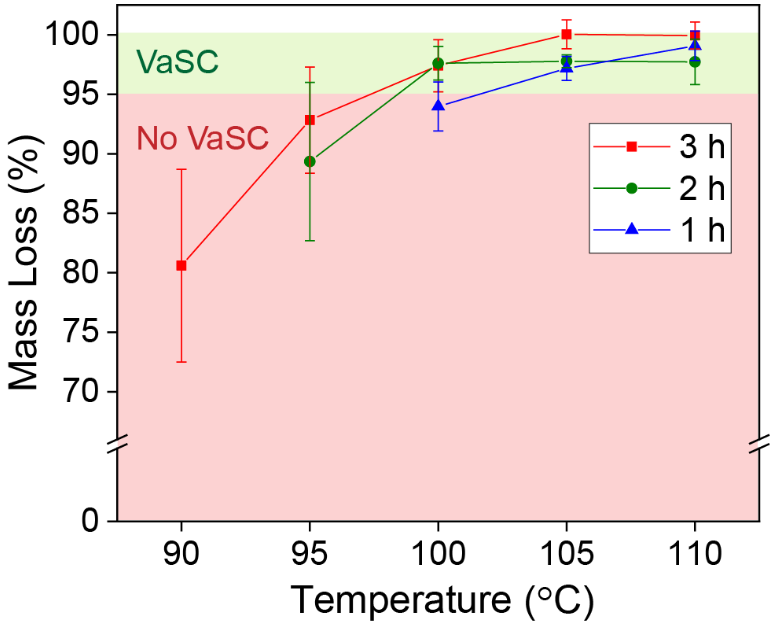

Figure 3.3. Mass loss characterization of cPPA films embedded in pDCPD matrix after vascularization in a heated vacuum oven at various times and temperatures. Mass loss of 95% or higher was deemed sufficient for successful vascularization. Error bars represent one standard deviation (n = 6).

Exposure for 3 hours at 100 °C led to successful vascularization with a mass loss of 98%. Optical and SEM images (**Figure 3.4a-d**) of the pDCPD matrix post-VaSC show residue-free microchannels with the same dimensions of the initial sacrificial cPPA templates. A dyed solution was injected into the microchannels to further confirm their clearance (**Figure 3.4b**). Specimens exposed to temperatures between 100-110 °C produced clear microchannels after a shorter duration of two hours. We were able to further reduce the exposure time to 1 hour through successful vascularization of specimens subjected to 105 °C and 110 °C, which is supported by the rapid mass loss of cPPA films at 110 °C in TGA experiments. These results show the high temperature-sensitivity of the cPPA mass loss kinetics. A marginal increase in exposure temperature from 90 to 100 °C allows complete evacuation of cPPA templates after 2 hours, and the exposure time reduces by 50% with a 5 °C increase in temperature to 105 °C. Thus, successful

VaSC with cPPA is demonstrated at significantly lower temperatures than PLA, and the VaSC time can be further lowered below 1 hour with a modest increase in temperature.

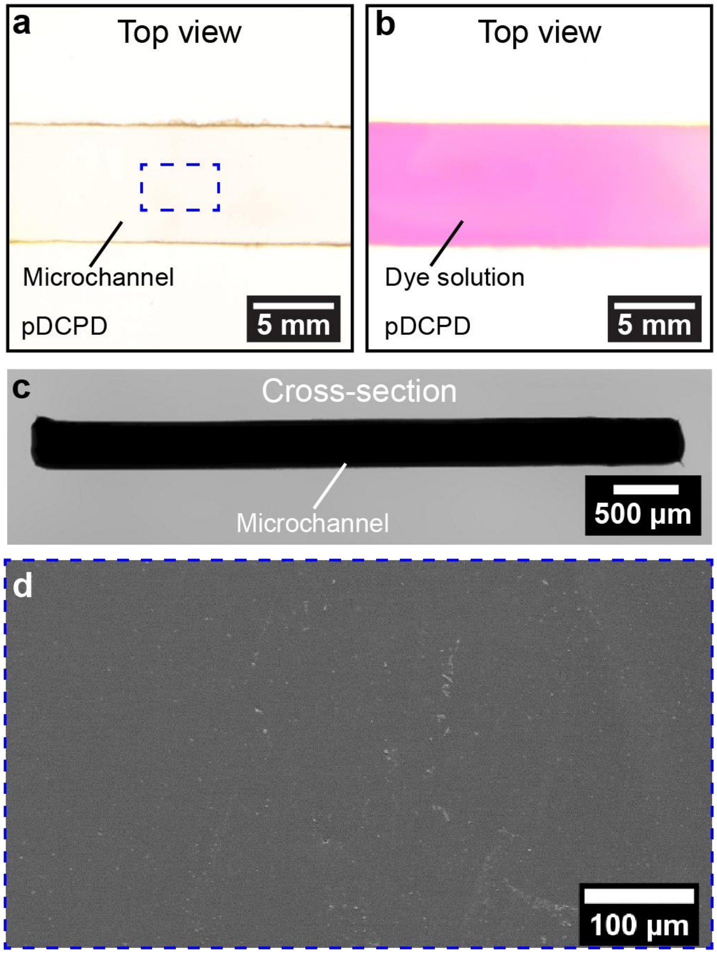

Figure 3.4. Optical and SEM images of a vascularized pDCPD sample. Optical images showing the top view of the microchannel in pDCPD matrix created (a) after VaSC of cPPA film at 100 °C for three hours and (b) after infiltration with a dye solution (Nile Red in ethanol). (c) Cross section of the rectangular channel. (d) SEM micrograph showing the surface of a microchannel. Any residual products from cPPA depolymerization were flushed away with organic solvents and no residual debris were observed inside the microchannels.

3.3.2 Low-temperature vascularization with sacrificial fibers

Since cPPA depolymerizes before observable glass or melt transition temperatures (**Figure 3.5**), solvent-based methods are required for producing sacrificial fibers. Solution-spinning methods including dry spinning and wet spinning are commonly used for polymers that cannot be melt-spun, including aramids, acrylics, and spandex [34], [35]. A range of fiber cross-sectional shapes are possible with these spinning techniques. Circular fibers are preferred for creating microchannels due to more regular fluid flow and lower stress concentrations in the host material [36]. During dry spinning, the polymer solution is extruded in a heated gas environment, which typically results in dumbbell or dog-bone shaped fiber cross-sections due to a non-uniform solvent evaporation process (see cPPA dry spinning results in **Appendix B**). In contrast, the polymer solution is extruded directly into a coagulation bath during wet spinning, allowing more control over the solvent removal process. Therefore, a wet-spinning approach [35] was adopted to form cPPA fibers with a uniform cross section (**Figure 3.6a**). A concentrated polymer solution (ca. 30 wt % cPPA in solvent) was extruded into a coagulant. Various solvent and coagulant combinations were screened for controlling the fiber cross-section. DCM and THF were employed as solvents since they are used for synthesizing cPPA. Methanol and water were used as coagulants (i.e., non-solvents) since they are used for precipitating cPPA after synthesis.

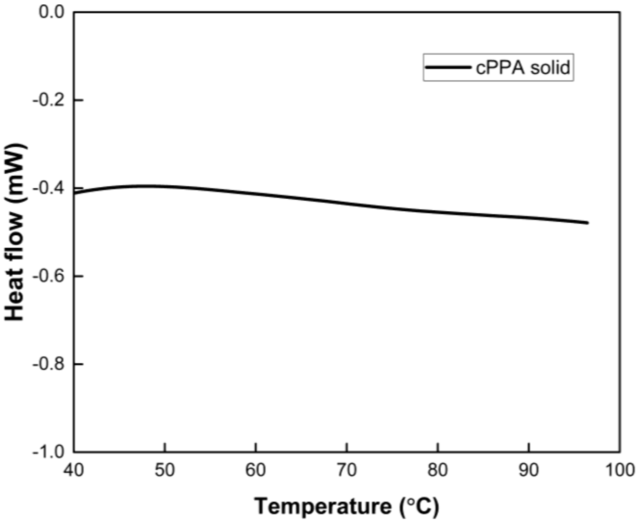

Figure 3.5. Differential scanning calorimetry of cPPA at 10 °C/min showing lack of observable glass or melt transition temperatures up to 95 °C, which limits cPPA processing to solution-based methods.

The difference in diffusion rates of the solvent exiting the fiber and counter-diffusion of non-solvent entering the fiber during coagulation plays a major role in dictating the cross-section of the freely extruded wet-spun fibers [37]. A slow coagulation process with roughly equal rates of diffusion and counter-diffusion results in a uniform fiber cross-section. In an early trial, cPPA dissolved in DCM was coagulated in a methanol bath and the resulting fibers had a bean-type cross-section without any voids (**Figure 3.6b**). This finding suggests that the fast diffusion rate of the solvent exceeded the counter-diffusion of methanol to yield a non-uniform fiber cross-section [38]. Subsequent iterations (**Figure 3.6c**) confirmed it was difficult to obtain circular fibers with DCM solvent and methanol-water solution as the coagulant. The solvent was switched to THF and fibers with a flat cross section were formed during coagulation of cPPA-THF solution in water (**Figure 3.6d**), which is likely due to predominant outward diffusion of a miscible solvent in a highly polar coagulant. When water was replaced with methanol to reduce the difference between diffusion and counter-diffusion rates, fibers with a circular cross section and a smooth surface were obtained (**Figure 3.6e**). A 50% reduction in polarity and a 12% increase in the molar volume of THF compared to DCM likely reduces its diffusion rate and facilitates a gentler coagulation process in methanol to form fibers with a uniform cross section [38], [39]. This hypothesis is also supported by a greater difference between the Hildebrand solubility parameter of methanol and THF (11.2) compared to methanol and DCM (9.5) [40]. The molecular weight of the starting cPPA was preserved after this wet-spinning step (**Table 3.1**), and the final diameter of the fibers was tuned from 0.2 to 1.6 mm by changing the nozzle diameters during extrusion.

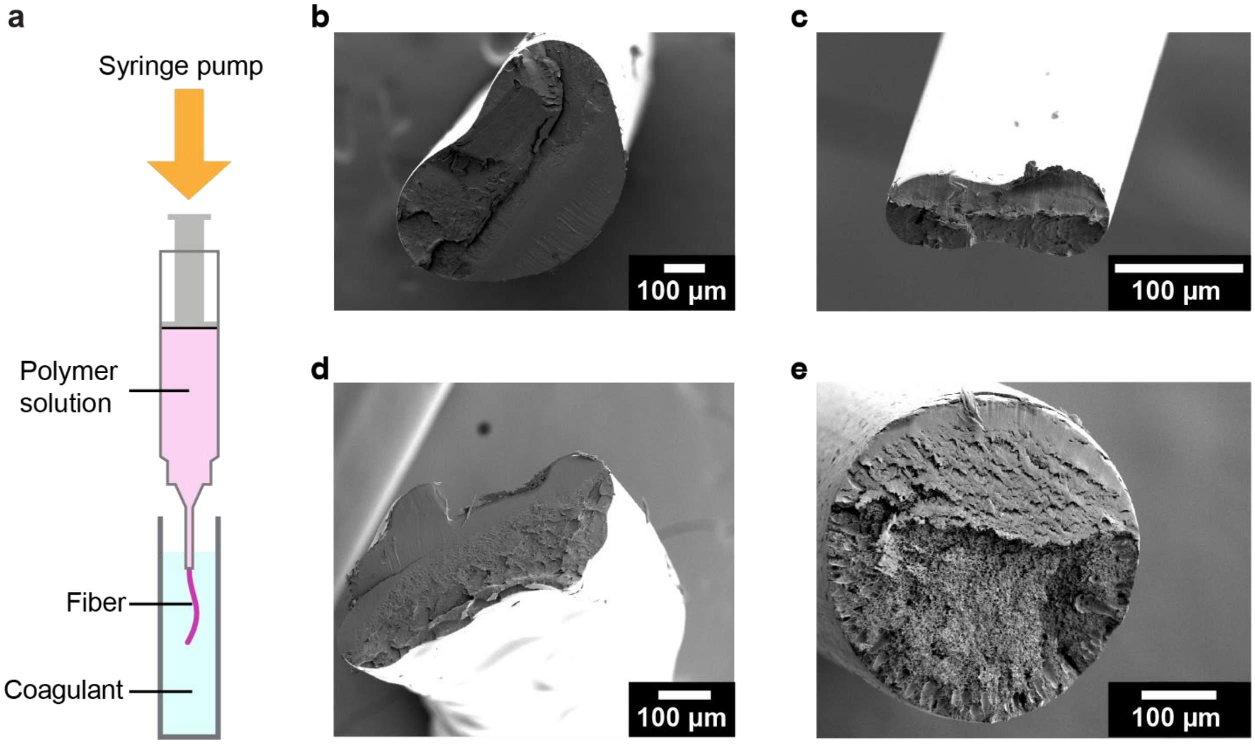

Figure 3.6. Wet spinning of sacrificial fibers with various cross-sectional shapes. (a) Schematic of the wet-spinning process in which a polymer solution containing 30 wt. % cPPA was extruded into a coagulation bath. (b-e) SEM micrographs showing cross section of wet-spun fibers with various solvent-coagulant combinations. (b) DCM as solvent and methanol as the coagulant. (c) DCM as solvent and 80:20 (v/v) methanol:water as the coagulant. (c) THF as solvent and water as the coagulant. (d) THF as solvent and methanol as the coagulant.

Table 3.1. The relative molecular weight of cPPA templates after different solvent processing routes using GPC. No significant reduction in average molecular weight was observed. Error represents one standard deviation from three different samples.

cPPA Sample	**M_w (kDa)**	**PDI**
Synthesized solid	138 ± 7	1.5
Solution-cast film	130 ± 7	1.5
Wet-spun fiber	128 ± 7	1.5

A depolymerization kinetics model [41] (**Equation 2.2**) was also developed for simulating the mass loss of cPPA fibers using dynamic TGA experiments. Since the T_d of a polymer is highly dependent on the heating rate [42], the kinetic parameters for cPPA depolymerization were extracted from three different ramp rates (**Figure 3.7**). The activation energy (*E*) of 89 kJ/mol and pre-exponential factor (*A*) of 4.4 x 10^9 s^{-1} accurately capture the mass loss behavior under various isothermal conditions (**Table 3.2**). This ~33% lower *E* compared to 133 kJ/mol for PLA containing 3% tin oxalate catalyst (shown in Chapter 2) results in rapid cPPA depolymerization at significantly lower temperatures.

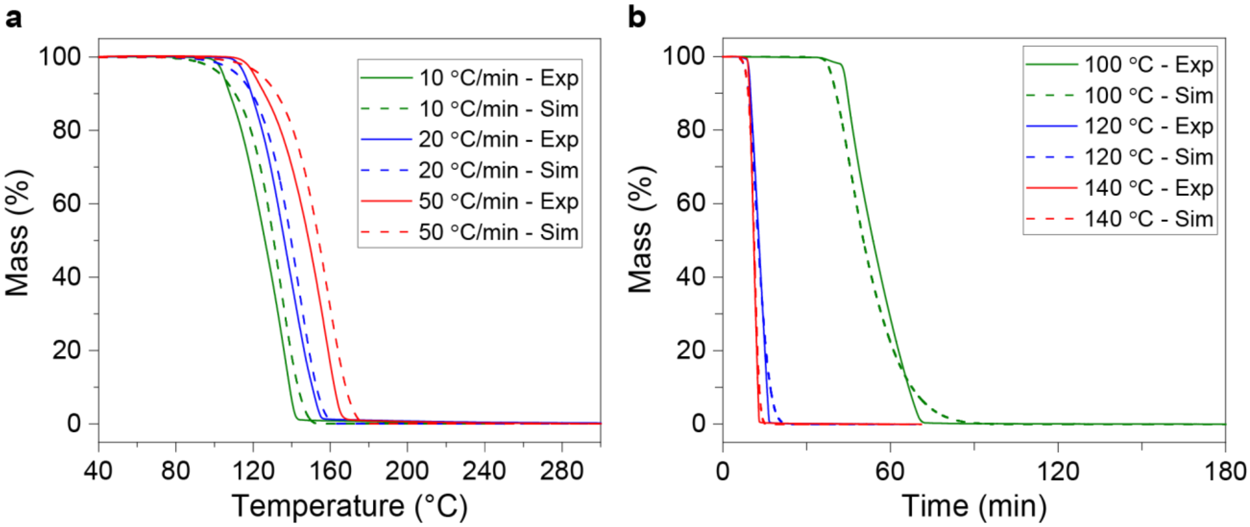

Figure 3.7. Comparison between TGA experiments (solid lines) and simulation (dashed lines) for cPPA fibers. (a) Dynamic TGA and (b) Isothermal TGA. Model optimization was performed using MATLAB. Simulation results were obtained in collaboration with Dr. Xiang Zhang.

Table 3.2. Kinetic parameters obtained using different isothermal and dynamic TGA experiments.

***E* (kJ/mol)**	***A* (s^{-1})**	***m***	***n***
89.5	4.4 x 10^9	0.23	0.81

The circular fibers as obtained in **Figure 3.6d** were embedded in a pDCPD matrix and subsequently depolymerized at 110 °C for one hour to obtain residue-free microchannels as shown in **Figure 3.8**. X-ray computed microtomographic (μCT) reconstruction of the resulting microchannels confirmed that the dimension of the channel matched well with the dimensions of the sacrificial precursor.

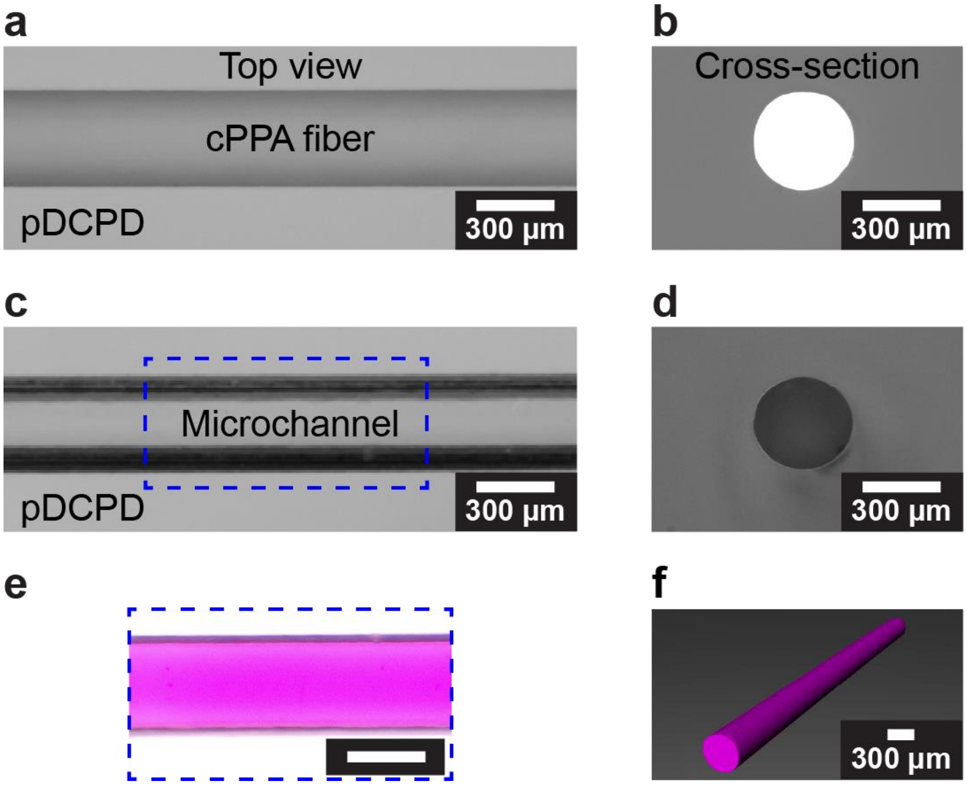

Figure 3.8. Vascularization of solution-processed cPPA fibers in p(DCPD) matrix. (a) Top and (b) cross-sectional view of a cPPA fiber embedded in the pDCPD matrix before VaSC. (c) Top and (d) cross-sectional view of a microchannel in the matrix after VaSC at 110 °C for one hour. (e) Top view of the microchannel after infiltration with a dye solution (scale bar is 300 μm) and (f) 3D reconstruction of a microchannel after infiltration with a radiocontrast fluid using X-ray microcomputed tomography (μCT).

cPPA fibers were embedded in three additional matrices with $T_g < 100$ °C (thiol-cured epoxy, amine-cured epoxy, and polydimethylsiloxane (PDMS)) (**Figure 3.9**) to further demonstrate the advantages of low-temperature vascularization. Clear microchannels after one hour at 110 °C were observed for the thiol- and amine-cured epoxy matrices with T_g ca. 42 °C and ca. 65 °C, respectively, without degradation of the host polymers (**Figure 3.10, 3.11**). Fibers embedded in clear PDMS matrix with a T_g ca. -125 °C were successfully evacuated under the same

110 °C / 1 h conditions (**Figure 3.12**). Increasing the temperature to 200 °C caused charring of the thiol-cured matrix (**Figure 3.13**), proving that sacrificial PLA is undesirable for vascularizing such matrices in short periods (< 3 h). Besides expanding vascularization to a broader range of matrices, cPPA allows substantial energy savings by cutting down the time and temperature required for the VaSC process. An estimation of the energy consumed in a 0.8 m^3 heated vacuum oven during vascularization shows a five-fold reduction in energy for evacuating cPPA templates compared to PLA (**Table 3.3**).

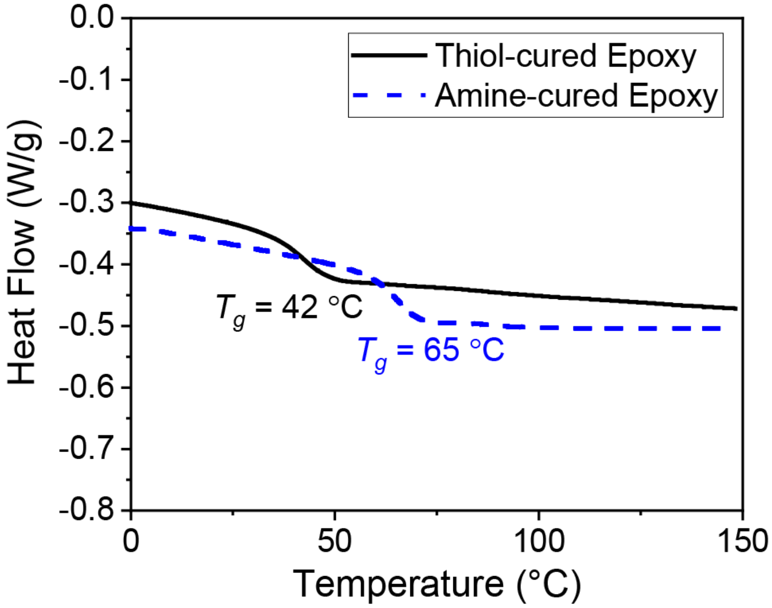

Figure 3.9. Differential scanning calorimetry on epoxy matrices at 10 °C/min.

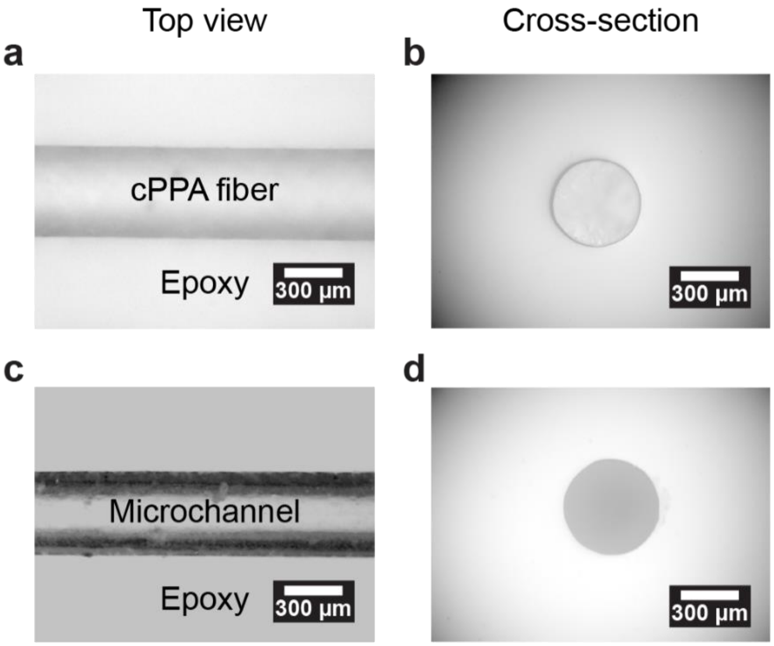

Figure 3.10. Vascularization of epoxy-based matrix cured using a thiolene-based crosslinker. (a) top and (b) cross-sectional view of a cPPA fiber embedded in the epoxy matrix before VaSC. (c) top and (d) cross-sectional view of a microchannel in the matrix after VaSC at 110 °C in 1 hour.

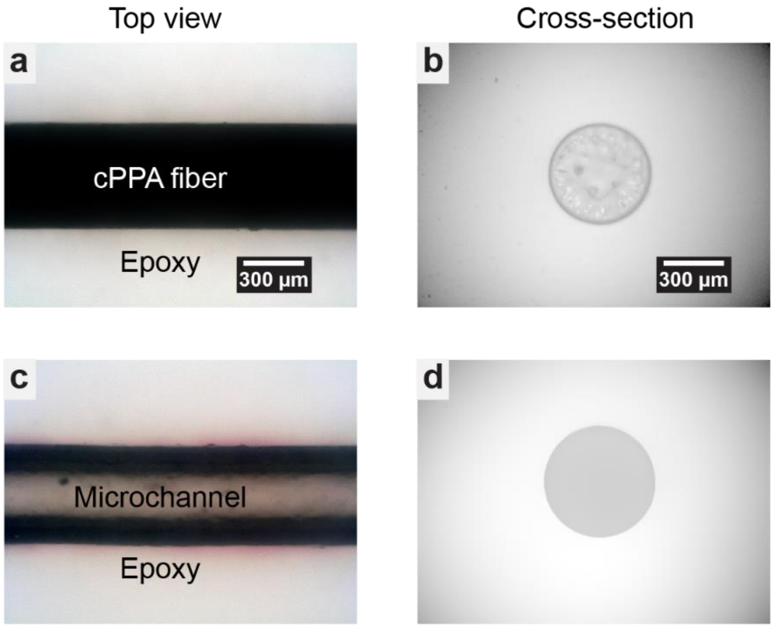

Figure 3.11. Vascularization of epoxy-based matrix cured using an amine-based crosslinker. (a) top and (b) cross-sectional view of a cPPA fiber embedded in the epoxy matrix before VaSC. (c) top and (d) cross-sectional view of a microchannel in the matrix after VaSC at 110 °C in 1 hour.

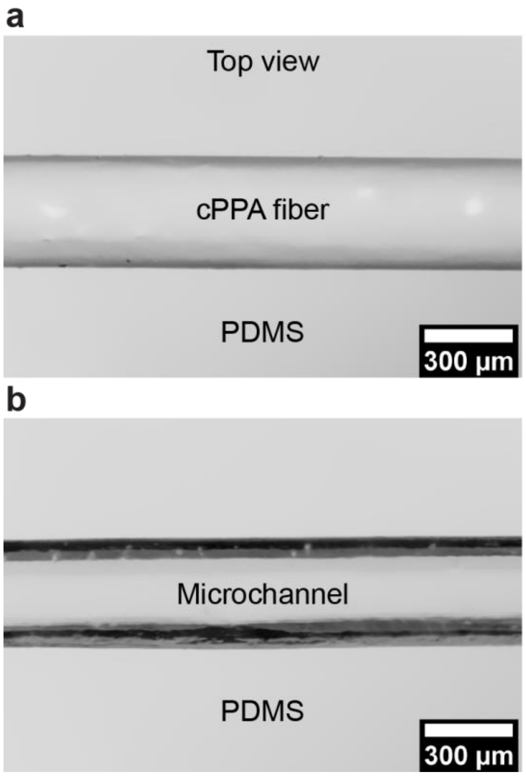

Figure 3.12. Vascularization of PDMS matrix. (a) top view of a cPPA fiber embedded in PDMS matrix before VaSC and (b) top view of a microchannel in the matrix after VaSC at 110 °C in 1 hour.

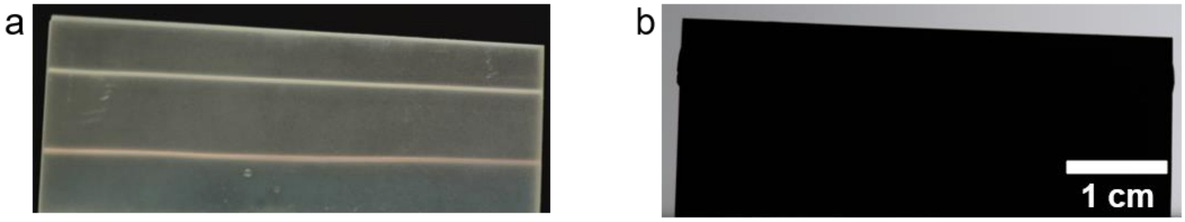

Figure 3.13. Thermal degradation of the thiol-crosslinked epoxy-based matrix after VaSC. (a) top view of the matrix with embedded PLA (top) and cPPA (bottom) fibers before VaSC. (b) top view of a charred matrix after VaSC at 200 °C for 12 hours.

Table 3.3. Energy estimation for vascularization cycles of PLA and cPPA (VaSC cycle and oven details in **Appendix A**)

Sacrificial Polymer	**Heating Step**	**Energy Consumption Rate (kWh/min)**[5]	**Step time (min)**	**Energy (MJ)**	**Total energy (MJ)**
PLA	Ramp	0.046	120	19.9	82.1
	Dwell	0.024	720	62.2	
cPPA	Ramp	0.046	60	9.9	15.1
	Dwell	0.024	60	5.18	

$$Energy\ consumption\ ratio\ for\ PLA\ vs.cPPA\ VaSC = \frac{82.1}{15.1} = 5.4$$

3.3.3 Low-temperature VaSC with printed sacrificial templates

3D-printing of cPPA can overcome the templating challenges of solvent-cast films, achieve multi-dimensionality beyond 1D fibers, and provide a scalable approach with fine control over template dimensions. Precision in channel dimensions becomes especially critical in microfluidic applications since the volumetric flow rate scales inversely with the fourth power of channel diameter [2]. Here we successfully demonstrate the planar printing of sacrificial cPPA. The direct ink writing setup, resembling a wet-spinning process, extrudes cPPA solution (35% in THF) onto a glass slide submerged in a methanol bath (**Figure 3.14a**). The concentrated cPPA solution adheres to the glass slide upon extrusion and sets into the printed shape upon solvent diffusion. cPPA was printed in a zig-zag pattern for demonstration (**Figure 3.14b**). Two zig-zag templates were overlaid and embedded in a thiol-cured epoxy matrix (**Figure 3.14c**). This specimen was vascularized at 110 °C for one hour, and the resulting microchannels were filled with dyed ethanol solution (**Figure 3.14d**). The two microchannels were interconnected at the overlapping regions where the sacrificial templates made physical contact before casting/evacuation. This demonstrates a viable method for creating 2.5D/3D vasculatures by printing planar templates separately and stacking them before resin infusion. Realizing free-form 3D cPPA templates will require a viscoplastic coagulant which can mechanically support the print while also facilitating uniform diffusion of the solvent from the extruded solution [43], [44]. A print bath with these desired features will allow the integration of complex sacrificial templates inside polymers and composites for manufacturing multifunctional vascular structures.

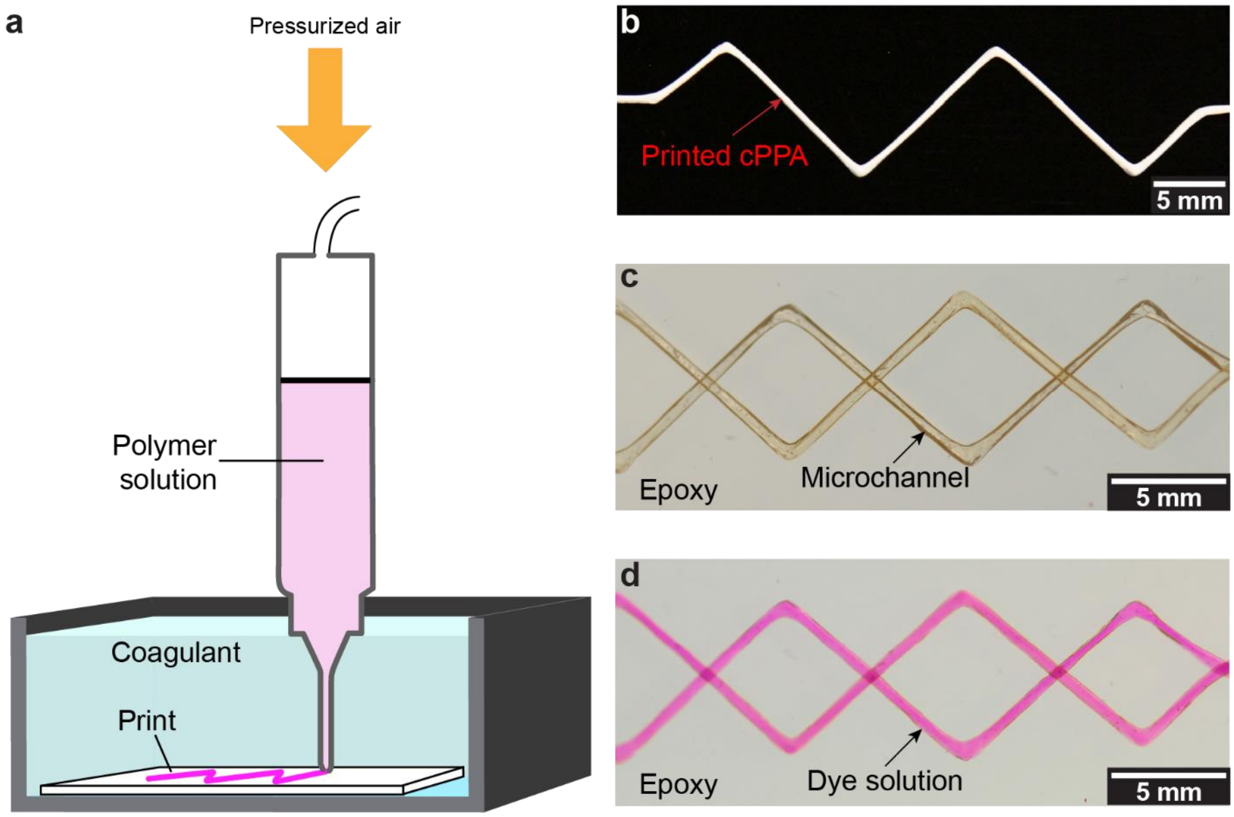

Figure 3.14 Printed cPPA templates for vascularization of a room temperature-cured epoxy matrix. (a) Solvent-cast printing of a polymer solution containing a 35 wt.% cPPA into a coagulation bath. (b) Solvent-cast printed template using tetrahydrofuran (THF) as solvent and methanol as coagulant. (c) Top view of microchannels in epoxy matrix after VaSC of two printed sacrificial templates at 110 °C for 1 hour. (d) Top view of the channels filled with a dye solution (Nile Red in ethanol) after VaSC.

3.3.4 Challenges with cPPA as a sacrificial polymer

Solution processing of cPPA has certain limitations related to the mechanical integrity of the sacrificial templates. Fibers made with wet spinning have voids distributed in the core (**Figure 3.15**), which make them susceptible to fracture during bending at small radii of curvature. These voids are likely caused by the formation of solvent pockets during fiber coagulation, which is an issue for making fibers greater than tens of microns in diameter [38]. Even though the tensile strength of cPPA films (> 23 MPa [23], [32]) suggests that they can be integrated into a fiber-reinforced polymer composite (FRPC) [4], cPPA fibers cannot be woven into a fabric reinforcement for making vascular composites due to brittle fracture. To overcome this challenge, attempts were made to thermally process cPPA by blending it with plasticizers but they proved to be largely unsuccessful due to severe thermal depolymerization during processing (see **Appendix B**). Another sacrificial polymer that can be thermally processed into robust fibers and printed architectures is needed to circumvent the above integration challenges, which has been explored in the next chapter.

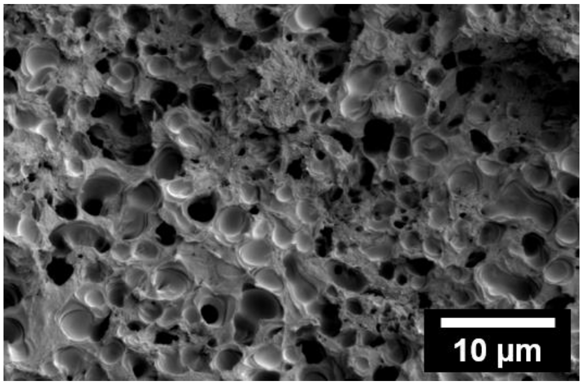

Figure 3.15. Cross-section of a wet-spun of sacrificial fibers (THF as the solvent and methanol as the coagulant) at higher magnification compared to **Figure 3.6e** shows 0.5-5 μm diameter voids present throughout the bulk of the fiber.

3.4 Summary

Internal microvascular architectures were created by rapid depolymerization of cPPA templates resulting in a five-fold reduction in thermal energy consumption compared to existing sacrificial polymers. Transient cPPA templates with varied size scales and dimensionality were fabricated by employing different solvent-exchange methods on concentrated polymer solutions. The cross section and morphology of the transient templates were tuned by changing the diffusion rate of the solvent in the coagulation bath. Complete depolymerization and vaporization of cPPA templates without the need for additional catalysts was observed within 1-3 hours near 100 °C in both *ex situ* TGA experiments and *in situ* vascularization experiments with templates embedded in host matrices (**Figure 3.16**). Even though a narrow temperature range is explored for successful vascularization in this chapter, a further reduction is VaSC time is possible with slight increases in temperature, as suggested by TGA experiments and modeling. Optical, SEM, and micro-CT characterization confirmed that the microchannels were residue-free after an ethanol rinse. Thus, cPPA expands the scope of vascularization to matrices with low glass transition temperatures (< 150 °C), such as thiol- and amine-crosslinked epoxies cured at room temperature. We aim to extend this low-temperature VaSC technique via 3D-printing to manufacture interconnected microvasculature in structural polymers and composites that resemble biological fluidic networks. This advancement hinges on obtaining mechanically robust templates that can survive the thermomechanical loads present during the fabrication of such host structures. The development of new processing routes to make complex cPPA templates may also find use in transient substrates for textiles and electronics applications.

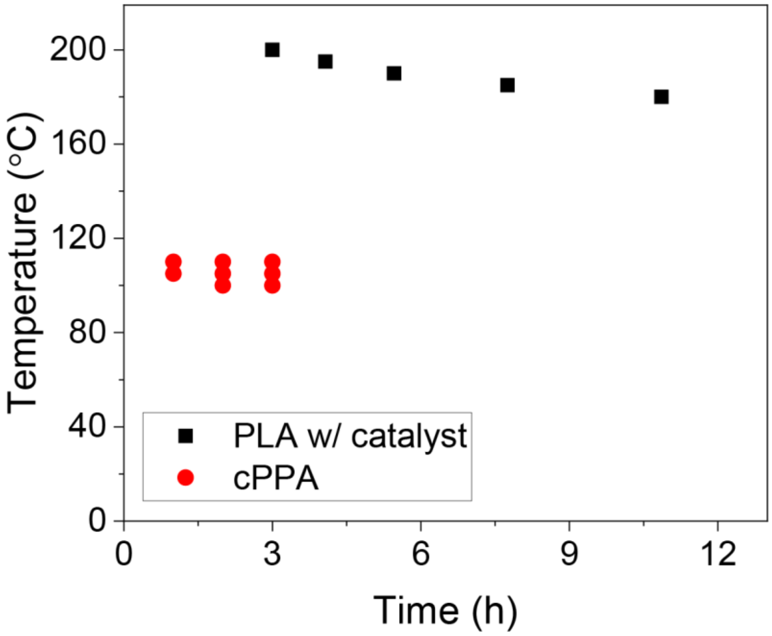

Figure 3.16. Successful VaSC protocols for cPPA showing significantly milder temperature conditions are required with this new sacrificial polymer compared to PLA.

3.5 References

[1] J. F. Patrick *et al.*, “Continuous Self-Healing Life Cycle in Vascularized Structural Composites,” *Advanced Materials*, vol. 26, no. 25, pp. 4302–4308, 2014, doi: 10.1002/adma.201400248.

[2] R. C. R. Gergely *et al.*, “Multidimensional Vascularized Polymers using Degradable Sacrificial Templates,” *Advanced Functional Materials*, vol. 25, no. 7, pp. 1043–1052, 2014, doi: 10.1002/adfm.201403670.

[3] J. F. Patrick *et al.*, “Robust sacrificial polymer templates for 3D interconnected microvasculature in fiber-reinforced composites,” *Composites Part A: Applied Science and Manufacturing*, vol. 100, pp. 361–370, 2017, doi: 10.1016/j.compositesa.2017.05.022.

[4] A. P. Esser-Kahn *et al.*, “Three-Dimensional Microvascular Fiber-Reinforced Composites,” *Advanced Materials*, vol. 23, no. 32, pp. 3654–3658, 2011, doi: 10.1002/adma.201100933.

[5] R. A. Witik, F. Gaille, R. Teuscher, H. Ringwald, V. Michaud, and J.-A. E. Månson, “Economic and environmental assessment of alternative production methods for composite aircraft components,” *J Clean Prod*, vol. 29, pp. 91–102, 2012, doi: 10.1016/j.jclepro.2012.02.028.

[6] H. Dong *et al.*, “Chemical Treatment of Poly(lactic acid) Fibers to Enhance the Rate of Thermal Depolymerization,” *ACS Applied Materials & Interfaces*, vol. 4, no. 2, pp. 503–509, 2012, doi: 10.1021/am2010042.

[7] M. Garg, S. R. White, and N. R. Sottos, “Rapid Degradation of Poly(lactic acid) with Organometallic Catalysts,” *Acs Appl Mater Inter*, vol. 11, no. 49, pp. 46226–46232, 2019, doi: 10.1021/acsami.9b17599.

[8] T. J. Spencer, Y.-C. Chen, R. Saha, and P. A. Kohl, “Stabilization of the Thermal Decomposition of Poly(Propylene Carbonate) Through Copper Ion Incorporation and Use in Self-Patterning,” *Journal of Electronic Materials*, vol. 40, no. 6, pp. 1350–1363, 2011, doi: 10.1007/s11664-011-1518-z.

[9] M. S. Baker, H. Kim, M. G. Olah, G. G. Lewis, and S. T. Phillips, “Depolymerizable poly(benzyl ether)-based materials for selective room temperature recycling,” *Green Chemistry*, vol. 17, no. 9, pp. 4541–4545, 2015, doi: 10.1039/c5gc01090j.

[10] B. Fan, J. F. Trant, R. E. Yardley, A. J. Pickering, F. Lagugné-Labarthet, and E. R. Gillies, “Photocontrolled Degradation of Stimuli-Responsive Poly(ethyl glyoxylate): Differentiating Features and Traceless Ambient Depolymerization,” *Macromolecules*, vol. 49, no. 19, pp. 7196–7203, 2016, doi: 10.1021/acs.macromol.6b01620.

[11] J.-B. Zhu, E. M. Watson, J. Tang, and E. Y. X. Chen, “A synthetic polymer system with repeatable chemical recyclability,” *Science*, vol. 360, no. 6387, pp. 398–403, 2018, doi: 10.1126/science.aar5498.

[12] A. M. Dilauro, A. Abbaspourrad, D. A. Weitz, and S. T. Phillips, “Stimuli-Responsive Core–Shell Microcapsules with Tunable Rates of Release by Using a Depolymerizable Poly(phthalaldehyde) Membrane,” *Macromolecules*, vol. 46, no. 9, pp. 3309–3313, 2013, doi: 10.1021/ma400456p.

[13] Y. Zhang, L. Ma, X. Deng, and J. Cheng, “Trigger-responsive chain-shattering polymers,” *Polymer Chemistry*, vol. 4, no. 2, pp. 224–228, 2013, doi: 10.1039/c2py20838e.

[14] S. Tang, M. Yourdkhani, C. M. P. Casey, N. R. Sottos, S. R. White, and J. S. Moore, “Low-Ceiling-Temperature Polymer Microcapsules with Hydrophobic Payloads via Rapid Emulsion-Solvent Evaporation.,” *ACS Applied Materials & Interfaces*, vol. 9, no. 23, pp. 20115–20123, 2017, doi: 10.1021/acsami.7b05266.

[15] E. Uzunlar, J. Schwartz, O. Phillips, and P. A. Kohl, “Decomposable and Template Polymers: Fundamentals and Applications,” *Journal of Electronic Packaging*, vol. 138, no. 2, pp. 020802–15, 2016, doi: 10.1115/1.4033000.

[16] A. M. DiLauro and S. T. Phillips, “End-capped poly(4,5-dichlorophthalaldehyde): a stable self-immolative poly(aldehyde) for translating specific inputs into amplified outputs, both in solution and the solid state,” *Polym Chem-uk*, vol. 6, no. 17, pp. 3252–3258, 2015, doi: 10.1039/c5py00190k.

[17] S. T. Phillips, J. S. Robbins, A. M. DiLauro, and M. G. Olah, “Amplified responses in materials using linear polymers that depolymerize from end-to-end when exposed to specific stimuli,” *J Appl Polym Sci*, vol. 131, no. 19, p. n/a-n/a, 2014, doi: 10.1002/app.40992.

[18] G. G. Lewis, J. S. Robbins, and S. T. Phillips, “A prototype point-of-use assay for measuring heavy metal contamination in water using time as a quantitative readout,” *Chemical Communications*, vol. 50, no. 40, pp. 5352–5354, 2014, doi: 10.1039/c3cc47698g.

[19] A. Sagi, R. Weinstain, N. Karton, and D. Shabat, “Self-Immolative Polymers,” *Journal of the American Chemical Society*, vol. 130, no. 16, pp. 5434–5435, 2008, doi: 10.1021/ja801065d.

[20] G. I. Peterson, M. B. Larsen, and A. J. Boydston, “Controlled Depolymerization: Stimuli-Responsive Self-Immolative Polymers,” vol. 45, no. 18, pp. 7317–7328, 2012, doi: 10.1021/ma300817v.

[21] W. Seo and S. T. Phillips, “Patterned Plastics That Change Physical Structure in Response to Applied Chemical Signals,” *Journal of the American Chemical Society*, vol. 132, no. 27, pp. 9234–9235, 2010, doi: 10.1021/ja104420k.

[22] J. P. Lutz, O. Davydovich, M. D. Hannigan, J. S. Moore, P. M. Zimmerman, and A. J. McNeil, "Functionalized and Degradable Polyphthalaldehyde Derivatives," *J Am Chem Soc*, vol. 141, no. 37, pp. 14544–14548, 2019, doi: 10.1021/jacs.9b07508.

[23] E. M. Lloyd *et al.*, "Fully Recyclable Metastable Polymers and Composites," *Chem Mater*, vol. 31, no. 2, pp. 398–406, 2018, doi: 10.1021/acs.chemmater.8b03585.

[24] A. M. Feinberg *et al.*, "Cyclic Poly(phthalaldehyde): Thermoforming a Bulk Transient Material," *ACS Macro Letters*, vol. 7, no. 1, pp. 47–52, 2018, doi: 10.1021/acsmacrolett.7b00769.

[25] A. M. Feinberg *et al.*, "Triggered Transience of Plastic Materials by a Single Electron Transfer Mechanism," *Acs Central Sci*, vol. 6, no. 2, pp. 266–273, 2020, doi: 10.1021/acscentsci.9b01237.

[26] H. L. Hernandez *et al.*, "Accelerated Thermal Depolymerization of Cyclic Polyphthalaldehyde with a Polymeric Thermoacid Generator," *Macromol Rapid Comm*, vol. 39, no. 11, p. 1800046, 2018, doi: 10.1002/marc.201800046.

[27] H. L. Hernandez *et al.*, "Triggered Transience of Metastable Poly(phthalaldehyde) for Transient Electronics," *Advanced Materials*, vol. 26, no. 45, pp. 7637–7642, 2014, doi: 10.1002/adma.201403045.

[28] C. W. Park *et al.*, "Thermally triggered degradation of transient electronic devices.," *Advanced Materials*, vol. 27, no. 25, pp. 3783–3788, 2015, doi: 10.1002/adma.201501180.

[29] C. E. Diesendruck *et al.*, "Mechanically triggered heterolytic unzipping of a low-ceiling-temperature polymer," *Nature Chemistry*, vol. 6, no. 7, pp. 623–628, 2014, doi: 10.1038/nchem.1938.

[30] J. A. Kaitz, C. E. Diesendruck, and J. S. Moore, "End group characterization of poly(phthalaldehyde): surprising discovery of a reversible, cationic macrocyclization mechanism.," *Journal of the American Chemical Society*, vol. 135, no. 34, pp. 12755–12761, 2013, doi: 10.1021/ja405628g.

[31] K. M. Lee, O. Phillips, A. Engler, P. A. Kohl, and B. P. Rand, "Phototriggered Depolymerization of Flexible Poly(phthalaldehyde) Substrates by Integrated Organic Light-Emitting Diodes," *Acs Appl Mater Inter*, vol. 10, no. 33, pp. 28062–28068, 2018, doi: 10.1021/acsami.8b08181.

[32] H. L. Hernandez *et al.*, "Processing-dependent mechanical properties of solvent cast cyclic polyphthalaldehyde," *Polymer*, vol. 162, no. J. Am. Chem. Soc. 135 2013, pp. 29–34, 2019, doi: 10.1016/j.polymer.2018.12.016.

[33] G. Yang and J. K. Lee, “Curing Kinetics and Mechanical Properties of endo - Dicyclopentadiene Synthesized Using Different Grubbs’ Catalysts,” *Ind Eng Chem Res*, vol. 53, no. 8, pp. 3001–3011, 2014, doi: 10.1021/ie403285q.

[34] Y. Imura, R. M. C. Hogan, and M. Jaffe, “10 Dry spinning of synthetic polymer fibers,” 2014, pp. 187–202.

[35] B. Ozipek and H. Karakas, “Wet spinning of synthetic polymer fibers,” 2014, pp. 174–186.

[36] C. J. Norris, I. P. Bond, and R. S. Trask, “Interactions between propagating cracks and bioinspired self-healing vascules embedded in glass fibre reinforced composites,” *Composites Science and Technology*, vol. 71, no. 6, pp. 847–853, 2011, doi: 10.1016/j.compscitech.2011.01.027.

[37] Y.-X. Wang, C.-G. Wang, Y.-J. Bai, and Z. Bo, “Effect of the drawing process on the wet spinning of polyacrylonitrile fibers in a system of dimethyl sulfoxide and water,” *Journal of Applied Polymer Science*, vol. 104, no. 2, pp. 1026–1037, 2007, doi: 10.1002/app.24793.

[38] J. P. Knudsen, “The Influence of Coagulation Variables on the Structure and Physical Properties of an Acrylic Fiber,” *Textile Research Journal*, vol. 33, no. 1, pp. 13–20, 1963, doi: 10.1177/004051756303300103.

[39] B. H. Ji, “Study on the Mass Transfer Process in Pan Wet-Spinning,” *Materials Science Forum*, vol. 650, pp. 336–342, 2010, doi: 10.4028/www.scientific.net/msf.650.336.

[40] A. F. M. Barton, “CRC Handbook of Solubility Parameters and Other Cohesion Parameters,” 2017, doi: 10.1201/9781315140575.

[41] P. Das and P. Tiwari, “Thermal degradation kinetics of plastics and model selection,” *Thermochimica Acta*, vol. 654, pp. 191–202, 2017, doi: 10.1016/j.tca.2017.06.001.

[42] T. J. Spencer and P. A. Kohl, “Decomposition of poly(propylene carbonate) with UV sensitive iodonium salts,” *Polymer Degradation and Stability*, vol. 96, no. 4, pp. 686–702, 2011, doi: 10.1016/j.polymdegradstab.2010.12.003.

[43] A. K. Grosskopf, R. L. Truby, H. Kim, A. Perazzo, J. A. Lewis, and H. A. Stone, “Viscoplastic Matrix Materials for Embedded 3D Printing,” *Acs Appl Mater Inter*, vol. 10, no. 27, pp. 23353–23361, 2018, doi: 10.1021/acsami.7b19818.

[44] J. T. Muth *et al.*, “Embedded 3D Printing of Strain Sensors within Highly Stretchable Elastomers,” *Adv Mater*, vol. 26, no. 36, pp. 6307–6312, 2014, doi: 10.1002/adma.201400334.

CHAPTER 4

ORTHOGONALLY-TRIGGERED SACRIFICIAL THERMOPLASTICS FOR LOW-TEMPERATURE VASCULARIZATION

4.1 Introduction

A major challenge to the successful fabrication of vascular thermosets and fiber-reinforced polymer composites (FRPCs) with complex microchannel architectures is the selection of a suitable sacrificial polymer. A polymer that can be processed into thermomechanically stable sacrificial templates for seamless integration into the host, yet depolymerizes rapidly at a temperature below the minimum VaSC temperature for PLA (ca. 160 °C) is required to reduce the energy and time needed for vascularization. As discussed in Chapter 3, cPPA satisfies the depolymerization criteria but it is difficult to process into mechanically robust templates. Thermoplastics that can be templated into desired architectures and remain stable until triggered to depolymerize with an orthogonal stimulus are promising sacrificial candidates for low-temperature VaSC.

Poly(propylene carbonate) (PPC) is an amorphous sacrificial thermoplastic with a glass transition temperature (T_g) between 25-46 °C [1] that has been used as a template for the fabrication of air cavities in microelectronic devices [2]. While thermal depolymerization of neat PPC occurs at relatively high temperatures (> 200 °C) [3], [4], acid- and base-catalyzed depolymerization of solvent-cast PPC films initiates at temperatures between 100-200 °C [5], [6]. The high acid sensitivity of PPC combined with its low softening temperature provides an opportunity to process robust templates that can be depolymerized at much lower temperatures than sacrificial PLA. Melt extrusion of PPC blended with an acid-based catalyst into fibers and 3D printed templates is not feasible due to the risk of severe depolymerization within the processing range (150-200 °C) [3]. In contrast, UV-triggered thermal depolymerization of solution-processed films [2], [5]–[14] and electrospun fiber mats (tens of microns in size) [15] blended with a latent photoacid generator (PAG) catalyst has been demonstrated previously. Although, most PAGs are unstable at the temperatures required for PPC processing [5], [9], a diaryliodonium-based photoacid generator (PAG) (commercially known as Rhodorsil-FABA) remains stable up to ca. 180 °C [2], [5], [7], [9]–[11], [14], [16]–[18]. This PAG has other advantages including high acidic strength and very low vapor pressure [5] [19], which facilitate complete depolymerization of PPC into propylene carbonate (PC) monomer (**Scheme 4.1**).

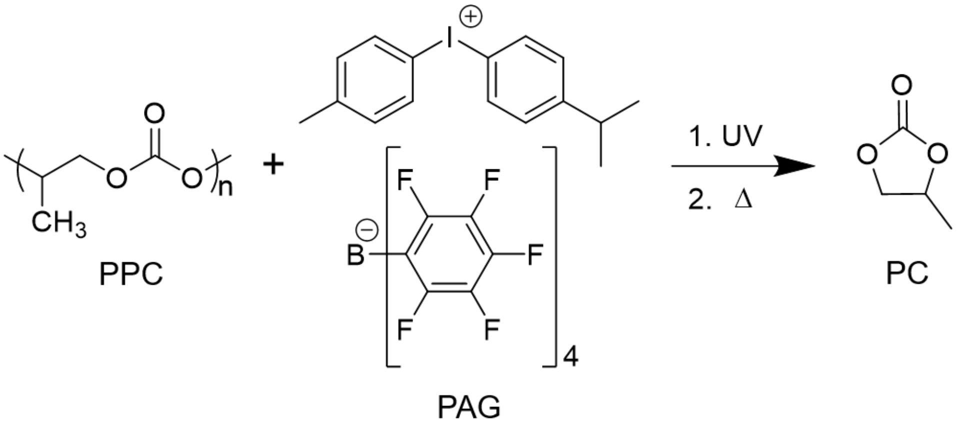

Scheme 4.1. UV-triggered thermal depolymerization of poly(propylene carbonate) (PPC) into propylene carbonate (PC) monomer.

In this chapter, depolymerization of melt-processed sacrificial PPC fibers and filaments blended with a UV-sensitive PAG is investigated. Mass loss of these templates after acid activation is characterized using a thermogravimetric analyzer (TGA). A depolymerization kinetics model is also developed to obtain a quantitative comparison of kinetic parameters with other sacrificial polymers discussed in previous chapters. Finally, sacrificial fibers are embedded into several low glass transition temperature host matrices and tested for successful VaSC at different temperatures and times.

4.2 Materials and methods

4.2.1 Materials

Poly(propylene carbonate) (PPC) pellets were acquired from Novomer. 4-Methylphenyl[4-(1-methylethyl)phenyl]iodonium tetrakis(pentafluorophenyl)borate photoacid generator (PAG), commercially known as Rhodorsil-FABA, was gifted by Bluestar Silicones. Anhydrous dichloromethane (DCM), pentaerythritol tetrakis(3-mercaptopropionate) (tetrathiol), N,N-diglycidyl-4-glycidyoxyaniline (DGOA), (dimethylaminomethyl) phenol (catalyst 1) were all purchased from Sigma Aldrich and used as received. EPON 828 and EPIKURE 3233 were obtained from Hexion. Clear PDMS (Sylgard 184) was purchased from DOW Corning. Polytetrafluoroethylene (PTFE) Petri dish liners were purchased from Welch Fluorocarbon Inc.

4.2.2 Solvent casting films containing latent catalyst

Films (thickness ca. 400 μm) were prepared under dark-room conditions using a similar solvent-casting setup as reported in Chapter 3. 10 mg PAG powder (1 wt. % w.r.t to PPC) was added to a glass vial containing 1 g of PPC pellets and the solids were dissolved in 6 mL DCM for 30 minutes on a vortexing machine. Films were air-dried for two days at room temperature (RT) and dissolved in acetonitrile (ACN) solvent to achieve a PAG concentration of 0.3 mg/mL for UV-vis spectroscopy. The dried films were laser cut into rectangular strips and stored in a freezer before running TGA experiments.

4.2.3 Melt-compounding PPC with PAG

Melt-blending of PPC with PAG was performed below 160 °C to minimize acidic depolymerization of PPC through thermal activation of the PAG during processing. Neat PPC pellets were blended with 1% - 3% PAG in a twin-screw melt compounder (Type Six, C.W. Brabender® Instruments). The twin-screw chamber was heated to 140 °C after which 40 g of PPC pellets were added to the chamber while rotating the mixing blades at 15 RPM until completely melted (ca. 10 min). The desired amount of PAG powder (per wt. % of PPC) was slowly added and then mixed at 45 RPM for 5 min. The melt-compounded material was removed from the chamber and cut into small pieces while still soft (with scissors) and allowed to cool to RT.

4.2.4 Melt-extrusion of sacrificial fibers and filaments

Sacrificial fibers and filaments were produced using a modified lab-scale melt-spinning apparatus (extruder). The blended polymer (20 g) was fed into a steel barrel and melted at 155 °C for 10 minutes. A polytetrafluoroethylene (PTFE) disc followed by a brass-capped steel piston was inserted into the top opening of the barrel to prevent the melted polymer from sticking to the piston. The sacrificial polymer was extruded through a 1.25 mm diameter spinneret at 3 g min^{-1} by mechanically advancing the piston. A metal pulley translated laterally and guided the extruded fiber to wrap uniformly around a spool mounted on an 88-mm diameter winding reel. The surface speed of the take reel was adjusted to control the final diameter of the fiber. For example, a surface speed of 120 m min^{-1} produced roughly 200 m of 400-μm diameter fiber. The sacrificial filaments (~2.85-mm diameter) were extruded through the same apparatus under the same temperature settings by replacing the smaller spinneret with a 2.5-mm diameter spinneret connected to 75-mm long hollow brass extension. The extruded filament entered a 1 m tall water column at RT instead of winding on a take-up drum. The filaments were vacuum dried at 40 °C for 24 hours before feeding into the 3D printer.

4.2.5 *UV Irradiation of sacrificial templates*

Activation of the PAG was carried out on an IntelliRay UV0320 parabolic flood curing system (Unitron International). Sacrificial films (20 mm x 5 mm x 400 µm) or fibers (15 cm long and 400-600 µm diameter) were placed on an aluminum foil. The fibers were taped at the ends to prevent shrinking during irradiation. The foil was secured on an adjustable metal shelf 75 mm below the lamp such that all the fibers were within the area projected by the lamp. The fibers were irradiated for a total of 10 min at 100% power (6-8 J cm^{-2} at 280 nm). The templates were flipped after 5 min to promote complete penetration of the UV light through the thickness of the polymer. The templates were either used immediately after irradiation or stored at -20 °C in a lightproof box until use.

4.2.6 *Depolymerization characterization*

Molecular weights of pellets and fibers were obtained via analytical gel permeation chromatography (GPC) on a system composed of a Waters (1515) Isocratic high-pressure liquid chromatography pump, a Waters (2414) Refractive Index Detector, a Waters (2707) 96-well autosampler, and a series of 4 Waters HR Styragel columns (7.8 x 300 mm, HR1, HR3, HR4, and HR5) in tetrahydrofuran (THF) at 30 °C. The GPC was calibrated using monodisperse polystyrene standards. Differential scanning calorimetry (DSC) was performed on a TA instruments Discovery DSC 250. Thermal depolymerization via mass loss of sacrificial templates (3 mg samples) in a nitrogen environment was measured on a TGA (Q500, TA instruments) equipped with an evolved gas analysis furnace. For dynamic tests, the mass loss was recorded during a heating cycle over the temperature range from 40 °C to 250 °C at a linear ramp rate of 1-100 °C/min. For isothermal tests, the temperature was ramped from 40 °C to 10 °C below the desired temperature at a linear ramp rate of 10 °C/min, then subsequently ramped to the desired temperature at a linear ramp rate of 5 °C/min to minimize temperature overshoot. The isothermal temperature was maintained for 3-6 hours for each test. Evolution of DCM (mass/charge (m/z) of 83 AMU), and PC (m/z of 87 AMU), corresponding to the mass loss observed in TGA traces, were monitored in real time with mass spectroscopy (MS) using a TA Instruments Discovery Mass Spectrometer. The mass spectrometer included a quadrupole detector equipped with a closed ion source, triple mass filter, and a dual (Faraday and secondary electron multiplier) detection system. The mass spectrometer and TGA were coupled with a heated transfer line maintained at 300 °C.

4.2.7 Specimen fabrication for VaSC experiments

PPC (1% - 3% PAG) fibers were irradiated with UV light (**Scheme 4.2**) followed by embedding in various host matrices using the same cell casting procedure mentioned in previous chapters. Specimens with fibers that were not irradiated with UV light were also fabricated as a control case. Successful vascularization for each time and temperature was determined after the thermal treatment of a separate set of specimens for each test in a heated vacuum oven (Jeio Tech Co. Ltd., OV-11). A steel wire (ca. 200 µm) and ethanol solution dyed with Nile Red were passed through the resulting channel after VaSC to determine successful vascularization. For vascularization experiments with a PDMS matrix, three specimens each containing three PPC (1% PAG) fibers, were tested for VaSC at different temperatures (40-100 °C) and times (1-12 h). For thiol-cured and amine-cured epoxy matrices, one 1% PAG and one 3% PAG fiber were embedded in each specimen to compare the influence of higher acid concentration on successful vascularization.

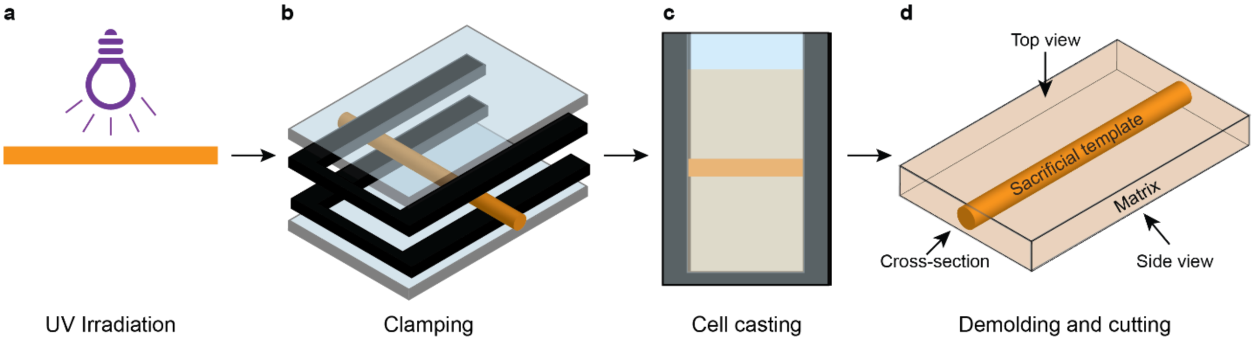

Scheme 4.2. Cell casting sacrificial templates in the thermoset matrix for vascularization experiments. (a) UV irradiation of a sacrificial PPC fiber (orange) to activate the latent catalyst. (b) Exploded isometric view of a fiber clamped by two rubber spacers (black) sandwiched between two glass plates (translucent blue). (c) Liquid resin (translucent brown) is poured into the cell casting mold to encapsulate the fiber. (d) The cured specimen is cut into shape with the transverse ends of the template exposed to the surrounding environment for VaSC experiments.

4.2.8 Microchannel visualization

VaSC samples were polished using a glycol-based polycrystalline diamond suspension on an Allied MetPrep 3™ with PH-4™ Power Head Grinder/Polisher (Allied High Tech Products Inclusive) before optical and electron microscopy. Optical images of the pDCPD, epoxy, and PDMS samples before and after VaSC were obtained on a Keyence VHX-5000 digital microscope at 200x magnification. Scanning electron micrographs (SEM) were acquired on an FEI Quanta FEG 450 ESEM. Samples were imaged at 5 kV after sputter coating with gold/palladium for 70 s using a Denton Desk II TSC-turbo-pumped sputter coater.

4.3 Results and discussion

4.3.1 Depolymerization characterization of sacrificial films

The thermal stability of PPC (1% PAG) films before and after UV irradiation was investigated to select suitable melt extrusion conditions that would not cause thermal depolymerization. First, we compared the absorbance spectra of the polymer and the PAG alone. As shown in **Figure 4.1a**, the PAG absorbed significantly, and PPC absorption was minimal in the 250-300 nm wavelength range. In prior work, UV irradiation of 1-4 J/cm^2 at 250 nm led to full activation of the PAG in films with different thicknesses (10-100 μm) [5], [9]. Since the thickness of PPC films in this work was much higher, the films were subjected to UV irradiation of 6-8 J/cm^2 (estimated at 280 nm based on instrument spectrum) and flipped half-way through UV exposure to ensure maximum activation of the PAG.

In subsequent TGA tests (**Figure 4.1b**), neat PPC films showed initial mass loss due to PC monomer at 200 °C (confirmed by the MS signal) followed by complete mass loss near 250 °C. In films containing latent PAG without UV irradiation, monomer mass loss began at 180 °C, which is attributed to thermal activation of PAG near this temperature, followed by a complete mass loss at 210 °C. In contrast, the UV-irradiated sacrificial PPC (1% PAG) films depolymerized completely into gaseous products below 150 °C. These results indicate that non-irradiated PPC blended with PAG can be melt extruded into stable sacrificial templates at processing temperatures less than 180 °C without triggering depolymerization.

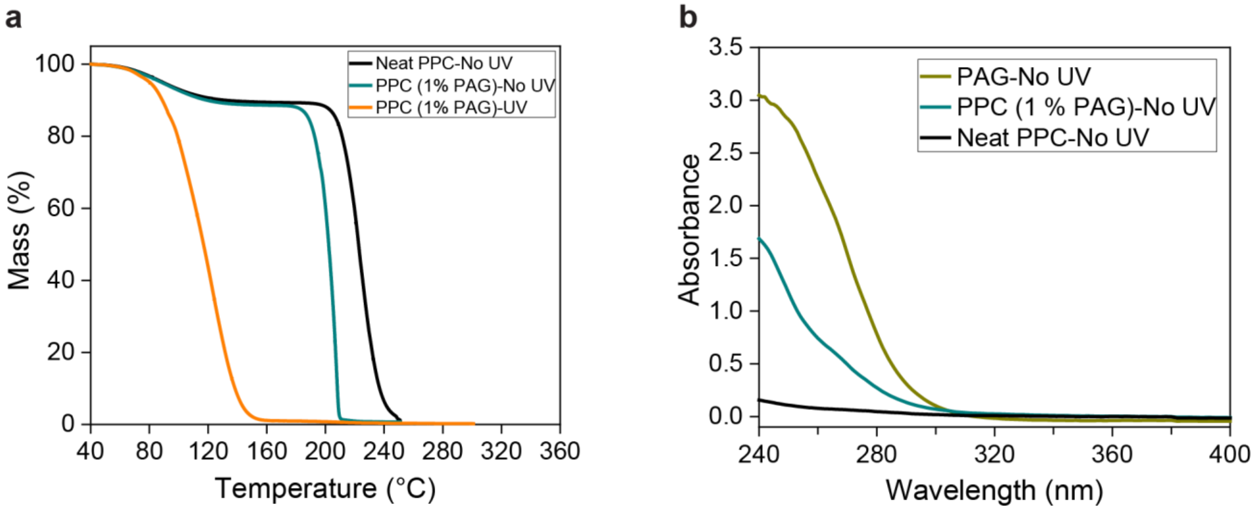

Figure 4.1. UV induced thermal depolymerization of sacrificial PPC: (a) UV absorbance of PPC blended with PAG, (b) dynamic TGA of PPC films at 2 °C/min (NI- not irradiated, I-irradiated with UV light). An initial mass loss plateau ca. 12% was seen in non-irradiated neat and 1% PAG films, due to loss of residual DCM, was confirmed by MS signal of the evolved gas in the mass spectrometer connected to the TGA.

4.3.2 Photo-triggered depolymerization of melt-extruded templates

The high thermal stability of the PAG allows the melt spinning of sacrificial PPC fibers and filaments in a custom melt spinning setup (**Figure 4.2a**). Approximately 200 m of PPC fiber containing 1% PAG was easily wound on a spool and bent around a relatively tight radius of curvature (< 5 mm) without any fracture (**Figure 4.2b**). Fibers had a circular cross-section (ca. 400 µm in diameter) without any voids (**Figure 4.2c**). Fibers with 3% PAG were also extruded with a similar cross-section (ca. 550 µm in diameter), mechanical integrity, and molecular weights.

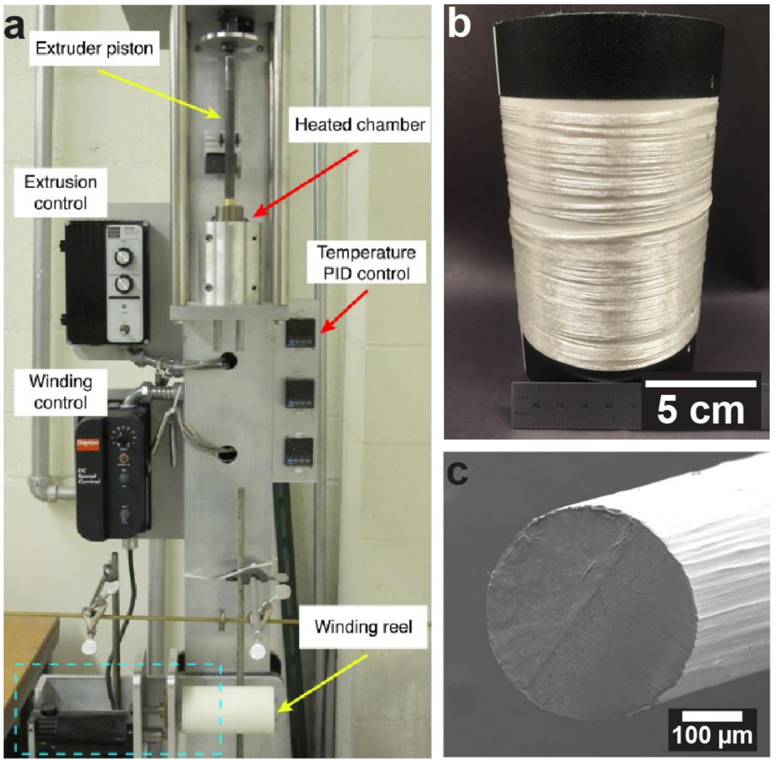

Figure 4.2. Melt spinning sacrificial PPC fibers: (a) a custom melt-spinning setup, (b) spool with PPC fibers, (c) SEM of a PPC fiber with a circular cross-section.

Fibers without any PAG were also produced using the same thermal processing cycle to investigate any thermal depolymerization effects. Molecular weights of both the neat fibers and PAG containing fibers were unchanged after melt extrusion (**Figure 4.3**). The glass transition temperature (T_g) of the PPC (1% PAG) fibers (**Figure 4.4**) was also close to that of the pellets (ca. 38 °C).

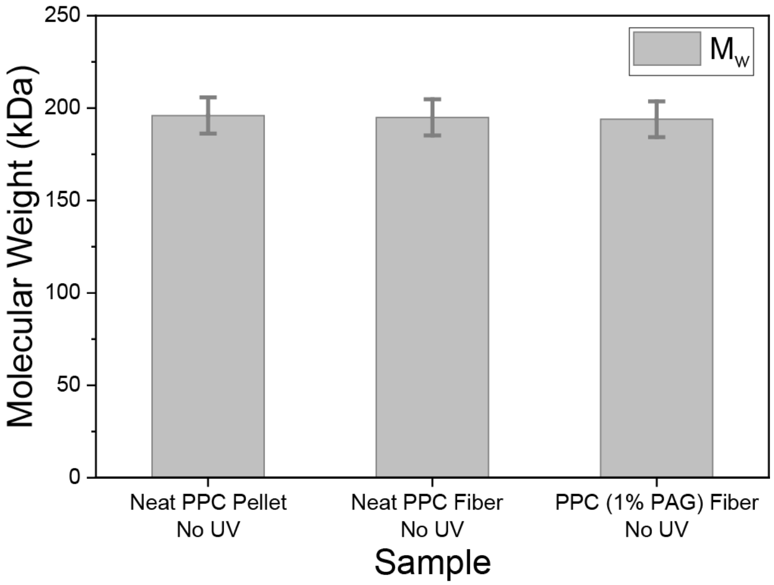

Figure 4.3. Gel permeation chromatography (GPC) of PPC samples at various stages of processing shows the thermal latency of the PAG during fiber spinning. No significant difference in weight averaged molecular weight between neat PPC pellet, melt-spun neat PPC fiber, and melt-spun PPC (1% PAG) fiber (155 °C for 15 minutes) is observed. Error bars represent one standard deviation (n =3)

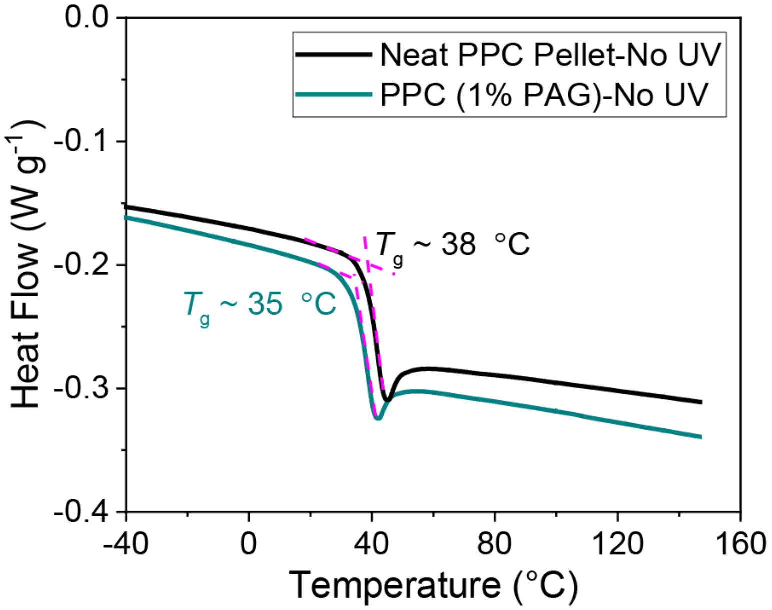

Figure 4.4. DSC at 5 °C min^{-1} showing a T_g of 38 °C for neat PPC pellets and 35 °C for PPC (1% PAG) fibers. Negative numbers on the y-axis indicate an endothermic process.

As shown in **Figure 4.5**, the depolymerization onset temperature (T_d, defined by 5% mass loss) of as-spun PPC (1% PAG) fibers occurred at 200 °C with complete mass loss at 230 °C, likely due to thermal activation of the PAG. In contrast, the T_d of UV-irradiated fibers was much lower (T_d ~ 93 °C) with complete mass loss at 130 °C, which is ca. 100 °C lower compared to PPC (1% PAG) fibers without UV-facilitated acid activation. Fibers with 3% PAG showed a negligible difference in the onset and complete mass temperatures.

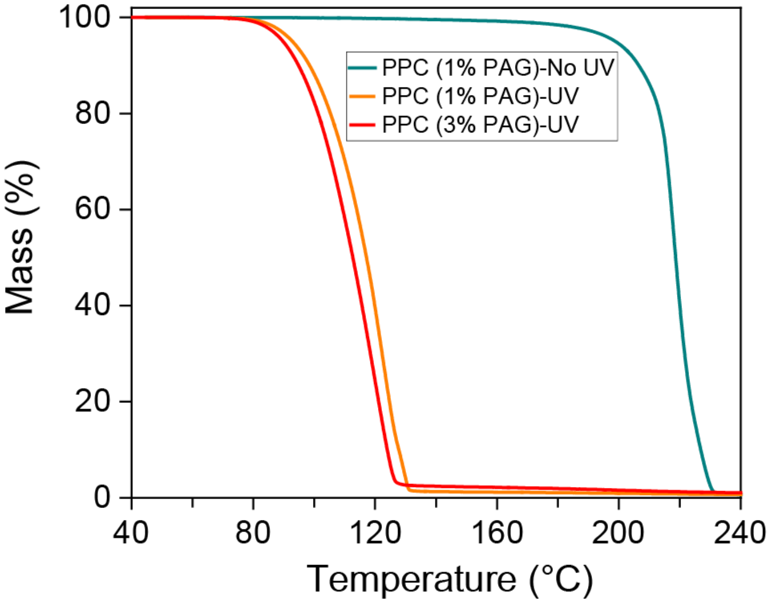

Figure 4.5. Thermal depolymerization of PPC fibers in dynamic thermogravimetric analysis (TGA) at 5 °C min^{-1} showing a ~100 °C difference in the mass loss temperatures for as-spun and UV-irradiated 1% PAG fibers.

Isothermal TGA was performed to better resolve the effect of PAG concentration and guide the temperature-time conditions for future vascularization experiments. PPC (1% PAG) fibers fully volatilized in 30 minutes at 100 °C (**Figure 4.6**) and 90 minutes at 80 °C, which is faster than the cPPA templates in Chapter 3 (isotherms at lower temperatures in **Appendix B**). PPC (1% PAG) fibers without UV irradiation did not show any mass loss after exposure to 100 °C for 30 minutes, and no reduction in molecular weight of the thermally cycled fibers was observed in GPC experiments either. At 60 °C, only 80% mass loss was observed after 360 minutes and a mere 11% mass loss occurred after 720 minutes (longest test time) at 50 °C for UV-irradiated PPC (1% PAG) fibers. Even though complete mass loss did not occur at these low temperatures, a brown-colored gum-like residue was collected from the TGA pans and transferred to GPC vials to check the molecular weight of the samples after this thermal cycling. Mostly low molecular weight (< 1 kDa) and monomeric products were seen in the GPC signals, suggesting that the slow depolymerization of PPC and low evaporation rate of the PC monomer (boing point (T_b) ca. 242 °C [22]) were responsible for incomplete mass loss at these temperatures. This incomplete depolymerization could also result from the neutralization of the protonic acid by ether linkages in the polymer backbone. Commercial PPC contains 1-10% ether linkages that can consume the acid by terminating the polymer chains with an alcoholic group during backbone scission and prevent regeneration of the catalyst [2], [9]. When the catalyst concentration was increased to 3% PAG, an approximately two-fold decrease in time for the complete mass loss was observed at 100 °C and at 60 °C, complete mass loss was achieved in 120 minutes. The mass loss plateaued at the initial PAG concentration for all isothermal TGA experiments as the PAG remains non-volatile under these mild temperatures. These isothermal experiments indicate that PPC (1% PAG) has a much lower vascularization temperature compared to cPPA (ca. 100 °C).

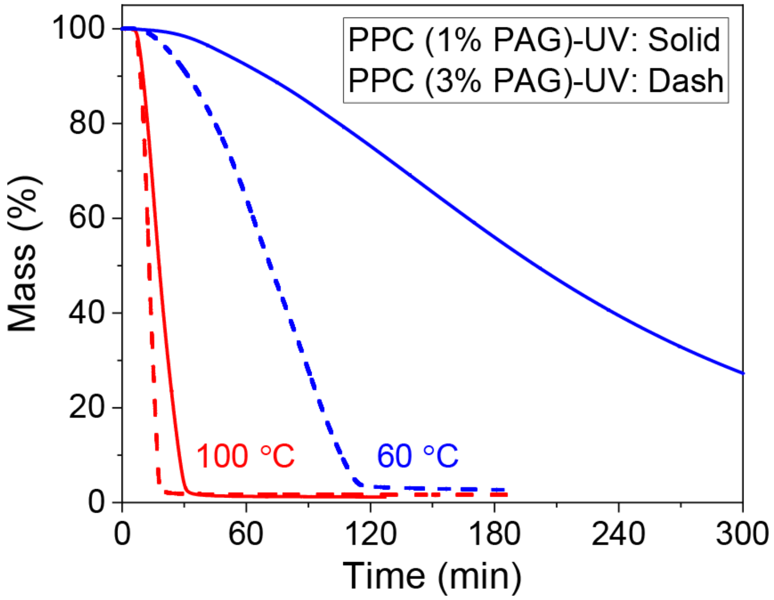

Figure 4.6. Mass loss of UV-irradiated PPC fibers with 1% and 3% PAG under isothermal TGA conditions.

A depolymerization kinetics model [23] (**Equation 2.2**) was also developed based on three dynamic ramp rates (2, 5, and 10 °C/min) for simulating the mass loss of PPC (1% PAG) fibers (**Figure 4.7**). Instrument limitations caused a nonlinear increase in furnace temperature from 40 to 100 °C for high ramp rates (> 40 °C/min), and the same temperature profile was used in corresponding simulations. The activation energy (*E*) of 110 kJ/mol and pre-exponential factor (*A*) of 4.0 x 10^{12} s^{-1} (**Table 4.1**) accurately capture the mass loss behavior under experimental conditions. This ca. 12 kJ/mol reduction in *E* and two orders of magnitude increase in *A* compared to PLA containing 3% tin acetate catalyst (shown in Chapter 2) promotes PPC depolymerization at significantly lower temperatures in much shorter time periods. The PAG has a melting point in the 120-133 °C range, which would lead to better dispersion of the catalyst in the PPC fibers during compounding and melt extrusion cycles with a substantially higher surface area compared to solvent-based blending without dissolution/melting of catalyst in PLA films. The activation energy is higher compared to metastable cPPA with an extremely low ceiling temperature (-36 °C).

However, the increase in the pre-exponential factor due to the presence of catalyst allows PPC depolymerization within the maximum isothermal TGA time (12 hours) at lower temperatures than possible with cPPA.

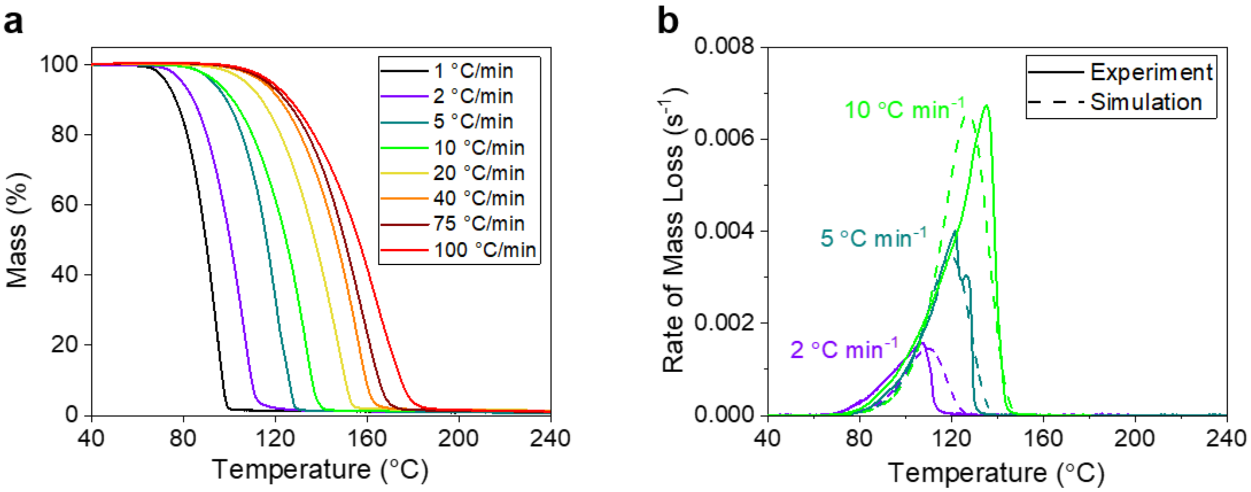

Figure 4.7. Modeling of depolymerization kinetics. (a) Dynamic TGA at various ramp rates for UV-irradiated PPC (1% PAG) fibers. (b) Depolymerization kinetics model using dynamic TGA data at three different ramp rates. Model optimization was performed using MATLAB. Simulation results were obtained in collaboration with Dr. Xiang Zhang.

Table 4.1. Kinetic parameters for sacrificial polymers obtained using different isothermal and dynamic TGA experiments.

Polymer	***E* (kJ/mol)**	***A* (s^{-1})**	***m***	***n***
PLA (3 % Sn(Ac)$_2$)	122.0	4.2 x 10^{10}	0.33	0.12
cPPA	89.5	4.4 x 10^{9}	0.23	0.81
PPC (1% PAG)	110.0	4.0 x 10^{12}	0.21	0.94

4.3.3 Low-temperature vascularization with sacrificial fibers

Vascularization experiments were carried out between 40-100 °C in 10 °C increments for a maximum time of 12 hours with sacrificial fibers embedded in three different low T_g matrices (PDMS (ca. -125 °C), thiol-cured epoxy (ca. 42 °C), and amine-cured epoxy (ca. 65 °C)). For UV-irradiated PPC (1% PAG) fibers in the PDMS matrix, clear microchannels were obtained after 1 hour at 100 °C (**Figure 4.8**). When the thermal cycling time was increased to three hours, successful vascularization was achieved at temperatures $\geq$ 70 °C (**Figure 4.9**). Incomplete depolymerization of the fibers caused obstructed microchannels after three hours at 60 °C. Increasing the time to six hours resulted in microchannels containing a gum-like residue that was easily flushed with ethanol to get clear channels. A direct correlation between TGA and VaSC protocols is difficult because a nitrogen environment is present in the TGA, and vascularization under vacuum changes the evaporation rate of the PC monomer. A further decrease in temperature to 50 °C led to partially clear channels after six hours, but increasing the treatment time to twelve hours and washing the gum-like residue with ethanol resulted in unobstructed channels. Lowering the thermal treatment temperature to 40 °C for twelve hours resulted in unsuccessful vascularization. For all test conditions, PPC (1% PAG) fibers without UV exposure remained intact inside the matrix. The VaSC temperature for PPC (1% PAG) is reduced by almost 50 °C compared to cPPA.

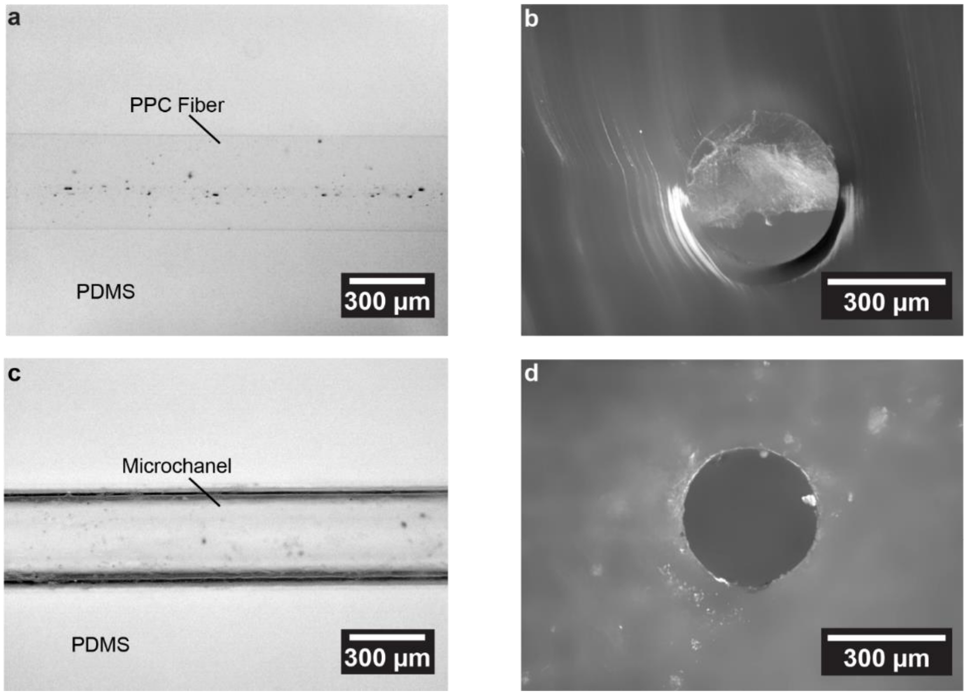

Figure 4.8. Vascularization of melt-spun PPC (1% PAG) fibers in PDMS matrix. (a) Top and (b) cross-sectional view of a PPC fiber embedded in the PDMS matrix before VaSC. (c) Top and (d) cross-sectional view of a microchannel in the matrix after VaSC at 100 °C for one hour.

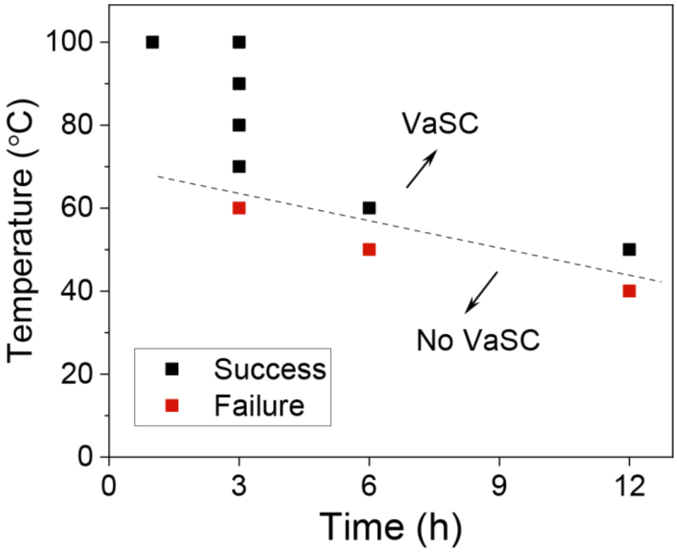

Figure 4.9. Successful VaSC conditions for PPC (1%PAG) fibers embedded in the PDMS matrix after the thermal treatment cycle in a vacuum oven at various times and temperatures. Three specimens, each with three embedded fibers, were used for each test and channel clearance was verified by passing a steel wire and flushing ethanol through the microchannel.

Vascularization experiments were also performed in thiol- and amine-cured epoxy-based host matrices with UV-irradiated PPC (1% PAG) and PPC (3% PAG) fibers. Contrary to the results for a PDMS matrix in **Figure 4.9**, PPC (1% PAG) fibers did not fully depolymerize and channels remained obstructed after one hour at 100 °C in both the epoxy matrices. We hypothesize that uncured/partially cured resin or hardener might neutralize the acidic hydrogen ions in the PPC template, which are responsible for continuing the depolymerization reaction, but further investigation is required. In contrast, PPC (3% PAG) fibers successfully evacuated after the same treatment cycle to leave a small amount of residue in the microchannel walls that was easily removed with an ethanol rinse (**Figure 4.10, Figure 4.11**). Successful vascularization with higher catalyst concentration is likely due to the formation of more hydrogen ions compared to the neutralizing effects of the epoxy matrix.

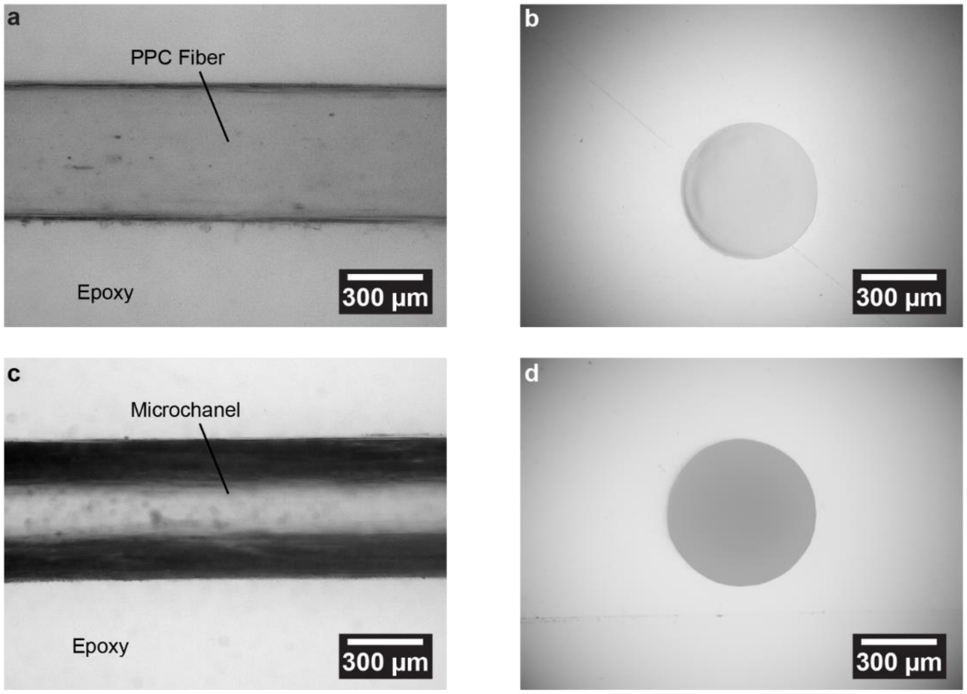

Figure 4.10. Vascularization of melt-spun PPC (3% PAG) fibers in an epoxy-based matrix cured using a thiolene-based crosslinker. (a) Top and (b) cross-sectional view of a PPC fiber embedded in the matrix before VaSC. (c) Top and (d) cross-sectional view of a microchannel in the matrix after VaSC at 100 °C for one hour.

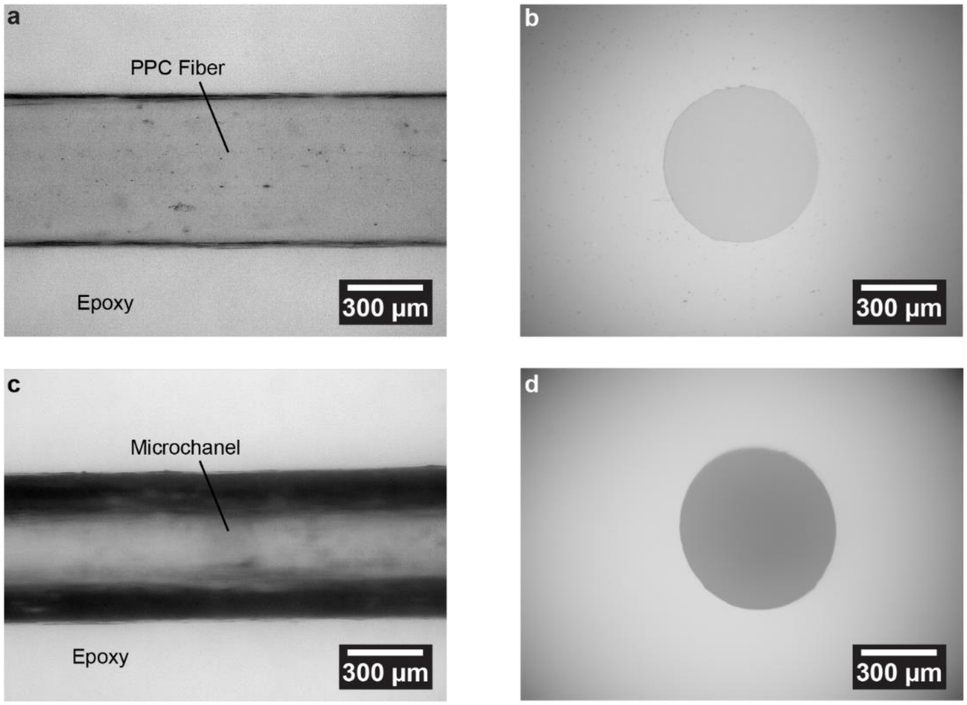

Figure 4.11. Vascularization of melt-spun PPC (3% PAG) fibers in an epoxy-based matrix cured using an amine-based crosslinker. (a) Top and (b) cross-sectional view of a PPC fiber embedded in the matrix before VaSC. (c) Top and (d) cross-sectional view of a microchannel in the matrix after VaSC at 100 °C for one hour.

4.4 Summary

Cylindrical microchannels were created in several host matrices at temperatures as low as 50 °C. PPC fibers containing a PAG were melt processed and embedded into the host matrix without any need for further drawing. Control over template cross-section, surface morphology, ductility, and shelf-stability under normal storage and handling conditions are substantial advantages of this new sacrificial polymer. This mechanical robustness combined with rapid transience at much lower temperatures than PLA or cPPA drastically expands the vascularization window (**Figure 4.12**), without increasing the energy footprint for VaSC compared to cPPA. PPC opens the possibility of creating more complex vascular structures with woven and additively manufactured melt-processed sacrificial templates inside neat thermosets and FRPCs. Further investigation of the effect of PAG concentration on vascularization is necessary to establish the processing window for VaSC in different host matrices.

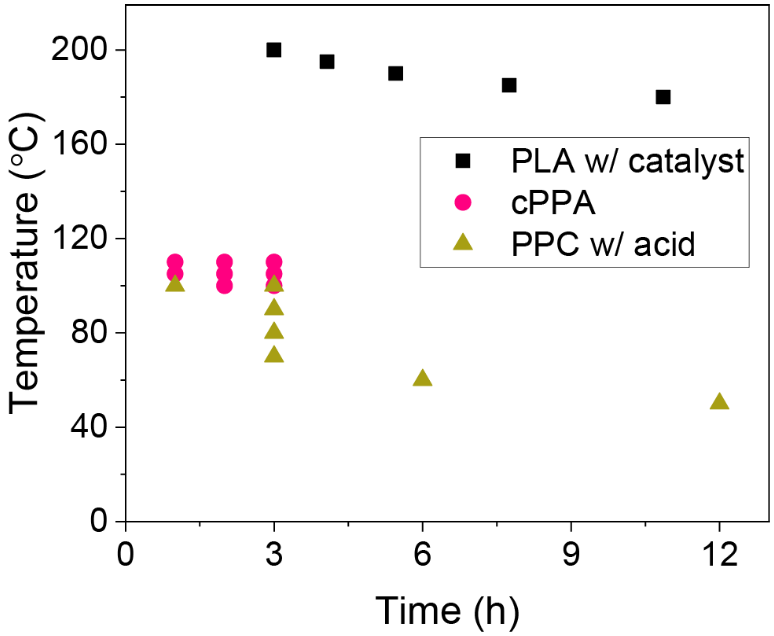

Figure 4.12 Successful VaSC protocols for PPC showing significantly lower temperature conditions are required with this new sacrificial polymer compared to PLA and cPPA.

4.5 References

[1] P. T. Altenbuchner, S. Kissling, and B. Rieger, "Green Chemistry and Sustainable Technology," pp. 163–200, 2014, doi: 10.1007/978-3-642-44988-8_7.

[2] E. Uzunlar, J. Schwartz, O. Phillips, and P. A. Kohl, "Decomposable and Template Polymers: Fundamentals and Applications," *Journal of Electronic Packaging*, vol. 138, no. 2, pp. 020802–15, 2016, doi: 10.1115/1.4033000.

[3] G. A. Luinstra and E. Borchardt, "Material Properties of Poly(Propylene Carbonates)," vol. 245, 2011, pp. 29–48.

[4] G. Luinstra, "Poly(Propylene Carbonate), Old Copolymers of Propylene Oxide and Carbon Dioxide with New Interests: Catalysis and Material Properties," *Polym Rev*, vol. 48, no. 1, pp. 192–219, 2008, doi: 10.1080/15583720701834240.

[5] M. G. Cupta, P. J. Joseph, and P. A. Kohl, “Photoacid generators for catalytic decomposition of polycarbonate,” *Journal of Applied Polymer Science*, vol. 105, no. 5, pp. 2655–2662, 2007, doi: 10.1002/app.26343.

[6] O. Phillips, J. M. Schwartz, and P. A. Kohl, “Thermal decomposition of poly(propylene carbonate): End-capping, additives, and solvent effects,” *Polymer Degradation and Stability*, vol. 125, pp. 129–139, 2016, doi: 10.1016/j.polymdegradstab.2016.01.004.

[7] J. P. Jayachandran *et al.*, “Air-channel fabrication for microelectromechanical systems via sacrificial photosensitive polycarbonates,” *Journal of Microelectromechanical Systems*, vol. 12, no. 2, pp. 147–159, 2003, doi: 10.1109/jmems.2003.809963.

[8] T. J. Spencer, Y.-C. Chen, R. Saha, and P. A. Kohl, “Stabilization of the Thermal Decomposition of Poly(Propylene Carbonate) Through Copper Ion Incorporation and Use in Self-Patterning,” *Journal of Electronic Materials*, vol. 40, no. 6, pp. 1350–1363, 2011, doi: 10.1007/s11664-011-1518-z.

[9] T. J. Spencer and P. A. Kohl, “Decomposition of poly(propylene carbonate) with UV sensitive iodonium salts,” *Polymer Degradation and Stability*, vol. 96, no. 4, pp. 686–702, 2011, doi: 10.1016/j.polymdegradstab.2010.12.003.

[10] E. Uzunlar and P. A. Kohl, “Thermal and photocatalytic stability enhancement mechanism of poly(propylene carbonate) due to Cu(I) impurities,” *Polymer Degradation and Stability*, vol. 97, no. 9, pp. 1829–1837, 2012, doi: 10.1016/j.polymdegradstab.2012.05.034.

[11] E. Uzunlar and P. A. Kohl, “Size-Compatible, Polymer-Based Air-Gap Formation Processes, and Polymer Residue Analysis for Wafer-Level MEMS Packaging Applications,” *Journal of Electronic Packaging*, vol. 137, no. 4, pp. 041001–13, 2015, doi: 10.1115/1.4030952.

[12] N. Fritz, H. Dao, S. A. B. Allen, and P. A. Kohl, “Polycarbonates as temporary adhesives,” *International Journal of Adhesion and Adhesives*, vol. 38, pp. 45–49, 2012, doi: 10.1016/j.ijadhadh.2012.04.001.

[13] R. Saha, N. Fritz, S. A. B. Allen, and P. A. Kohl, “Packaging-compatible wafer level capping of MEMS devices,” *Microelectronic Engineering*, vol. 104, pp. 75–84, 2013, doi: 10.1016/j.mee.2012.11.010.

[14] K. L. Camera, B. Wenning, A. Lal, and C. K. Ober, “Transient materials from thermally-sensitive polycarbonates and polycarbonate nanocomposites,” *Polymer*, vol. 101, pp. 59–66, 2016, doi: 10.1016/j.polymer.2016.08.050.

[15] P. Ohlendorf *et al.*, “Transient Fiber Mats of Electrospun Poly(Propylene Carbonate) Composites with Remarkable Mechanical Strength,” *ACS Applied Materials & Interfaces*, vol. 9, no. 30, pp. 25495–25505, 2017, doi: 10.1021/acsami.7b04710.

[16] R. D. Allen *et al.*, “Positive photoresist system for near-UV to visible imaging,” 1993.

[17] J. Abdallah, M. Silver, S. A. B. Allen, and P. A. Kohl, “UV-induced porosity using photogenerated acids to catalyze the decomposition of sacrificial polymers templated in dielectric films,” *J. Mater. Chem.*, vol. 17, no. 9, pp. 873–885, 2007, doi: 10.1039/b606438h.

[18] J. V. Crivello and U. Bulut, “Curcumin: A naturally occurring long-wavelength photosensitizer for diaryliodonium salts,” *Journal of Polymer Science Part A: Polymer Chemistry*, vol. 43, no. 21, pp. 5217–5231, 2005, doi: 10.1002/pola.21017.

[19] M. G. Cupta, “Characterization and Optimization of Photoacid Generators for use in poly(propylene carbonate) Sacrificial Polymer Systems,” 2006.

[20] A. P. Esser-Kahn *et al.*, “Three-Dimensional Microvascular Fiber-Reinforced Composites,” *Advanced Materials*, vol. 23, no. 32, pp. 3654–3658, 2011, doi: 10.1002/adma.201100933.

[21] J. F. Patrick *et al.*, “Robust sacrificial polymer templates for 3D interconnected microvasculature in fiber-reinforced composites,” *Composites Part A: Applied Science and Manufacturing*, vol. 100, pp. 361–370, 2017, doi: 10.1016/j.compositesa.2017.05.022.

[22] C. S. Hong, R. Wakslak, H. Finston, and V. Fried, “Some thermodynamic properties of systems containing propylene carbonate and ethylene carbonate,” *J Chem Eng Data*, vol. 27, no. 2, pp. 146–148, 1982, doi: 10.1021/je00028a012.

[23] P. Das and P. Tiwari, “Thermal degradation kinetics of plastics and model selection,” *Thermochimica Acta*, vol. 654, pp. 191–202, 2017, doi: 10.1016/j.tca.2017.06.001.

CHAPTER 5

RAPID, ONE-STEP FABRICATION OF VASCULARIZED THERMOSETS AND COMPOSITES

5.1 Introduction

Bioinspired vascular networks in synthetic materials serve as heat and mass transport conduits in biocompatible hydrogels [1], [2], microfluidics [3]–[6], self-healing and self-cooling structures [7]–[10], filtration [11], and energy [12], [13] applications. However, lengthy multistep processes involving solvents [1], [2], [14]–[17], external heat [15], [18]–[21], and vacuum [9], [15], [18], [19], [22], [23] make large-scale manufacture of vascular thermosets and composites energy- and time-intensive. The two-step VaSC process with sacrificial PLA (**Figure 5.1**) consumes > 10^8 joules for a 0.8 m^3 oven to cure the matrix and subsequently evacuate the template (refer to **Appendix A** for calculations). Low-temperature vascularization achieved with cPPA (Chapter 2) and PPC (Chapter 3) templates translate to a five-fold reduction in thermal energy consumption compared to PLA but still takes several hours, and the external heat source scales with sample size. For example, only the curing step for the fuselage of a Boeing 777x aircraft in an autoclave for 8 hours would consume greater than 10^{11} joules of thermal energy [24]. Adding a VaSC cycle to the fabrication sequence at this scale would further increase the total energy consumption to nearly 10^{12} joules. In contrast, biological materials rely on cellular processes for simultaneously depositing and removing material to create vasculature (**Figure 1.3**) [25]. Inspired by this coordinated approach, we developed a new strategy for simultaneous matrix polymerization and sacrificial template depolymerization at lower temperatures.

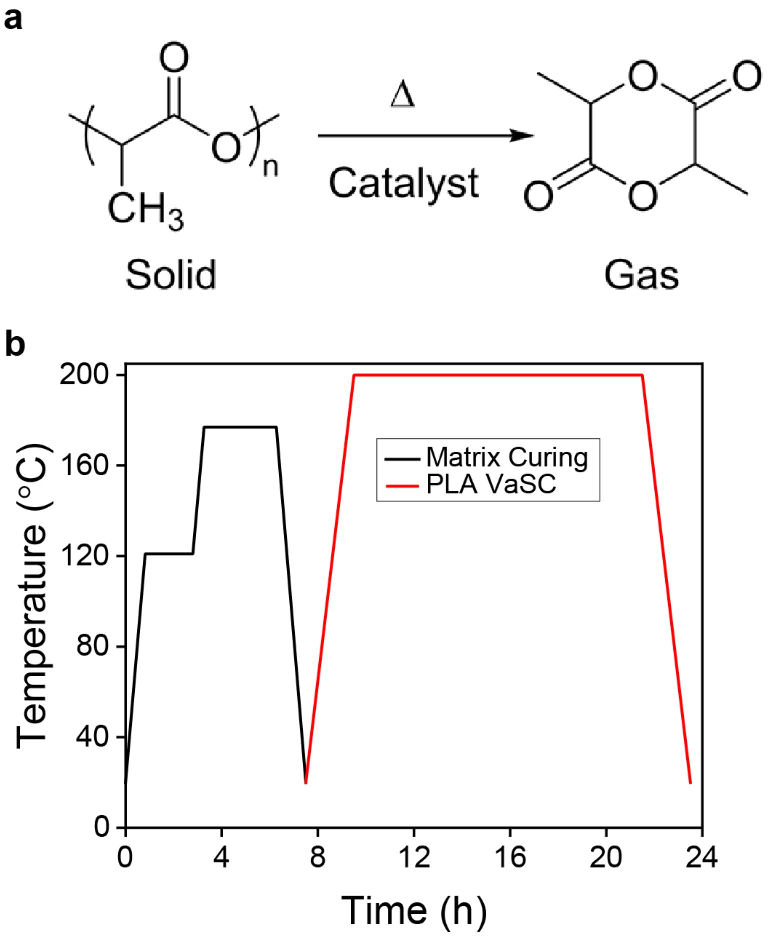

Figure 5.1. Two-step curing and VaSC cycle for sacrificial PLA (tin oxalate catalyst) embedded in a BPA- epoxy matrix.

Frontal polymerization of epoxy, polyurethane, and olefin monomers has emerged as an alternative strategy for manufacturing functionally graded polymers, hydrogels, sensors, and thermoset composites compared to bulk curing [26], [27]. Recently, rapid manufacturing of high-performance thermosets and FRPCs was achieved through frontal polymerization (FP) of dicyclopentadiene (DCPD) monomer [28]. During FP, a localized thermal stimulus activates a latent catalyst to initiate a highly exothermic self-propagating reaction wave that converts liquid or gelled DCPD resin into a rigid poly(dicyclopentadiene) (pDCPD) thermoset at room temperature (RT) without further external energy. A fraction of the released chemical enthalpy drives the curing reaction, while the remaining energy is lost into the surroundings as heat.

In this chapter, we harness the surplus energy for concurrent depolymerization of the embedded sacrificial templates, eliminating the need for a sustained external heat source to manufacture vascular thermosets and fiber-reinforced polymer composites (FRPCs) (**Scheme 5.1**). We also explore the processing window for successful coupling between the curing and depolymerization reactions through experiments and computational modeling. The sacrificial polymer is programmed to decompose and leave a hollow replica in the host matrix during FP, reducing the energy consumption and fabrication time by several orders of magnitude compared to existing methods. Microchannel shape is modulated before and during FP of the matrix, thereby expanding the scope of vascular structures that can be achieved beyond conventional VaSC. This one-step strategy obviates the need for sustained external energy to manufacture vascular structural materials with dynamic multifunctional properties [29].

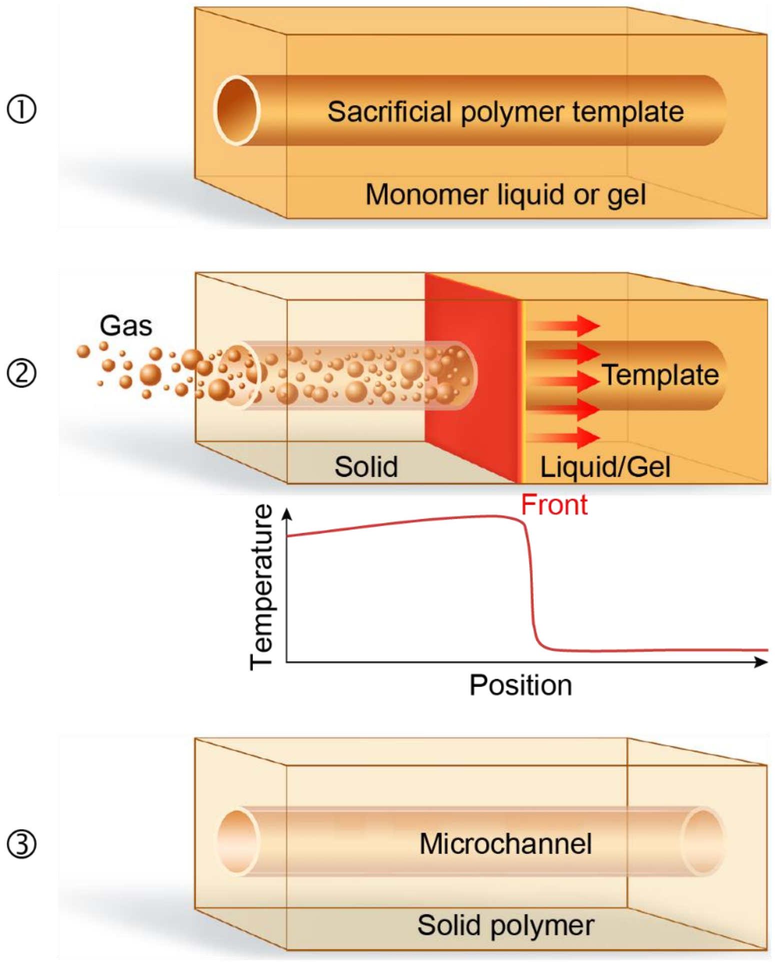

Scheme 5.1. Simultaneous polymerization and vascularization concept. Representative volume element depicting concurrent fabrication of a microvascular structure. ① A sacrificial polymer template is embedded inside a liquid or gelled host matrix. ② A self-propagating exothermic FP reaction is triggered to transform the host into a solid matrix and concurrently depolymerize the sacrificial template into small molecules through a localized increase in temperature. ③ A durable thermoset with microchannels mirroring the starting template is manufactured within minutes.

5.2 Materials and methods

5.2.1 Materials

Dicyclopentadiene (DCPD), 5-ethylidene-2-norbornene (ENB), second-generation Grubbs' catalyst (GC2), phenylcyclohexane (PCH), tributyl phosphite inhibitor (TBP), ethanol, and 5-(N-2,3-Dihydroxypropylacetamido)-2,4,6-triiodo-N,N′-bis(2,3-dihydroxypropyl)isophthalamide (Histodenz^{TM}) were purchased from Sigma-Aldrich and used as received. The sources for PPC and PAG are mentioned in Section 4.2.1. The reinforcement for vascular composite specimens was a Toray T300 carbon fiber 2 × 2 twill weave fabric (tow size 3,000; areal density 204 g m^{-2}). A 26-gauge Kanthal wire (diameter 0.40 mm; resistivity 1.4×10^{-4} Ω cm) was used to trigger FP of neat resin specimens in glass molds. Post FP curing, 200-μm diameter steel wires were used to verify channel clearance in neat and FRPC specimens.

5.2.2 Host matrix resin formulation

Since *endo*-DCPD is a solid at 20 °C, we melt it in an oven at 40 °C and then add 5 wt. % ENB to depress the freezing point below room temperature (RT). For the rest of the procedure, this 95/5 DCPD/ENB solution is simply referred to as DCPD solution. The solution is degassed at 15 kPa for 8 hours before further use. The resin formulation for a typical experiment begins with weighing out 62.7 mg GC2 in a 4 mL scintillation vial, followed by dissolution in 3.12 mL PCH using a sonication bath. One molar equivalent of TBP (20 μL) is added to the catalyst solution using a volumetric syringe. The GC2/PCH/TBP solution is then thoroughly mixed with 97.4 g DCPD solution (10,000 molar equivalents with respect to GC2). The resulting resin is used for experiments involving a neat matrix. For composite experiments, 0.3 molar equivalents of TBP was used. Unless otherwise specified, FP is initiated under standard ambient conditions (20 °C and 1 atm).

5.2.3 Resin rheology

The storage and loss moduli of the DCPD resin as it incubates (slowly cures) under isothermal conditions (20 °C) are extracted from time sweep measurements at 0.1% strain and 1 Hz frequency on an AR-G2 rheometer (TA Instruments). Approximately 0.5 mL of resin is placed between a 25-mm-diameter steel top plate equipped with a solvent trap and a bottom Peltier plate on the instrument for each test. A loading gap of ca. 1000 μm is used for each test. A storage modulus of 30 kPa ($\alpha_0 > 0.20$) indicates the formation of elastomeric gels that can be removed from glass molds without any tack on the contact surfaces (**Figure 5.2**). Gels with $\alpha_0 < 0.20$ (G' < 30 kPa) are challenging to demold due to plastic deformation of the viscous resin, and irregular globs on the surface are permanently locked in shape after FP, which is undesirable.

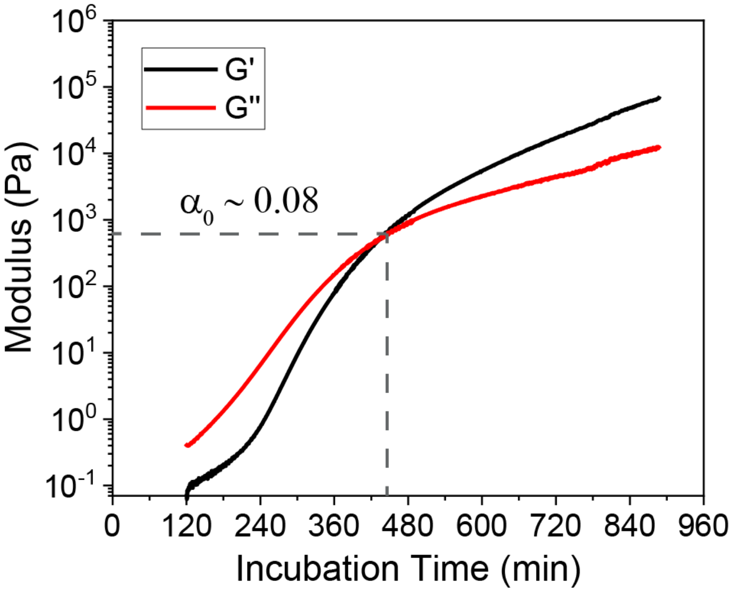

Figure 5.2. Storage (G') and loss (G") moduli of DCPD resin incubated at 20 °C under oscillatory shear. The G' and G" crossover occurs at $\alpha_0 \sim 0.08$.

5.2.4 Thermal characterization of resin

The degree of precure (α_0) of the resin is measured during incubation at 20 °C using differential scanning calorimetry (DSC) in a Discovery DSC Q250 (TA Instruments) equipped with an RCS 90 cooling system. Approximately 2-3 mg of resin is placed in an aluminum hermetic DSC pan and sealed before loading onto the DSC autosampler. Loading a small mass of each sample ensures a constant temperature gradient in the instrument despite the highly exothermic nature of the curing reaction. Each sample is subjected to a constant ramp rate of 7 °C min^{-1} between -50 °C and 250 °C to determine the thermal cure profile (**Figure 5.3**). The baseline-corrected exothermic peak in the heat flow signal is integrated to extract the enthalpy of reaction (H_{r1}) and calculate the degree of precure of each sample using the equation: $\alpha_0 = 1 - \frac{H_{r1}}{H_{r0}}$, where H_{r0} is the enthalpy of reaction of freshly prepared liquid (uncured) resin and H_{r1} is the calculated enthalpy of gelled (partially cured) resin. The specific heat capacity of the matrix (C_{p1}) is averaged between 20 °C and 200 °C after calibration with a sapphire standard. The degree of precure (α_0) of the DCPD resin for different incubation times is summarized in **Table 5.1**.

Table 5.1. Degree of precure (α_0) of DCPD resin during incubation at 20 °C.

Incubation Time (min)	**Degree of precure (α_0)***
0-30	0.01
450	0.08
720	0.22
780	0.25
840	0.31
900	0.35
960	0.40

* Error of 0.01 represents one standard deviation from 5 samples for each incubation time.

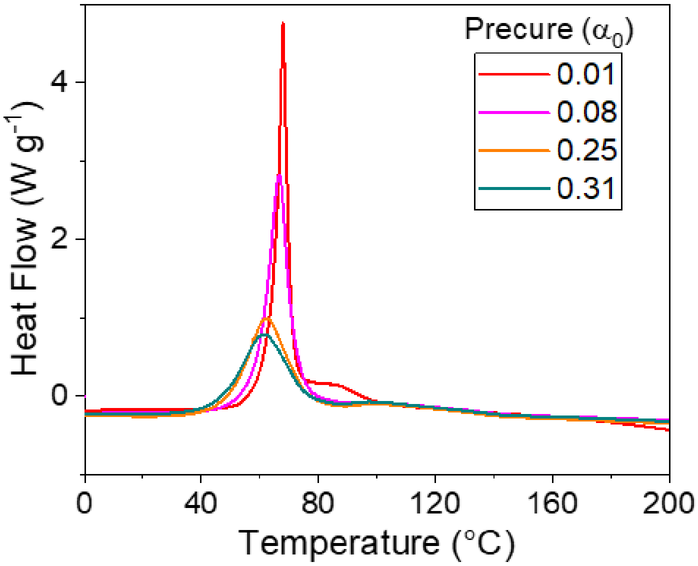

Figure 5.3. DSC data (ramp rate of 7 °C min^{-1}) for the resin incubated for different time intervals at 20 °C.

5.2.5 Thermal characterization of sacrificial polymer

The melt-extruded PPC templates described in Section 4.3 are used for all experiments. The heat capacity (C_{p2}) and enthalpy of depolymerization (H_{r2}) of PPC fibers is measured by DSC as described in Section 4.26. Approximately 2-3 mg of the sacrificial polymer is sealed in an aluminum hermetic DSC pan and exposed to a constant ramp rate of 5 °C min^{-1} between -50 °C and 180 °C (**Figure 5.4a**). The specific heat capacity of the fibers is averaged between 20 °C and 140 °C after calibration with a sapphire standard. The H_{r2} of the sacrificial polymer is extracted by integrating the baseline-corrected endothermic peak in the heat flow signal between 50 °C and 180 °C. For open-pan DSC experiments, a TA instruments Q20 DSC connected to a CFL-50 cooling system is used. The enthalpy of vaporization of PC monomer (integrated between 60 °C and 150 °C) is subtracted from the enthalpy of vaporization of PPC (1% PAG) fiber to estimate the enthalpy of depolymerization of the fiber (**Figure 5.4b**).

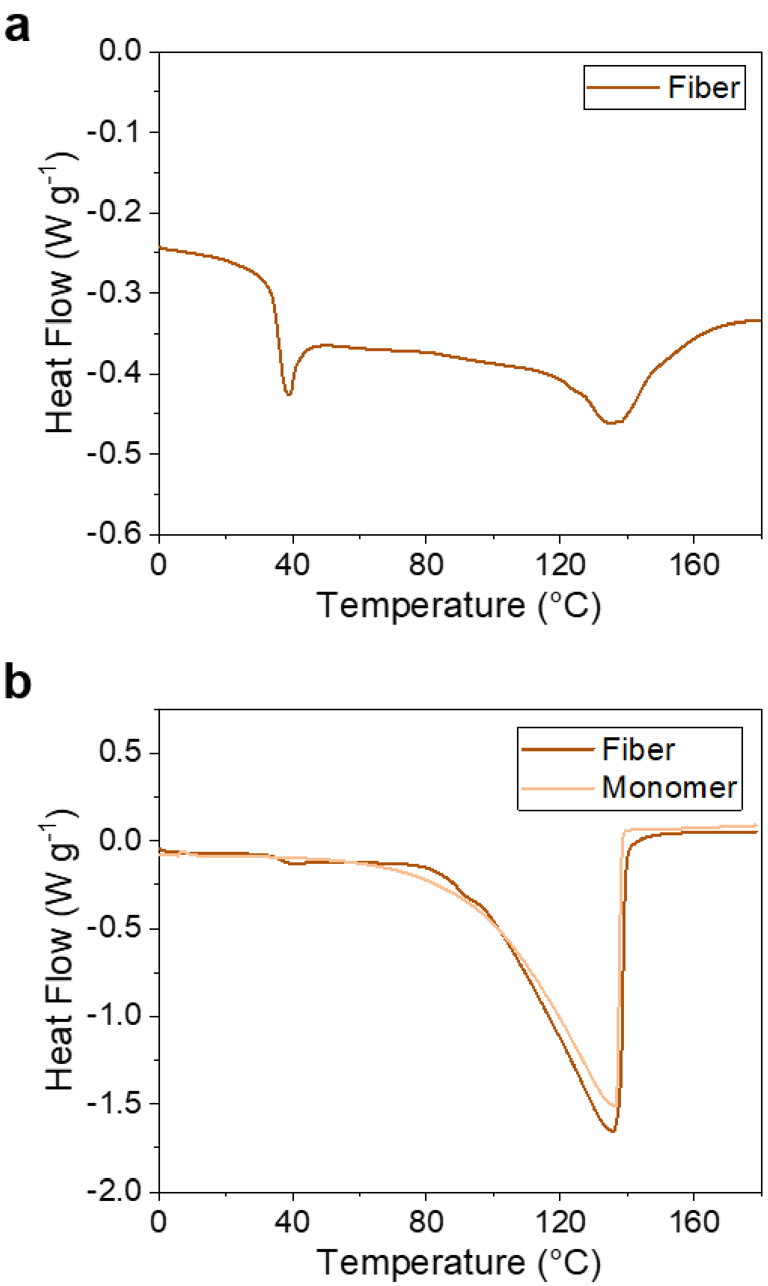

Figure 5.4. Thermal analysis of PPC fibers. (a) DSC of PPC (1% PAG, UV irradiated) at 5 °C min^{-1} in closed-pan setting. The total heat absorbed by the fiber between 50 and 180 °C amounts to 21 J g^{-1}. (b) DSC of PPC (1% PAG, UV irradiated) and PC monomer at 5 °C min^{-1} in open-pan setting. The heat of vaporization of PC matched reported values [30] and an additional H_{r2} = 19 J g^{-1} is consumed during PPC depolymerization, which is close to the calculated H_{r2} from closed-pan tests.

5.2.6 Specimen fabrication for vascularized neat polymer

For FP of specimens in glass molds, a single PPC (1% PAG) fiber is clamped between two polyurethane spacers (outer dimensions: 76.0 mm x 50.0 mm x 3.0 mm) and sandwiched between two 76.2 mm x 50.8 mm x 6.4 mm glass plates in a cell casting mold (**Scheme 5.2**). Liquid resin is poured in each mold to completely submerge the fiber in 60 mm x 34 mm x 6 mm of resin. A resistive wire perpendicular to the fiber orientation is placed in the resin near the top edge and is briefly powered (6 W for ~3 seconds) to initiate FP. Resin-filled molds are incubated in an environmental test chamber (MicroClimate, Cincinnati Sub-Zero Products) at 20 °C for several minutes to achieve the desired degree of precure (α_0). As summarized in Table 5.1, incubation for 450 minutes results in $\alpha_0 \sim 0.08$. Once the desired α_0 is reached, FP of the gelled sample is initiated with the resistive wire.

For FP of specimens without the glass mold, the precured elastomeric gel specimens are removed from the cell casting mold once $\alpha_0 > 0.20$ (approximately twelve hours). The edges of the specimens are trimmed with a razor blade to expose the transverse ends of the sacrificial fiber. FP is then initiated by applying a soldering iron to one end. For the helical microchannel, a PPC fiber (1% PAG) is heat-set at 40 °C into the desired shape before embedding in the glass mold and filling with resin.

For dynamic modulation experiments, DCPD gels containing a single sacrificial fiber (located at 1 mm from the surface of a 4 mm thick sample) are fixed between tensile grips on an Instron 8841 fatigue frame with a gauge length of 50 mm. FP is thermally initiated using a soldering iron at one end of the sample, and dynamic (sinusoidal) loading is applied as the front propagates. Front propagation, applied tension, and fiber orientation are all in the same direction. The displacement amplitude is maintained at 4 mm for all samples and the frequency is varied from 0.1–1 Hz.

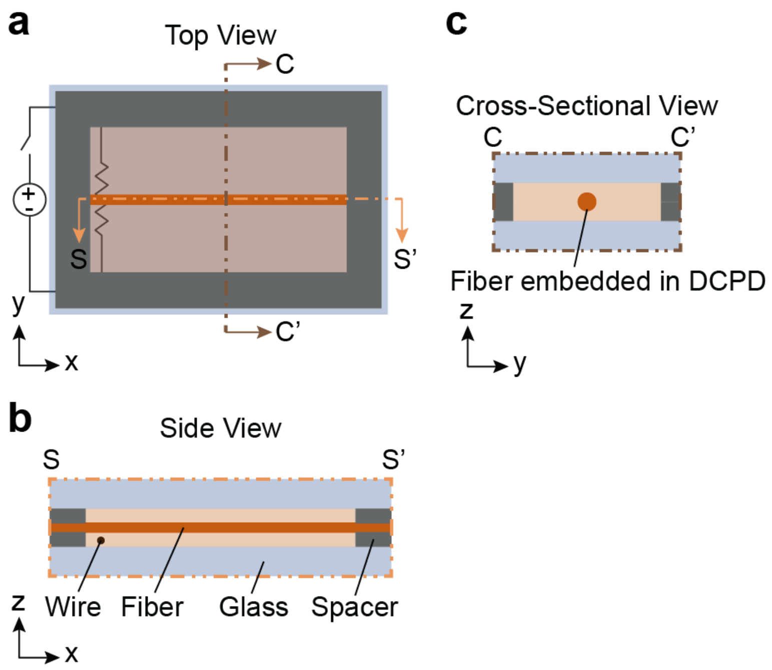

Scheme 5.2. Cell casting of sacrificial fibers in DCPD resin. The sacrificial PPC fiber (orange) is clamped by two rubber spacers (dark grey) sandwiched between two glass plates (translucent blue). Liquid resin (translucent brown) is poured in the cell casting mold to encapsulate the fiber.

5.2.7 *Front velocity and temperature measurements*

A T-type thermocouple (TMQSS, Omega) is inserted into the neat matrix and composite specimens to determine the peak front temperature. For neat resin specimens with embedded sacrificial fibers, we place the thermocouple at the center of the specimen, oriented perpendicular to the fiber, and ~15 mm away from the fiber to avoid any influence on the shape of the polymerization front near the fiber. For composite specimens, the thermocouple is placed at the mid-plane of the fabric layup.

For the neat matrix experiments, a Canon EOS 7D digital camera is focused on the plane of the sacrificial fiber embedded in the specimen during FP. Tracker software (Open Source Physics) is used to determine the location of the polymerization front along the specimen length based on color and refractive index mismatch between the uncured and cured matrix in the optical images extracted from the Canon video. The front velocity is obtained from the slope of the best-fit trendline for the position of the polymerization front as a function of time.

5.2.8 Specimen fabrication for vascular fiber-reinforced composites

Composites specimens are fabricated with 10 plies of 2 × 2 twill weave carbon fiber fabric. The DCPD resin solution is prepared with 0.3 equivalents of TBP with respect to GC2. A wet layup technique is used to infuse the liquid DCPD resin into a 10 cm by 13 cm stack of dry carbon fiber fabric with a PPC fiber (3% PAG, 400 μm diameter) secured on the fifth fabric layer (midplane of the fabric stack). The layup is prepared on a resistive heater (OMEGALUX®), which is secured onto an insulator tool plate (448-D, Fibre Glast Developments Corp.). Silicone spacers (4 mm thick) are placed adjacent to the layup to dictate the cured composite thickness. An additional insulator tool plate is rested on top of the layup, and then the entire setup is moved to a hydraulic press (MTP-13, Tetrahedron). A platen force of 2 kN is applied onto the setup, and then FP is initiated by powering the resistive heater. The heater is powered for ca. 30 sec until the thermocouples embedded within the fabric stack indicate that the front has propagated through the composite thickness.

Depolymerization of the sacrificial fiber post FP is evaluated by passing a steel wire through the channel. The channel fidelity and void content in the cured composite are measured by polishing the cross-sections of samples cut along the panel, then imaging the polished surfaces via a digital optical microscope (VHX-5000, Keyence). ImageJ software is used to measure the circularity of the channel and to calculate the ratio of void to cross-sectional area for each polished sample. The composite fiber volume fraction, V_f, is calculated as $V_\mathrm{f} = \frac{f_\mathrm{A} n}{\rho_\mathrm{f} t}$, where f_A is the areal weight of the fabric, ρ_f is the fiber density, n is the number of plies, and t is the composite thickness.

5.2.9 Microchannel characterization and reconstruction

After FP, optical images of polished cross sections are captured on a Keyence VHX-5000 digital microscope at 100x-200x magnification. Microchannels within the host matrices are also visualized with X-ray computed microtomographic (μCT) imaging (Xradia MicroXCT-400 using TXM Controller software). The μCT scans are conducted after infiltrating the empty microchannels with a contrast solution (350 mg Histodenz^{TM} in 1 g DI water). For 5 mm long channels, 360° scans are obtained in rotation intervals of 0.4° with a 4x objective (5 μm per pixel) at 5 s exposure times with 40 kV (200 μA, 8W) source. For 20 mm long microchannels, imaging settings are changed to rotation intervals of 0.5° with a 1x objective (20 μm per pixel) at 3 s exposure times with 60 kV (133 μA, 8W) source. Scan reconstructions are completed in a proprietary software and images are produced via Amira^{TM} (v. 6.4.0).

5.3 Results and discussion

5.3.1 Coordinated manufacturing of vascular thermosets

We measured the front temperature profile during FP of DCPD (**Scheme 5.3a**) for different degrees of precure (α_0). With a glass mold, the temperature exceeds 200 °C for low α_0. For higher α_0, the maximum temperature is significantly reduced. (**Figure 5.5**). Sacrificial poly(lactic acid) (PLA) blended with the organometallic catalyst studied in Chapter 2 is thermally stable for several hours at these temperatures [19], [22], [31]. In contrast, both cPPA (Chapter 3) and PPC (1% PAG) (Chapter 4) have depolymerization onset temperatures near 100 °C with complete mass loss below 150 °C. Rapid transience in this temperature window makes both cPPA and PPC suitable candidates for depolymerization during FP. Successful vascularization of cPPA films, fibers, and printed templates embedded in neat DCPD gels and carbon-FRPCs is reported in **Appendix C** along with the limitations. Here, we report vascularization through depolymerization of PPC templates containing activated catalyst (**Scheme 5.3b**).

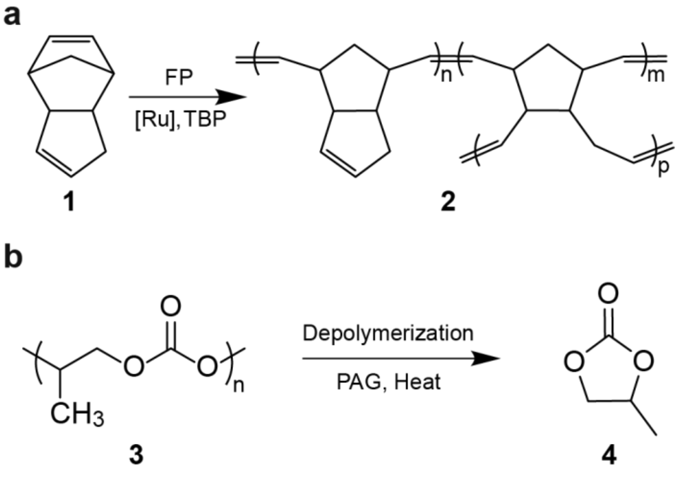

Scheme 5.3. Matrix and sacrificial materials for simultaneous polymerization and vascularization. (a) Scheme for FP of a DCPD monomer (**1**) into crosslinked pDCPD (**2**) using a ruthenium catalyst (Ru; that is, second-generation Grubbs' catalyst) and a tributyl phosphite inhibitor (TBP). (b) Scheme for acid-catalyzed thermal depolymerization of PPC (**3**) into PC monomer (**4**).

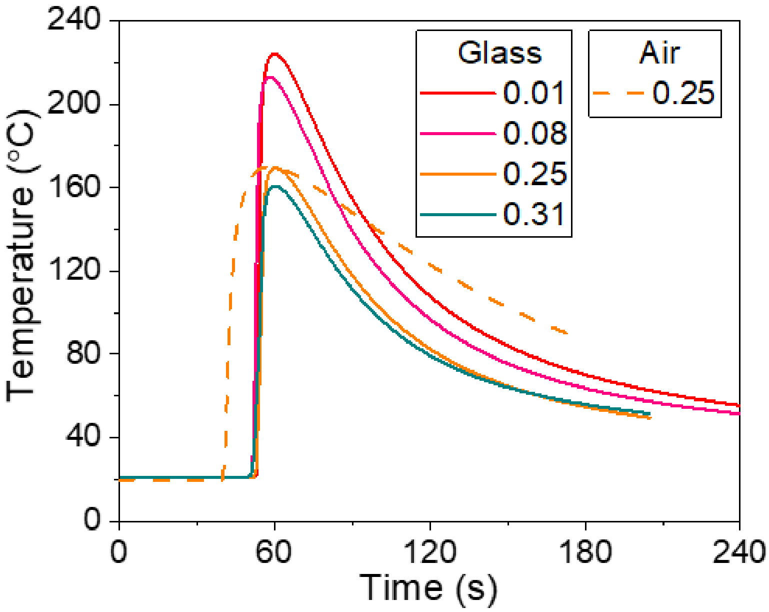

Figure 5.5. Temperature profile at a fixed location inside DCPD specimens with different levels of precure during and after FP, with and without the glass mold (RT = 20 °C).

First, we investigated a single UV-irradiated PPC (1% PAG) fiber in a neat DCPD matrix. As shown in **Figure 5.6a**, the PPC fiber successfully depolymerizes into liquid and gaseous molecules as the polymerization front propagates across the sample. The vascularized pDCPD specimen was created in less than 2 minutes under ambient conditions. Optical microscopy of the microchannel cross-section and X-ray computed microtomography (μCT) reconstruction of the microchannel volume reveal that the dimensions and morphology of the channel match the sacrificial fiber, establishing the fidelity of this rapid, concurrent process (**Figure 5.7**). Moreover, only a small energy input is required for FP, saving ca. 10^6 joules of thermal energy compared to conventional curing and VaSC steps for similar size samples (refer to **Appendix A**). As expected, fibers without UV irradiation did not depolymerize in similar experiments (**Figure 5.8**).

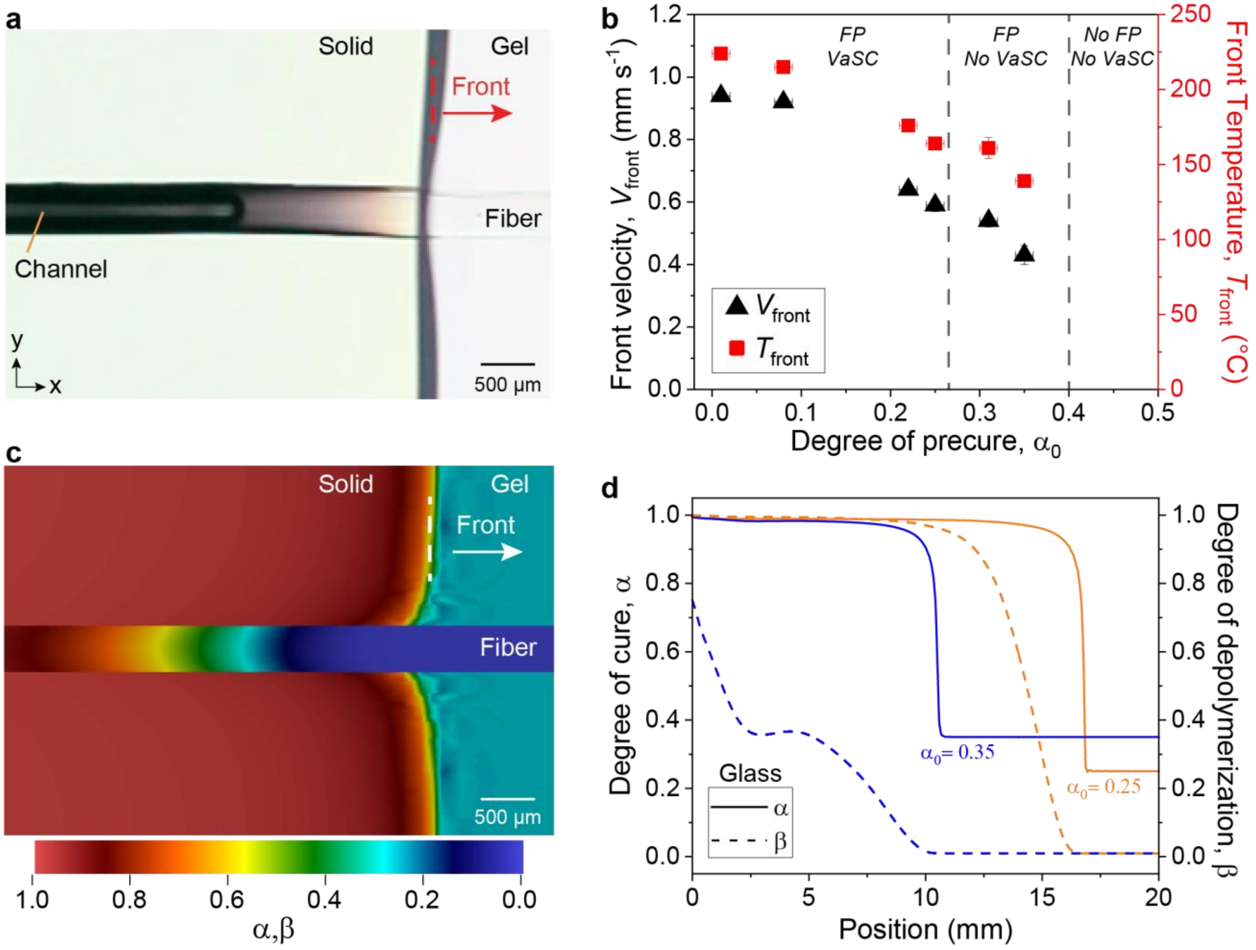

Figure 5.6. Experimental investigation and thermochemical modeling of the competition between FP and depolymerization reactions. (a) Optical snapshot of propagating FP reaction in a DCPD gel (α_0 = 0.25) with concurrent depolymerization of an embedded PPC (1% PAG) fiber to create a vascular pDCPD. (b) Representative front velocity and maximum temperature during FP as a function of precure revealing three different regimes for concurrent FP and VaSC. Error bars represent one standard deviation from the mean (n = 3). (c) Simulation snapshot of a DCPD gel (α_0 = 0.25) showing the spatial distribution of the degree of cure (α) of the DCPD matrix and the degree of depolymerization (β) of the PPC template during FP. (d) Computational model tracks α (solid lines) and β (dashed lines) in the direction of the fronts. Simulation results were obtained by Dr. Xiang Zhang.

We explored the effect of precure on the vascularization process (**Figure 5.6b**). As α_0 increases, both the front velocity (V_{front}) and maximum front temperature (T_{front}) decrease. For $\alpha_0 \leq 0.25$, successful FP and vascularization are achieved. The depolymerization kinetics of PPC is highly temperature-sensitive (Section 4.3.2) and successful vascularization depends on the surplus enthalpy released by the host matrix during FP. The chemical enthalpy decreases with increasing degree of precure of DCPD (α_0) due to a reduction in the fraction of chemical bonds capable of propagating FP [28]. FP still propagates in gels with $0.30 \leq \alpha_0 \leq 0.35$ but produces obstructed channels due to insufficient energy for completing the fiber depolymerization (**Figure 5.9**). Heat loss to the glass interface dominates heat generation during FP in gels with $\alpha_0 \geq 0.40$, and propagation is no longer possible.

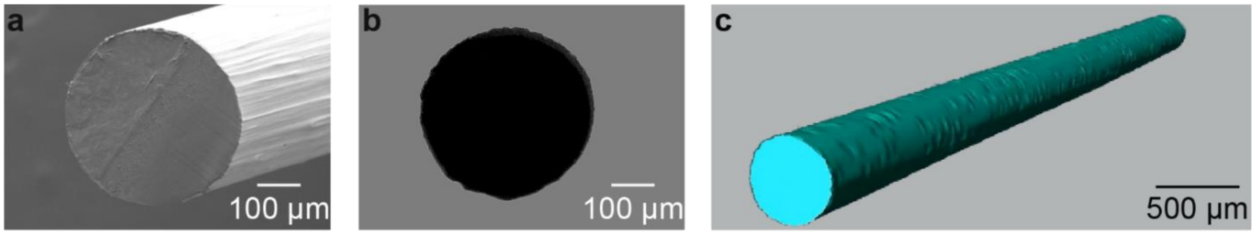

Figure 5.7. (a) SEM micrograph of an as-spun PPC (1% PAG) fiber. (b) optical micrograph of a microchannel in pDCPD matrix after FP-VaSC of a gel ($\alpha_0 = 0.25$) containing a UV-irradiated PPC (1% PAG) fiber. (c) X-Ray computer microtomographic (μCT) reconstruction of a cylindrical microchannel after FP-VaSC.

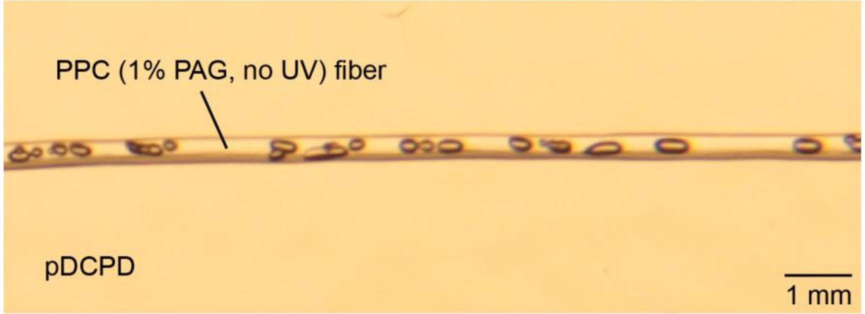

Figure 5.8. Unsuccessful FP-VaSC of a PPC (1%PAG, no UV irradiation) fiber in a DCPD gel ($\alpha_0 = 0.25$).

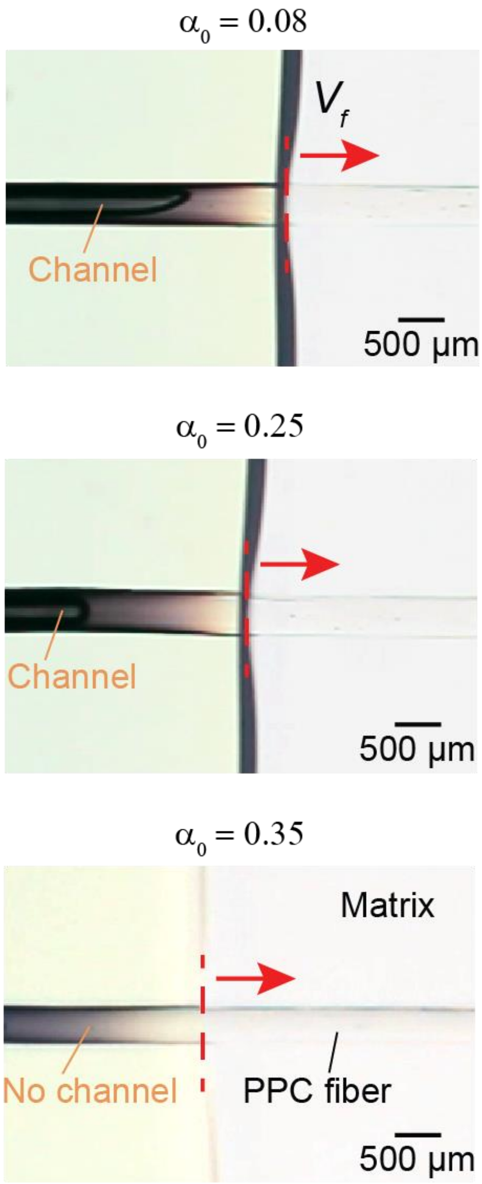

Figure 5.9. Optical snapshots of DCPD gels inside glass molds during FP with concurrent depolymerization of an embedded PPC (1% PAG) fiber at various α_0.

Since the thermal conductance of glass is 3x compared to the convective film coefficient of air, similar experiments were performed without the glass mold. DCPD gels with $\alpha_0 > 0.20$ are easily removed from the glass molds. Slightly higher V_{front} and T_{front} at the corresponding α_0 are observed without the mold (**Figure 5.10**), and the matrix cooling profile is substantially slower (**Figure 5.5**). The prolonged heat retention inside the matrix increases the surplus enthalpy available for depolymerization and extends the vascularization window to a higher α_0 of 0.35. Quenching of the front does not occur until $\alpha_0 \sim 0.50$. For the successful vascularization snapshots in **Figure 5.9**, a slight distortion in the shape of the polymerization front near the fiber with a spatial separation between the front and the trailing channel is also seen. This spatial separation also seems to increase with α_0. We hypothesize that a competition between the surplus heat generated during FP, and the heat consumed during endothermic depolymerization of the fiber as well heat dissipation into the surroundings is responsible for these observations.

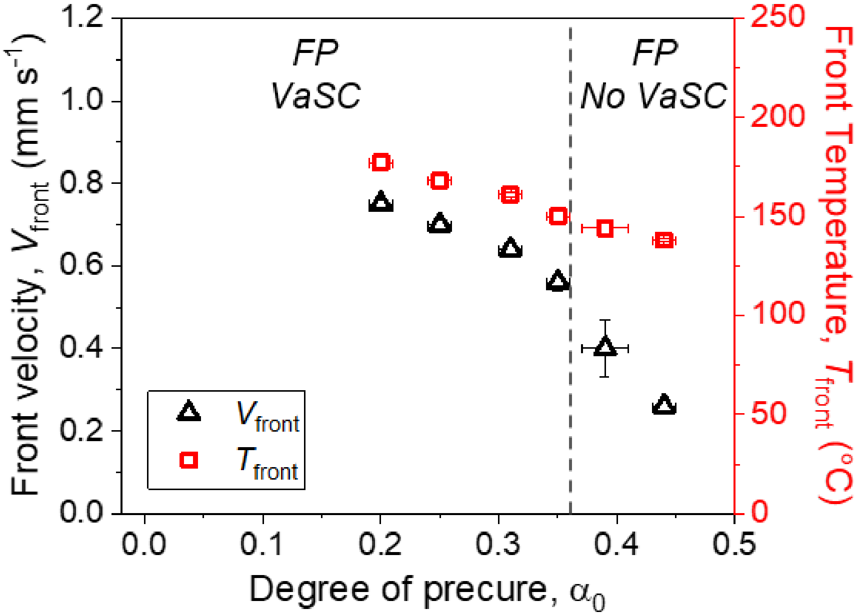

Figure 5.10. Representative front velocity and maximum temperature during FP as a function of precure showing two different regimes for FP and VaSC. Error bars represent one standard deviation from the mean (n = 3).

5.3.2 *Modeling of concurrent depolymerization and frontal polymerization*

In collaboration, we developed a coupled thermochemical curing (α: degree of cure of DCPD) and depolymerization (β: degree of depolymerization of PPC) model using a transient, non-linear finite-element solver model to gain analytical insight into the effect of such initial and boundary conditions on the concurrent vascularization process (see model formulation and parameters in **Appendix D**). Successful polymerization and vascularization are defined numerically by $\alpha \geq 0.90$ and $\beta \geq 0.90$, respectively. The 3D simulation domain consists of a 20 mm x 4 mm x 6 mm matrix with an embedded sacrificial fiber (diameter = 400 μm) surrounded by 6-mm thick glass plates on the top and bottom surfaces. Once the FP was initiated using a line trigger on the left-hand side (perpendicular to the longitudinal axis of the fiber), α of the matrix and β of fiber were simultaneously computed for each element in the simulation domain. The x-y plane in the domain (**Figure 5.6c)** captures the spatial variation in α and β during the coordinated phenomena. First, a slight deceleration of the polymerization front is predicted near the fiber for an initial precure state (α_0 = 0.25, in **Figure 5.6c**). V_{front} and T_{front} predictions for different α_0 match closely with experiments (**Figure 5.11**). Moreover, complete depolymerization trailing the curing front is numerically verified (**Figure 5.6d**) for experimental specimens with clear channels (α_0 = 0.25), whereas only partial depolymerization of the fiber is predicted in samples with obstructed microchannels (α_0 = 0.35). The simulations also predict an extension of the successful vascularization window without the glass mold (**Figure 5.12**). The V_{front} predictions are higher compared to simulations with glass mold (**Figure 5.12a**), corroborating experimental observations. The successful vascularization window is extended to $\alpha_0 \leq 0.35$ due to longer heat retention in the matrix after FP, and quenching is not predicted up to $\alpha_0 \sim 0.50$. At $\alpha_0 > 0.35$, partial depolymerization of the sacrificial fibers is predicted, which is experimentally verified by clogged microchannels in specimens with $\alpha_0 \sim 0.40$ (**Figure 5.12b**). These simulation results confirm that a thermochemical competition between the heat generated by the host matrix and the heat consumed both by the depolymerizing fiber and by the surroundings causes a time delay between curing and depolymerization phenomena. This coupled model is a promising tool to design optimal distribution and volume fraction of the sacrificial component that would predict the successful fabrication of complex vascular structures.

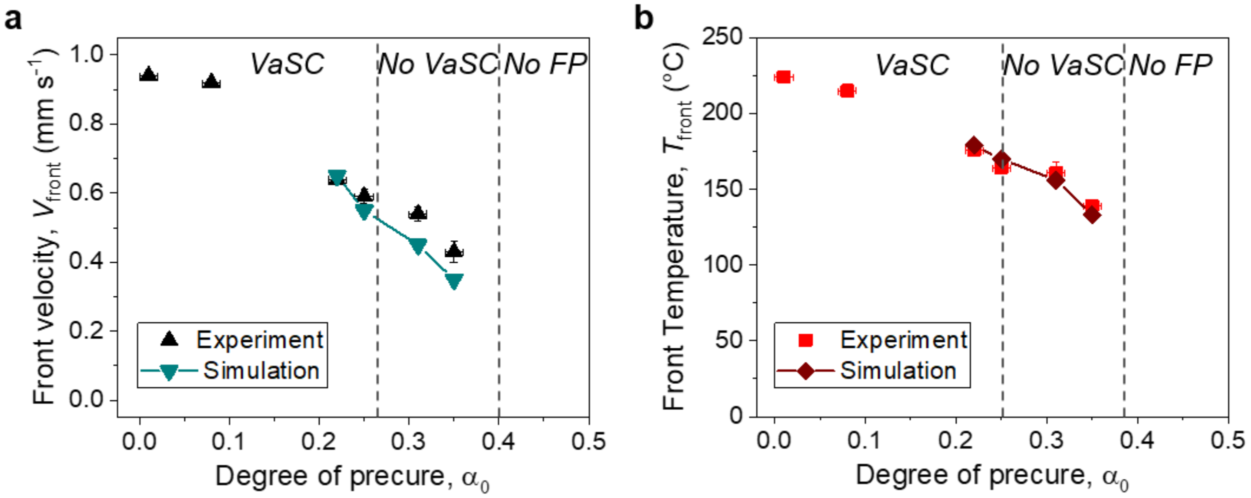

Figure 5.11. Comparison between experimental and simulation results for (a) front velocity (V_{front}) and (b) front temperature (T_{front}) in neat matrices with glass mold. Simulation results were obtained by Dr. Xiang Zhang.

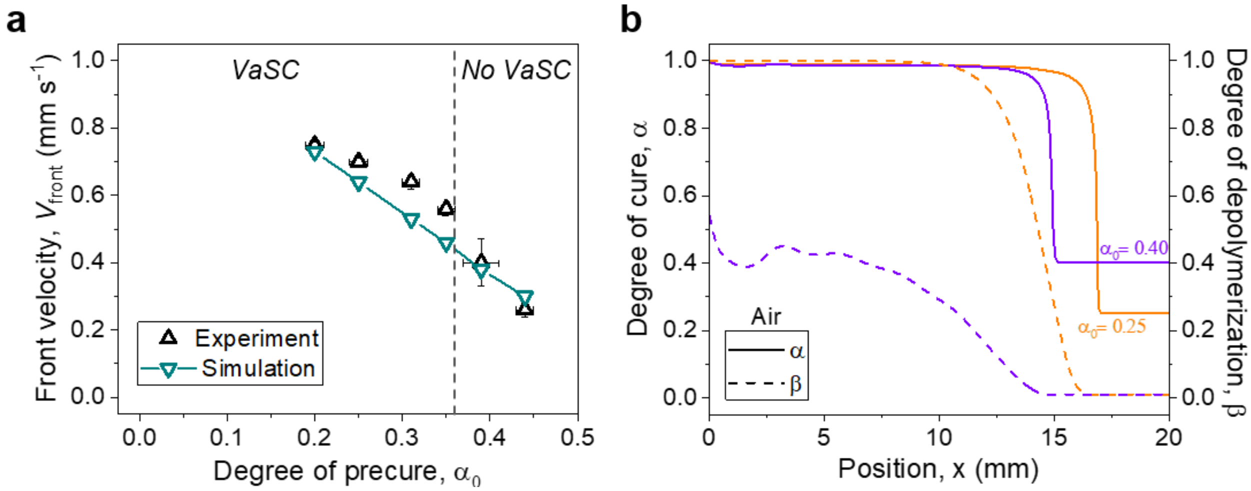

Figure 5.12. Comparison between experimental and simulation results for specimens with convective boundaries (no glass mold). (a) Front velocity (V_{front}) in neat matrices. (b) The computational model predicts complete depolymerization for $\alpha_0 = 0.25$ case but partial depolymerization for $\alpha_0 = 0.40$ specimens, which is verified experimentally. Simulation results are obtained by Dr. Xiang Zhang.

5.3.3 Modulation of microchannel architecture

The free-standing elastomeric gels with embedded PPC (1% PAG, UV-irradiated) fibers offer *ex situ* and *in situ* control over the host and channel architecture (**Figure 5.13**). First, a helical microchannel spanning the 3D space inside pDCPD was created from a heat-set fiber (**Figure 5.13a,b**). The X-ray microcomputed tomographic (µCT) reconstruction of the channel shows a good dimensional and morphological agreement with the sacrificial template. In the second example, a flat gel with a straight fiber was bent into a horseshoe shape prior to FP and the resulting microchannel preserved the sharp curvature (**Figure 5.13c**). This technique for altering microchannel geometry without fracturing or debonding the template enables rapid manufacturing of vascular thermosets with complex shapes.

In a third demonstration, *in situ* modulation of the microchannel geometry from a 1D sacrificial template is achieved by applying dynamic loading during FP (**Figure 5.13d**). The instantaneous out-of-plane deformation experienced by the gel and the fiber under an oscillatory strain was permanently fixed by the polymerization front (**Figure 5.13e**). The pitch and amplitude of the channel were tuned by controlling the oscillation frequency (**Figure 5.13f**). Such control over vascular features may find use in particle/cell separation [32] or serve as conduits for enhanced mixing of multiple fluids via non-laminar flow [33].

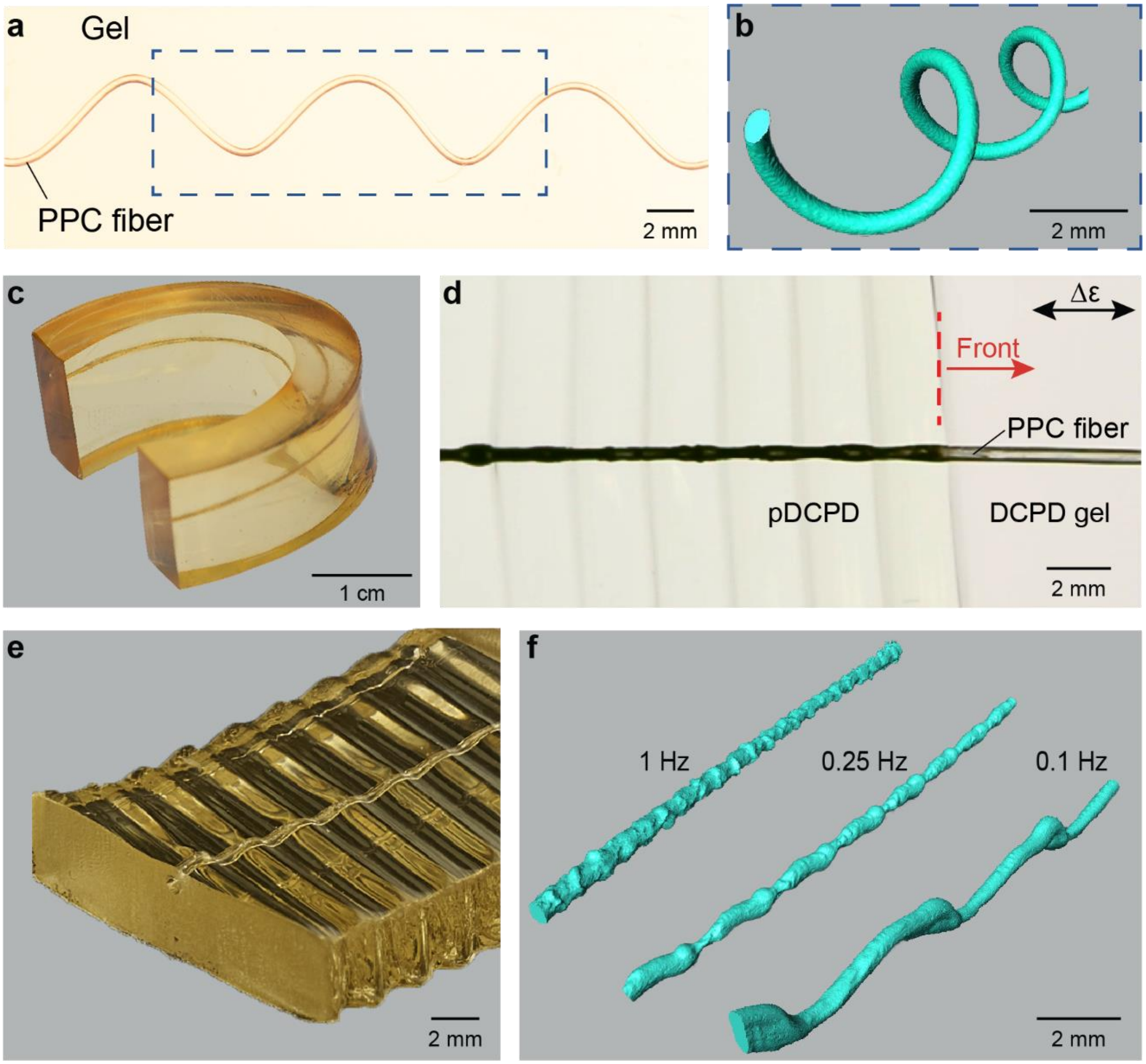

Figure 5.13. Free-standing elastomeric DCPD gels ($\alpha_0 = 0.25$) with embedded PPC (1% PAG) fibers enable on-demand modulation of the microchannel architecture. (a) A helical sacrificial template embedded in a DCPD gel and (b) µCT reconstruction of the helical microchannel after filling with a radiocontrast fluid in the cured pDCPD matrix. (c) A rectangular gel with a straight sacrificial fiber is bent into a horseshoe shape prior to FP and the resulting microchannel traces the curvature of the solid pDCPD. (d-f) Concurrent polymerization and vascularization under oscillatory strain. (d) optical snapshot during and (e) after FP of a pDCPD sample to create sinusoidal microchannel from a straight fiber using dynamic strain (frequency: 0.25 Hz, amplitude: 4 mm). (f) µCT reconstructions of the microchannels after filling them with a radiocontrast fluid show an increase in out-of-plane deformation with a decrease in oscillation frequency. Oscillatory experiments were performed in collaboration with Leon Dean.

5.3.4 Bioinspired interconnected vasculature

The ability to 3D print templates further expands our ability to create complex vascular structures, more analogous to biological systems (**Figure 5.14**). A sacrificial PPC (1% PAG, UV-irradiated) network resembling primary and secondary veins of an impatiens leaf was printed via fused-deposition modeling (FDM). To create the sacrificial template, a scanned image of the leaf was processed in ImageJ to map the key coordinates of the primary and secondary veins (**Appendix C**). These coordinates were then converted into a G-code and loaded into a TAZ6 FDM printer (Lulzbot). A PPC (1% PAG) printing filament (diameter ca. 2.85 mm) was fed into the printer and extruded at 160 °C through a 500 μm diameter nozzle, onto an 80 °C bed. The template was printed at a 0.4-mm print height and 35 mm/min material feed-rate.

The printed leaf template is embedded in DCPD gel ($\alpha_0 = 0.25$) before initiating FP by briefly powering a resistive wire. As shown in **Figure 5.14a**, the liquid and gaseous depolymerization products escape the rapidly forming microchannels behind the polymerization front. A vascular pDCPD structure was formed in 80 seconds at ambient conditions. μCT reconstruction in **Figure 5.14b** shows an excellent match between the template and microchannel architecture. Such interconnected vascular networks have garnered interest in designing multifunctional structures with extended lifetimes [10], [15], [18], [29], [34]–[40], and solar microreactors for synthesizing pharmaceutically relevant drugs [41], [42]. These structures can also serve as rapidly prototyped imaging phantoms for understanding fluid/gas flow through complex capillary networks in plant and animal systems.

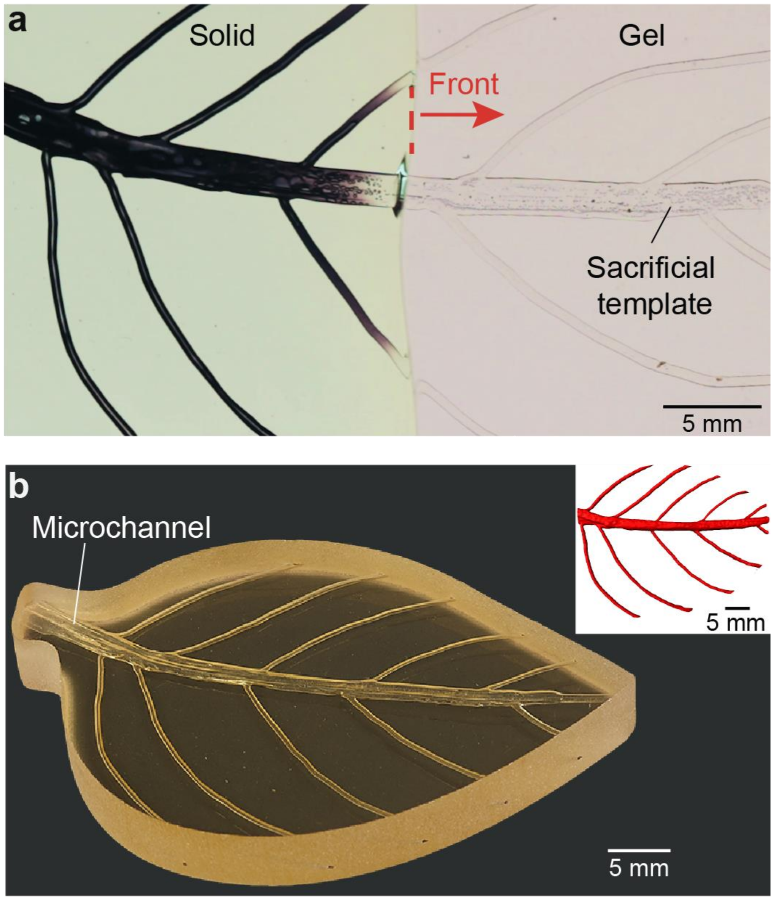

Figure 5.14. Bioinspired vascular network using a 3D printed PPC template. (a) Optical snapshot during simultaneous polymerization and vascularization of a free-standing DCPD gel ($\alpha_0 = 0.25$) with an embedded 3D printed PPC template (1% PAG). The depolymerization products escape through the central vein and vascularization is completed within 80 seconds. (b) Macro image and µCT reconstruction after injecting a radiocontrast fluid in the resulting vasculature (inset) showing interconnectivity between the initial template and resulting microchannels. 3D printing of PPC was done by Jia En Aw.

5.3.5 Rapid vascularization in fiber-reinforced composites

Vascularized woven-FRPCs were also manufactured. Sacrificial PPC (3% PAG) fiber was sandwiched between layers of carbon fiber fabric, which was then infused with liquid DCPD monomer using a wet layup scheme, as shown in **Figure 5.15**. FP was triggered through the thickness of the impregnated fabric preform by briefly powering a resistive heating mat underneath the layup. The heater was switched off as soon as a spike in the thermocouple temperature was observed (ca. 30 seconds) (**Figure 5.16**). A void-free composite with a fiber volume fraction (V_f) of 36% and circular microchannels was achieved (**Figure 5.15b**). The fabrication time and energy are reduced by three and four orders of magnitude, respectively, compared to oven curing and VaSC of similar size samples with sacrificial PLA templates.

FP manufacturing of vascular composites is challenging due to the presence of fiber reinforcement, which reduces the exotherm and maximum front temperature compared to neat resin. A higher catalyst concentration of 3% was needed in the PPC fibers to achieve complete vascularization, owing to the faster depolymerization kinetics compared to 1% PAG fibers (Section 4.3.2). Additionally, a 2D heating mat was used to supply enough thermal energy for facilitating complete fiber depolymerization during through-thickness FP compared to a linear trigger. A lower V_f compared to traditional high-performance composites ($V_f > 50$ %) was used to generate more chemical energy for PPC depolymerization during FP of the composite. The PPC fiber was sandwiched in the middle of the fabric preform to retain the thermal energy for a longer period after completion of FP. These challenges with fiber placement and sufficient energy for concurrent depolymerization need to be surmounted to create vascular composites with high V_f. Such vascularized composites have applications in self-healing, self-cooling, and electromagnetically reconfigurable structures [8], [19], [40], [43], [44].

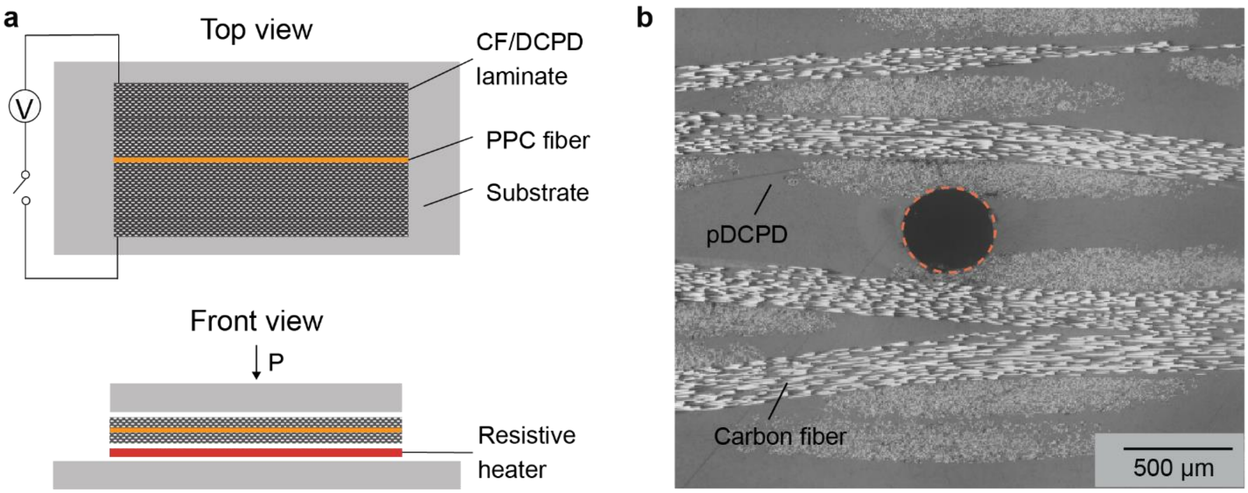

Figure 5.15. Concurrent polymerization and vascularization in FRPC. (a) Press-assisted composite fabrication scheme showing a PPC fiber (3% PAG) sandwiched between fabric layers and a resistive heater mat triggers through-thickness FP. (b) Optical cross section showing a circular microchannel inside a void-free composite cured within 30 seconds at RT, reducing the fabrication time by three orders of magnitude and processing energy by four orders of magnitude compared to a traditional autoclave cycle. Composite fabrication was achieved in collaboration with Polette Centellas.

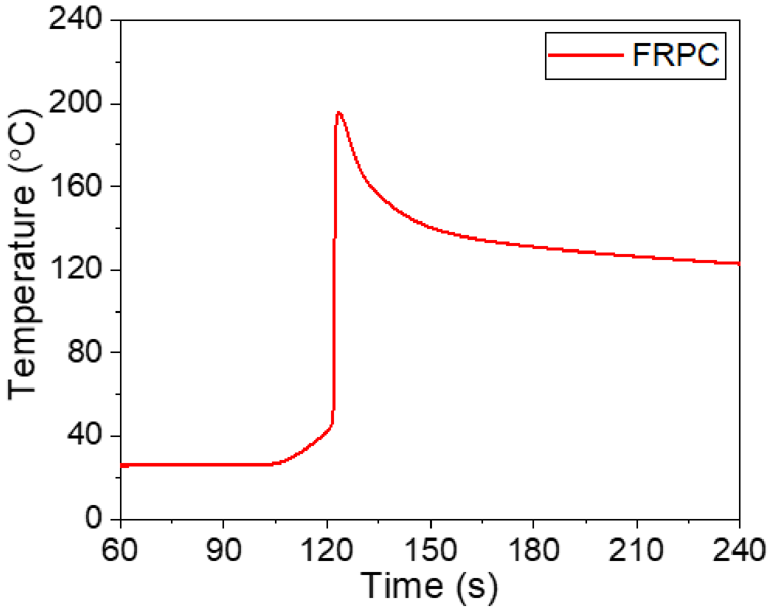

Figure 5.16. Thermocouple reading during FP of FRPC. The heater was switched off as soon as a sharp spike in thermocouple reading (indicating initiation of FP) was seen.

5.4 Summary

In conclusion, we have demonstrated a rapid, energy-efficient technique for manufacturing thermosets and FRPCs with embedded microfluidic networks. Precise control over the microchannel shape, size, and complexity was achieved through the seamless integration of orthogonally triggered sacrificial templates. The competition between the reaction enthalpy of DCPD, and the energy consumed during depolymerization of the template and dissipation into the surroundings was investigated experimentally and validated computationally. This technology can help accelerate the use of high-performance vascular structures by minimizing the energetic and temporal footprint for fabrication by several orders of magnitude.

5.5 References

[1] B. Grigoryan *et al.*, “Multivascular networks and functional intravascular topologies within biocompatible hydrogels,” *Science*, vol. 364, no. 6439, pp. 458–464, 2019, doi: 10.1126/science.aav9750.

[2] J. S. Miller *et al.*, “Rapid casting of patterned vascular networks for perfusable engineered three-dimensional tissues,” *Nat Mater*, vol. 11, no. 9, pp. 768–774, 2012, doi: 10.1038/nmat3357.

[3] D. Lim, Y. Kamotani, B. Cho, J. Mazumder, and S. Takayama, “Fabrication of microfluidic mixers and artificial vasculatures using a high-brightness diode-pumped Nd:YAG laser direct write method.,” *Lab on a chip*, vol. 3, no. 4, pp. 318–323, Nov. 2003, doi: 10.1039/b308452c.

[4] H. Wu, T. W. Odom, D. T. Chiu, and G. M. Whitesides, “Fabrication of complex three-dimensional microchannel systems in PDMS.,” *Journal of the American Chemical Society*, vol. 125, no. 2, pp. 554–559, Jan. 2003, doi: 10.1021/ja021045y.

[5] J. R. Anderson *et al.*, “Fabrication of Topologically Complex Three-Dimensional Microfluidic Systems in PDMS by Rapid Prototyping,” *Anal Chem*, vol. 72, no. 14, pp. 3158–3164, 2000, doi: 10.1021/ac9912294.

[6] J. Wang, M. M. Maw, X. Yu, B. Dai, G. Wang, and Z. Jiang, “Applications and perspectives on microfluidic technologies in ships and marine engineering: a review,” *Microfluid Nanofluid*, vol. 21, no. 3, p. 39, 2017, doi: 10.1007/s10404-017-1873-z.

[7] S. J. Pety, P. X. L. Chia, S. M. Carrington, and S. R. White, “Active cooling of microvascular composites for battery packaging,” *Smart Mater Struct*, vol. 26, no. 10, p. 105004, 2017, doi: 10.1088/1361-665x/aa84e7.

[8] S. J. Pety, M. H. Y. Tan, A. R. Najafi, P. R. Barnett, P. H. Geubelle, and S. R. White, “Carbon fiber composites with 2D microvascular networks for battery cooling,” *International Journal of Heat and Mass Transfer*, vol. 115, pp. 513–522, Dec. 2017, doi: 10.1016/j.ijheatmasstransfer.2017.07.047.

[9] C. J. Norris, I. P. Bond, and R. S. Trask, “The role of embedded bioinspired vasculature on damage formation in self-healing carbon fibre reinforced composites,” *Composites Part A*, vol. 42, no. 6, pp. 639–648, Jun. 2011, doi: 10.1016/j.compositesa.2011.02.003.

[10] G. Williams, R. Trask, and I. Bond, “A self-healing carbon fibre reinforced polymer for aerospace applications,” *Compos Part Appl Sci Manuf*, vol. 38, no. 6, pp. 1525–1532, 2007, doi: 10.1016/j.compositesa.2007.01.013.

[11] K. Brubaker, A. Garewal, R. C. Steinhardt, and A. P. Esser-Kahn, “Bio-inspired counter-current multiplier for enrichment of solutes,” *Nat Commun*, vol. 9, no. 1, p. 736, 2018, doi: 10.1038/s41467-018-03052-y.

[12] K. J. Maloney, K. D. Fink, T. A. Schaedler, J. A. Kolodziejska, A. J. Jacobsen, and C. S. Roper, “Multifunctional heat exchangers derived from three-dimensional micro-lattice structures,” *Int J Heat Mass Tran*, vol. 55, no. 9–10, pp. 2486–2493, 2012, doi: 10.1016/j.ijheatmasstransfer.2012.01.011.

[13] A. Z. Weber, M. M. Mench, J. P. Meyers, P. N. Ross, J. T. Gostick, and Q. Liu, “Redox flow batteries: a review,” *J Appl Electrochem*, vol. 41, no. 10, pp. 1137–1164, 2011, doi: 10.1007/s10800-011-0348-2.

[14] D. J. Beebe *et al.*, “Functional hydrogel structures for autonomous flow control inside microfluidic channels,” *Nature*, vol. 404, no. 6778, pp. 588–590, 2000, doi: 10.1038/35007047.

[15] C. J. Hansen, W. Wu, K. S. Toohey, N. R. Sottos, S. R. White, and J. A. Lewis, “Self-Healing Materials with Interpenetrating Microvascular Networks,” *Advanced Materials*, vol. 21, no. 41, pp. 4143–4147, Nov. 2009, doi: 10.1002/adma.200900588.

[16] L. M. Bellan, S. P. Singh, P. W. Henderson, T. J. Porri, H. G. Craighead, and J. A. Spector, “Fabrication of an artificial 3-dimensional vascular network using sacrificial sugar structures,” *Soft Matter*, vol. 5, no. 7, pp. 1354–1357, 2009, doi: 10.1039/b819905a.

[17] C. Gualandi, A. Zucchelli, M. F. Osorio, J. Belcari, and M. L. Focarete, “Nanovascularization of Polymer Matrix: Generation of Nanochannels and Nanotubes by Sacrificial Electrospun fibers,” *Nano Lett*, vol. 13, no. 11, pp. 5385–5390, 2013, doi: 10.1021/nl402930x.

[18] K. S. Toohey, N. R. Sottos, J. A. Lewis, J. S. Moore, and S. R. White, “Self-healing materials with microvascular networks,” *Nat Mater*, vol. 6, no. 8, pp. 581–585, Aug. 2007, doi: 10.1038/nmat1934.

[19] A. P. Esser-Kahn *et al.*, “Three-Dimensional Microvascular Fiber-Reinforced Composites,” *Advanced Materials*, vol. 23, no. 32, pp. 3654–3658, Jul. 2011, doi: 10.1002/adma.201100933.

[20] D. G. Moore, L. Barbera, K. Masania, and A. R. Studart, “Three-dimensional printing of multicomponent glasses using phase-separating resins,” *Nat Mater*, vol. 19, no. 2, pp. 212–217, 2019, doi: 10.1038/s41563-019-0525-y.

[21] E. Uzunlar, J. Schwartz, O. Phillips, and P. A. Kohl, “Decomposable and Template Polymers: Fundamentals and Applications,” *Journal of Electronic Packaging*, vol. 138, no. 2, pp. 020802–15, Jun. 2016, doi: 10.1115/1.4033000.

[22] R. C. R. Gergely *et al.*, “Multidimensional Vascularized Polymers using Degradable Sacrificial Templates,” *Advanced Functional Materials*, vol. 25, no. 7, pp. 1043–1052, Dec. 2014, doi: 10.1002/adfm.201403670.

[23] D. Therriault, S. R. White, and J. A. Lewis, “Chaotic mixing in three-dimensional microvascular networks fabricated by direct-write assembly,” *Nat Mater*, vol. 2, no. 4, pp. 265–271, 2003, doi: 10.1038/nmat863.

[24] A. J. Timmis *et al.*, “Environmental impact assessment of aviation emission reduction through the implementation of composite materials,” *Int J Life Cycle Assess*, vol. 20, no. 2, pp. 233–243, 2014, doi: 10.1007/s11367-014-0824-0.

[25] N. Little, B. Rogers, and M. Flannery, “Bone formation, remodelling and healing,” *Surg Oxf*, vol. 29, no. 4, pp. 141–145, 2011, doi: 10.1016/j.mpsur.2011.01.002.

[26] J. A. Pojman, “Polymer Science: A Comprehensive Reference,” vol. 4, K. Matyjaszewski and M. Möller, Eds. Elsevier B.V., 2012, pp. 957–980.

[27] J. A. Pojman and Q. Tran-Cong-Miyata, *Nonlinear Dynamics with Polymers*. Wiley-VCH Verlag GmbH & Co. KGaA, 2010.

[28] I. D. Robertson *et al.*, “Rapid energy-efficient manufacturing of polymers and composites via frontal polymerization,” *Nature*, vol. 557, no. 7704, pp. 223–227, May 2018, doi: 10.1038/s41586-018-0054-x.

[29] I. P. S. Qamar, N. R. Sottos, and R. S. Trask, “Grand challenges in the design and manufacture of vascular self-healing,” *Multifunct Mater*, vol. 3, no. 1, p. 013001, 2020, doi: 10.1088/2399-7532/ab69e2.

[30] C. S. Hong, R. Wakslak, H. Finston, and V. Fried, “Some thermodynamic properties of systems containing propylene carbonate and ethylene carbonate,” *J Chem Eng Data*, vol. 27, no. 2, pp. 146–148, 1982, doi: 10.1021/je00028a012.

[31] H. Dong *et al.*, “Chemical Treatment of Poly(lactic acid) Fibers to Enhance the Rate of Thermal Depolymerization,” *ACS Applied Materials & Interfaces*, vol. 4, no. 2, pp. 503–509, Feb. 2012, doi: 10.1021/am2010042.

[32] W. Lee *et al.*, “3D-Printed Microfluidic Device for the Detection of Pathogenic Bacteria Using Size-based Separation in Helical Channel with Trapezoid Cross-Section,” *Sci Rep-uk*, vol. 5, no. 1, p. 7717, 2015, doi: 10.1038/srep07717.

[33] L. M. Dean, B. P. Krull, K. R. Li, Y. I. Fedonina, S. R. White, and N. R. Sottos, “Enhanced Mixing of Microvascular Self-Healing Reagents Using Segmented Gas–Liquid Flow,” *Acs Appl Mater Inter*, vol. 10, no. 38, pp. 32659–32667, 2018, doi: 10.1021/acsami.8b09966.

[34] B. J. Blaiszik, S. L. B. Kramer, S. C. Olugebefola, J. S. Moore, N. R. Sottos, and S. R. White, “Self-Healing Polymers and Composites,” *Annual Review of Materials Research*, vol. 40, no. 1, pp. 179–211, Jun. 2010, doi: 10.1146/annurev-matsci-070909-104532.

[35] A. R. Hamilton, N. R. Sottos, and S. R. White, “Self-Healing of Internal Damage in Synthetic Vascular Materials,” *Adv Mater*, vol. 22, no. 45, pp. 5159–5163, 2010, doi: 10.1002/adma.201002561.

[36] S. R. White, J. S. Moore, N. R. Sottos, B. P. Krull, W. A. S. Cruz, and R. C. R. Gergely, “Restoration of Large Damage Volumes in Polymers,” *Science*, vol. 344, no. 6184, pp. 620–623, 2014, doi: 10.1126/science.1251135.

[37] K. R. Hart *et al.*, “Repeated healing of delamination damage in vascular composites by pressurized delivery of reactive agents,” *Composites Science and Technology*, vol. 151, pp. 1–9, Oct. 2017, doi: 10.1016/j.compscitech.2017.07.027.

[38] J. F. Patrick *et al.*, “Continuous Self-Healing Life Cycle in Vascularized Structural Composites,” *Advanced Materials*, vol. 26, no. 25, pp. 4302–4308, Apr. 2014, doi: 10.1002/adma.201400248.

[39] C. J. Norris, I. P. Bond, and R. S. Trask, “Healing of low-velocity impact damage in vascularised composites,” *Composites Part A: Applied Science and Manufacturing*, vol. 44, pp. 78–85, Jan. 2013, doi: 10.1016/j.compositesa.2012.08.022.

[40] J. F. Patrick *et al.*, “Robust sacrificial polymer templates for 3D interconnected microvasculature in fiber-reinforced composites,” *Composites Part A: Applied Science and Manufacturing*, vol. 100, pp. 361–370, Sep. 2017, doi: 10.1016/j.compositesa.2017.05.022.

[41] D. Cambié *et al.*, “Energy-Efficient Solar Photochemistry with Luminescent Solar Concentrator Based Photomicroreactors,” *Angewandte Chemie Int Ed*, vol. 58, no. 40, pp. 14374–14378, 2019, doi: 10.1002/anie.201908553.

[42] D. Cambié, F. Zhao, V. Hessel, M. G. Debije, and T. Noël, “A Leaf-Inspired Luminescent Solar Concentrator for Energy-Efficient Continuous-Flow Photochemistry,” *Angewandte Chemie Int Ed*, vol. 56, no. 4, pp. 1050–1054, 2016, doi: 10.1002/anie.201611101.

[43] A. M. Coppola *et al.*, “Active Cooling of a Microvascular Shape Memory Alloy-Polymer Matrix Composite Hybrid Material ,” *Adv Eng Mater*, vol. 18, no. 7, pp. 1145–1153, 2016, doi: 10.1002/adem.201600020.

[44] A. M. Coppola, L. G. Warpinski, S. P. Murray, N. R. Sottos, and S. R. White, “Survival of actively cooled microvascular polymer matrix composites under sustained thermomechanical loading,” *Compos Part Appl Sci Manuf*, vol. 82, pp. 170–179, 2016, doi: 10.1016/j.compositesa.2015.12.010.

CHAPTER 6

CONCLUSIONS AND FUTURE WORK

6.1 Conclusions

In its current state, manufacturing vascular thermosets and fiber-reinforced polymer composites (FRPCs) through sustained external heating and/or vacuum for curing the host matrix and evacuating the embedded sacrificial templates is an extremely energy- and time-intensive process. The high thermal stability of poly(lactic acid) (PLA) up to 280 °C [1] leads to a lengthy vascularization step at elevated temperatures, even with a depolymerization-promoting tin oxalate catalyst (200 °C for 12 hours). In this dissertation, depolymerization of three different sacrificial precursors: PLA blended with a more efficient catalyst in Chapter 2, cyclic poly(phthalaldehyde) (cPPA) in Chapter 3, and poly(propylene carbonate) (PPC) blended with a photoacid generator (PAG) in Chapter 4 was explored for rapid, energy-efficient manufacturing of vascular thermosets and composites at lower temperatures. The precursors were templated into films, fibers, and printed architectures through solution- and melt-processing methods and mass loss after depolymerization was characterized *ex situ* by thermogravimetric analysis (TGA) (**Figure 6.1**) and *in situ* after embedding in the host matrix (**Figure 6.2**).

Sacrificial templates that could survive the thermomechanical stresses encountered during the processing of thermosets and fiber-reinforced polymer composites (FRPCs) were integrated into several host matrices. These templates were successfully evacuated at significantly lower temperatures than sacrificial PLA to create vascular structures. The clearance, surface morphology, and dimensions of the microchannels after vaporization of sacrificial components

(VaSC) were compared with the initial templates using various microscopy and tomographic reconstruction techniques to prove the fidelity of this process with the new sacrificial polymers.

An Arrhenius-type kinetics model, based on mass loss experiments on templates in TGA, was developed in a collaborative effort to compare the critical parameters dictating the depolymerization of the sacrificial polymers at various temperatures (**Table 6.1**). The lower activation energy for cPPA and PPC compared to PLA explained higher sensitivity to thermal depolymerization near 100 °C. A 100x increase in the pre-exponential factor for the depolymerization kinetics model of PPC explained faster depolymerization compared to cPPA at temperatures below 90 °C, whereas negligible mass loss of cPPA was experimentally observed below this temperature after twelve hours. Microvascular fiber-reinforced polymer composites (FRPCs) with high-temperature resistant host matrices were previously fabricated with energy- and time-intensive VaSC protocol (200 °C for 12 hours). In comparison, the new sacrificial polymers, cPPA and PPC, expanded the scope of this vascularization strategy to a broader range of host materials with low glass transition temperatures (< 100 °C) by allowing a significant reduction in the VaSC temperature (50-100 °C), as shown in **Figure 6.2**. These low-temperature VaSC protocols translated to a five-fold reduction in thermal energy consumption during manufacturing compared to the evacuation of PLA.

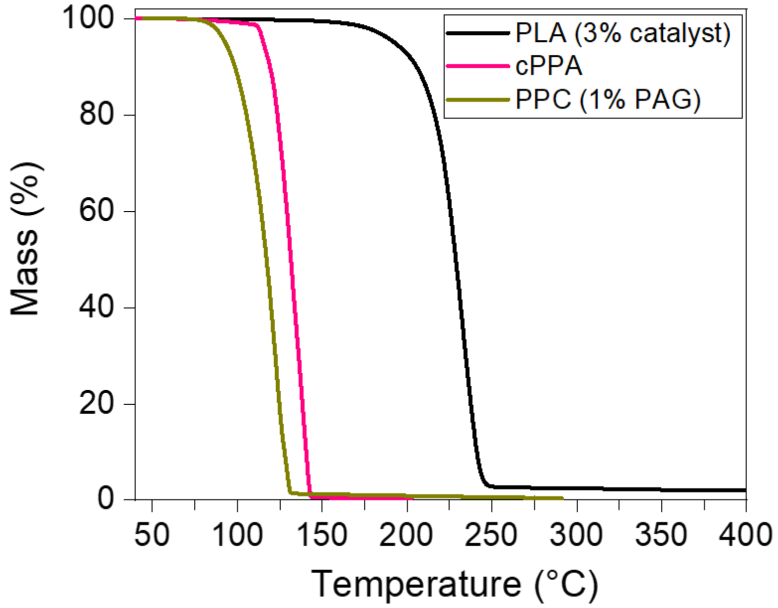

Figure 6.1 Dynamic TGA on sacrificial polymers at 5 °C/min.

Table 6.1. Kinetic parameters of the depolymerization models obtained using TGA experiments.

Polymer	**Stimulus**	**Activation energy (kJ mol^{-1})**	**Pre-exponential factor (s^{-1})**
PLA	Catalyst + Heat	122	4.2×10^{10}
cPPA	Heat	89	4.4×10^{9}
PPC	Acid + Heat	110	4.0×10^{12}

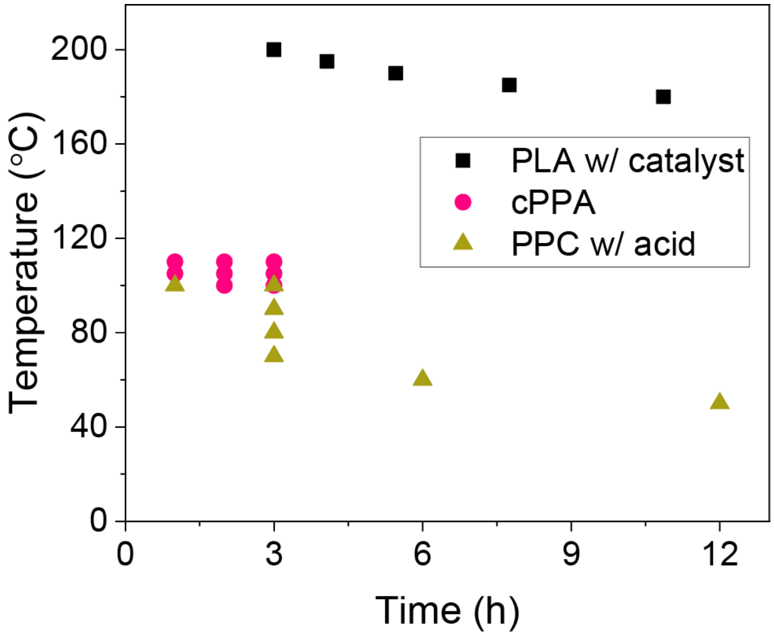

Figure 6.2 Summary of successful VaSC times and temperatures for PLA, cPPA, and PPC.

Beyond the traditional VaSC method, a concurrent approach to create vascular structures was developed. This new method is inspired by vessel formation in bones through selective deposition and removal of material via coordinated cellular processes (Section 1.1). As a first demonstration of concurrent vascularization, we investigated coupled DCPD matrix polymerization and sacrificial fiber depolymerization in Chapter 5. The surplus heat released during self-sustained exothermic frontal polymerization (FP) of the matrix was simultaneously consumed by the depolymerizing template (cPPA or PPC) to leave behind hollow channels. Using this rapid process, a vascular poly(dicyclopentadiene) (pDCPD) thermoset with interconnected microchannels and microvascular carbon-FRPC were created within seconds under ambient conditions, reducing the fabrication energy by four orders of magnitude and the fabrication time by three orders of magnitude. Additionally, the compliance of the gelled DCPD matrix provided another advantage over conventional VaSC by allowing modulation of the microchannel shape and spatial arrangement.

The processing window for successful coupling between the curing and vascularization processes was investigated both experimentally and numerically with a transient non-linear finite element solver. Since depolymerization of the sacrificial polymer is an endothermic process, a competition exists between the surplus heat generated during FP, and the heat consumed during template depolymerization and dissipated into the boundary conditions. The effect of initial conditions such as degree of precure of the host resin before FP and boundary conditions such as an adiabatic glass container vs. an open mold with air convection on the complete evacuation of the sacrificial templates was studied. At higher degrees of precure (> 0.25), longer heat retention in the FP matrix through more insulating boundary conditions extended the successful coupling regime with an agreement between experiments and simulations. This combined thermochemical model demands further development for guiding the optimal distribution of the sacrificial component that would dictate the successful fabrication of vascular structures under given initial and boundary conditions.

6.2 Future work

6.2.1 Volume fractions and Configurations

The vascular structures produced in this work contained very low volume fractions of microchannels (< 1%), but structures such as heat exchangers and filtration devices require a large fraction of porosity/channels in the host material to maximize fluid or mass transport. However, increasing the total volume fraction of the sacrificial precursors or localized network densification could result in incomplete depolymerization or worse, quenching of FP due to a greater amount of heat required to depolymerize the templates. Additionally, all the experiments in Chapter 5 were performed with the sacrificial fiber (diameter < 600 μm) placed in the center of a 6-mm-thick matrix to ensure maximum heat conduction for depolymerization. In contrast, creating vasculature just near the surface of the host matrix is advantageous for active cooling applications in samples exposed to external heat flux [2]–[6]. Fibers placed nearer to the matrix surface will inevitably receive a smaller portion of the surplus energy from FP due to faster heat loss to the surroundings. Precursor placement, dimensions, and volume fraction of the sacrificial templates that can be evacuated completely in a given matrix geometry need to be investigated experimentally and numerically to design structures with pervasive vascular networks spanning 3D space in the host. Experiments performed with multiple fibers placed at various distances from the matrix surface will reveal some of these constraints on the successful coupling between curing and vascularization. Incorporating such constraints into the computational framework to optimize template location and volume fraction inside the matrix at a certain degree of precure, boundary conditions, and host matrix dimensions would help converge on successful solutions of network configurations.

The vascular FRPCs created with the concurrent vascularization process had a fiber-reinforcement volume fraction (V_f) ca. 36 % to get unobstructed microchannels by minimizing the amount of another heat sink (carbon-fiber) in the process. Eventually, vascular FRPCs with V_f greater than 50 % need to be manufactured for aerospace and automotive parts using press-assisted wet layup or vacuum-assisted resin transfer molding (VARTM) processes. Furthermore, blockage-tolerant redundant vascular pathways inside these composites are required for maintaining structural performance under extreme environments [3], [5]–[7]. While both these goals can be accomplished with energy-intensive two-step VaSC [8], additional thermal energy will be required to complete the vascularization process in high-performance vascular composites manufactured with FP compared to currently provided with linear and through-thickness heaters. The resin formulation could also be altered to increase the FP temperature by adding other crosslinkers or higher catalyst loadings and achieve the desired result. The effect of template architecture (increased tortuosity e.g., sinusoidal networks) and volume fraction on the clearance and fidelity of the resulting microchannels also need to be evaluated with various triggering energies. A homogenized numerical model that incorporates V_f as an additional parameter will provide computational insights into the energy balance of this process in FRPCs and help push the applicability of this manufacturing technique in high-performance structural vascular materials.

6.2.2 Library of new matrix materials

All experimental demonstrations of the concurrent vascularization process were done with a pDCPD matrix. While the tensile strength and modulus of neat pDCPD are comparable to BPA-based epoxies, FRPCs made with this matrix have inferior mechanical properties in matrix-dominated delamination experiments due to poor reinforcement-matrix interface. In contrast, epoxy-based matrices offer much better interfacial strength due to the epoxy-tailored sizing of the reinforcement fibers but they suffer from low heat generation during FP [9]. Attempts to improve the interface in pDCPD-based composites or improve the reactivity in epoxy-based systems to manufacture vascular FRPCs with superior mechanical properties would promote industrial adoption of this fabrication process in aerospace, automotive, and marine applications.

Besides developing stronger composites, microfluidic devices for synthesizing molecules [10], studying macromolecular relaxation [11], and mimicking actuation and fluid flow in biocompatible matrices [12] are other interesting application spaces for this one-step process. The host matrices in the above-mentioned applications are generally “soft” hydrogels or rubbery materials to replicate the mechanical and chemical properties of biological materials of interest. Although DCPD cures into a “stiff” matrix, FP of a blended cyclooctadiene (COD)-DCPD resins into elastomeric materials with T_g between -90 °C to 135 °C and tensile modulus between 3 MPa to 2 GPa was reported recently using a similar catalyst-inhibitor system [13]. One-step fabrication of vascular "soft" materials with tunable mechanical properties should be explored through FP of DCPD-COD mixtures with embedded templates to demonstrate the versatility of this technology beyond structural vascular materials. Interestingly, hydrogels with pH-responsive backbones, chemical sensing abilities, self-healing functions, and controlled drug release have been synthesized using FP [14]–[17]. Such systems should be explored to create vascular hydrogels with the one-step method to truly achieve the physical and chemical properties required for biocompatible microfluidic devices without lengthy manufacturing methods. As mentioned in previous chapters, multi-step processes are required to fabricate interconnected microchannel geometries, and techniques like stereolithography are not reliable for creating high fidelity channels with diameters below 200 μm as poor light attenuation in the z-direction can cause undesirable curing with blocked microchannels [12]. Moreover, removal of uncured resins from the channels through dissolution is challenging at smaller diameters due to high wettability and dominant capillary forces. In contrast, VaSC offers superior geometrical control over the microchannel diameter from few microns to centimeters through the escape of gaseous monomer, resembling the wide range of capillary sizes in biological materials [18]. In principle, similar size scales could also be achieved with one-step VaSC but warrant further verification using melt-spun sacrificial PPC fibers with diameters near tens of microns.

The conventional or concurrent vascularization technology should also be extended to thermoplastic matrices and composites. Thermoplastic materials are fast to manufacture, currently used in the automotive sector, and are less detrimental to the environment after end-of-life due to higher recyclability [19]. Unfortunately, none of the three sacrificial polymers explored in this work will survive the melt processing temperatures (> 200 °C) experienced during manufacturing of thermoplastic composites. New sacrificial materials that remain stable at such extreme temperatures (270 °C for Nylon [20]) but can be later triggered orthogonally (radiation, mechanical, or magnetic stimuli) to depolymerize at a lower temperature are required to accomplish this goal. While the one-step process will rely on the parallel development of FP in thermoplastics, tackling this problem with the two-step process may be more fruitful in the near future.

6.2.3 Surface functionalization of the vasculature

The microchannel walls after template vaporization in all previous attempts were either covered with unremovable catalyst residue [21] or rinsed with solvents to obtain a non-permeable surface representing the bulk of the matrix. Additionally, placing two sacrificial fibers next to each other during embedding in the host matrix results in fused microchannels after template evacuation [22]. While this is good for interconnectivity, it is undesirable for flowing two or more different fluids in close proximity without mixing or chemical reactions. In contrast, natural systems deploy countercurrent exchange systems through vascular networks that may be permeable to heat and/or mass transfer. Trees have vascular bundles with xylem channels transporting water upwards from the roots and phloem channels transporting sugars downwards from the leaves [23]. In the human circulatory system, blood flows in opposite directions in the arteries and veins for heat exchange [24], while the gills in the piscine respiratory system rely on oxygen uptake from the surrounding water through gas permeable capillaries [25]. The exchange efficiency of such systems depends on the proximity of the adjacent hollow channels. Inspired by this design, synthetic countercurrent systems for more efficient heat transfer, chemical purification, and gas exchange have been reported [26]. Previously, sacrificial PLA fibers coated with dimethyl-siloxane-based and polyimide- based polymers (ca. 100 μm coating thickness) were used to create non-permeable and semipermeable vascular bundles through a two-step VaSC process [22] but single-step manufacturing of coated microchannels remains to be demonstrated. The fibers can be dip-coated or air-sprayed with a resin that is subsequently cured. The coating should not degrade during the depolymerization of the fiber and instead adhere to the FP matrix. Besides allowing vascular bundles for heat or mass exchange, coatings could also help tailor the wettability of the channel walls to facilitate better fluid flow. Rigid coatings could also compensate for the knockdown in the mechanical properties of the matrices with high vascular network density [6]. Lastly, the coating could also be a catalyst that lines the channel wall during fiber depolymerization and chemically bonds to the FP matrix to create a vascular microreactor. Leaf-inspired photomicroreactors in which the fluid containing the catalyst and the reactants are converted into pharmaceuticals have been reported previously with 1D microchannels [27]. Rapid manufacturing of such synthetic analogs with more complex vascular architectures may enable material synthesis through the concentration of readily available solar energy in inhospitable environments (e.g., Mars) [10] where setting up large-scale manufacturing plants may prove to be even more challenging.

6.3 References

[1] H. Dong *et al.*, “Chemical Treatment of Poly(lactic acid) Fibers to Enhance the Rate of Thermal Depolymerization,” *ACS Applied Materials & Interfaces*, vol. 4, no. 2, pp. 503–509, Feb. 2012, doi: 10.1021/am2010042.

[2] A. M. Coppola, A. S. Griffin, N. R. Sottos, and S. R. White, “Retention of mechanical performance of polymer matrix composites above the glass transition temperature by vascular cooling,” *Composites Part A: Applied Science and Manufacturing*, vol. 78, pp. 412–423, Nov. 2015, doi: 10.1016/j.compositesa.2015.07.012.

[3] S. J. Pety, M. H. Y. Tan, A. R. Najafi, P. R. Barnett, P. H. Geubelle, and S. R. White, “Carbon fiber composites with 2D microvascular networks for battery cooling,” *International Journal of Heat and Mass Transfer*, vol. 115, pp. 513–522, Dec. 2017, doi: 10.1016/j.ijheatmasstransfer.2017.07.047.

[4] S. J. Pety, P. X. L. Chia, S. M. Carrington, and S. R. White, “Active cooling of microvascular composites for battery packaging,” *Smart Mater Struct*, vol. 26, no. 10, p. 105004, 2017, doi: 10.1088/1361-665x/aa84e7.

[5] A. M. Coppola, “Thermal Regulation of Vascularized Fiber-Reinforced Polymer Composites,” 2015.

[6] S. J. Pety, “Microvascular Composites as a Multifunctional Material for Electric Vehicles,” 2017.

[7] S. J. Pety *et al.*, “Design of redundant microvascular cooling networks for blockage tolerance,” *Appl Therm Eng*, vol. 131, no. Int. J. Heat Mass Transf. 103 2016, pp. 965–976, 2018, doi: 10.1016/j.applthermaleng.2017.10.094.

[8] A. P. Esser-Kahn *et al.*, “Three-Dimensional Microvascular Fiber-Reinforced Composites,” *Advanced Materials*, vol. 23, no. 32, pp. 3654–3658, Jul. 2011, doi: 10.1002/adma.201100933.

[9] J. A. Pojman, “Polymer Science: A Comprehensive Reference,” vol. 4, K. Matyjaszewski and M. Möller, Eds. Elsevier B.V., 2012, pp. 957–980.

[10] D. Cambié *et al.*, “Energy-Efficient Solar Photochemistry with Luminescent Solar Concentrator Based Photomicroreactors,” *Angewandte Chemie Int Ed*, vol. 58, no. 40, pp. 14374–14378, 2019, doi: 10.1002/anie.201908553.

[11] D. Kumar, C. M. Richter, and C. M. Schroeder, “Double-mode relaxation of highly deformed anisotropic vesicles,” *Phys Rev E*, vol. 102, no. 1, p. 010605, 2020, doi: 10.1103/physreve.102.010605.

[12] B. Grigoryan *et al.*, “Multivascular networks and functional intravascular topologies within biocompatible hydrogels,” *Science*, vol. 364, no. 6439, pp. 458–464, 2019, doi: 10.1126/science.aav9750.

[13] L. M. Dean, Q. Wu, O. Alshangiti, J. S. Moore, and N. R. Sottos, “Rapid Synthesis of Elastomers and Thermosets with Tunable Thermomechanical Properties,” *Acs Macro Lett*, vol. 9, no. 6, pp. 819–824, 2020, doi: 10.1021/acsmacrolett.0c00233.

[14] Y. Liu, C.-F. Wang, and S. Chen, “Facile access to poly(DMAEMA-co-AA) hydrogels via infrared laser-ignited frontal polymerization and their polymerization in the horizontal direction,” *Rsc Adv*, vol. 5, no. 39, pp. 30514–30521, 2015, doi: 10.1039/c5ra01366f.

[15] T. Chen, Y. Li, S.-Y. Yang, C.-F. Wang, and S. Chen, “Synthesis of versatile poly(PMMA-b-VI) macromonomer-based hydrogels via infrared laser ignited frontal polymerization,” *J Polym Sci Part Polym Chem*, vol. 54, no. 9, pp. 1210–1221, 2015, doi: 10.1002/pola.27961.

[16] Q. Li, J.-D. Liu, S.-S. Liu, C.-F. Wang, and S. Chen, “Frontal Polymerization-Oriented Self-Healing Hydrogels and Applications toward Temperature-Triggered Actuators,” *Ind Eng Chem Res*, vol. 58, no. 9, pp. 3885–3892, 2019, doi: 10.1021/acs.iecr.8b05369.

[17] Q. Feng, F. Li, Q.-Z. Yan, Y.-C. Zhu, and C.-C. Ge, “Frontal polymerization synthesis and drug delivery behavior of thermo-responsive poly(N-isopropylacrylamide) hydrogel,” *Colloid Polym Sci*, vol. 288, no. 8, pp. 915–921, 2010, doi: 10.1007/s00396-010-2224-8.

[18] R. C. R. Gergely *et al.*, “Multidimensional Vascularized Polymers using Degradable Sacrificial Templates,” *Advanced Functional Materials*, vol. 25, no. 7, pp. 1043–1052, Dec. 2014, doi: 10.1002/adfm.201403670.

[19] W. Tan, B. G. Falzon, M. Price, and H. Liu, “The role of material characterisation in the crush modelling of thermoplastic composite structures,” *Compos Struct*, vol. 153, pp. 914–927, 2016, doi: 10.1016/j.compstruct.2016.07.011.

[20] X. Xu, B. Li, H. Lu, Z. Zhang, and H. Wang, “The effect of the interface structure of different surface-modified nano-SiO2 on the mechanical properties of nylon 66 composites,” *J Appl Polym Sci*, vol. 107, no. 3, pp. 2007–2014, 2007, doi: 10.1002/app.27325.

[21] M. Garg, S. R. White, and N. R. Sottos, “Rapid Degradation of Poly(lactic acid) with Organometallic Catalysts,” *Acs Appl Mater Inter*, vol. 11, no. 49, pp. 46226–46232, 2019, doi: 10.1021/acsami.9b17599.

[22] H. Dong, “Synthetic Vascular Materials via a Vaporization of Sacrificial Component Approach,” 2013.

[23] T. T. Kozlowski and S. G. Pallardy, “Physiology of Woody Plants,” no. Bot. Rev.611995, pp. 7–33, 1997, doi: 10.1016/b978-012424162-6/50019-3.

[24] A. Coccarelli, E. Boileau, D. Parthimos, and P. Nithiarasu, “An advanced computational bioheat transfer model for a human body with an embedded systemic circulation,” *Biomech Model Mechan*, vol. 15, no. 5, pp. 1173–1190, 2015, doi: 10.1007/s10237-015-0751-4.

[25] R. Fänge, “Reviews of Physiology, Biochemistry and Pharmacology,” pp. 111–158, 1982, doi: 10.1007/bfb0035347.

[26] K. Brubaker, A. Garewal, R. C. Steinhardt, and A. P. Esser-Kahn, “Bio-inspired counter-current multiplier for enrichment of solutes,” *Nat Commun*, vol. 9, no. 1, p. 736, 2018, doi: 10.1038/s41467-018-03052-y.

[27] D. Cambié, F. Zhao, V. Hessel, M. G. Debije, and T. Noël, “A Leaf-Inspired Luminescent Solar Concentrator for Energy-Efficient Continuous-Flow Photochemistry,” *Angewandte Chemie Int Ed*, vol. 56, no. 4, pp. 1050–1054, 2016, doi: 10.1002/anie.201611101.

APPENDIX A

ENERGY CONSUMPTION FOR MANUFACTURING VASCULAR STRUCTURES

A.1 Equipment and process assumptions

The energy consumed during any heating step is determined by multiplying the energy consumption rate with the step time. The energy consumption rate during ramp and dwell steps for an oven with a power rating of 4.8 kW and an interior volume of 0.8 m^3 were chosen to be 0.046 kWh min^{-1} and 0.024 kWh min^{-1}, respectively [1]. The following equipment and protocols are used for each process:

BPA-epoxy oven-cure cycle: 50 min from 20 to 121 °C and dwell for 2 hours followed by a ramp for 25 min to 177 °C and dwell for 3 hours

DCPD oven-cure Cycle: 30 min from 20 to 70 °C and dwell for 2 hours followed by a ramp to 170 °C for 50 min and dwell for 1.5 hours

PLA VaSC cycle: 2 hours from 20 °C to 200 °C and then 12 hours at 200 °C

cPPA VaSC cycle: 1 hour from 20 °C to 110 °C followed by 1 hour at 110 °C

PPC VaSC cycle: 1 hour from 20 °C to 100 °C followed by 1 hour at 100 °C

DCPD FP initiation with resistive wire: A DC source with 3 Amperes at 2 Volts was switched on for 3 seconds

FRPC FP initiation with heating mat: A 300 W heater was powered on for 30 seconds

UV irradiation cycle for PPC: 10 minutes at 10 mW cm^{-2} for a 15 cm long fiber

A.2 Energy consumption calculations

Table A.1. Energy estimation for two-step and one-step vascularization.

Process	Step	Time (min)	Energy (J)	Total Energy (J)
Two-step (A)	BPA Oven-Cure	375	3.80×10^7	1.20×10^8
	PLA VaSC	840	8.20×10^7	
Two-step (B)	DCPD Oven-Cure	290	3.10×10^7	1.13×10^8
	PLA VaSC	840	8.20×10^7	
Two-step (C)	DCPD Oven-Cure	290	3.10×10^7	4.60×10^7
	cPPA/PPC VaSC	120	1.50×10^7	
One-step (DCPD)	FP + PPC VaSC	1	1.08×10^2	1.08×10^2
One-step (FRPC)	FP + PPC VaSC	0.5	9.09×10^3	9.09×10^3

A.3 Consumption ratios for VaSC with PLA vs. cPPA/PPC

$$Energy\ consumption\ ratio\ for\ VaSC\ in\ thermosets = \frac{8.20 \text{ x } 10^7}{1.50 \text{ x } 10^7} = 5.47$$

A.4 Consumption ratios for two-step vs. one-step vascularization

$$Energy\ consumption\ ratio\ for\ thermosets = \frac{\text{Two−step (A)}}{\text{One−step (DCPD)}} = \frac{1.20 \text{ x } 10^8}{1.08 \text{ x } 10^2} = 1.09 \text{ x } 10^6$$

$$Energy\ consumption\ ratio\ for\ composites = \frac{\text{Two−step (A)}}{\text{One−step (FRPC)}} = \frac{1.20 \text{ x } 10^8}{9.09 \text{ x } 10^3} = 1.32 \text{ x } 10^4$$

$$Time\ consumption\ ratio\ for\ thermosets = \frac{\text{Two−step (A)}}{\text{One−step (DCPD)}} = \frac{1215}{1} = 1.21 \text{ x } 10^3$$

$$Time\ consumption\ ratio\ for\ composites = \frac{\text{Two−step (A)}}{\text{One−step (FRPC)}} = \frac{1215}{0.5} = 2.43 \text{ x } 10^3$$

A.5 References

[1] R. A. Witik, F. Gaille, R. Teuscher, H. Ringwald, V. Michaud, and J.-A. E. Månson, "Economic and environmental assessment of alternative production methods for composite aircraft components," *J Clean Prod*, vol. 29, pp. 91–102, 2012, doi: 10.1016/j.jclepro.2012.02.028.

APPENDIX B

PROCESSING AND CHARACTERIZATION OF SACRIFICIAL POLYMERS

B.1 Dry spinning cPPA fibers

Since wet-spun cPPA fibers were challenging to handle due to brittle fracture during bending, two different strategies to get mechanically strong fibers with a circular cross-section were adopted. First, dry spinning of cPPA fibers was attempted. Dry spinning involves dissolving the polymer in a low boiling point (T_b) solvent and extruding it at high temperatures to remove the solvent before collection. Concentrated solutions of cPPA (20-30 wt. % in solution) were prepared using two different solvents, DCM (T_b = 40 °C) and THF (T_b = 66 °C), and extruded in a heated environment using a custom dry spinning setup (**Figure B.1a**). A syringe pump expelled the polymer solution and the fiber was collected on a solvent-resistant roller inside a fume hood. Two concave ceramic resistive heaters (20 cm in length) connected to a PID controller were placed opposite to each other to form a heated cylindrical tube half-way in the vertical distance between the tip of the syringe and the roller (total distance ca. 60 cm). The heaters were maintained at a constant temperature before beginning the extrusion for all tests. The solvents type, solvent concentration, and winding speed were varied to study the influence on final fiber cross-section and mechanical handleability. Representative cross-sections are shown in **Figure B.1b-e**. The wound fibers were sticky with non-uniform cross sections for both solvents when no external heat was applied. Dry fibers (ca. 100 μm diameter) were collected when the heater temperature was higher than 75 °C but the cross sections remained non-circular. Unlike wet-spun fibers, the cross-sections did not show porosity but the fibers remained fragile against repeated bending around a tight radius of curvature (5 mm). As mentioned extensively in the dry spinning literature [1], it was challenging to tune the cross-section of the final fibers in this diameter range, so the focus was shifted to melt spinning plasticized cPPA fibers.

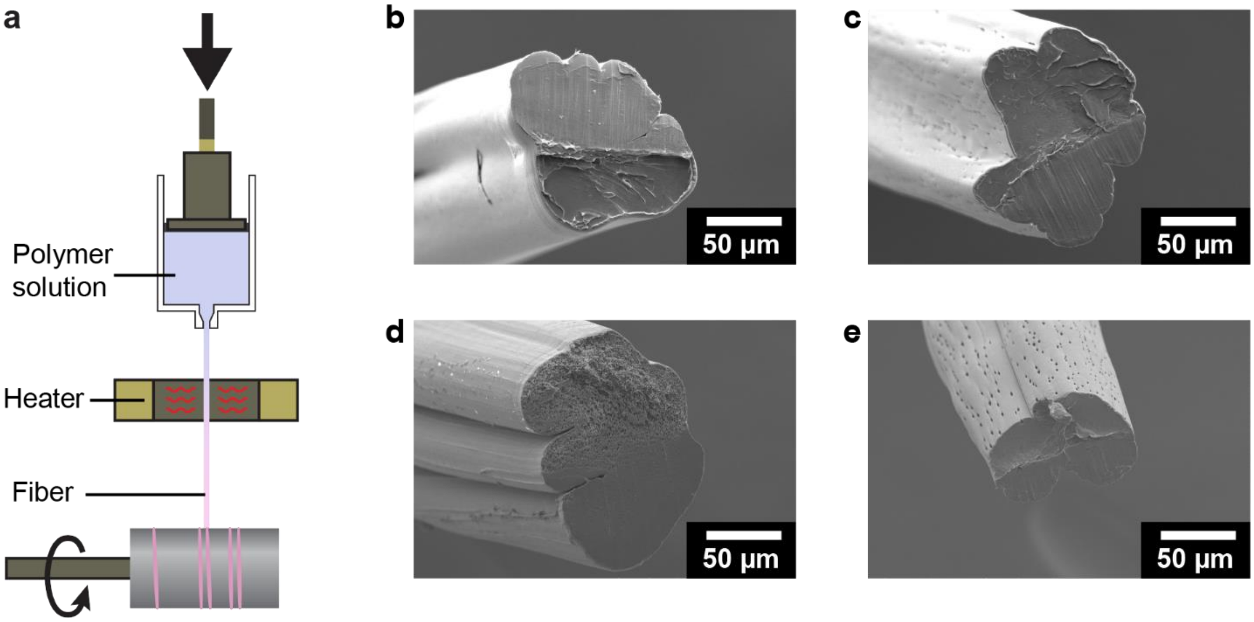

Figure B.1. Dry-spinning cPPA fibers. (a) Dry-spinning setup. (b-e) Dry-spun cPPA fibers using 25 wt. % polymer solutions. (b) DCM solvent without any heating at room temperature. (c) DCM solvent with the heater at 80 °C. (d) THF solvent without heating. (e) THF solvent with the heater at 100 °C.

B.2 Melt-extrusion of plasticized cPPA

Solvent-blending phthalate-based plasticizers has shown promise in thermoforming cPPA into planar structures such as dog bones by depressing the glass transition temperature of cPPA from 180 °C (estimated in [2]) to as low as 25 °C [3]. Since negligible mass loss was observed for solid cPPA at 85 °C in TGA (Chapter 3), this temperature was selected for melt-extrusion experiments in the custom melt-spinning setup described in Chapter 4. Another consideration for extrusion was the T_g of plasticized cPPA. The T_g needs to be such that the templates retain their shape near room temperature but are pliable enough for extrusion at 85 °C. In one trial, solvent-cast cPPA films plasticized with 25 wt. % (w.r.t cPPA) dibutyl phthalate (DBP) were obtained with a T_g of 34 °C

(**Figure B.2a**). These films were chopped into small pieces and fed into the heated barrel of the melt-extruder for obtaining plasticized filaments. The feedstock was softened for 30 minutes at 85 °C and extruded through a 1.5 mm diameter spinneret. The degree of softening was insufficient for winding a continuous filament and approximately 10 cm long pieces were collected. A circular cross section with a diameter ca. 1.6 mm and a solid microstructure was obtained for these filaments (**Figure B.2b**).

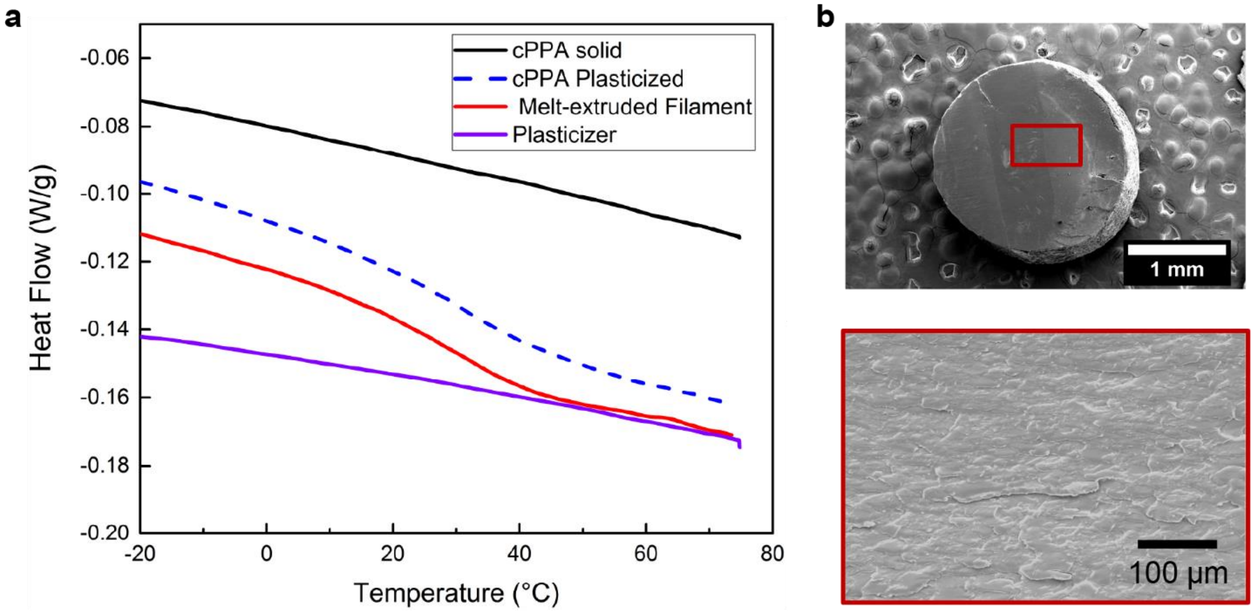

Figure B.2. Melt-extrusion of plasticized cPPA. (a) DSC on plasticized film (dashed blue line) and filament (solid red line) at 5 °C/min. (b) Cross section of a plasticized cPPA filament after melt extrusion.

While circularity and homogeneous cross section were achieved, the thermal stability of these templates was compromised in the extrusion process. First, a drop in the weight-averaged molecular weight of the filament (75 kDa) compared to film (310 kDa) was indicated by the higher retention time for the filament samples in GPC experiments (**Figure B.3**). This depolymerization was further confirmed by isothermal TGA experiments at 85 °C. While solid cPPA showed negligible mass loss as expected, the plasticized film showed a gradual decrease in mass to 93%

after three hours (**Figure B.4**). We surmise this reduction in thermal stability may have been caused by residual impurities from cPPA synthesis, which could diffuse and react faster with the plasticized cPPA chains [3]. The melt-extruded filament showed ca. 80% mass loss solely due to monomer (confirmed by MS) and the residual mass was attributed to the plasticizer due to very low vapor pressure at this temperature. When the extruded samples were stored in a -20 °C freezer, a liquid residue (mostly *o*PA) was obtained after six months, unlike solid cPPA which showed negligible reduction in molecular weight under the same conditions. These observations confirmed that the extrusion process had initiated partial depolymerization of some polymer chains, which the depolymerization continued in the freezer above their ceiling temperature (-36 °C [4]). Additionally, only discontinuous strands were obtained with this method and the extrusion pressure was insufficient for fiber spinning attempts at smaller diameters. Usually, extrusion temperatures of greater than 150 °C are used to achieve the right viscosities for melt-spinning amorphous polymers with T_g near 40 °C. However, no further extrusion attempts with cPPA were made due to the severe hazard of depolymerization into a highly toxic and corrosive monomer at such temperatures. Significant steps for enhancing the thermal stability of cPPA while plasticizing it need to be taken to pursue melt-processing routes in the future.

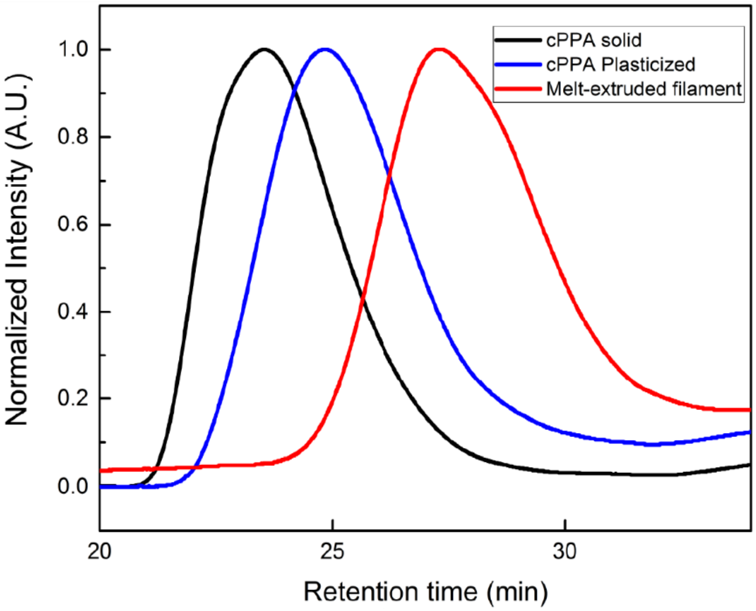

Figure B.3. GPC traces of cPPA solid (black), film (blue), and filament (red).

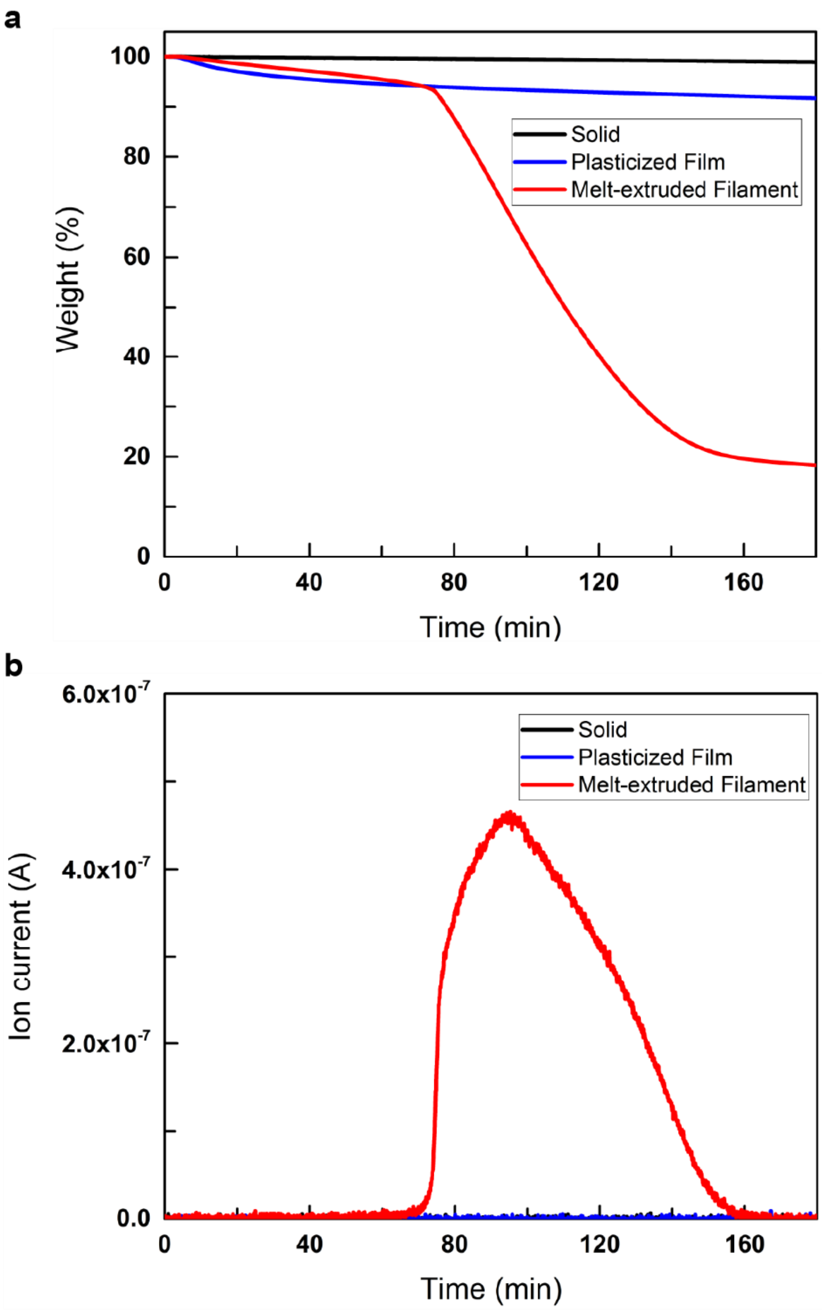

Figure B.4. Monitoring cPPA depolymerization in TGA-MS experiments. (a) Mass loss during isothermal TGA (85 °C) of cPPA templates at various stages of processing. (b) Detection of *o*PA (105 AMU) monomer using MS on the evolved gas from TGA experiments.

B.3 Thermal stability of melt-spun sacrificial PPC fibers

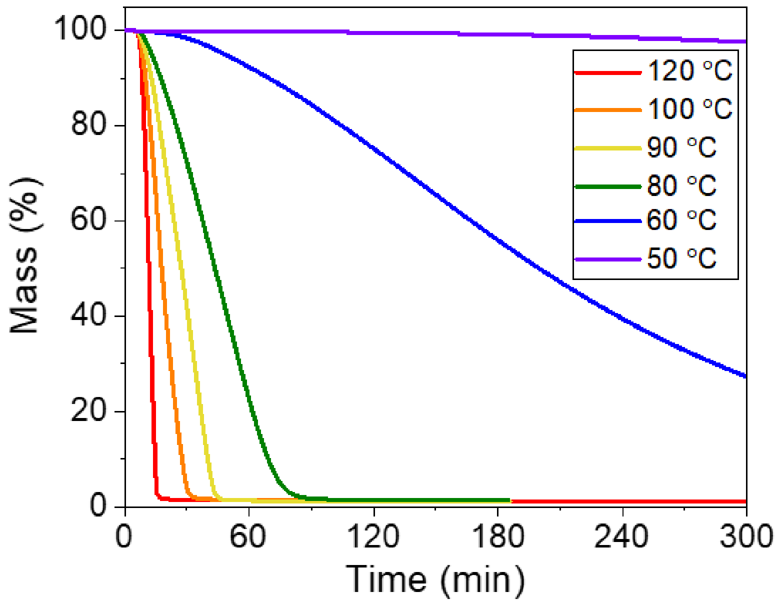

Figure B.5. Mass loss of PPC (1% PAG, UV-irradiated) fibers during isothermal TGA experiments.

B.4 References

[1] Y. Imura, R. M. C. Hogan, and M. Jaffe, “10 Dry spinning of synthetic polymer fibers,” Elsevier, 2014, pp. 187–202.

[2] J. A. Kaitz and J. S. Moore, “Copolymerization of o-Phthalaldehyde and Ethyl Glyoxylate: Cyclic Macromolecules with Alternating Sequence and Tunable Thermal Properties,” *Macromolecules*, vol. 47, no. 16, pp. 5509–5513, Aug. 2014, doi: 10.1021/ma5013557.

[3] A. M. Feinberg *et al.*, “Cyclic Poly(phthalaldehyde): Thermoforming a Bulk Transient Material,” *ACS Macro Letters*, vol. 7, no. 1, pp. 47–52, Jan. 2018, doi: 10.1021/acsmacrolett.7b00769.

[4] J. P. Lutz, O. Davydovich, M. D. Hannigan, J. S. Moore, P. M. Zimmerman, and A. J. McNeil, “Functionalized and Degradable Polyphthalaldehyde Derivatives,” *J Am Chem Soc*, vol. 141, no. 37, pp. 14544–14548, 2019, doi: 10.1021/jacs.9b07508.

APPENDIX C

CONCURRENT POLYMERIZATION AND VASCULARIZATION

cPPA can depolymerize rapidly in the 100-145 °C range without any catalyst (Chapter 3), and at lower temperatures using acidic triggers [1], [2]. Its high sensitivity to heat and pH triggers, despite the processing challenges discussed previously, make it an excellent sacrificial candidate for vascularization during FP. Before exploring PPC as a more suitable candidate with more processing advantages, the heat released during FP was used to concurrently depolymerize embedded cPPA templates for vascularizing neat thermosets and FRPCs.

C.1 Vascularization in neat matrix

Gel scaffolds with embedded solution-processed sacrificial templates were fabricated for initial experiments using the cell-casting method reported in Chapter 5. The DCPD resin was prepared according to a modified literature procedure [3]. Two equivalents of TBP inhibitor (with respect to GC2) were used and the cell-casting mold was incubated in an environmental chamber maintained at 25 °C for 14.5 h, yielding a gel scaffold 50 mm x 34 mm x 6 mm with a degree of precure (α_0) ca. 0.30. The scaffold was removed from the mold and touched on one end with a soldering iron to initiate FP. The heat supplied to the cPPA template during FP was sufficient to completely depolymerize the sacrificial films and fibers and create a vascular network within the poly(DCPD) matrix (**Figure C.1**). A thermocouple embedded in the gel showed a peak temperature of ca. 162 °C during frontal polymerization, which subsequently cooled to 100 °C within 2 minutes. 3D reconstruction of the channel created **Figure C.1b** using μCT showed clear channels with surface morphology and dimensions similar to the initial template.

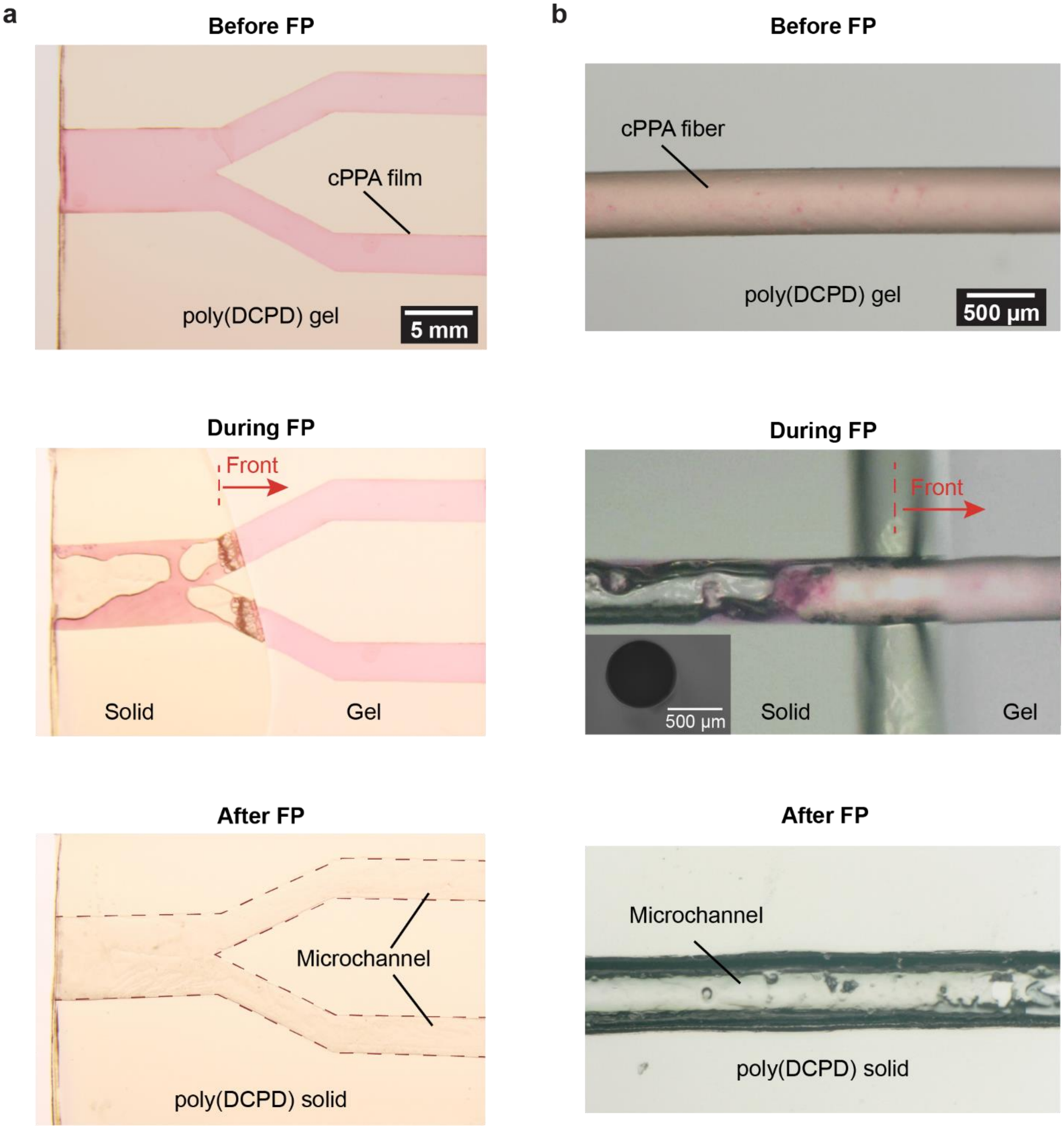

Figure C.1. Rapid vascularization of DCPD gels with embedded cPPA templates. (a) Optical snapshots of the gel scaffold with a bifurcating film before (top image), during FP (center), and after (bottom) FP. (b) Optical snapshots of the scaffold with a 500 μm diameter cPPA fiber before (top image), during FP (center), and after (bottom) FP. The inset image during FP shows cross section of the microchannel. All channels were flushed with ethanol to remove any residual monomer.

Increasing the incubation time in the environmental chamber decreased the front temperature and front velocity (**Figure C.2**). This is attributed to a reduction in the number of exothermic reactions happening per unit volume during FP due to an increase in α_0. FP of a gel scaffold with an α_0 of 51% was insufficient to depolymerize the embedded cPPA fiber, resulting in clogged channels. Furthermore, factors like changes in the geometry of the gel scaffold, the surrounding insulation conditions, and dimensions of the sacrificial template will also influence the successful vascularization at lower α_0.

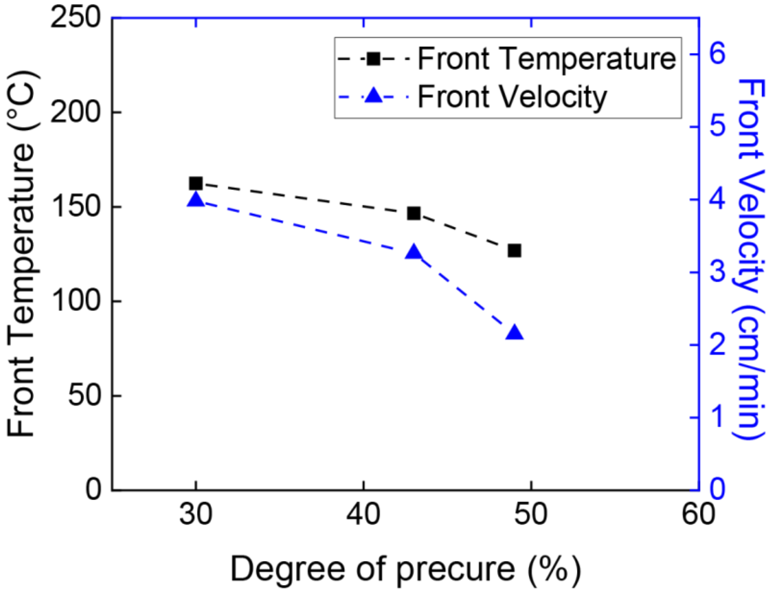

Figure C.2. FP velocity and temperature in the successful vascularization window ($\alpha_0 < 50\%$).

To demonstrate the fidelity of the process with precise control over interconnectivity in the microchannels, two fibers were placed perpendicular to each other while in physical contact at one junction and incubated in a gel scaffold ($\alpha_0 = 0.30$). After FP, both channels cleared and 3D reconstruction of the microchannels in the contact region revealed a fused architecture (**Figure C.3**). An ethanol solution dyed with Nile Red was injected into one channel and the fluid was successfully transported to the perpendicular channel through this junction, further confirming the successful formation of an interconnected network.

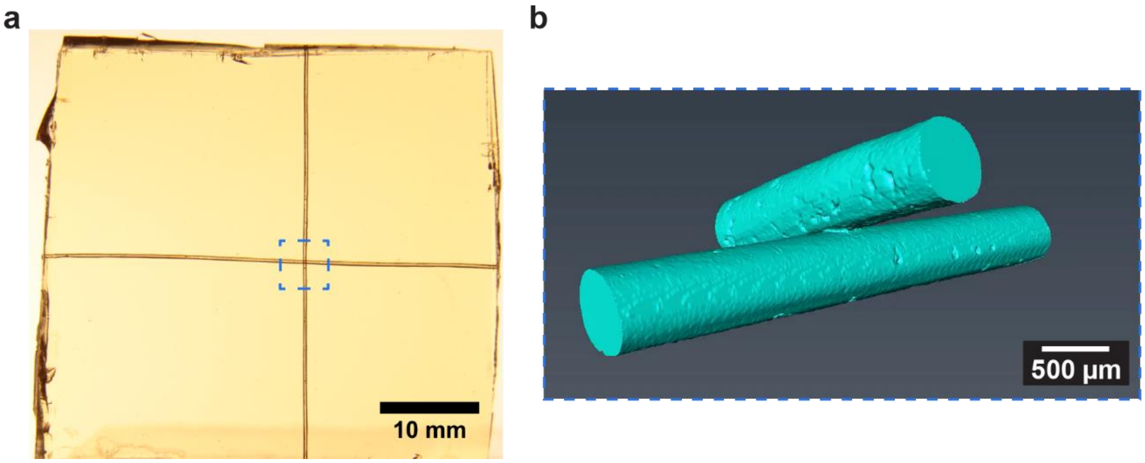

Figure C.3. Interconnected microchannels in a neat pDCPD matrix. (a) Optical snapshot after FP. (b) µCT reconstruction of the junction region.

Besides vessels that were hundreds of microns in diameter, channels with larger diameters (1.5 mm) were also created with thick cPPA filaments (**Figure C.4a**). The larger diameter translated to a ca. 10x increase in the volume of sacrificial material, which clearly distorts the shape of the front in the region of the matrix near the fiber due to increased heat consumption. This experiment suggests the need for a parametric study with volume fractions and configurations of sacrificial templates similar to the future work with PPC templates discussed in Chapter 6. Besides creating 1D channels, 2D vessels were also formed with printed cPPA templates (**Figure C.4b**).

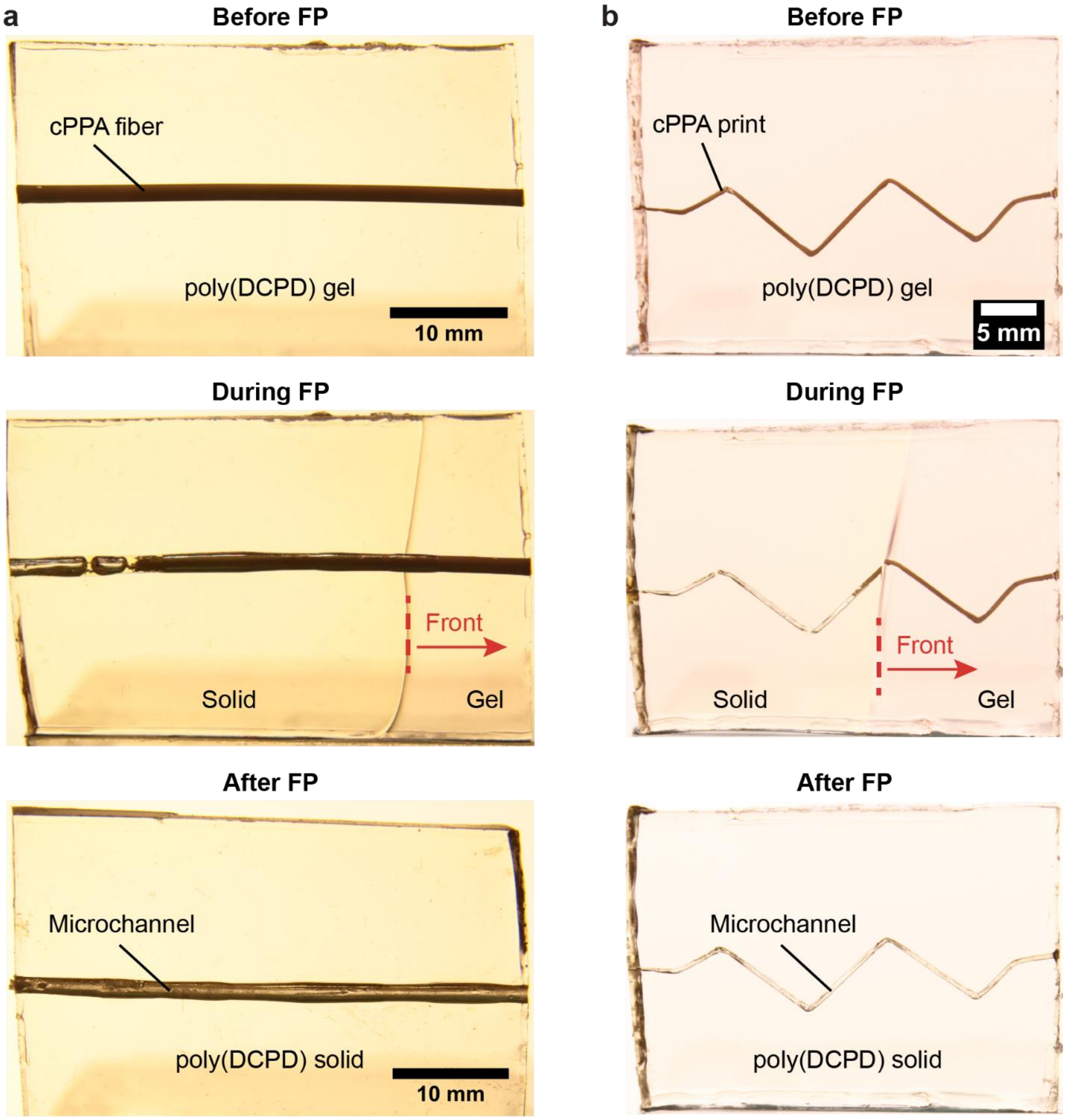

Figure C.4. Rapid vascularization of DCPD gels with embedded fibers and printed templates. (a) Optical snapshots of the scaffold with a 1.5 mm diameter cPPA fiber before (top image), during FP (center), and after (bottom) FP. (b) Optical snapshots of the scaffold with a printed sacrificial template before (top image), during FP (center), and after (bottom) FP. All channels were flushed with ethanol to remove any residual monomer.

C.2 Vascularization in fiber-reinforced polymer composites

FP of continuous carbon-FRPCs using a linear initiation was demonstrated using FP of DCPD resin via a vacuum-assisted resin transfer molding (VARTM) process (**Figure C.5a,b**). However, a significant portion of the heat released during FP of FRPCs is consumed by the fiber-reinforcement due to thermal conductivity and high-volume fraction (50 % and higher for high-performance composites) [3]. In a preliminary experiment (refer to Chapter 5 for resin formulation in FRPC specimens), a significantly lower peak temperature of 125 °C (**Figure C.5c**) compared to poly(DCPD) gel was observed during VARTM of a 175 x 100 x 4 mm FRPC with twelve plies of 2 x 2 twill weave carbon fiber-reinforcement (volume fraction ca. 50 %). A wet-spun cPPA fiber was embedded in the middle of the laminate parallel to the length of the plies, and the fiber was still present after FP due to insufficient heat available for depolymerization (**Figure C.5d**). Two materials and processing strategies to facilitate complete depolymerization were combined for obtaining vascular FRPCs with cPPA fibers.

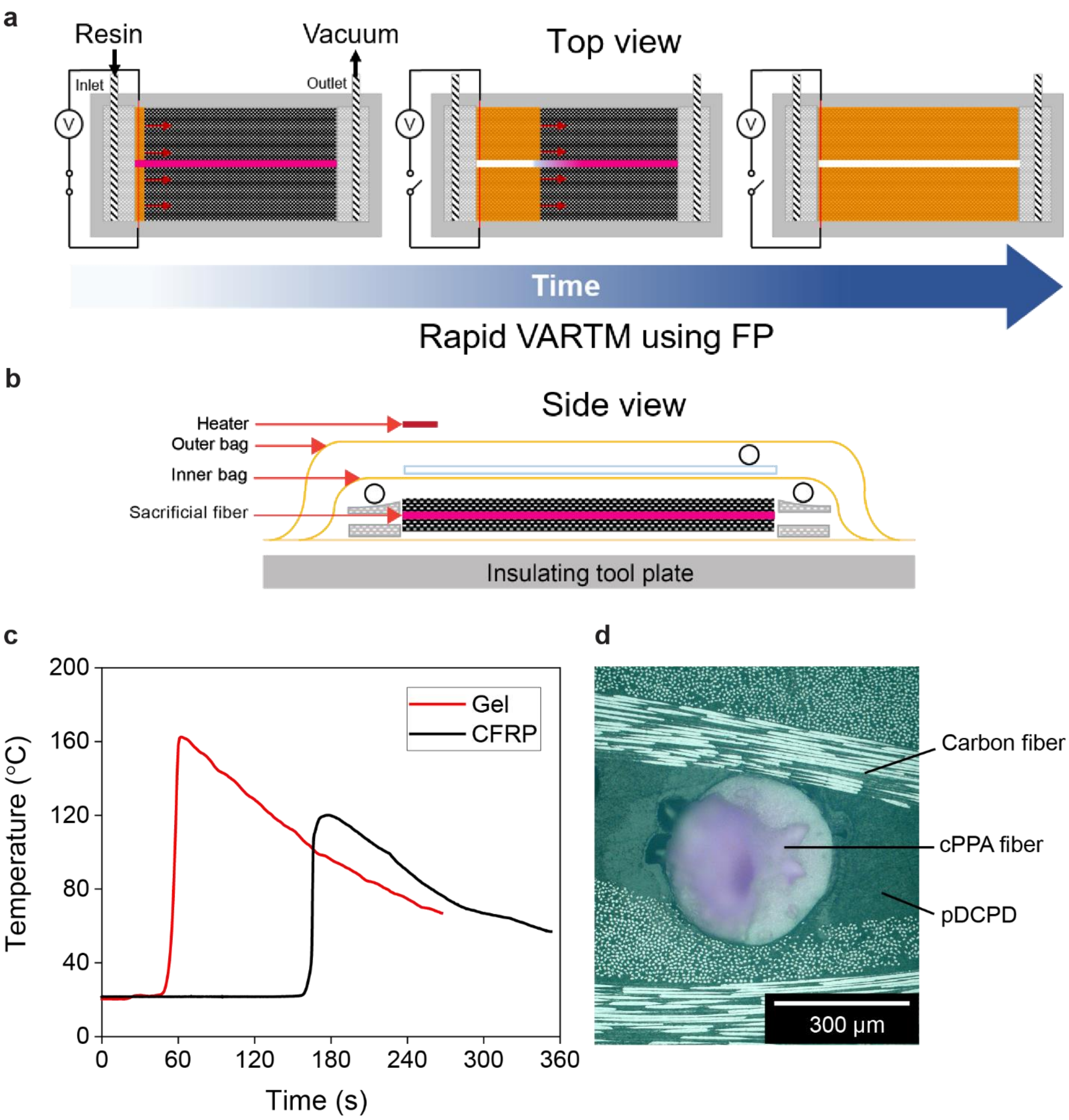

Figure C.5. Concept and experiments for rapid vascularization of FRPCs with embedded cPPA fibers (pink). (a) Top view of FRPC during FP showing initiation and completion of FP with an embedded cPPA fiber. (b) Side view of the FRPC showing the sacrificial fiber placed in the midplane of the fabric preform (black). (c) Temperature profile during FP of a carbon-FRPC measured by a thermocouple. (d) Optical snapshots of the cross section of the FRPC after FP, showing an intact sacrificial fiber.

First, the PAG used for PPC in Chapter 5 was also blended with the cPPA fibers during the wet spinning process to facilitate acid-catalyzed depolymerization at lower temperatures. Even with very low concentrations of PAG (0.1% of cPPA), fibers irradiated with UV light for 2 minutes depolymerized at 80 °C in less than 1 hour (red lines **Figure C.6a**). Fibers without any PAG (black lines) showed a negligible mass loss in three hours at this temperature. Second, a top insulating plate similar to the bottom tool plate in **Figure C.5a,b** was added to the VARTM samples for longer heat retention. This modification helped maintain the composite temperature above 60 °C for nearly 10 mins after FP had propagated in any given location (**Figure C.6b**), which was significantly longer than the previous setup. Two fibers perpendicular to the front direction were placed 2 cm apart in the midplane of the fabric preform. While the neat cPPA fiber did not depolymerize during FP, the UV-irradiated PAG-containing fiber depolymerized completely to create a hollow channel (**Figure C.6c,d**). Unfortunately, the channel shape was not circular, and the volatile monomer caused voids near the microchannel. Further optimization of the depolymerization rate is required to refine the channel fidelity.

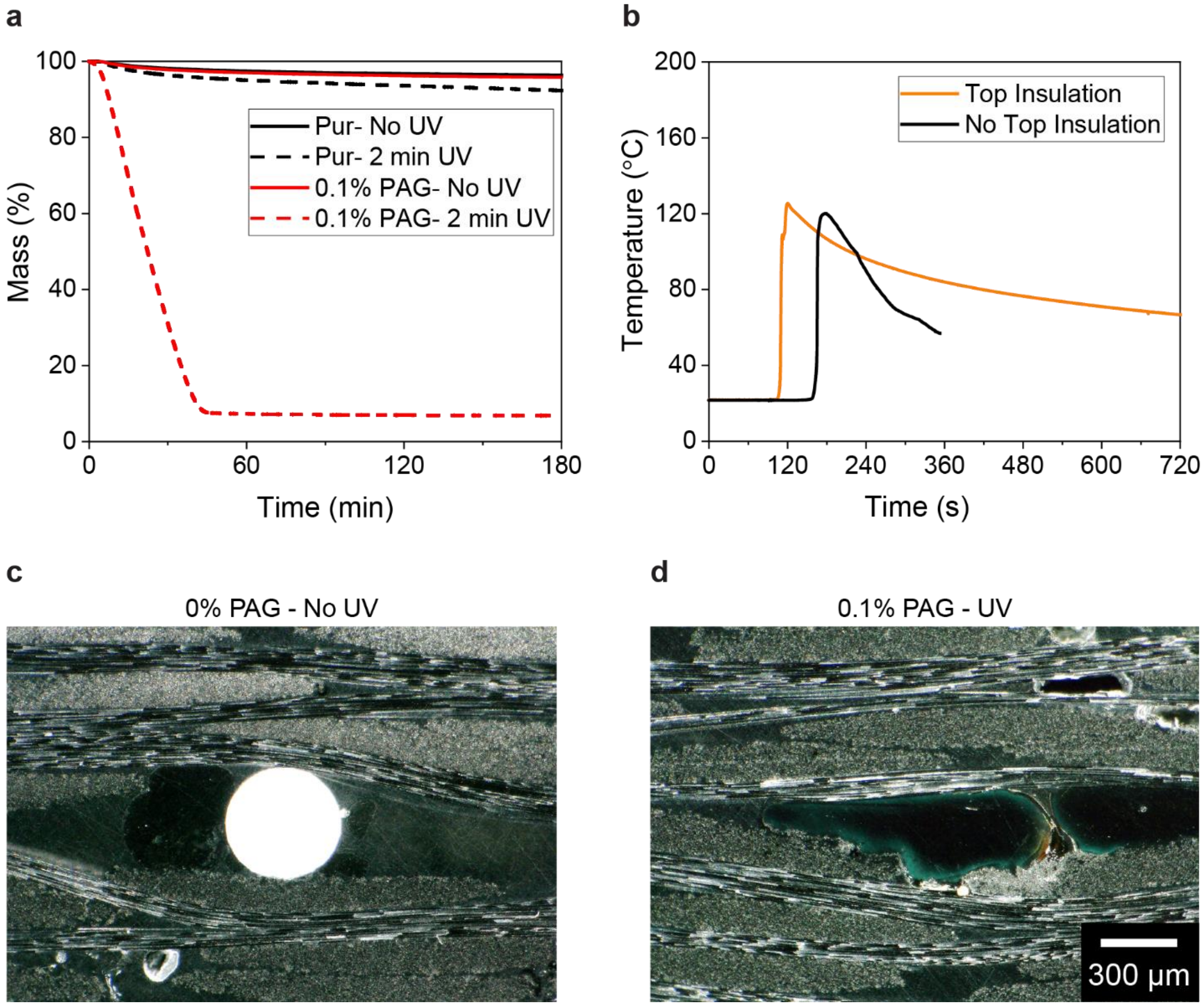

Figure C.6. Rapid vascularization of FRPCs with more insulated boundary conditions. (a) Mass loss of cPPA fibers (pure and with PAG) during isothermal TGA experiments at 80 °C. (b) The temperature profile of a carbon-FRPC with liquid DCPD was measured by a thermocouple during FP. The scheme in Figure C.5 was modified by adding a top insulating plate for longer heat retention (orange line) inside the composite compared to no top insulation (black line). (c) Cross-section of a composite showing an intact cPPA fiber after FP. (d) Cross-section of the composite showing a deformed microchannel after depolymerization of a PAG containing fiber.

C.3 3D printing PPC leaf network

The digital image of an impatiens leaf was scanned, and coordinates of the primary and secondary veins were mapped, as shown by blue dots in **Figure C.7a**. A G-code was written based on these coordinates, which was then used to print the PPC filament in the areas marked by the black regions in **Figure C.7b**.

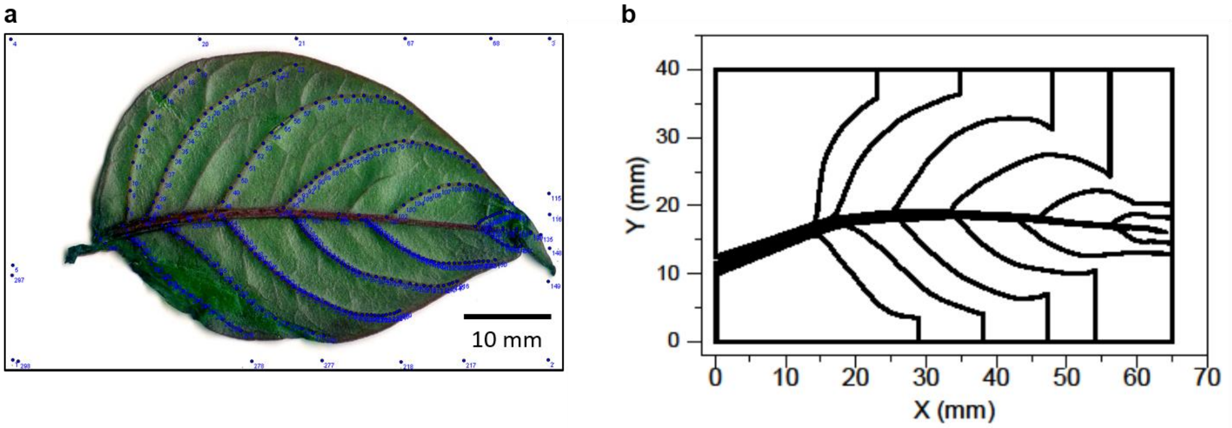

Figure C.7. 3D printing sacrificial PPC (1% PAG) templates. (a) A digital image of a leaf is used to map coordinates of the primary and secondary veins. (b) The coordinates are then converted into a G-code, which is then loaded into a 3D printer. The printed extrudes the PPC (1% PAG) filament in the areas marked by the black pixels.

C.4 References

[1] H. L. Hernandez *et al.*, “Triggered Transience of Metastable Poly(phthalaldehyde) for Transient Electronics,” *Advanced Materials*, vol. 26, no. 45, pp. 7637–7642, Oct. 2014, doi: 10.1002/adma.201403045.

[2] C. W. Park *et al.*, “Thermally triggered degradation of transient electronic devices.,” *Advanced Materials*, vol. 27, no. 25, pp. 3783–3788, Jul. 2015, doi: 10.1002/adma.201501180.

[3] I. D. Robertson *et al.*, “Rapid energy-efficient manufacturing of polymers and composites via frontal polymerization,” *Nature*, vol. 557, no. 7704, pp. 223–227, May 2018, doi: 10.1038/s41586-018-0054-x.

APPENDIX D

COMPUTATIONAL MODELING OF ONE-STEP VASCULARIZATION

D.1 Model equations

The frontal polymerization of DCPD and the depolymerization of PPC are coupled chemo-thermal processes described by their own reaction-diffusion model. In the DCPD domain, the thermo-chemical model expressed in terms of the temperature, T (in K), and degree-of-cure, α, takes the form:

$$\begin{cases} \kappa_1 \nabla^2 T + \rho_1 H_{r1} \frac{\partial \alpha}{\partial t} = \rho_1 C_{p1} \frac{\partial T}{\partial t} \\ \frac{\partial \alpha}{\partial t} = A_1 exp\left(-\frac{E_{a1}}{RT}\right)(1-\alpha)^{n_1}\alpha^{m_1}\frac{1}{1+\exp[C(\alpha-\alpha_c-\alpha_0)]} \end{cases} \qquad \text{D.1}$$

where $\alpha = 0$ denotes the neat resin and $\alpha = 1$, the fully cured polymer. In the first equation in (1), ∇^2 denotes the spatial Laplacian operator, κ_1 (in $\mathrm{W/(m \cdot K)}$) denotes the thermal conductivity, ρ_1 (in $\mathrm{kg}/(m^3)$) the density, C_{p1} (in $\mathrm{J/(kg \cdot K)}$) the specific heat, and H_{r1} (in $\mathrm{J/g}$) the total enthalpy of reaction. Subscript 1 indicates quantities are associated with DCPD. The second equation in (1) captures the cure kinetics, with A (in s^{-1}) denoting the pre-exponential constant, E_a (in $\mathrm{kJ/mol}$) the activation energy, and R (= 8.314 $\mathrm{J/(mol \cdot K)}$) the universal gas constant. The additional terms appearing in the cure kinetic model are based on the Prout-Tompkins auto-catalytic model $(1-\alpha)^{\mathrm{n}}\alpha^m$ augmented by a diffusion factor $(1 + \exp[C(\alpha - \alpha_c)])^{-1}$ [1]. This model has been successfully used to model FP in DCPD monomer [2], DCPD gels, and DCPD-based composites [3]–[5]. **Table D.1** provides the material properties and **Table D.2** provides cure kinetic parameters for DCPD.

Table D.1. Material properties of the various components used in computational modeling.

Material	κ **(W m^{-1}K^{-1})**	ρ **(kg m^{-3})**	***C*$_p$ (J kg^{-1} K^{-1})**	***H*$_r$ (J g^{-1})**
DCPD resin	0.15	980	1,600	380
PPC (1% PAG) fiber	0.25	1,260	1,800	20
Glass plate	1.14	2000	800	NA

Table D.2. Kinetic parameters for the conversion for materials used in computational modeling.

Material	**E (kJ mol^{-1})**	**A (s^{-1})**	***m***	***n***
DCPD resin	113.2	8.5 x 10^{15}	0.7	1.74
PPC (1% PAG)	110.0	4.0 x 10^{12}	0.2	0.94

The depolymerization process of the PPC fiber is described similarly in terms of the thermal field and the degree of depolymerization β, with $\beta = 0$ corresponding to the intact PPC and $\beta = 1$ the fully depolymerized state:

$$\begin{cases} \kappa_2 \nabla^2 T - \rho_2 H_{r2} \frac{\partial \beta}{\partial t} = \rho_2 C_{p2} \frac{\partial T}{\partial t}, \\ \frac{\partial \beta}{\partial t} = A_2 exp\left(-\frac{E_{a2}}{RT}\right)(1-\beta)^{n_2}\beta^{m_2}, \end{cases} \tag{D.2}$$

where the subscript ‘2’ denotes quantities associated with PPC, and H_{r2} the total heat absorbed per unit mass by the depolymerization of the sacrificial material. To extract the parameters defining the depolymerization kinetics of PPC, a constrained nonlinear multi-variable optimization algorithm [6] is adopted to match dynamic TGA data obtained at different ramping rates (Chapter 4). The material properties and depolymerization kinetics parameters used in this study for PPC are listed in **Table D.1** and **Table D.2**.

D.2 Modeling geometry and boundary conditions

For the 3D simulation during FP of a DCPD matrix with an embedded PPC template, **Figure D.1a** demonstrates the repeating unit cell consisting of a PPC fiber embedded in a block of DCPD matrix exposed to convective air cooling along its top and bottom surfaces. Owing to symmetry, only a quarter of the unit cell (**Figure D.1b**) is simulated, with all planes of symmetry captured as adiabatic (insulated) surfaces and a convective boundary condition (with a convective coefficient of 75 W/(m^2K) and an ambient temperature of 20 °C applied along the top surface exposed to air. In the simulation, the inter-fiber spacing (S) is 4 mm, the thickness of the host matrix (H) is 6 mm, and the length of the domain (L) is 20 mm. Initiation of the FP process is achieved by prescribing a temperature (200 °C) at one end of the simulation domain for one second. For the simulations involving a glass slide placed along the top and bottom of the specimen (**Scheme 5.2** in Chapter 5), a 6-mm thick glass layer is added along the top of the simulation domain. In that glass layer, the transient heat conduction equation (no reaction term) is solved, with the convective boundary condition applied to the surface of the glass layer exposed to air.

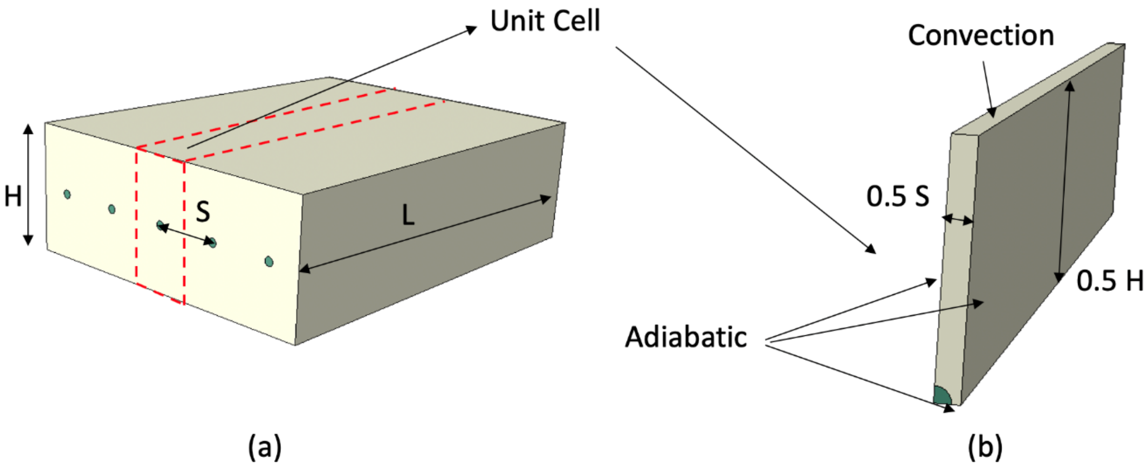

Figure D.1. Simulation domain: (a) Entire specimen with multiple parallel PPC fibers (green) embedded in a DCPD matrix; (b) Simulated domain with adiabatic conditions applied along the symmetry planes and convective conditions along the top surface.

The analysis is performed with Multiphysics Object-Oriented Simulation Environment (MOOSE), an open-source C++ math library and nonlinear finite element solver [7] that provides the mesh adaptivity needed to accurately and efficiently capture the sharp gradients in temperature and in the degree of cure/depolymerization in the vicinity of the advancing front.

D.3 References

[1] G. Yang and J. K. Lee, "Curing Kinetics and Mechanical Properties of endo - Dicyclopentadiene Synthesized Using Different Grubbs' Catalysts," *Ind Eng Chem Res*, vol. 53, no. 8, pp. 3001–3011, 2014, doi: 10.1021/ie403285q.

[2] E. Goli, I. D. Robertson, P. H. Geubelle, and J. S. Moore, "Frontal Polymerization of Dicyclopentadiene: A Numerical Study," *J Phys Chem B*, vol. 122, no. 16, pp. 4583–4591, 2018, doi: 10.1021/acs.jpcb.7b12316.

[3] S. Vyas, E. Goli, X. Zhang, and P. H. Geubelle, "Manufacturing of unidirectional glass-fiber-reinforced composites via frontal polymerization: A numerical study," *Compos Sci Technol*, vol. 184, p. 107832, 2019, doi: 10.1016/j.compscitech.2019.107832.

[4] S. Vyas, X. Zhang, E. Goli, and P. H. Geubelle, “Frontal vs. bulk polymerization of fiber-reinforced polymer-matrix composites,” *Compos Sci Technol*, vol. 198, p. 108303, 2020, doi: 10.1016/j.compscitech.2020.108303.

[5] E. Goli *et al.*, “Frontal polymerization of unidirectional carbon-fiber-reinforced composites,” *Compos Part Appl Sci Manuf*, vol. 130, p. 105689, 2020, doi: 10.1016/j.compositesa.2019.105689.

[6] M. J. D. Powell, “Numerical Analysis, Proceedings of the Biennial Conference Held at Dundee, June 28–July 1, 1977,” pp. 144–157, 2006, doi: 10.1007/bfb0067703.

[7] D. Gaston, C. Newman, G. Hansen, and D. Lebrun-Grandié, “MOOSE: A parallel computational framework for coupled systems of nonlinear equations,” *Nucl Eng Des*, vol. 239, no. 10, pp. 1768–1778, 2009, doi: 10.1016/j.nucengdes.2009.05.021.